Copenhagen, May 12, 2022

PhD Dissertation

Adiabatic evolution of driven quantum systems in the presence of dissipation and noise possessing spatial and temporal correlations

Jan A. Krzywda

Institute of Physics Polish Academy of Sciences

Under the supervision of dr hab. Ł. Cywiński, prof. IF PAN

Asi za wsparcie,
Tadkowi za pomysły,
Rodzicom za motywację,
Łukaszowi za cierpliwość

– Dziękuję
Jan A. Krzywda

Academic Achievements

Up to date the author has published seven scientific papers and a single preprint [1–8] . This thesis is mostly based on two research papers on charge transfer between semiconductor quantum dots in presence of a realistic environment [1, 2]. It presents and extends these results to include spin dephasing during shuttling of a spin qubit between two quantum dots. The theory developed in the thesis has become also useful in writing of a recent preprint, in which the blueprint of realistic spin qubit shuttle in Si/SiGe device was proposed [3]. This work has been done in collaboration within the international QuantERA Si-QuBus consortium. The relation between the thesis and [3] is explained in the closing chapter.

Apart from the above works on spin qubit shuttling in semiconductor quantum dots, during his PhD the author has published a paper on characterizing spatial and temporal correlations of environmental noise using decoherence of a many-qubit register [4]. This was a final achievement of author's work on a previous research subject, which concentrated on the characterizing and utilizing noise correlations in two-qubit quantum registers [5, 7, 8]. The author has been also involved in writing a topical review on the possibility of using single qubits as a spectrometers of environmental noise [6].

The author acknowledge financial support from the National Science Centre (NCN), Poland, under:

- QuantERA Si-QuBus programme (Grant No. 2017/25/Z/ST3/03044),
- ETIUDA doctoral scholarship (Grant No. 2020/36/T/ST3/00569),
- PRELUDIUM grant (Grant No. 2021/41/N/ST3/02758),

[1]: J. A. Krzywda and Ł. Cywiński, 'Adiabatic electron charge transfer between two quantum dots in presence of 1/f noise', Physical Review B **101** (2020)
[2]: J. A. Krzywda and Ł. Cywiński, 'Interplay of charge noise and coupling to phonons in adiabatic electron transfer between quantum dots', Physical Review B **104** (2021)
[3]: V. Langrock, J. A. Krzywda, N. Focke, I. Seidler, L. R. Schreiber, and Ł. Cywiński, 'Blueprint of a scalable spin qubit shuttle device for coherent mid-range qubit transfer in disordered Si/SiGe/SiO$_2$', (2022)
[4]: J. Krzywda, P. Szańkowski, and Ł. Cywiński, 'The dynamical-decoupling-based spatiotemporal noise spectroscopy', New Journal of Physics **21** (2019)
[5]: J. Krzywda, P. Szańkowski, J. Chwedeńczuk, and Ł. Cywiński, 'Decoherence-assisted detection of entanglement of two qubit states', Physical Review A **98** (2018)
[6]: P. Szańkowski, G. Ramon, J. Krzywda, D. Kwiatkowski, and Ł. Cywiński, 'Environmental noise spectroscopy with qubits subjected to dynamical decoupling', Journal of Physics: Condensed Matter **29** (2017)
[7]: J. Krzywda, Ł. Cywiński, and P. Szańkowski, 'Localization of a magnetic moment using a two-qubit probe', Physical Review A **96** (2017)
[8]: J. Krzywda and K. Roszak, 'Phonon-mediated generation of quantum correlations between quantum dot qubits', Scientific Reports **6** (2016)

Abstract in English

The main purpose of the thesis is to understand potential threats present during coherent shuttling of a semiconductor quantum dot based spin qubit. As long-distance electron transport can be realized by multiple transitions between quantum dots in an array, we have concentrated here on a single event electron transfer between two quantum dots. The main difficulty of the analysis lies in the complexity of the environment in which the spin qubit is embedded. Apart from nuclear spin noise, which directly affects spin coherence, the experiments in semiconductor quantum dot show a combination of low- and high-frequency environmental charge noise. It can be attributed to lattice vibrations, and random fluctuations of electric fields, which are expected to influence the motion of the charge. Additionally, finite correlation between charge and spin degree of freedom, activated by non-zero spin-orbit coupling, is expected to make the spin degree of freedom sensitive to these environmental noises, and affect the state of the shuttled spin qubit. As coherent shuttling is necessary for building large, scalable quantum processor based on quantum dots, this thesis is devoted to quantification of both charge transfer error, and spin dephasing during electron transfer between two realistically described quantum dots.

The charge can be moved between the dots using change of voltages controlling the dots. For slow-enough change, the electron stays in the lowest-energy state, which is moved between the dots. According to Landau-Zener model, such an adiabatic evolution takes place if the sweep is slow enough in comparison to tunnel coupling. However, we show that in presence of realistic environment, charge transfer error can increase also for slower sweeps. We describe how the function of charge transfer error becomes non-monotonic as a function of sweep rate in realistic models of silicon quantum dots, and compare this result with a typically monotonic behaviour in gallium-arsenide quantum dots.

In the second part of the thesis we add the spin degree of freedom, and analyze to what extent the electron shuttling modifies coherence of spin qubit in a superposition state. The presence of spin-orbit coupling leads to a correlation between spin and charge degrees of freedom, and the driving of the system in presence of this correlation leads to perturbation of the spin state by the electron motion. In this way, the spin qubit that is relatively protected from environmental noises when it is stationary, becomes sensitive to spatially-dependent environmental fields (phonons, charge noise). This leads to non-deterministic evolution, and hence spin dephasing. We show that dephasing of the spin qubit is activated by non-zero difference in dot-dependent Zeeman splitting, and non-zero tunnel coupling with spin-flip, both of which are make the spin sensitive to spatio-temporal correlations of the environmental noise. We use realistic models of Si and GaAs quantum dots in presence of their typical environments, to predict achievable electron spin qubit transfer fidelities.

Abstrakt po polsku

Celem pracy doktorskiej jest zrozumienie zagrożeń stojących na drodze do realizacji koherentnego transportu elektronu w komputerze kwantowym zbudowanym z półprzewodnikowych kropek kwantowych. Koncentruję się na procesie tunelowania elektronu wzdłuż łańcucha kropek kwantowych, rozważając pojedyńcze przejście pomiędzy dwoma kropkami. Głównym wyzwaniem jest złożoność realistycznego otoczenia kubitu spinowego, na które składają się spiny jądrowe, bezpośrednio sprzęgające się ze spinem elektronu, ale też, jak pokazują eksperymenty przeprowadzane w bramkowanych kropkach kwantowych, wysoko i niskoczęstotliwościowe fluktuacje pól elektrycznych (szum ładunkowy), oraz drgania sieci krystalicznej (fonony). Obecność niekontrolowanych pól elektrycznych nie tylko wpływa na ruch elektronu, ale także, w obecności skończonego odziaływania spinowo-orbitalnego, modyfikuje jego stan spinowy. Ponieważ koherentna komunikacja pomiędzy oddalonymi rejestrami kwantowymi jest konieczna dla konstrukcji skalowalnego komputera kwantowego, praca ta poświęcona jest realistycznemu oszacowaniu błędu transferu ładunku, oraz utraty koherencji spinowej wywołanej przemieszczeniem się elektronu pomiędzy dwoma kropkami kwantowymi.

Transport ładunku wywołany jest za pomocą zmienianego w czasie napięcia na bramkach, które kontrolują potencjał kropek kwantowych. Ruch elektronu wymuszany jest poprzez zmianę odstrojenia energii stanów podstawowych kropek, podczas której elektron powinien pozostać w stanie podstawowym, którego położenie zmienia się pomiędzy kropkami. Z rozwiązania modelu Landaua-Zenera wiemy, że wystarczająco powolna zmiana odstrojenia prowadzić będzie do udanego transferu ładunku. Jak jednak pokazuję w tej pracy, w wyniku sprzężenia elektronu z otoczeniem, prawdopodobieństwo pozostawienia ładunku w początkowej kropce może także rosnąć dla wolniejszych przejść. Opisuję wyniki pokazujące, że błąd transferu ładunku jest opisany niemotoniczną funkcją czasu przejścia w realistycznym modelu podwójnej kropki kwantowej w krzemie, zaś w arsenku galu monotonicznie zanika z rosnącym czasem przejścia.

W drugiej części pracy dodaję spinowy stopień swobody, analizując wpływ transferu na fazę pomiędzy stanami spinowymi. Pokazuję, że wymuszona ewolucja ładunkowego stopnia swobody, w obecności sprzężenia spinowo-orbitalnego prowadzi do chwilowej korelacji spinu i ładunku. W rezultacie, częściowa zmiana charakteru kubitu ze spinowego na ładunkowy wystawia jego stan na wpływ fononów oraz szumu ładunkowego. Prowadzi to do defazowania stanów spinowych, którego charakter wrażliwy jest na czasowo-przestrzenne korelacje szumu. W rozprawie prezentuję mechanizmy utraty fazy przesyłanego kubitu, które zachodzą w obecności: różnicy rozszczepień Zeemana w kropkach oraz niezachowującego spin sprzężenia tunelowego pomiędzy kropkami. Głównym wynikiem jest oszacowanie błędu transferu ładunku, oraz ilości utraty koherencji kubitu spinowego, w wyniku przejścia elektronu pomiędzy dwoma kropkami w realistycznych układach opartych na krzemie i arsenku galu.

Contents

1 Introduction

Quantum information processing is attractive from the point of view of solving classically hard problems, which include database search [9] and prime number factorization [10], but also simulating dynamics of the systems which are subject to quantum mechanical laws [11]. Recently, largest working devices consisting of a few tens of qubits, are realized in superconducting microstructures [12, 13] and trapped ions [14]. They already allow to show the so-called " quantum supremacy" over state-of-the art classical simulation in some artificially created problems [15], and allow for efficient simulation of small molecules [16]. However, any real-life benefit from quantum computers requires at least hundreds (if not many orders of magnitude more) of controlled qubits with sufficiently long coherence times [17, 18]. For this reason there is an ongoing effort to create large, scalable architecture for both quantum computing and quantum simulation.

1.1 Spin qubits

The architecture on which we concentrate in this thesis, is based on the semiconductor spin qubits. It takes advantage of encoding quantum information on the internal degree of freedom (spin) of a single electron. The electron itself is trapped in an electrically defined potential well, known as the quantum dot (QD). Semiconductor spin qubits offer relatively small sizes of the physical qubit[1] , and allow for leveraging achievements of the already existing semiconductor industry [20].

1: The typical size of the qubit in semiconductor quantum dot is $\sim 100nm$, which compared with typical size of superconductor qubit $\sim 100\,\mu$m [19] shows almost three orders of magnitude difference.

There already exists roadmaps for building scalable semiconductor quantum devices. Most of them uses silicon electron spin qubits [21–23]. However proposals involving germanium and silicon holes also exist [24]. Concentrating on the electron spins, we now summarize recent progress in Si and GaAs spin qubits, and the way in which they fulfil the Vincenco criteria [25] for efficient and scalable quantum computation.

Source of errors

The main reason for which large scalable quantum computers based on semiconductor devices have been not constructed yet, is the environment of spin qubits, the presence of which is a natural consequence of embedding a controllable two-level system in a solid-state physical material.

Using internal states of the electron allows to exploit naturally weak coupling between the spin and electric field, that includes its random fluctuations[2] . In absence of significant spin-orbit coupling, a spin qubit remains sensitive only to magnetic noise, generated by the spinful nuclei in the semiconductor lattice. Historically first spin qubits, developed in GaAs nanostructures, suffered from hyperfine coupling to nuclear spins,

2: present in the semiconductor nanostructures in form of Johnson and 1/f noise [26, 27]

which significantly limited their coherence to nanosecond timescale [28, 29]. More recently, spin qubits in silicon-based nanostructures[3] allow to take advantage of the process of isotopic purification [31], which is used to gradually get rid of spinful nuclei[4] . As a result, measured coherence times of spin qubits in Si-based quantum dots are orders of magnitude larger than in GaAs. However, being the group IV semiconductor, Si introduces additional ground state degeneracy due to presence of multiple minima of conduction band, known as the valley states [20]. Their presence poses new challenges to quantum information processing in Si-devices [32].

3: Most relevant nanostructures involve Si/SiGe heterostructures and SiMOS nanostructures resembling a single electron transistor [30].

4: Note that this process would not work for GaAs, since no spinless isotopes of Ga and As exist.

In absence of nuclear spins performance of a semiconductor qubit is limited by its interaction with uncontrolled environmental fields in form of magnetic and charge noise, as well as lattice vibrations (phonons).[5] These interactions lead to two physically distinguishable processes: that of energy dissipation, and of loss of definite phase between the qubit states, i.e. *dephasing*.

5: See [20, 30, 33] for the reviews on the semiconductor spin qubits.

Dissipation

Dissipation follows from the possibility of energy exchange between the environment and the qubit, and leads to modification of the probability of occupying qubit's energy eigenstates.[6] In a semiconductor spin qubit, the energy transfer is mediated by the lattice vibrations (phonons) and Coulomb interaction (charge noise). Typical time scale on which the excited state of the qubit relaxes to the ground state is given by relaxation time T_1. In general, the relaxation time is reported to be relatively short for orbital eigenstates [34, 35] and orders of magnitude longer for the relaxation between spin eigenstates [36, 37]. As a result, superposition of spin states (a spin qubit) is expected to be much more robust against environmental noise in comparison to the superposition of orbital states. [7] The main reason for such a difference is that the spin does not couple directly to position-dependent electric fields generated by lattice deformations, or other sources of charge noise. Only in presence of spin-orbit coupling[8] , a spin qubit can become sensitive to such fields, due to presence of correlation between spin and orbital degrees of freedom.

6: Most often identified with computational states of the qubit.

7: which is often termed a charge qubit.

8: intrinsic or synthetic due to spatial dependence of the spin Hamiltonian

Dephasing

The power of quantum information processing lies in the exploiting quantum interference effect, which requires preservation of phase relations in superpositions of states of qubits [38]. For this reason, loss of a definite phase between the states, known as the dephasing, is as dangerous to quantum computation as energy relaxation of the qubits. However, contrary to the dissipative evolution, the process of dephasing does not require exchange of energy with the environment. For spin qubits based on III-V materials (such as GaAs), or natural silicon, the dephasing time of freely evolving spin qubit is limited by low-frequency noise coming from nuclear spins [29, 33, 39–41], while in isotopically purified Si the charge noise (affecting the spin due to presence of spin-orbit couplings) is the dominant source of dephasing [42–44]

Error mitigation and correction

There are several methods to minimize the influence of non-controlled evolution of the qubits. Dephasing due to low-frequency[9] noise can be significantly limited by active control of the qubit in form of dynamical decoupling [6, 45]. A more general method of dealing with unwanted errors is quantum error correction,[10] which employs redundancy and entanglement in encoding of quantum information [46–49]. Note that error correction approach additionally increases the number of physical qubits needed to realize a given computational task.

9: compared to energy splitting of the qubit, see Chapter 4 for in-depth discussion

10: that in principle can protect against sufficiently rare bit- and phase-flip errors.

Realisation of spin qubit

In this thesis we concentrate on a spin qubit based on a single electron in a single QD, known as the Loss-DiVincenzo qubit [21]. In gate-defined quantum dots the electron from a 2-dimensional electron gas (2DEG)[11] is trapped by electric potential controlled by voltages applied to metallic gates above the 2DEG. There are alternative ways of trapping the electron in other semiconductor nanostructures, which include point defects [50], shallow donors [51], or self-assembled QDs [52], but we do not consider them in this thesis.

11: formed by the semiconductor heterostructure or the interface between two semiconductors.

Apart from using a spin of a single electron, quantum information in the gate-defined QDs can be encoded and processed using two levels of multi-electron systems, which include singlet-triplet qubit in double QDs [53–55], and exchange-only qubits in triple QDs [56, 57].

Initialization

The initialization is performed by state dependent tunneling from the reservoir of electron to the ground energy state inside the quantum dot [58]. It requires sufficiently low temperature to minimize occupation of higher energy state[12] . Once the electron tunnels into the quantum dot, its state can be modified by coherent control[13] [59–61].

12: Note that for box model of $L = 20$nm the energy gap between ground and excited state is given by $E \approx 1$meV, which corresponds to temperature of $T \approx 10$K.

13: see logic gates below

Coherence time

Phase coherence between the states of the qubit should be sustained for much longer then any of the elementary unitary operations, called logic gates [62]. Without significant spin-orbit coupling, an electron spin qubit is sensitive to nuclear field (so-called *Overhauser field*), and hence its coherence time is expected to increase as number of spinful nuclei in the volume occupied by the electron wavefunction decreases. For this reason, coherence times measured in a free induction decay experiment[14] in isotopically purified[15] Si are $T_2^* \approx 10\,\mu$s [32, 43, 63], which is much longer than $T_2^* \approx 10$ns measured in GaAs [55, 64]. Since dephasing in GaAs is dominated by slow nuclear noise, the presence of refocusing in a spin-echo type experiment allows to extend the coherence times of spin qubits in GaAs to $T_{\text{echo}} > 1\,\mu$s [28, 64, 65].

14: Evolution without active control of the qubit,

15: The natural Si has the abundance of about 4.7% of spinful ^{29}Si nuclei,

In absence of magnetic noise, coherence times are limited by ubiquitous in semiconductor devices random fluctuations of electric field, that couple

to the spin qubit by the spin-orbit interaction. For this reason, coherence times of electron spin qubits are lower in presence of synthetic spin-orbit interaction, which is generated by the magnetic field gradients [66, 67].

Logic gates

The universal set of quantum gates has to be realizable. For instance the set can consist of single qubit gates (rotations around each axis) and a two-qubit gate (CNOT) [62].

Single qubit gates in single-electron semiconductor spin qubits are realized by transverse pulses of ac field, that are resonant with the Zeeman splitting of the spin.[16] The pulses can be time-dependent magnetic field or time-dependent electric field (that couples to the qubit via spin-orbit interaction), with the latter allowing for faster control and more flexible design. The all-electrical control has been recently demonstrated in Si [39, 69], and earlier in GaAs [70, 71]. However in order to affect a spin qubit state with electric field, alocal magnetic field gradient or intrinsic spin-orbit coupling is needed. As mentioned above, their presence effectively correlates spin and orbit degree of freedom, and to some extent exposes the spin qubit to fluctuations of electric fields.

16: see [68] for original Rabi proposal.

Two-qubit gates were realized in Si [72–75] and GaAs [55, 71]. Their operation exploits exchange interaction[17] , which however requires the two electrons to occupy neighbouring dots [76, 77]. Recent attempts to extend its range[18] are not expected to work beyond a distance of few quantum dots.

17: Exchange interaction between nearby electrons (the wavefunctions of which have nonzero overlap) is a consequence of Coulomb interaction between them and Pauli Exclusion principle. For the two qubits of the same spin splitting it is equivalent to Heisenberg interaction

$$H_{\text{heis}} = \frac{J}{2}\sigma_1 \cdot \sigma_2, \tag{1.1}$$

where J is the exchange constant.

18: in form of superexchange interaction [77, 78],

Readout

In a semiconductor spin qubit, the commonly used method of readout of its state is the so-called spin-to-charge conversion, which correlates position of the electron charge with its spin state. The two most relevant realizations are the energy-dependent tunneling to the reservoir dot [61], and qubit tunneling to a dot already occupied with a single electron, which exploits Pauli Exclusion Principle [55]. Recently, also reflectometry methods has been used, which relate phase and amplitude of transmitted/reflected signal to the state of the qubit [79].

1.2 The problem with coherent communication

From the above it is clear that an effective operation of the QD-based spin qubits requires their close proximity (due to need for two-qubit gates). At the same time, the initialization and coherent control of the qubits requires finite breathing space around the quantum dots needed for classical wiring, and charge sensors required for the readout.

One way of dealing with these conflicting requirements is to first build small quantum registers, which can host limited number of fully functional logical qubits, however if such an idea is pursued, a coherent link between distant registers is needed to provide scalability of a semiconductor quantum computer [22, 23, 80]. The problem of realizing long-range

coherent coupling of distant spin qubits remains to be solved. Below we present the most promising methods to achieve this task.

Spin chains

One way to deal with long range transfer of quantum information encoded in spin degrees of freedom are the spin chains [81]. In such an application a one-dimensional chain of spin qubits coupled via nearest-neighbor Heisenberg interaction allows for realising multiple SWAP gates, and in consequence communicating distant spins [82]. However, this method introduces a large overhead in terms of quantum operations needed for coherent state transport. An alternative approach uses adiabatic state transfer, where continuous control of parameters of the qubit chain allows for physical movement of spin state [83], with the first realization in GaAs device demonstrated in [84]

Photons as flying qubits

Coherent communication between stationary qubits can be provided by a physically moving quantum system, known as a flying qubit. A natural candidate for such a flying qubit is a photon. However, coupling between spin and light is difficult to achieve, due to small magnetic dipole of the single electron [85]. The intrinsic coupling is much smaller then the inverse of dephasing times of spin qubit, and for this reason recent demonstrations of coherent spin-photon coupling take advantage of artificially created electric dipole moment in the double quantum dot structure [86–88]. However the presence such a dipole moment induces finite qubit-orbit couplings, which enable coupling of the spin to charge noise, creating thus an efficient dephasing and dissipation channel. Consequently, further development of photon-mediated coupling between two dots, i.e. realization of photon-mediated two-qubit gate, will require relatively low amplitude of the charge noise, or a method of its mitigation (passive or active).

Charge transfer

An alternative method is to turn a stationary qubit into a flying one, and communicate distant registers simply by a physical movement of the spin qubit [89, 90]. In this way, contrary to photon-based approach, no conversion of the quantum information from spin degree of freedom to photon's degrees of freedom is needed. In general, the electron can be moved by properly designed modulation of confinement potential, which can be seen as the dynamical drive of its orbital states. Below we discuss three methods of such spin qubit shuttling.

Surface acoustic waves

In polar materials, the prominent example of which are GaAs-based quantum dots, the electron can be shuttled in a moving potential of a surface acoustic wave (SAW) [91]. Coherent electron transfer with SAWs

was demonstrated in GaAs [92–95], however this method will not work in non-polar group-IV semiconductors that include the Si-based devices.

Conveyor Belt

Another way of physically shuttling the electron is to use a single moving quantum dot, which is occupied by the electron spin qubit. Recently, first demonstration of such *conveyor belt* charge transfer over distance of $\sim 0.5\,\mu$m in Si/SiGe was shown [96]. For our blueprint of scalable conveyor belt design we refer to [3]. We highlight that the results for spin coherence in conveyor belt described there can be understood in terms of theory developed in this thesis, see the outlook.

Bucket Brigade

In this thesis we focus on a method of electron shuttling applicable to any material hosting electrically-controlled QDs, in which one uses adiabatic transfer through an array of pre-defined quantum dots. We will call this method of transfer the *bucket brigade* (BB). The BB transfer consists of consecutive transitions between tunnel-coupled neighbouring dots. For each pair, the electron is transferred by sufficiently slow modulation of energy detuning between the ground states of the dots, which is schematically illustrated in Fig. 1.1

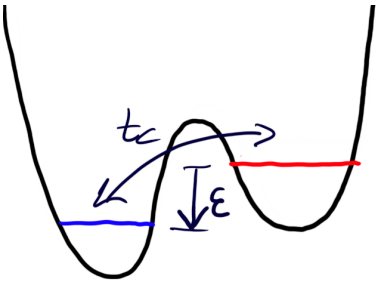

Figure 1.1: Schematic picture of double quantum dot (DQD) system. We denote detuning between the lowest energy levels of each dot as ϵ and tunnel coupling between them as t_c.

If the electron remains in the ground state while the detuning is slowly changed between positive and negative values, it is moved between the dots. The minimal model of such an interdot charge transfer can be viewed as a realization of Landau-Zener adiabatic transition [97]. Up to date, experimental demonstrations of charge transfer using this method include transfer across 9 QDs is silicon [98], and coherent transfer across up to 4 QDs in GaAs [99]. High-fidelity coherent transfer between 2-3 neighbouring dots in Si has also been recently shown [100, 101]. However, deeper understanding of the role of environment, which will be needed for long-range coherent shuttling is missing. In this thesis we focus on transfer of spin qubit from one quantum dot to another, while taking into account the presence of realistic environment, that possesses nontrivial temporal and spatial correlation.

1.3 Context of the thesis

We now put this thesis in context of the other works on multilevel adiabatic transitions.

Landau-Zener transition for an open quantum system

The modification of Landau-Zener dynamics due to an open character of the system was considered in many works. Most of them treated the environment of an adiabatically driven two-level system as a bosonic bath with Ohmic spectrum[102–108]. More recently, a method of computing the non-unitary evolution of a driven quantum system in form of an

adiabatic Master equation formalism, has been developed in the context of adiabatic quantum computing and research on quantum annealers [103, 109–111]. From those considerations, it is well known that the probability of effectively adiabatic transfer, which in our case corresponds to successful interdot charge transfer, is expected to increase in presence of zero-temperature bath, and decrease if thermal energy becomes comparable with the size of the avoided crossing [102, 111–113]. Furthermore, a high-temperature environment, modeled by stochastic modification of Hamiltonian parameters [1, 114–117] is expected to increase the probability of non-adiabatic transition. However, this is not true for low-frequency modification of the tunnel coupling, which in some regime of parameters can help in the adiabatic transfer, as it was first discussed in [116], and then independently demonstrated in the relevant for this thesis context of silicon quantum dots [118]. Corrections to Landau-Zener probability due to presence of another low-frequency noise in form of nuclear spins have been also considered [119].

Multilevel adiabatic transition

With quantum information encoded in spin degree of freedom, and in presence of valley state in the Si-based case, the charge transfer is only a part of the story. Full analysis of electron transfer requires a theoretical treatment of multilevel adiabatic transition. Outside of the application to spin qubits, the multilevel Landau-Zener transition for the closed quantum system was previously analyzed in [120–122]. However, these works focused on effective treatment of Landau-Stuckelberg-Majorana interference [97], which is expected to be hard to observe in presence of environmental noise. Non-trivial spectral density of environmental noise was considered in [123], where the analysis did not go beyond a three-level system, and in [124], where analytical treatment was possible in the limit of many avoided crossings.

More recently, multilevel problem has been put in context of the electron transfer between double quantum dot in Si and GaAs devices [125–128], however in these works, the open quantum system aspect is still missing. The multilevel description of double quantum dot system coupled to environmental field is also at the core of the electron-photon coupling [87, 129], however there the dynamical aspect of driving charge degrees of freedom is not present.[19] Similarly for the undriven system, of two self-assembled quantum dots, the dephasing of spin degrees of freedom caused by the relaxation between the charge levels characterized by a different spin splitting has been predicted [130].

19: Nevertheless, we will show that correlating spin and charge degree of freedom, that is commonly used to increase spin-photon coupling [85, 88], can in our context lead to noise-induced spin dephasing

Results of this thesis

In this thesis we attempt to go beyond the above-mentioned analyses, and consider an open quantum system, the electron undergoing charge transition between two realistic quantum dots, with its internal degree of freedom, the spin. In this effectively four-level Landau-Zener transition we focus on coherence of the spin degree of freedom, that is weakly coupled to charge degree of freedom driven through adiabatic transition in presence of the environmental noise[20] . The results will be put in context

20: To concentrate on the relevant physics, we mostly neglect the valley degree of freedom, and discuss consequences of including it in the outlook.

of realising coherent, long-range coupling by physical displacement of spin qubit in a realistic semiconductor device. We attempt to predict the charge transfer error, and loss of spin coherence during spin qubit shuttling between two state-of-the-art Si and GaAs quantum dots. We include models of their respective spin-orbit coupling, and realistic environmental noises: magnetic due to nuclear spins, and electric due to various sources of charge noise and coupling to phonons.

Among many results we show that:

1. The charge transfer error and the loss of spin coherence can be a non-monotonic function of detuning sweep rate. As a result, there might exist an optimal sweep rate, for which the loss of spin coherence is minimized.
2. In an experimentally relevant regime, coherent spin qubit shuttling is typically limited by the charge transfer error (in Si) and phase error (in GaAs).
3. Successful charge transfer over $\sim 10\,\mu$m range requires large tunnel coupling of $t_c > 60\,\mu$eV, characterizing all the coupled dots along the chain.
4. Spin dephasing during the interdot transfer is enabled by a difference in spin splitting between the two dots, which can scale with magnetic field (if it is due to distinct g-factors in the two dots). Using Zeeman splittings smaller than the tunnel coupling, $E_z < t_c$, allows to avoid of spin-flip interference, which also affects spin coherence. Thus, using as small fields as possible is highly beneficial.
5. Stronger coupling between the spin qubit and the environment can decrease the transfer error in certain ranges of parameters. In particular the relaxation process between the orbital levels can aid the charge transfer by recovering the occupation of the ground adiabatic state that have been lost around the avoided crossing.

The analysis presented in the thesis combines results of two published articles [1, 2], and the unpublished results on the loss of spin coherence during the transfer. Results of my research contained in [3], which concern the problem of qubit shuttling by making the quantum dot potential move in a desired direction, are briefly discussed in the outlook. In particular we show there relation between these results and those presented in the thesis.

1.4 Outline of basic results for interdot spin qubit transfer

Let us now outline the problem of electron spin qubit transfer between two quantum dots, i.e. within the double quantum dot (DQD) system.

Orbital evolution as the Landau-Zener problem

First we neglect the spin degree of freedom, and take two into account the lowest-lying orbital states located in the left and right dot, i.e. $|L\rangle$, $|R\rangle$ respectively. In the minimal model we neglect the presence of valley

degree of freedom in Si. We assume the dots are coupled with tunnel coupling t_c, and the time-dependent[21] detuning between the dots is given by $\epsilon(t) = E_L(t) - E_R(t)$. In the basis of the $|L\rangle, |R\rangle$ states, the orbital Hamiltonian reads:

$$\hat{H}_o(t) = \frac{\epsilon(t)}{2}\hat{\sigma}_z + \frac{t_c}{2}\hat{\sigma}_x, \tag{1.2}$$

where $\hat{\sigma}_x = |L\rangle\langle R| + |R\rangle\langle L|$, $\hat{\sigma}_z = |L\rangle\langle L| - |R\rangle\langle R|$. In all the cases considered in this thesis, we will start the evolution at initial time t_i at large negative detuning,

$$\epsilon(t_i) \ll -t_c, \tag{1.3}$$

for which the ground state is located in the left dot. Note that we assume t_c to be positive and real. By sweeping to large positive detuning at final time t_f,

$$\epsilon(t_f) \gg t_c, \tag{1.4}$$

the ground state is moved to the right dot. The time dependent gap between ground and excited state of DQD system[22] is given by

$$\Omega(t) = \sqrt{\epsilon^2(t) + t_c^2}. \tag{1.5}$$

In Fig. 5.1 we schematically illustrate the instantaneous energy spectrum of Hamiltonian $\hat{H}_o(t)$ as a function of $\epsilon(t)$ and the relation between the instantaneous states at large detunings and dot-like states.

We assume the sweep is linear in time, $\epsilon(t) = vt$, where v denotes the detuning sweep rate or the *sweep rate* for short. This allows us to use the Landau-Zener model of non-adiabatic excitations [97], according to which the probability of non-adiabatic evolution, i.e. the electron not following the ground state into the target right dot $|R\rangle$, is given by

$$Q_{\mathrm{LZ}} = \exp\left(-\frac{\pi}{2}\frac{t_c^2}{v}\right). \tag{1.6}$$

For larger part of the thesis we concentrate on the adiabatic limit of $t_c^2 \gg v$, for which Q_{LZ} is exponentially small.

21: i.e. controlled by voltages applied to hates that define the QDs

22: or simply *the orbital gap*

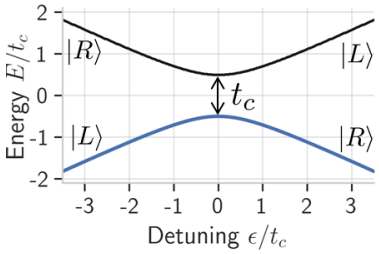

Figure 1.2: Energy spectrum of the Hamiltonian $\hat{H}_o(t)$ from Eq. (1.2) as a function of detuning $\epsilon(t)$. The ground state is denoted using blue color. In the figure we marked the dot-basis, which correspond to adiabatic states at large positive/negative detuning, in particulair for the ground state we have $|-(t_i)\rangle \approx |L\rangle$ and $|-(t_f)\rangle \approx |R\rangle$. In the ideal case the transfer of charge from left to right dot amounts to staying in the ground instantaneous state.

Transferred electron as an open quantum system

To show the most relevant modification introduced by taking into account the presence of the environment, let us consider stationary classical noise in detuning,

$$\epsilon(t) \to \epsilon(t) + \delta\epsilon(t). \tag{1.7}$$

It is convenient to concentrate on the region of avoided crossing, i.e. set $\epsilon = 0$ at which the orbital Hamiltonian (1.2) reduces to $\hat{H}_o(0) = \frac{t_c}{2}\hat{\sigma}_x$, and hence its eigenstates correspond to symmetric and anti-symmetric combination of the dot-like states, i.e.

$$|\pm(0)\rangle = \frac{1}{\sqrt{2}}\left(|L\rangle \pm |R\rangle\right), \tag{1.8}$$

where $|\pm(t)\rangle$ is the ground and excited energy state of $\hat{H}_o(t)$ at time-instant t. Around the avoided crossing the total Hamiltonian reads then:

$$\hat{H}_o(0) + \hat{V}_{\text{noise}}(t) = \frac{t_c}{2}\hat{\sigma}_x + \frac{\delta\epsilon(t)}{2}\hat{\sigma}_z, \tag{1.9}$$

from which we read that the detuning noise is transverse in the basis of $|\pm(0)\rangle$.

Probability of losing the electron

Following [131, 132], one can show that the presence of time-dependent transverse noise $\xi_\perp(t) = \delta\epsilon(t)$ leads to transitions between the eigenstates, with a transition rate around the avoided crossing given by

$$\Gamma_+(t_c) = \frac{1}{4}S_\perp(t_c), \tag{1.10}$$

which is proportional to the Fourier transform of the correlation function $S_\perp(\omega) = \int_{-\infty}^{\infty} \mathrm{d}t' e^{-i\omega t'}\langle\xi_\perp(t')\xi_\perp(0)\rangle$ known as the *Spectral Density of transverse noise* $S_\perp(\omega)$, evaluated at angular frequency corresponding to the gap $\omega = t_c$.

During the adiabatic passage the electron spends only a limited amount of time around the avoided crossing. We estimate this time period as:

$$t_{\text{LZ}} = \frac{2t_c}{v}, \tag{1.11}$$

such that for times $|t| < t_{\text{LZ}}$ the orbital gap $\Omega(t) \approx t_c$. Using this, and the excitation rate $\Gamma_+(t_c)$, we estimate the noise induced level of non-adiabaticity[23] as

$$Q_1 \approx \int_{t_i}^{t_f} \Gamma_+(\Omega[t])\mathrm{d}t \approx \frac{1}{2}S_\perp(t_c)\frac{t_c}{v}, \tag{1.12}$$

This simple result will be confirmed by more involved calculations presented in Part II, where the possibility of charge transfer in realistic DQD systems is analyzed.

23: in the leading order of perturbation theory, where subsequent relaxation process is ignored,

Trade-off between fast and slow adiabatic transition

Importantly, the noise-induced correction to the probability of leaving the electron behind is inversely proportional to sweep rate $1/v$, i.e. contrary to Landau-Zener model slower sweeps lead to higher occupation of the excited state. This competition between noise-induced transitions and standard Landau-Zener excitations results in a non-monotonic behaviour of the charge transfer error Q as a function of v.

This effect can be observed in Fig. 1.4, where among other quantities we plot a numerically computed[24] probability of leaving the electron behind[25] Q (solid red line), and the linear correction Q_1 from Eq. (1.12) (dashed red line). In the figure we can see that at $v > 400$ μeV/ns the charge transfer is limited by Q_{LZ} (black line), and hence the error grows for faster sweeps. For 100 μeV/ns$< v <$ 400 μeV/ns the noise-induced correction shows $Q \sim 1/v$ relation predicted by Q_1, i.e. the charge transfer error decreases for faster sweeps.

24: for the method used in the numerical simulation see Sec. 5.4

25: associated with occupation of higher energy state at the end of the sweep

Finally, for the slowest sweeps, the charge transfer error can be decreased by the relaxation processes, which is expected to dominate over the excitation if the energy gap exceeds thermal energy $\Omega > k_B T$. However, long transfer time, while possibly beneficial for the purpose of getting the electron into the desired final location (due to the relaxation-aided transfer), negatively affects the spin coherence of the transferred spin qubit. We briefly discuss these effects below.

Internal degree of freedom - the spin of the electron

We now add the spin degree of freedom. Crucially, we assume that the spin splitting in the two dots differs, and we define the average and the difference in the spin splittings as:

$$\overline{E}_z = \frac{E_Z^{(L)} + E_Z^{(R)}}{2}, \qquad \Delta E_z = E_Z^{(L)} - E_Z^{(R)}, \tag{1.13}$$

respectively. Using them we write the Hamiltonian describing the spin degree of freedom and its coupling to the orbital degrees of freedom:

$$\hat{H}_{\text{spin}} = \frac{\overline{E}_z}{2}\hat{\sigma}_z + \frac{\Delta E_z}{4}\hat{\sigma}_z\hat{s}_z, \tag{1.14}$$

where $\hat{s}_i$ is the Pauli operator associated with the spin degree of freedom.[26] The spin-dependent orbital gap is given by

$$\Omega_s = \sqrt{(\epsilon(t) + \tfrac{\sigma_s}{2}\Delta E_z)^2 + t_c^2}, \tag{1.15}$$

where $\sigma_s = \pm 1$ for $s = \uparrow$ and $\downarrow$ respectively. In Fig. 1.3 we plot the energy spectrum of the joint Hamiltonian $\hat{H}_o(\epsilon) + \hat{H}_{\text{spin}}$ as a function of ϵ, and use thick lines to denote orbital ground states associated with spin up (red) and spin down (blue). As it can be seen, the non-zero value of ΔE_z

26: i.e. $\hat{s}_z = |\uparrow\rangle\langle\uparrow| - |\downarrow\rangle\langle\downarrow|$

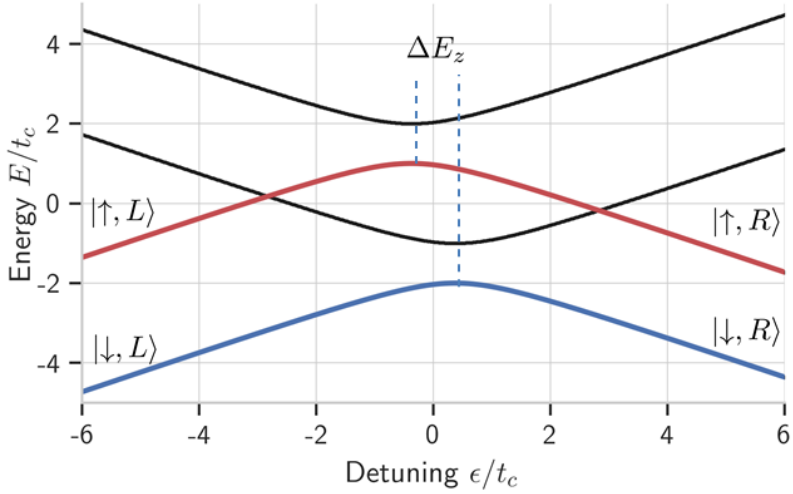

Figure 1.3: Spectrum of the spin-charge Hamiltonian $\hat{H}_o(t)+\hat{H}_{\text{spin}}$, where the thick lines correspond to ground orbital spin-down (blue) and spin-up (red) states, i.e. $|-,\downarrow\rangle$ and $|+,\uparrow\rangle$ respectively. We also denoted their dot composition at large negative, and large positive detuning. To show the effect of ΔE_z we used its value that is exaggerated by a factor of ~ 10 compared to the values typical for quantum dots considered in this thesis.

desynchronises the adiabatic transitions corresponding to spin-up and spin-down component. For this analysis we assume that the electron is initialized in the ground orbital state[27] in equal spin superposition, s0

27: left dot for $\epsilon \ll -t_c$

that at initial time $t = t_i$ we can write:

$$|\psi(t_i)\rangle = \frac{|\uparrow\rangle + |\downarrow\rangle}{\sqrt{2}} \otimes |L\rangle \,. \tag{1.16}$$

Note that in the vicinity of $\epsilon = 0$ the eigenstates exhibit a nontrivial correlation of spin and orbital degrees of freedom[28] .

28: In the limit of large ΔE_z at $\epsilon = 0$, the ground state spin superposition is approximately given by:

$$|\psi\rangle \approx \tfrac{1}{\sqrt{2}}(|R,\uparrow\rangle + e^{i\phi}\,|L,\downarrow\rangle), \tag{1.17}$$

which shows strong correlation between spin and orbital states

Loss of coherence

In view of using adiabatic transfer to distribute quantum information in the future quantum computer, the goal of the thesis is to compute the spin coherence of an electron that is finally occupying the target location (the right dot in the context here). For large detuning this is equivalent to the coherence left in the ground orbital state at $vt_f \gg t_c$, which we write as:

$$W_-(t_f) = \mathrm{Tr}\big\{\hat{s}_- \,\langle R|\,\hat{\rho}(t_f)\,|R\rangle\big\}. \tag{1.18}$$

We define the loss of coherence as

$$\delta W_- = 1 - |W_-(t_f)|, \tag{1.19}$$

and additionally concentrate on small error, i.e. $\delta W_-(t_f) \ll 1$, which is relevant for future quantum computers[29] . In this limit, we will argue that the loss of coherence can be expressed as:

$$\delta W_- = \frac{1}{2}\big(Q_\uparrow + Q_\downarrow + \langle\delta\phi^2\rangle\big), \tag{1.20}$$

which shows that the phase coherence is diminished due to three different mechanisms:

29: that are expected to operate at the threshold of error correction code i.e. $\delta W_-(t_f) < 10^{-2}$ [46–49]

- Probability of leaving one of the spin components in the initial, left dot Q_s.[30]
- The phase error $\langle\delta\phi^2\rangle$, that is associated with random contribution to the relative phase between two spin components $\delta\phi = \phi - \phi_0$, which is being averaged over many realizations of the experiment.

30: or equivalently in the excited orbital state

Apart from the above-mentioned competition between the L-Z physics and the environmental noise induced excitation, the Q_s charge transfer error can be additionally modified by the subsequent relaxation processes and the spin-flip interference, which we discuss later in the thesis. In Fig. 1.4, we show numerically computed loss of coherence for an example of a DQD system. In the figure we can identify the limit of fast sweeps, for which the loss of coherence (red line with squares) is limited by the charge transfer (red line), and the limit of slow sweeps for which it becomes limited by the loss of well-defined phase relation due to finite $\langle\delta\phi^2\rangle$ (blue dotted line). Let us now discuss two possible origins of the latter.

Temporary spin to charge conversion

First let us assume that the evolution is adiabatic, i.e. both coherent and incoherent non-adiabatic effects are weak, $Q_1 \ll 1$ and $Q_{\mathrm{LZ}} \ll 1$. In such a case the relative phase between the two spin components can

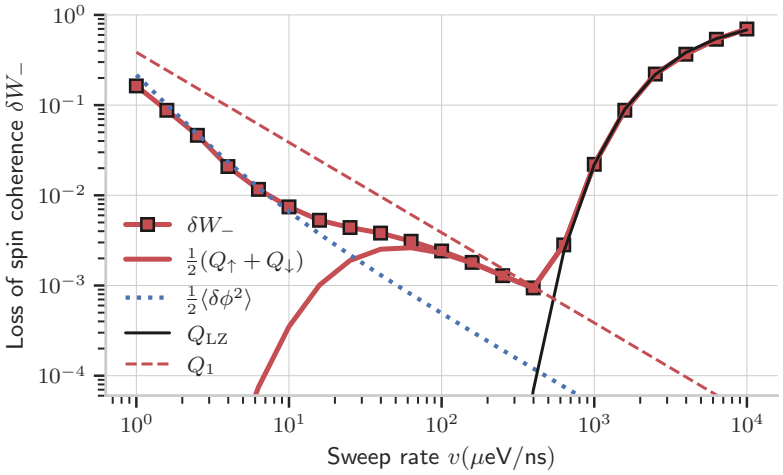

Figure 1.4: Numerically calculated loss of coherence δW_- (red line with squares) from Eq. (1.19) compared against spin-averaged occupation of excited orbital state $(Q_\uparrow + Q_\downarrow)/2$ (red line). We decompose the δW_- into various contributions: the Landau-Zener probability Q_{LZ} (black solid line), the noise induced excitation from ground to excited state Q_1 (red dashed line) and the purely dephasing processes $\langle\delta\phi^2\rangle$ (blue dotted line). For presentation purpose we used $t_c = 40\,\mu$eV, $\Delta E_z = 0.4\,\mu$eV, $\Gamma_-(t_c) = 0.01\,\mathrm{ns}^{-1}$,$T = 100\,$mK, $\sigma_\epsilon = 1\,\mu$eV. To compute numerical result we used the method described in ref. A and averaged over $N = 100$ realizations of the quasistatic noise in detuning.

be computed by integrating the spin-dependent orbital splitting from Eq. (1.15):

$$\phi = -\frac{1}{2}\int_{t_i}^{t_f} \mathrm{d}t' \Big(\Omega_\uparrow(t') - \Omega_\downarrow(t')\Big). \tag{1.21}$$

We now add low-frequency noise in detuning

$$\epsilon(t) \to \epsilon(t) + \delta\epsilon, \tag{1.22}$$

where $\delta\epsilon$ is modeled as Gaussian quasistatic noise, which remains constant during single run but varies between the consecutive realizations of the experiment. In introduces random contribution to dephasing, which in the leading order[31] gives:

$$\delta\phi = \frac{\Delta E_z}{v}\delta\epsilon. \tag{1.23}$$

Averaging over realizations of slow noise gives

$$\langle\delta\phi^2\rangle \approx \left(\frac{\Delta E_z}{v}\right)^2 \sigma_\epsilon^2, \tag{1.24}$$

where the $\sigma^2 = \langle\delta\epsilon^2\rangle$ is the variance of the quasistatic noise. Note that in contrast to charge transfer error computed in Eq. (1.12), the phase-error-limited dephasing scales as $\delta W_- \propto 1/v^2$ as it can be seen in Fig. 1.4 for $v < 10\ \mu$eV/ns. Due to difference in scaling there will always exist a sweep rate at which purely phase error $\langle\delta\varphi^2\rangle$ dominates over charge transfer error $Q_\uparrow + Q_\downarrow$.

31: In the limit of $\delta\epsilon, \Delta E_z \ll t_c$

Transition induced dephasing

The second mechanism, which gives purely dephasing contribution $\langle\delta\phi^2\rangle$, is associated with at least two inelastic transitions between the orbital states in presence of non-zero ΔE_z. It can be understood as a consequence of random amount of time spent in the orbital states that have slightly different Zeeman splittings.

To show relevant physics we focus on a simplified scenario, in which the electron gets excited in vicinity of the avoided crossing.[32] After this

32: Approximately this happens with the probability Q_1, given by Eq. (1.12)

event, after a sufficiently long evolution time the electron will relax to the orbital ground state. We assume that the characteristic relaxation rate is given by the Γ_-, which is assumed here to be time-independent.[33] Thus in presence of non-zero ΔE_z, the electron spin qubit acquires an additional phase given by:

$$\delta\phi = \int_0^{t_r} \left(\Omega_\uparrow(t') - \Omega_\downarrow(t')\right) \approx \frac{\Delta E_z}{v}\left(\sqrt{t_c^2 + v^2 t_r^2} - t_c\right), \tag{1.25}$$

where t_r is the time spent in the excited state and we have used the leading order expression in $\Delta E_z/t_c$. We concentrate on the limit of slow relaxation, i.e. $vt_r \gg t_c$ for which $\delta\phi(t_r) \approx \Delta E_z t_r$. We average over distribution of the relaxation times,[34] which gives:

$$\langle\delta\phi^2(t_r)\rangle_{t_r} = \int_0^\infty \left(p(t_r)(\Delta E_z t_r)^2\right)\mathrm{d}t_r = \left(\frac{\Delta E_z}{\Gamma_-}\right)^2. \tag{1.26}$$

This shows that the coherence loss is proportional to the time spent in the excited state, i.e. the dephasing is smaller if the relaxation is faster. The above error should be multiplied by the probability of excitation around the avoided crossing $\approx Q_1$, which together leads to the prediction that the contribution from transition induced dephasing reads

$$\delta W_- \approx \Gamma_+ \frac{t_c}{v}\left(\frac{\Delta E_z}{\Gamma_-}\right)^2, \tag{1.27}$$

Note that in the limit of $\Delta E_z \approx \Gamma_-$, the loss of phase equals to the probability of excitation at avoided crossing, i.e. $\delta W_- \approx Q_1$. This is true even if the relaxation process successfully recovers occupation of ground adiabatic state, and hence charge transfer takes place.

33: The functional form of realistic time-dependent relaxation and excitation rates as a function of the gap $\Omega(t)$ and state composition for realistic semiconductor devices, will be computed in the thesis

34: which corresponds to the Poisson distribution, i.e.

$$p(t_r) = \Gamma_- e^{-\Gamma_- t_r}$$

for assumed constant Γ_-

1.5 Thesis structure

The thesis is separated into three parts, which we describe in details below:

I. Driven open two-level system

First part introduces the relevant tools needed for numerical and analytical analysis performed in the latter parts. Chapters 2-4 present textbook knowledge on the dynamics of the undriven, two-level open quantum system. In Chapter 2 we introduce the Hamiltonian of a two-level system and define transverse and longitudinal couplings to the environment, which we then relate to dissipative and purely dephasing processes. In Chapter 3 we discuss how the transverse coupling to an environment with typically short correlation time, gives rise to relaxation and the excitation rates, and we derive there the Master equation in the Linblad form. Next in Chapter 4 we discuss the dephasing caused by longitudinal coupling, and explain the role of the environmental correlation time. We show that for a freely evolving electron the dephasing is dominated by slow fluctuations of the environment, which we model as a classical noise. We introduce 1/f noise and effectively quasistatic noise model that are relevant for further analysis.

In Chapter 5 we consider a driven two-level system, and discuss the Landau-Zener model of its adiabatic transition. We include the effects of the environment on the system's adiabaticity by first considering classical fluctuations of Hamiltonian parameters, and then by using the adiabatic Master equation. We finally describe our approach to modeling the adiabatic transition in presence of both high- and low-frequency noise, which will be used in subsequent chapters.

II. Charge transfer of spin qubit

The beginning of the second part is dedicated to modeling of a realistic double quantum dot. In Chapter 6 we describe our model of electron wavefunction in semiconductor quantum dot and define sets of parameters for three DQD systems that correspond to typical Si-based and GaAs-based devices. Next, in Chapter 7 we discuss the effects of the coupling between the orbital degree of freedom and the environment. In particular, for the models of DQDs we compute the orbital relaxation rates due to environmental electric fields, in form of lattice vibrations (phonons) and charge noise. In the process we describe the relation between the non-unitary evolution of spatial degree of freedom of the two-level system and the spatial correlations of the environmental field. Finally in Chapter 8 we discuss analytical and numerical results on charge transfer error in the interdot transition, which were published in [1, 2].

III. Spin degree of freedom in charge transfer

In this we introduce the spin degree of freedom, and discuss the implications of its coupling to the charge degree of freedom. In Chapter 9 we briefly discuss the origin of spin-orbit coupling in semiconductor QDs, and discuss its implications for the stationary spin qubit. In particular, we show that it leads to correlation between spin and orbital degrees of freedom, and makes the spin qubit vulnerable to the previously discussed fluctuations of electric fields. Next, in Chapter 10 we discuss the implications of finite spin-orbit coupling in context of the DQD transition and extend the adiabatic Master equation to the case of four-level system.

We use these tools in Chapter 11, where we discuss the processes leading to non-ideal interdot transfer of the excited spin state. In particular, we show the effects of spin-flip interference (which has been omitted in the example above) and spin relaxation due to spin-orbit mixing. Among others, we use the thoery developed before to propose a realization of the Elizur-Veidman bomb testing experiment, and finally compute spin-up charge transfer error for realistic DQD devices. In the last Chapter 12 we compute the loss of spin coherence during interdot transition. We discuss there in detail the two processes leading to spin dephasing, which are both activated by non-zero difference in dot-dependent Zeeman splittings. The first of them leads to temporal separation of two spin-components, and becomes sensitive to low-frequency charge noise, and the second of them introduces random phase due to multiple inelastic transitions between the instantaneous levels.

IV. Outlook and discussion

We conclude the thesis by the summary and the discussion, which includes the elucidation of the implication of the results presented in the thesis for the long-distance coherent electron transfer in semiconductor devices. In the outlook we show the relation of the thesis to our work on the electron transfer in the moving dot, and discuss the possibility of using the electron shuttling to characterize spatiotemporal correlations of the environmental noise.

I. Driven open two-level system

2 General description of a two-level quantum system

In the thesis we will consider dynamical driving of the charge degree of freedom to which the spin degrees of freedom (the spin two-level system) are coupled. Before we do it we concentrate on the dynamics of undriven Two-Level System (TLS) coupled to the environment, and the way in which the non-unitary evolution of the TLS can emerge. Then in Chapter 3 and Chapter 4 we will separately discuss dissipative and dephasing evolution of the TLS.

2.1 Unitary evolution

For the isolated TLS, we assume the time-independent Hamiltonian,

$$\hat{H}_q = \frac{1}{2}\Omega\hat{\sigma}_z, \tag{2.1}$$

using which the unitary evolution of any pure state is given by

$$|\psi(t)\rangle = e^{-i\hat{H}_q t}\,|\psi(0)\rangle\,, \tag{2.2}$$

where $|\psi(0)\rangle$ is some initial state of the TLS[1] . The general form of the pure state at time t can be written as:

$$|\psi(t)\rangle = \cos\frac{\theta}{2}\,|\downarrow\rangle + \sin\frac{\theta}{2}e^{i\varphi}\,|1\rangle = \begin{bmatrix}\cos\frac{\theta}{2}\\ \sin\frac{\theta}{2}e^{i\varphi},\end{bmatrix} \tag{2.3}$$

where θ and ϕ might correspond to a azimuthal and polar angle in the spherical coordinate system (see Fig. 2.1 for graphical representation of the state).

The statistics of any measurement performed on the TLS is encoded in the *density matrix* defined as:

$$\hat{\rho}_q(t) = |\psi(t)\rangle\langle\psi(t)| = \frac{1}{2}\begin{bmatrix}1+\cos\theta & \sin\theta e^{-i\varphi}\\ \sin\theta e^{i\varphi} & 1-\cos\theta\end{bmatrix} = \frac{1}{2}\left(\hat{\mathbb{1}} + \mathbf{n}\cdot\hat{\boldsymbol{\sigma}}\right), \tag{2.4}$$

where we introduced the unit vector $|\mathbf{n}| = 1$ and the vector of Pauli matrices $\hat{\boldsymbol{\sigma}} = [\hat{\sigma}_x, \hat{\sigma}_y, \hat{\sigma}_z]^T$.

1: often corresponding to the ground energy state of $\hat{H}_q\,|\downarrow\rangle = -\frac{\Omega}{2}\,|\downarrow\rangle$, where we assumed that $\Omega > 0$.

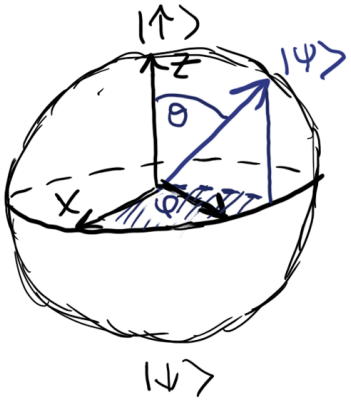

Figure 2.1: The pure state of the two-level system $|\psi\rangle$ from Eq. (2.2) plotted on the Bloch sphere with azimuthal and polar angles θ and φ.

2.2 Emergence of non-unitary evolution

We now consider a realistic situation in which presence of environment leads to non-unitary evolution.

Reduced density matrix

We first extend the Hilbert space by considering the presence of typically large environment. We assume that the TLS and environment are initially uncorrelated, i.e. the initial state of the composite system reads:

$$\hat{\rho}_{qe}(0) = \hat{\rho}_q(0) \otimes \hat{\rho}_e(0), \tag{2.5}$$

where $\hat{\rho}_e(0)$ is the initial density matrix of the environment. The evolution of the composite system is described in terms of unitary dynamics, i.e. $\hat{\rho}_{qe}(t) = \hat{U}(t)\hat{\rho}_{qe}(0)\hat{U}^\dagger(t)$, generated by the evolution operator:

$$\hat{U}(t) = \exp\left\{-i \int_0^t \left(\hat{H}_q + \hat{V}_{qe} + \hat{H}_e\right) \mathrm{d}t\right\}, \tag{2.6}$$

where in addition to TLS Hamiltonian $\hat{H}_q$ (2.1), we introduced TLS-environment coupling $\hat{V}_{qe}$ and the Hamiltonian of the environment $\hat{H}_e$.

The evolution of the composite system will remain unitary, which might not be true for the evolution observed from the perspective of the measurements performed on the TLS alone[2] . In principle effects of the environmental presence can be minimized if the coupling $\hat{V}_{qe}$ becomes as small as possible by isolating the TLS from the rest of the world, however at some point isolated TLS would be difficult to control or measure[3] .

2: note that usually only the TLS is accessible.

3: as for both electromagnetic fields are often used.

Measurement performed on the qubit could be used to estimate the expectation value of some observable of interest $\hat{A}$, which is mathematically defined via the expression $\langle \hat{A} \rangle = \mathrm{Tr}\{\hat{A}\hat{\rho}_{qe}(t)\}$. The statistics of each measurement can be equivalently represented by so-called reduced density matrix $\hat{\rho}_q(t) = \mathrm{Tr}_e\{\rho_{qe}(t)\}$, which amounts to averaging over environmental degrees of freedom. Substituting $\hat{U}(t)\hat{\rho}_{qe}(0)\hat{U}^\dagger(t)$ to the definition of reduced density matrix allows to write:

$$\begin{aligned}\hat{\rho}_q(t) = \mathrm{Tr}_e\{\hat{U}\hat{\rho}_{qe}(0)\hat{U}^\dagger\} &= \sum_{n,m} p_n \langle m|\hat{U}|n\rangle \hat{\rho}_q(0) \langle n|\hat{U}^\dagger|m\rangle \\ &= \sum_n p_n \left(\sum_m \langle m|\hat{U}|n\rangle \hat{\rho}_q(0) \langle n|\hat{U}^\dagger|m\rangle \right),\end{aligned} \tag{2.7}$$

where we expressed the initial environmental state as $\hat{\varrho}_e = \sum_n p_n |n\rangle\langle n|$. We highlight that above expression for reduced density matrix of TLS has a form of Eq. (2.4), however with possibly reduced length of the vector $|\mathbf{n}| \leq 1$. If $|\mathbf{n}| < 1$ the state of the TLS becomes mixed as a result of non-unitary evolution.

Let us now define two processes leading to the non-unitary evolution. To do so, we write reduced density matrix of the TLS in terms of its *polarization*[4] :

4: or equivalently the occupation of energy eigenstates

$$Z(t) = p_\uparrow(t) - p_\downarrow(t) = \mathrm{Tr}\{\hat{\sigma}_z\hat{\rho}_{qe}(t)\}, \tag{2.8}$$

and *the coherence* between its eigenstates:

$$W(t) = 2\,\mathrm{Tr}\{|\downarrow\rangle\langle\uparrow|\,\hat{\rho}_{qe}(t)\} = 2\,\mathrm{Tr}\{\hat{\sigma}_-\hat{\rho}_{qe}(t)\}. \tag{2.9}$$

Note that using the above definitions, the reduced density of the TLS, at any time instant can be written as:

$$\hat{\rho}_q(t) = \frac{1}{2}\begin{bmatrix} 1+Z(t) & W(t) \\ W^*(t) & 1-Z(t) \end{bmatrix}. \tag{2.10}$$

Modification of $Z(t)$ requires transfer of the energy between the TLS and the environment, that is associated with the *dissipative* evolution. As we will show in Chapter 3 the energy dissipation will also affect the coherence $W(t)$. In contrast in Chapter 4, we will consider the second relevant mechanism of the *dephasing*, in case of which the decrease of $W(t)$ does not require the energy transfer between the TLS and the environment and hence leaves the $Z(t)$ unchanged.

Longitudinal and transverse couplings to environment

The general coupling between the TLS and the environment has a form

$$\hat{V}_{\mathrm{qe}} = \frac{1}{2}(\hat{\sigma}_z\hat{V}_\phi + \hat{\sigma}_-\hat{V}_- + \hat{\sigma}_+\hat{V}_+), \tag{2.11}$$

where $\hat{\sigma}_i$ are the Pauli operator acting on the TLS of interest, which later in the thesis will correspond to two lowest lying in energy orbital states or the spin qubit. In subsequent chapters we will show how the above Hamiltonian gives rise to both dissipation and dephasing of TLS.

Transverse coupling

In particular in Chapter 3, we will show that the energy dissipation is associated with the transverse part of the above coupling, which we define as

$$\hat{V}_\perp \equiv \frac{1}{2}\left(\hat{\sigma}_-\hat{V}_- + \hat{\sigma}_+\hat{V}_+\right). \tag{2.12}$$

As we will show, the dissipative contribution to non-unitary evolution due to transverse noise is dominated by the fluctuations in resonance with the energy gap of TLS. We highlight that due to typically weak TLS-environment coupling, in this thesis we neglect effects of energy renormalization due to off-resonant transverse coupling [29, 133].

Longitudinal coupling

On the other hand, in Chapter 4 we will analyze loss of definite phase between TLS eigenstates without exchange of energy between the TLS and environment. We associate such pure-dephasing process, with the longitudinal part of the coupling:

$$\hat{V}_\parallel \equiv \frac{\hat{\sigma}_z}{2}\hat{V}_\phi. \tag{2.13}$$

As we will discuss, for the system of interest the dephasing due to longitudinal noise will be dominated by the environmental fluctuations with characteristic frequencies below the gap of TLS. For this reason the effects of longitudinal coupling will be simulated by the classical low-frequency noise.

Due to effective separation of time-scales, i.e. the high-frequency noise associated with transverse and low-frequency with longitudinal coupling, and also in the limit of typically small dephasing error, both contributions will be treated as independent[5] .

5: For the numerical test and discussion, see Appendix A

3 Dissipative evolution of a two-level system

In this section we concentrate on the ab-initio calculation of the effects of coupling between the two-level systems and its environment. We start with the dissipative evolution caused by the transverse coupling $\hat{V}_\perp$, which together with Two-Level System (TLS) Hamiltonian $\hat{H}_q$ gives:

$$\hat{H}_\perp = \frac{1}{2}\Omega\hat{\sigma}_z + \frac{1}{2}(\hat{\sigma}_-\hat{V}_- + \hat{\sigma}_+\hat{V}_+), \tag{3.1}$$

where $\hat{\sigma}_\pm$ are the ladder operators $(\hat{\sigma}_x \pm i\hat{\sigma}_y)/2$. First in Sec. 3.1 we will compute leading order contribution to polarization and the phase error and relate them to spectral density of the environment. Next in Sec. 3.2, we combine this limit with short correlation time of the environment and derive Master equation in the Linblad form.

3.1 Weak coupling limit

Fermi Golden Rule and relaxation rate

We assume the TLS is initialed in the excited state $|\psi_0\rangle = |\uparrow\rangle$[1] , which is uncorrelated with the initial state of the environment $\hat{\rho}_e$, that assumed to be in equilibrium with respect to environmental Hamiltonian $\hat{H}_e$.[2] In such case the evolution operator in the interaction picture reads:

$$\hat{U}'(t) = \mathcal{T}\exp\left\{-i\int_0^t U_0^\dagger(t')\hat{V}_{qe}U_0(t')\mathrm{d}t'\right\}, \tag{3.2}$$

where $\hat{V}_{qe} = \frac{1}{2}(\hat{\sigma}_-\hat{V}_- + \hat{\sigma}_+\hat{V}_+)$ and $\hat{U}_0(t) = e^{-i\Omega\hat{\sigma}_z t/2}e^{-i\hat{H}_e t}$ while $\mathcal{T}$ stands for time-ordering operator [134]. The probability of measuring the TLS ground state at time t, i.e. $p_\downarrow(t) = \mathrm{Tr}\{|\downarrow\rangle\langle\downarrow|\,\rho'(t)\}$ [3] can be written as:

$$p_\downarrow(t) = \mathrm{Tr}\left\{|\downarrow\rangle\langle\downarrow|\,\hat{U}'(t)\,|\uparrow\rangle\langle\uparrow|\,\rho_e(0)U_I^\dagger(t)\right\} = \sum_{nm} p_n|\langle\downarrow,m|\,\hat{U}_I(t)\,|\uparrow,n\rangle|^2, \tag{3.3}$$

We now assume the evolution time is sufficiently short, or the perturbation is sufficiently weak, such that the evolution operator can be expanded up to a leading order as $\hat{U}'(t) = 1 - i\int_0^t U_0^\dagger(t)\hat{V}_{qe}U_0(t)$, which substituted above gives:

$$\begin{aligned}\delta p_\downarrow(t) &= \sum_{mn} p_n\left|\langle\downarrow,m|\,\hat{V}_{qe}\,|\uparrow,n\rangle\right|^2\int_0^t\int_0^t \mathrm{d}t_1\mathrm{d}t_2\, e^{-i(E_{nm}+\Omega)(t_1-t_2)}\\ &= \sum_{mn} p_n\left|\langle\downarrow,m|\,\hat{V}_{qe}\,|\uparrow,n\rangle\right|^2 t^2\mathrm{sinc}^2\left(\frac{E_{mn}-\Omega}{2}t\right),\end{aligned} \tag{3.4}$$

where $\delta p_\downarrow$ represents leading order correction to spin-down probability. The last term illustrates Heisenberg time-energy uncertainty principle.

1: i.e. we assume the TLS splitting to be positive, i.e. $\Omega > 0$,

2: i.e. we assume completely mixed state of environment in thermal equilibrium, for which $\hat{\rho}_e = e^{-\beta\hat{H}_e}/\mathfrak{Z}$, where $\mathfrak{Z} = \mathrm{Tr}\{e^{-\beta\hat{H}_e}\}$ is the partition function and $\beta = 1/k_\mathrm{B}T$.

3: where the density matrix in the interaction picture reads $\hat{\rho}'(t) = \hat{U}_0^\dagger(t)\hat{\rho}(t)\hat{U}_0(t)$,

The energy might by not conserved, i.e. $\Omega - E_{mn} \neq 0$ as long as t is sufficiently small. Typically however, the t is long enough to enforce conservation of energy and at the same time $1/t$ remains larger then the level spacing of typical environmental,[4] which allow us to treat the density of environmental states as continuous and hence take the limit:

$$t\mathrm{sinc}^2(xt/2) \to 2\pi\delta(x). \tag{3.5}$$

From the above the probability of TLS relaxation becomes linear in time:

$$\delta p_\downarrow(t) = \frac{t\,\pi}{2}\sum_{mn} p_n \left|\langle m|\,\hat{V}_-\,|n\rangle\right|^2 \delta(E_{mn}-\Omega) \equiv \Gamma_-(\Omega)t. \tag{3.6}$$

It is convenient to define the spectral density of transversely coupled environment, which from the Eq. (3.6) can be written as:

$$\begin{aligned} S_\perp(\Omega) &= 2\pi\sum_{mn} p_n \left|\langle m|\,\hat{V}_-\,|n\rangle\right|^2 \delta(E_{mn}-\Omega) \\ &= \int_{-\infty}^{\infty} \mathrm{Tr}\Big(\hat{V}'_+(t)\hat{V}'_-(0)\hat{\rho}_{qe}\Big)e^{i\Omega t}\mathrm{d}t = \int_{-\infty}^{\infty} C_{+-}(t)e^{i\Omega t}\mathrm{d}t, \end{aligned} \tag{3.7}$$

where we have used the identity $2\pi\delta(E_{mn}-\Omega) = \int_{-\infty}^{\infty}\mathrm{d}t e^{-i(E_{mn}-\Omega)t}$, the interaction picture $\hat{V}'_\pm(t) = e^{i\hat{H}_e t}\hat{V}_\pm e^{-i\hat{H}_e t}$ and introduced correlation function

$$C_{+-}(t) = \mathrm{Tr}\big\{\hat{V}'_+(t)\hat{V}'_-(0)\hat{\rho}_e\big\}. \tag{3.8}$$

The spectral density of transverse noise can be directly related to relaxation rate, since

$$\Gamma_-(\Omega) \equiv \frac{1}{4}S_\perp(\Omega), \tag{3.9}$$

where for the used sign convention of $\Omega > 0$ the relaxation process the energy is emitted from the TLS to the environment[5] . In general the relaxation process will be associated with the positive arguments ($\omega > 0$) of the transverse spectral density $S_\perp(\omega)$.

4: For instance phonons, for which the spacing between the levels $\propto 1/V$, where V is the macroscopic volume of the crystal.

5: since the energy of the final state of environment is above the initial one, which means that $E_{mn} = \Omega > 0$,

Excitation rate and detailed balance condition

To complete the microscopic characterization of the dissipation process we will now consider the opposite situation, in which the environment induces transition from ground to excited state, which requires the energy absorption from the environment. If one repeats the above calculations for the case of initial and final states $|\downarrow\rangle, |\uparrow\rangle$ respectively, the excitation rate will become related to a differently ordered correlation function, i.e.:

$$\Gamma_+(\Omega) = \frac{1}{4}\int_{-\infty}^{\infty} C_{-+}(-t)e^{i\Omega t}\mathrm{d}t, \tag{3.10}$$

where $C_{-+}(t) = \mathrm{Tr}\big\{\hat{V}'_-(t)\hat{V}'_+(0)\hat{\rho}_e\big\}$.

We are now left with the question, what is the connection between two correlation functions $C_{+-}(t)$ and $C_{-+}(t)$? For the environment in thermal equilibrium at temperature T with respect to its Hamiltonian,[6] the relation between the correlation functions can be derived with the

6: i.e. $\hat{\rho}_e = e^{-\beta\hat{H}_e}/\mathfrak{Z}$ where $\mathfrak{Z}$ is the partition function.

help of imaginary time formalism,

$$\begin{aligned} C_{+-}(t) &= \mathrm{Tr}\Big(\hat{V}'_+(t)\hat{V}'_-(0)\hat{\rho}_e\Big) = \frac{1}{\mathcal{Z}}\,\mathrm{Tr}\Big(e^{i\hat{H}_e t}\hat{V}_+ e^{-i\hat{H}_e t}\hat{V}_- e^{-\beta\hat{H}_e}\Big) \\ &= \frac{1}{\mathcal{Z}}\,\mathrm{Tr}\Big(e^{i(i\beta H_e)}e^{-i(i\beta\hat{H}_e)}e^{-i\hat{H}_e t}\hat{V}_- e^{i\hat{H}_e t}e^{i(i\beta\hat{H}_e)}\hat{V}_+\Big) \\ &= \mathrm{Tr}\Big(e^{-i\hat{H}_e(t+i\beta)}\hat{V}_- e^{i\hat{H}_e(t+\beta)}\hat{V}_+\hat{\rho}_e\Big) = C_{-+}(-t-i\beta), \end{aligned} \tag{3.11}$$

which can be alternatively[7] written as $C_{-+}(-t') = C_{+-}(t'-i\beta)$. When this expression is substituted to Eq. (3.10), the excitation rate reads:

7: Note that in Eq. (3.11) the time variable can be shifted by $t = t' - i\beta$

$$\Gamma_+(\Omega) = \frac{1}{4}\int_{-\infty}^{\infty} C_{+-}(t-i\beta)e^{i\Omega t}\mathrm{d}t = \frac{1}{4}S_\perp(\Omega)e^{-\beta\Omega}. \tag{3.12}$$

In this way we derived the condition:

$$\Gamma_+(\Omega) = \Gamma_-(\Omega)e^{-\beta\Omega}, \tag{3.13}$$

which is commonly known as the detailed balance or Kubo-Martin-Schwinger condition [135, 136]. Finally it is convenient to write the relaxation and excitation rates in the common form as:

$$\Gamma_\pm(\Omega) = \frac{1}{4}S_\perp(\mp\Omega), \tag{3.14}$$

where $S_\perp(-\Omega) = S_\perp(\Omega)e^{-\beta\Omega}$ as a consequence.

Dissipation contribution to dephasing

Transverse coupling to environment can also lead to losing of definite phase between the TLS eigenstates, which can be related to dephasing rate Γ_W. To show it, we now take previously introduced in Eq. (3.1) transverse Hamiltonian $\hat{H}_\perp$ with environment at thermal equilibrium with $\hat{H}_e$, and compute the off-diagonal element of the reduced TLS density matrix in the interaction picture as:

$$W'(t) = \mathrm{Tr}\{\hat{\sigma}_-\hat{\rho}'(t)\} = e^{i\Omega t}W(t). \tag{3.15}$$

Now up to second order in the coupling $\hat{V}_\pm$, the change in the above, i.e. $\delta W'_\perp = W'(t) - W(0)$ is given by:

$$\begin{aligned} \delta W'_\perp = &\frac{1}{4}\int_0^t\int_0^t \langle\hat{V}'_+(t_1)\hat{V}'_+(t_2)\rangle e^{-i\Omega(t_1+t_2)}\mathrm{d}t_1\mathrm{d}t_2 \\ &- \frac{1}{4}\int_0^t\int_0^{t_2}\Big(\big(\langle\hat{V}'_-(t_1)\hat{V}'_+(t_2)\rangle + \langle\hat{V}'_+(t_2)\hat{V}'_-(t_1)\rangle\big)e^{-i\Omega(t_1-t_2)}\Big)\mathrm{d}t_1\mathrm{d}t_2. \end{aligned} \tag{3.16}$$

For the time being we skip the first *non-secular* term, which does not conserve the energy and rapidly oscillates with twice the frequency, that corresponds to the energy gap of the TLS.[8] We now rewrite the second part of the expression, in terms of the correlation functions[9] from

8: see Sec. 3.2 for more detailed discussion in context of master equation

9: $C_{\pm\mp}(t) = \mathrm{Tr}\Big(\hat{V}'_\pm(t)\hat{V}'_\mp(0)\rho_e\Big)$

Eq. (3.8):

$$\delta W'_{\perp} = -\frac{1}{4}\int_0^t \int_0^{t_2} \Big(\big[C_{-+}(t_1 - t_2) + C_{+-}(t_2 - t_1)\big] e^{-i\Omega(t_1 - t_2)} \Big) \mathrm{d}t_1 \mathrm{d}t_2. \tag{3.17}$$

We now change the variables into $T = (t_1 + t_2)/2$ and $\tau = t_2 - t_1$, which allows to write:

$$\delta W'_{\perp} = -\frac{1}{4}\int_0^t \Big((t - \tau)\big[C_{-+}(-\tau) + C_{+-}(\tau)\big] e^{i\Omega\tau} \Big) \mathrm{d}\tau. \tag{3.18}$$

It is often assumed that transverse noise has relatively short correlation time[10] τ_c, i.e. $t \gg \tau_c$, which allows to 1) extend limits of the integral to infinity and 2) neglect the term proportional to τ in the integral. Next we introduce spectral densities i.e. $C_{\pm\mp}(\pm t) = \int \frac{\mathrm{d}\omega}{2\pi} S_{\perp}(\pm\omega) e^{-i\omega t}$. Together it gives:

$$\delta W'_{\perp} = \frac{t}{4}\int_{-\infty}^{\infty} \frac{\mathrm{d}\omega}{2\pi} \big[S_{\perp}(\omega) + S_{\perp}(-\omega)\big] F(\omega - \Omega), \tag{3.19}$$

where we introduced the filter function, defined as:

$$F(\Omega - \Omega) = \int_0^{\infty} \mathrm{d}t e^{i(\omega - \Omega)t} = \pi\delta(\omega - \Omega) + \mathrm{PV}\left(\frac{1}{i(\omega - \Omega)}\right). \tag{3.20}$$

The first term proportional to Dirac delta is related to incoherent transitions between ground and excited states, while the latter, proportional to principal value[11] is related to the so-called Lamb shift, additional deterministic phase shift due to renormalization of TLS gap (see Eq. (3.38) and discussion there). Since the latter contribution can be often calibrated out, as it is not random in its nature, we concentrate on the first term and finally write the leading order contribution to dephasing due to inelastic transition rates as:

$$\delta W'_{\perp} = -\frac{\Gamma_-(\Omega) + \Gamma_+(\Omega)}{2}\, t \equiv -\Gamma_W t, \tag{3.22}$$

where we have derived the dephasing rate due to transverse coupling to environment with short correlation time as

$$\Gamma_W = \Gamma_-(\Omega) \coth(\beta\Omega/2) e^{-\beta\Omega/2}. \tag{3.23}$$

10: By the correlation time we mean the timescale at which the correlation function effectively vanishes, i.e. $C(t) \to 0$ for $t \gg \tau_c$

11: Formally the principal value is defined as the distribution, for instance for the function $f(x)$ we have:

$$\mathrm{PV}(1/x)[f] = \lim_{\delta\to 0}\left(\int_{-\infty}^{-\delta} f(x)\mathrm{d}x + \int_{\delta}^{\infty} f(x)\mathrm{d}x\right) \tag{3.21}$$

3.2 Master equation approach

After considering dissipation mechanisms in the second order in time expansion, we now extrapolate them to more general treatment of non-unitary evolution of the TLS coupled to the environment of typically short correlation time,[12] known as the Master equation approach.

12: short in comparison to the timescale at which the environment affects the TLS state

Bloch-Redfield equation

First we briefly derive Bloch-Redfield Master equation following standard textbook approach [137], where to some extent we repeat calculation up to second order in the transverse coupling $\hat{H}_{\perp}$ given in Eq. (3.1). However

this time we start, from the Von-Neumann equation for TLS-environment density matrix, which in the interaction picture reads

$$\dot{\hat{\rho}}'(t) = -i\left[\hat{V}'_\perp(t), \rho'(t)\right], \tag{3.24}$$

where $\hat{V}'_\perp(t) = e^{i(\hat{H}_q+\hat{H}_e)t} V_\perp e^{-i(\hat{H}_q+\hat{H}_e)t}$ and $\rho'(t) = e^{i(\hat{H}_q+\hat{H}_e)t}\rho(t)e^{-i(\hat{H}_q+\hat{H}_e)t}$. We now iterate the equation once[13] and write:

$$\dot{\hat{\rho}}'(t) = -i\left[\hat{V}'_\perp(t), \rho'(0)\right] - \left[\hat{V}'_\perp(t), \left[\int_0^t \mathrm{d}t' V'_\perp(t'), \rho'(t')\right]\right]. \tag{3.25}$$

13: i.e.

$$\rho'(t) = \rho'(0) - i\int_0^t \mathrm{d}t'[V'_\perp(t'), \hat{\rho}'(t')]$$

The reduced density matrix of the TLS is obtained by tracing environmental degrees of freedom, using assumption of the uncorrelated states $\hat{\rho}'(t) = \hat{\rho}'_q(t) \otimes \hat{\rho}_e$. Note that due to typically large size of environment in this derivation $\hat{\rho}_e$ is assumed constant, i.e. unaltered by the interaction with the TLS. Finally we assume the expectation value of the single interaction operator is zero, i.e. $\mathrm{Tr}_e\{\hat{V}_\pm(t)\hat{\rho}_0\}$, which is typically the case in thermal equilibrium, and write:

$$\dot{\hat{\rho}}'_q(t) = -\mathrm{Tr}_e\left\{\left[\hat{V}'_\perp(t), \int_0^t \mathrm{d}t'\hat{V}'_\perp(t')\hat{\rho}'_q(t')\hat{\rho}_e\right]\right\} + h.c, \tag{3.26}$$

where we also replaced double commutator by the single one plus its Hermitian conjugate.

Markov approximation

We will now assume the environment memory is short, i.e. the typical correlation time, during which the integral gives non-zero contribution is much shorter then the characteristic timescale of TLS's evolution due to its interaction with the environment[14] . Mathematically this allows us to first extend the lower bound to $-\infty$, and then introduce new variable $r = t - t'$, such that:

$$\dot{\hat{\rho}}'_q(t) = -\mathrm{Tr}_e\left\{\left[\hat{V}'_\perp(t), \int_0^\infty \mathrm{d}r\hat{V}'_\perp(t-r)\hat{\rho}'_q(t-r)\hat{\rho}_e\right]\right\} + h.c., \tag{3.27}$$

14: It formally means that correlation functions $C_{\pm\mp}(t)$ goes to zero as the TLS relaxation $T_1 \approx 1/\Gamma_-$ time exceeds the environmental correlation time $T_1 \gg \tau_c$

the Markov approximation is now completed by replacing $\hat{\rho}'_q(t-r) \to \hat{\rho}'_q(t)$, i.e. neglecting TLS evolution that takes place on the timescale of short correlation time of environment.

Bloch-Redfield tensor

We now substitute the coupling Hamiltonian,

$$\hat{V}'_\perp(t) = \frac{1}{2}\left(\hat{V}'_+(t)\sigma'_+(t) + \hat{V}'_-(t)\hat{\sigma}'_-(t)\right), \tag{3.28}$$

and go to Schrodinger representation, which amounts to unwinding interaction picture with respect to TLS Hamiltonian[15] . As a result the Bloch-Redfield equation can be written in the simple form:

$$\dot{\hat{\rho}}_q(t) = i\left[\hat{\rho}_q(t), \hat{H}_q\right] - \sum_{k,l=\pm}\left[\hat{s}_k, \hat{R}_{kl}\hat{\rho}_q(t)\right] + h.c. \tag{3.29}$$

15: This means we substitute $\hat{\rho}'_q(t) = \hat{U}_q^\dagger(t)\hat{\rho}_q(t)\hat{U}_q(t)$, where $\hat{U}_q(t) = e^{-i\hat{H}_q t}$, and multiply from the left by $\hat{U}_q(t)$ and from the right by $\hat{U}_q^\dagger(t)$

where we have defined the Bloch-Redfield tensor as

$$\hat{R}_{kl}(t) = \frac{1}{4}\int_0^\infty \hat{\sigma}'_l(-r)C_{kl}(r)\mathrm{d}r, \tag{3.30}$$

written in terms of previously introduced correlation function $C_{kl}(r) = \mathrm{Tr}\{\hat{V}'_k(r)\hat{V}'_l(0)\hat{\rho}_e\}$ and the operators in the interaction picture: $\hat{V}'_l(t) = e^{i\hat{H}_e t}\hat{V}_l e^{-i\hat{H}_e t}$ and $\hat{\sigma}'_l(-r) = e^{-i\Omega r\hat{\sigma}_z/2}\hat{\sigma}_l e^{i\Omega r\hat{\sigma}_z/2}$.

As we have shown in the previous section, transitions between the TLS eigenstates are caused by the energy exchange with environment. In analogy to Eq. (3.4) in the limit of weak coupling, or equivalently relatively long evolution time, the terms which do not conserve energy will effectively vanish. Below we will show that for typically weak coupling, the contribution from such *non-secular terms* $\hat{R}_{++}, \hat{R}_{--}$ are negligibly small, mostly due to fast oscillations with the frequency given by twice the TLS splitting 2Ω (see below). Later we will explicitly calculate more relevant *secular terms* $\hat{R}_{\pm\mp}$, which will allow us to arrive at the Linblad form of the Master equation. Note that in Chapter 10, where we will generalize master equation to the four-level system of spin and driven orbital states, we will use local-secular approximation [138], in which we will leave "slightly" non-conservative terms, as they will be crucial to understand TLS dephasing in presence of the orbital dissipative evolution.

Non-secular terms $R_{\pm\pm}$

We now go back to interaction picture with respect to the TLS, i.e.

$$\dot{\hat{\rho}}'_q(t) = \sum_{k,l=\pm} e^{i(k+l)\Omega t}\left[\hat{s}_k, \hat{R}_{kl}(t)\hat{\rho}'_q\right] + h.c, \tag{3.31}$$

and concentrate on a single non-secular term, for instance $i = j = +$. We compute the coherence element[16] :

$$\dot{W}'(t) = \left(\frac{1}{4}\int_0^\infty \mathrm{d}r C_{++}(r)e^{-i\Omega r}\right)e^{i2\Omega t}W'^*(t) = C_0 e^{i2\Omega t}W'^*(t), \tag{3.32}$$

where C_0 is some time-independent constant involving Fourier transform of the correlator $\mathrm{Tr}\{\hat{V}'_+(r)\hat{V}'_+(0)\hat{\rho}_e\}$ at the TLS frequency Ω. Not only the C_0 is usually smaller then the spectral densities in the secular terms, but the expression involves rapidly oscillating phase $e^{i2\Omega t}$. For the weak coupling one can use perturbation theory, which in the leading order predicts:

$$\delta W(T) = C_0\int_0^T e^{i2\Omega t} \tag{3.33}$$

which oscillates and becomes negligible for sufficiently large ΩT and small C_0, i.e. in weak coupling limit. As we will show, this feature is absent in the secular terms, where $i \neq j$, on which we concentrate now.

16: $W'(t) = \mathrm{Tr}\{\hat{\sigma}_-\rho'_q(t)\}$. Note that $Z'(t) = Z(0)$.

Secular terms $\hat{R}_{\pm\mp}$

We now move to non-oscillatory secular terms, that corresponds to elements of Bloch-Redfield tensor with $i \neq j$. In particular, the term responsible for relaxation can be identified as

$$\begin{aligned}\hat{R}_{+-} &= \frac{\hat{\sigma}_-}{4}\int_0^\infty \langle \hat{V}'_+(s)\hat{V}'_-(0)\rangle e^{i\Omega s}\mathrm{d}s = \frac{\hat{\sigma}_-}{4}\int_{-\infty}^\infty \frac{\mathrm{d}\omega}{2\pi}S_\perp(\omega)\int_0^\infty e^{-i(\omega-\Omega)s} \\ &= \frac{\hat{\sigma}_-}{4}\left(\frac{1}{2}S_\perp(\Omega) - iA_{\mathrm{LS},-}(\Omega)\right),\end{aligned} \tag{3.34}$$

where we have used Fourier transform of the correlation function, i.e. spectral density $C_{+-}(s) = \int \frac{\mathrm{d}\omega}{2\pi}S_\perp(\omega)e^{-i\omega s}$, and denoted correction due to principal value[17] as $A_{\mathrm{LS},-}(\Omega)$, see Eq. (3.36) for its exact form. Similarly for the element corresponding to excitation from ground to excited TLS state (energy absorption) we have:

17: $\int_0^\infty e^{-iat} = \pi\delta a + i\mathrm{PV}[1/a]$

$$\begin{aligned}\hat{R}_{-+} &= \frac{\hat{\sigma}_+}{4}\int_0^\infty \langle V'_-(s)V'_+(0)\rangle e^{-i\Omega s}\mathrm{d}s = \frac{\hat{\sigma}_+}{4}\int_0^\infty C_{-+}(s)e^{-i\Omega s}\mathrm{d}s \\ &= \frac{\hat{\sigma}_+}{4}\int_{-\infty}^\infty \frac{\mathrm{d}\omega}{2\pi}S_\perp(-\omega)\int_0^\infty e^{i(\omega-\Omega)s} = \frac{\hat{\sigma}_+}{4}\left(\frac{1}{2}S_\perp(-\Omega) + iA_{\mathrm{LS},+}(\Omega)\right),\end{aligned} \tag{3.35}$$

where we have used the previously derived $C_{-+}(s) = \int \frac{\mathrm{d}\omega}{2\pi}S_\perp(-\omega)e^{i\omega s}$, and introduced the term related to the principal value as $A_{\mathrm{LS},+}(\Omega)$, which can be written as:

$$A_{\mathrm{LS},\mp}(\Omega) = \frac{1}{2\pi}\int \mathrm{d}\omega S_\perp(\pm\omega)\mathrm{PV}[(\omega-\Omega)^{-1}], \tag{3.36}$$

where for environment in thermal equilibrium we have $S_\perp(-\Omega) = S_\perp(\Omega)e^{-\beta\Omega}$.

The secular terms together with the unitary part provide differential equation for the TLS density matrix. That is the celebrated *Gorini – Kossakowski – Sudarshan – Lindblad Master equation* (GKSL Master equation) [139, 140] of the form:

$$\dot{\hat{\rho}}_q = -i\left[\hat{H}_q + \hat{H}_{\mathrm{LS}}, \rho_q\right] + \sum_{j=\pm} L_j\hat{\rho}_q\hat{L}_j^\dagger - \frac{1}{2}\left\{\hat{L}_j^\dagger\hat{L}_j, \hat{\rho}_q\right\}, \tag{3.37}$$

where by inspection of Eqs. (3.34) and (3.35) one can reconstruct exact form of *Linblad operators* $\hat{L}_+ = \hat{\sigma}_+\sqrt{\Gamma_+}$ and $\hat{L}_- = \hat{\sigma}_-\sqrt{\Gamma_-}$, expressed in terms of transition rates related to spectral densities via $\Gamma_\pm(\Omega) = \frac{1}{4}S_\perp(\mp\Omega)$. We have denoted contribution from the principal value of the integrals as $\hat{H}_{\mathrm{LS}}$. It generates correction to unitary dynamics, which stems from renormalization of the TLS energy gap due to virtual transitions, commonly known as *the Lamb-shift*, i.e.

$$\hat{H}_{\mathrm{LS}} = \frac{A_{\mathrm{LS},+}(\Omega) + A_{\mathrm{LS},-}(\Omega)}{8}\hat{\sigma}_z. \tag{3.38}$$

We follow analysis of other solid-state systems [141, 142] and assume its effect can be neglected.

Equations of motion

Master equation derived above can be used to write equations of motion for the polarization and the coherence of the TLS. With the constant and diagonal Hamiltonian $\hat{H}_q = \frac{1}{2}\Omega\hat{\sigma}_z$ they can be analytically integrated to give the polarization at time t as

$$Z(t) = Z_0 e^{-(\Gamma_- + \Gamma_+)t} + Z_{\mathrm{eq}}\left(1 - e^{-(\Gamma_- + \Gamma_+)t}\right), \tag{3.39}$$

where we have introduced equilibrium value of $Z_{\mathrm{eq}} = \frac{\Gamma_+ - \Gamma_-}{\Gamma_+ + \Gamma_-}$. On the other hand solving Linblad equations for $W(t)$ gives

$$W'(t) = W(0)e^{-\Gamma_W t}, \tag{3.40}$$

where $\Gamma_W = \frac{1}{2}(\Gamma_+ + \Gamma_-)$. In principle, the equations of motion can be generalized to the case where the rates are time-dependent $\Gamma_\pm(t)$, for which the observables are given by:

$$\begin{aligned} Z(t) &= Z_0 e^{-\int_0^t [\Gamma_-(t') + \Gamma_+(t')]\mathrm{d}\,t'} - \int_0^t \mathrm{d}s[\Gamma_+(s) - \Gamma_-(s)]e^{-\int_s^t [\Gamma_+(s') + \Gamma_-(s')]\mathrm{d}s'}, \\ W'(t) &= W'(0)e^{-\int_0^t \Gamma_W(t')}. \end{aligned} \tag{3.41}$$

Note that with time-dependent rates one can only define the polarization $Z_{\mathrm{eq}}(t)$ to which $Z(t)$ tries to tend at every moment of time[18] .

18: This leads to asymmetric hysteresis curve in the driven systems [143]

4 Dephasing of a two-level system

The second process considered in this thesis amounts to losing the definite phase between the qubit eigenstates without energy transfer. We now relate its origin to the longitudinal qubit-environment coupling $\hat{V}_\parallel$, which together with the qubit Hamiltonian reads:

$$\hat{H}_\phi = \frac{\Omega}{2}\hat{\sigma}_z + \frac{\hat{V}_\phi}{2}\hat{\sigma}_z. \tag{4.1}$$

4.1 Master equation approach

We start by considering memory-less environment (short correlation time) and hence reuse Bloch-Redfield Master equation approach[1] for the longitudinal coupling $\hat{V}_\phi$. We will generally assume that longitudinal coupling is statistically independent from the transverse one[2] , which means that in the Bloch-Redfield equation (3.29), any terms involving $\langle \hat{V}_\pm \hat{V}_\phi \rangle = 0$ can be ignored. As a result the only additional term to Bloch-Redfield tensor is the dephasing term:

$$\hat{R}_\phi + \hat{R}_\phi^\dagger = \frac{1}{4}\int_0^\infty \hat{\sigma}_z \left(\langle \hat{V}'_\phi(s)\hat{V}'_\phi(0)\rangle + \langle \hat{V}'_\phi(0)\hat{V}'_\phi(s)\rangle \right) \mathrm{d}s = \frac{S_\phi(0)}{4}, \tag{4.2}$$

where the contribution from principle value cancels. In the above we introduced spectral density of longitudinally coupled environment:

$$S_\phi(\omega) = \frac{1}{2}\int_{-\infty}^{\infty} \mathrm{d}t \left\langle \{\hat{V}'_\phi(t), \hat{V}'_\phi(0)\} \right\rangle_e e^{i\omega t}, \tag{4.3}$$

with operators in the interaction picture $\hat{V}'_\phi(t) = e^{i\hat{H}_e t}\hat{V}_\phi e^{-i\hat{H}_e t}$. By computing the commutator

$$\left[\hat{\sigma}_z, \hat{R}_\phi \hat{\rho}_q\right] + h.c. = \frac{1}{4}S_\phi(0)\left(\hat{\rho} - \hat{\sigma}_z\hat{\rho}\hat{\sigma}_z\right), \tag{4.4}$$

one can find the dephasing Linbladian operator:

$$\hat{L}_\phi = \sqrt{\frac{S_\phi(0)}{4}}\hat{\sigma}_z, \tag{4.5}$$

which substituted to the GKSL Master equation from Eq. (3.37), generates decay of off-diagonal density matrix element i.e.

$$W'(t) = W(0)\exp\left(-\frac{S_\phi(0)}{2}t\right), \tag{4.6}$$

1: We highlight here that later in the thesis we will be considering spectral densities, which are irregular at zero frequency. This includes both typical for semiconductor 1/f-noise and the model of quasistatic noise, which are divergent at $\omega = 0$. As we will show for those relevant cases, the Master equation approach fails.

2: As we will show later this can be related to a separation of the timescales associated with the environmental noise.

and does not modify $Z(t)$. In this way we showed that dephasing rate for the environment with short correlation lengths, such that Born-Markov approximation holds reads is given by $\Gamma_\phi = \frac{1}{2}S_\phi(0)$.

4.2 Weak coupling limit δW_ϕ

We now move to computation of more general environment, where correlation time is not essentially shorter then any other time scale. In the interaction picture[3] the coherence reads:

3: i.e. $W_\phi(t) = \mathrm{Tr}\{\sigma_- \rho'(t)\}$

$$W'_\phi(t) = W(0)e^{-i\Omega t}\left\langle \tilde{\mathcal{T}} \exp\left\{\frac{i}{2}\int_0^t \hat{V}'_\phi(\tau)\right\} \mathcal{T} \exp\left\{-\frac{i}{2}\int_0^t \hat{V}'_\phi(\tau)\right\}\right\rangle_e . \tag{4.7}$$

where $\tilde{\mathcal{T}}$ denotes anti-chronological time-ordering and we used the interaction picture $\hat{V}'_\phi(t) = e^{i\hat{H}_e t}\hat{V}_\phi e^{-i\hat{H}_e t}$. We assume the environmental operator has zero average, $\langle V'_\phi(t)\rangle$ and write the difference in phase coherence $\delta W'_\phi = W'(t) - W(0)$ in first non-vanishing order as

$$\begin{aligned}\delta W'_\phi(t) = &-\frac{W(0)}{4}\int_0^t \mathrm{d}t_2 \int_0^t \mathrm{d}t_1 \langle \hat{V}'_\phi(t_1)\hat{V}'_\phi(t_2)\rangle + \\ &-\frac{W(0)}{4}\int_0^t \mathrm{d}t_2 \int_0^{t_2} \mathrm{d}t_1 \langle \hat{V}'_\phi(t_2)\hat{V}'_\phi(t_1) + \hat{V}'_\phi(t_1)\hat{V}'_\phi(t_2)\rangle. \end{aligned} \tag{4.8}$$

After a few careful operations on two integrals above, one can express the loss of initial phase coherence using symmetric 2-point correlation function of the environmental operator, i.e.

$$\delta W'_\phi(t) = -\frac{W(0)}{2}\int_0^t \int_0^t C_\phi(t_1 - t_2)\mathrm{d}t_1\mathrm{d}t_2. \tag{4.9}$$

where the correlation function is defined using anti-commutator

$$C_\phi(t_1 - t_2) = \tfrac{1}{2}\langle\{\hat{V}'_\phi(t_1), \hat{V}'_\phi(t_2)\}\rangle, \tag{4.10}$$

where the dependence on the difference in time, requires the environment to be in thermal equilibrium, in which $[\hat{H}_e, \hat{\rho}_e] = 0$. The presence of the anti-commutator ensures that the correlation function is real even for asymmetric couplings[4] .

4: However for such asymmetric coupling, i.e. $\hat{V}_{qe} = \hat{V}_\uparrow |\uparrow\rangle\langle\uparrow| + \hat{V}_\downarrow |\downarrow\rangle\langle\downarrow|$, where $\hat{V}_\uparrow \neq -\hat{V}_\downarrow$, the δW_ϕ acquires additional phase shift related to the commutator $[\hat{V}'_\phi(t_1), \hat{V}'_\phi(t_2)]$ [144, 145].

Effects of finite correlation time

We now distinguish different ways in which dephasing can depend on the evolution time t. Using equation Eq. (4.9) for leading order loss of phase coherence, and in analogy to relaxation considerations from Sec. 3.1, we introduce Fourier transform of correlation function, or the spectral density of longitudinally coupled noise $S_\phi(\omega)$ as

$$C_\phi(t_1 - t_2) = \int_{-\infty}^{\infty} \frac{d\omega}{2\pi} S_\phi(\omega) e^{-i\omega(t_1 - t_2)}, \tag{4.11}$$

which if substituted to expression for $\delta W'_\phi$ produces:

$$\delta W'_\phi(t) = -\frac{t^2}{2}\int_{-\infty}^{\infty}\frac{\mathrm{d}\omega}{2\pi}\mathrm{sinc}^2\left(\frac{\omega t}{2}\right)S_\phi(\omega). \tag{4.12}$$

The overall dependence on t is given by the interplay between the functions $\mathrm{sinc}(\omega t/2) = 2\sin(\omega t/2)/\omega t$ and $S_\phi(\omega)$. For the spectral density sufficiently flat in low frequencies, i.e. very short correlation time τ_c in comparison to t, we can use limiting expression $\lim_{t\to\infty} t\,\mathrm{sinc}^2(xt/2) = 2\pi\delta(x)$ and arrive at rate-like behaviour $\delta W_\phi(t) \propto tS_\phi(0)$, derived using Master Equation approach in Eq. (4.6).

In the opposite limit of relatively slowly decaying $C_\phi(t)$, the spectral density is expected to be peaked at low-frequencies. Thus with evolution time $t < \tau_c$ the sinc function effectively is flat with respect to spectral density $S_\phi(\omega)$, and $\delta W_\phi(t) \propto t^2\int S_\phi(\omega)$.[5] In these two limiting cases we have:

$$\delta W'_\phi(t) = \begin{cases} -\frac{1}{2}S_\phi(0)\,t, & \text{for } t \ll t_c\text{, i.e. fast noise} \\ -\frac{1}{2}C_\phi(0)\,t^2, & \text{for } t \gg t_c\text{, i.e. slow noise} \end{cases} \tag{4.13}$$

5: The quadratic scaling can be seen from Eq. (4.9), if one assumes that correlation function remains constant on the timescale of the experiment $C_\phi(t_1 - t_2) = C_\phi(0)$, using which $\delta W'_\phi(t) = -\frac{1}{2}C_\phi(0)$

Hence we have showed that in the two limiting cases the dephasing is caused by the fluctuations of environment, which can be either attributed to zero-frequency component of the fast noise or total power of the slow noise $C_\phi(0) = \int_{-\infty}^{\infty} S_\phi(\omega)\mathrm{d}\omega$. Note that for the spectral density divergent at $\omega = 0$, for instance $1/f$ noise from the following Sec. 4.3, the dephasing cannot be linear in time, as the spectrum cannot be effectively replaced by a constant value $S_\phi(0)$.

Decoherence from many weakly coupled sources

We conclude this section on quantum dephasing noise by considering a typical case in which the environment consist of many weakly coupled systems, e.g. nuclear spins or two-level fluctuators,

$$\hat{V}_\phi = \sum_k \hat{V}_{\phi,k}. \tag{4.14}$$

If contribution to dephasing from each of them is small enough, it can be computed in the leading order. If additionally on the time-scale of the experiment coupling between them is negligible, the evolution operators factorizes, i.e. $\hat{U} = \prod_k \hat{U}_k$, and thus the qubit coherence reads:

$$W_\phi = \prod_k W_{\phi,k} \approx \prod_k (1 - \delta W_{\phi,k}) \approx \exp\left(-\sum_k \delta W_\phi(t)\right) = \exp\big(-\chi_\phi(t)\big), \tag{4.15}$$

in this way we introduced decoherence factor $\chi_\phi(t)$ using the fact that $\delta W_{\phi,k} \ll 1$. The above argument is the reminiscence of central limiting theorem, since it allowed us to effectively "Gaussify"[6] the environmental contribution. In the following section, we will show that for Gaussian classical noise approximation the decoherence factor is equivalent to variance of random phase $\delta\phi$ due to environmental fluctuations, i.e. $\chi_\phi(t) \equiv \frac{1}{2}\langle\delta\phi^2\rangle$.

6: By Gaussification we mean that the overall coherence of the form of characteristic function is given in terms of second-order correlation function, which is a feature of Gaussian random variable x, i.e. $\langle e^{ix}\rangle = e^{-\langle x^2\rangle/2}$

4.3 Classical noise approach

In this section we present an alternative approach to dynamics of open quantum system, in which instead of dealing with typically large and complicated dynamics of the environment we replace it by the "equivalent" classical noise, which stochastically modifies unitary evolution of the qubit. The conditions under which this is a good approximation have been discussed in many papers [4–7, 146–153]. Here we discuss elements of the theory needed for the purpose of the thesis.

Model of classical dephasing - quasistatic noise

Imagine the qubit is subject to random rotations, which for instance are caused by the uncontrolled part of classical electronics that modifies the energy gap Ω by the random quantity ξ. Now we assume the time interval between consecutive realizations of the measurement scheme is long enough such that the value of ξ can significantly change. As a result statistical properties of ξ will modify expectation value of any observable. The simplest example is the free evolution of spin-superposition. We model influence of ξ by introducing the Hamiltonian:

$$\hat{H}(\xi) = \frac{\Omega}{2}\hat{\sigma}_z + \frac{\xi}{2}\hat{\sigma}_z. \tag{4.16}$$

If we measure the qubit coherence after time t, its value is conditioned on ξ and given by:

$$W(t|\xi) = \mathrm{Tr}\left\{|\uparrow\rangle\langle\downarrow| \, e^{-i\hat{H}(\xi)t}\hat{\rho}_0 e^{i\hat{H}(\xi)t}\right\} = W_0 e^{-i\xi t}, \tag{4.17}$$

and hence the current value of ξ accounts for the additional phase evolution. Similarly to any measurable quantity, the estimation of coherence W requires multiple projective measurements along x and y axis, which can be seen from the identity: $W = \langle\hat{\sigma}_-\rangle = \frac{1}{2}\langle\hat{\sigma}_x - i\hat{\sigma}_y\rangle$. As a result an attempt to estimate the coherence gives us only access to the statistical average,

$$W(t) \approx \frac{1}{N}\sum_{n=1}^{N} W(t|\xi_n) \to W_0\langle e^{-i\xi t}\rangle_\xi, \tag{4.18}$$

where in the last expression we used the limiting case of large number of repetitions, such that the average over repetitions of experiment (temporal average) can be replaced by overaging over statistical ensemble of possible values of ξ, i.e. $\langle\ldots\rangle_\xi$. The model of the noise considered above is often termed *quasistatic*, as it remains constant during single run of the experiment but varies between consecutive runs.

From the above considerations it is clear that averaging over many random phases will result in dephasing of the qubit. Above we have shown that the decoherence can be expressed in terms of characteristic function of the distribution of ξ. It also means, that $W(t)$ after sufficiently long period, will decay to zero for any distribution with non-zero variance. In particular the initial decay can be seen by considering leading order contribution to $\delta W'(t) = W'(t) - W(0)$, i.e.

$$\delta W'(t) = -i\langle\delta\phi\rangle - \frac{1}{2}\langle\delta\phi^2\rangle. \tag{4.19}$$

where $W(t) = W'(t)e^{-i\Omega t}$ and the random phase for quasistatic noise reads $\delta\phi = \xi t$. Note that any non-zero average can be incorporated to definition of the bare splitting $\Omega \to \Omega + \langle\xi\rangle$. As a consequence we will assume $\langle\delta\phi\rangle = 0$ and hence the short-time loss of coherence is proportional to the variance of random phase

$$\delta W'(t) = -\tfrac{1}{2}\langle\delta\phi^2\rangle \tag{4.20}$$

which for quasistatic noise is quadratic in time.

Another way of looking at the formula for decoherence is in terms of the cumulats of random variable $\delta\phi$. The cumulats are defined in terms of Taylor expansion of the logarithm of characteristic function, i.e. nth cumulant κ_n is implicitly defined as:

$$\log\langle e^{i\delta\phi}\rangle = \sum_n \kappa_n \frac{i^n}{n!}, \tag{4.21}$$

which can be immediately related to

$$\langle e^{i\delta\phi}\rangle = \exp\left\{-i\kappa_1 - \frac{1}{2}\kappa_2 + i\frac{1}{6}\kappa_3 \ldots\right\}. \tag{4.22}$$

Gaussian quasistatic noise

The only random variable, for which the number of nonzero cumulant is finite[7] is the Gaussian random variable, for which $\kappa_1 = \langle\delta\phi\rangle$ and $\kappa_2 = \langle\delta\phi^2\rangle - \langle\delta\phi\rangle^2$, while $\kappa_n = 0$ for $n > 2$ [154]. At the same time Gaussian statistics of $\delta\phi$ is expected on the basis of central limiting theorem due to typically complex structure of environment, reflected in a sum over many weakly coupled sources. Thus for the most part of this thesis the quasistatic classical noise will be assumed Gaussian.[8] In this case dephasing can be computed from the simple expression:

$$W'(t) = W_0 \exp\left(-\frac{1}{2}\langle\delta\phi^2\rangle\right) = W_0 \exp\left(-\frac{1}{2}\sigma^2 t^2\right) \tag{4.23}$$

where $\sigma^2 = \langle\xi^2\rangle$.

7: and actually equal to 2

8: Note that Gaussian statistics of $\delta\phi$ implies that for quasistatic noise ξ is itself a Gaussian random variable

Dynamical noise

We will now show that analogous expression can be obtained in presence of the environment modelled as dynamical stochastic process. As an extension of the previous section we take the Hamiltonian:

$$\hat{H}(t) = \frac{\Omega}{2}\hat{\sigma}_z + \frac{\xi(t)}{2}\hat{\sigma}_z. \tag{4.24}$$

In this case the evolution operator is also diagonal in spin operators $\hat{U}(t) = \exp\left(-i\frac{1}{2}\int \xi(t)\hat{\sigma}_z\right)$, and thus the coherence can be easily computed as:

$$W'(t) = W_0\left\langle \exp\left\{-i\int_0^t \xi(t')\mathrm{d}t'\right\}\right\rangle_\xi, \tag{4.25}$$

where $\langle \dots \rangle$ denotes averaging over realizations of $\xi(t)$. We can now relate to the previous section by introducing variable:

$$\delta\phi(t) = \int_0^t \xi(t')\mathrm{d}t, \tag{4.26}$$

using which $W'(t) = \langle e^{-i\delta\phi(t)} \rangle$. $\delta\phi$ can be now interpreted as the random variable generated by $\xi(t')$ process. The above expression for the coherence in the interaction picture can be computed analytically for many classical noise processes $\xi(t)$ [6, 155], including any noise with Gaussian statistics.

9: see discussion around Eq. (4.15)

Motivated by the presence of multiple weakly coupled noise sources,[9] we concentrate on the Gaussian stochastic process $\xi(t)$, which by definition produces the Gaussian random variable $\delta\phi$. In such case the coherence reads

$$W'(t) = W_0 \exp\left(-\frac{1}{2}\langle\delta\phi^2(t)\rangle\right) \equiv W_0 \exp\left(-\frac{1}{2}\int_0^t\int_0^t \mathrm{d}t_1\mathrm{d}t_2\langle\xi(t_1)\xi(t_2)\rangle\right), \tag{4.27}$$

and hence the loss of coherence can be related to the variance of random phase $\langle\delta\phi^2\rangle$. In analogy to the quantum case it is convenient to express $\langle\delta\phi^2\rangle$ in terms of correlation function of the environment:

$$\langle\delta\phi^2\rangle = \frac{1}{2}\int_0^t\int_0^t C_\phi(t_1 - t_2)\mathrm{d}t_1\mathrm{d}t_2 = \frac{1}{2}\int_0^t\int_0^t \langle\xi(t_1)\xi(t_2)\rangle\mathrm{d}t_1\mathrm{d}t_2, \tag{4.28}$$

where we assumed the noise is stationary, meaning that $\langle\xi(t_1)\xi(t_2)\rangle = \langle\xi(t_1 - t_2)\xi(0)\rangle$.

Classical-quantum correspondence

The relation between quantum and classical correlation function can be explicitly seen, when the coherence is expanded up to the second order in the coupling, in case of which the error is directly related to the correlation function

$$\delta W'(t) = -\frac{W_0}{2}\int_0^t \mathrm{d}t_1 \int_0^t \mathrm{d}t_2 C(t_1 - t_2), \tag{4.29}$$

where we can insert the proper correlation function:

$$C_\phi(\Delta t) = \begin{cases} \frac{1}{2}\,\mathrm{Tr}_e\left[\{\hat{V}_\phi(\Delta t), \hat{V}_\phi(0)\}\hat{\rho}_e\right], & \text{for the quantum case} \\ \left\langle \xi(\Delta t)\xi(0)\right\rangle_\xi, & \text{for the classical case.} \end{cases} \tag{4.30}$$

Naturally this means the statistical properties of the process $\xi(t)$, should be chosen to reconstruct the quantum correlation function. Note also that the anti-commutator of quantum correlation functions means that it has the same symmetry as the classical one.

Note that the classical spectral density, defined as:

$$S_{\phi,cl}(\omega) = \int_{-\infty}^{\infty} \mathrm{d}t e^{i\omega t}\langle\xi(t)\xi(0)\rangle = \int_{-\infty}^{\infty} \mathrm{d}t e^{i\omega t}\langle\xi(0)\xi(t)\rangle = S_{\phi,cl}(-\omega), \tag{4.31}$$

is by definition symmetric in the frequencies. Although transverse quantum noise appears classical only in the limit of $\Omega \ll k_B T$,[10] the longitudinal quantum noise is always symmetrized. As a result dephasing can be often simulated by the classical noise. However only in the limit of $\Omega \ll k_B T$ the classical noise can be thought of as a physical model of the environment, and not just a mathematically equivalent model. Finally we use Eq. (4.13) to argue that for sufficiently long correlation time of environment dephasing is dominated by the low-frequency part of the $S_\phi(\omega)$, that fulfills the relation $\omega < k_B T$.

10: for which the spectral densities $S(\omega) = S(-\omega)$. This happens if the Fourier transforms of $C_\pm(t)$ and $C_\mp(t)$ are equal for physcially relevant $\omega < k_B T$.

4.4 Relevant noise processes

We now discuss the two relevant noise process: the Ornstein-Uhlenbeck noise and the highly relevant for QDs systems 1/f noise [27, 43, 44, 156–160].

Ornstein-Uhlenbeck process

We start with the only Gaussian, Markovian and stationary process, known as the Ornstein-Uhlenbeck noise. Historically it corresponds to velocity of Brownian particle [161]. Mathematical definition of O-U noise $\xi(t)$ can be made using differential equation known as the Langevin equation [155] of the form:

$$\dot{\xi}_{\mathrm{ou}}(t) = -\frac{1}{\tau_c}\xi_{\mathrm{ou}}(t) + \sqrt{\frac{2\sigma^2}{\tau_c}}w(t), \tag{4.32}$$

where[11] $\sigma^2 = \int \frac{\mathrm{d}\omega}{2\pi} S(\omega)$ is the power of the noise τ_c is the correlation time and $w(t)$ is derivative of the Wiener process, commonly known as the *Gaussian white noise* with the correlation function $\langle w(t_1)w(t_2)\rangle = \delta(t_1 - t_2)$. The correlation function of $\xi_{\mathrm{ou}}(t)$ is exponential i.e.

$$C_{\mathrm{ou}}(t_1 - t_2) = \langle \xi_{\mathrm{ou}}(t_1)\xi_{\mathrm{ou}}(t_2)\rangle = \sigma^2 \exp\left(\frac{-|t_1 - t_2|}{\tau_c}\right), \tag{4.33}$$

By direct computation of Fourier transform the spectral density of O-U noise is a Lorenzian curve, i.e.

$$S_{\mathrm{ou}}(\omega) = \int_{-\infty}^{\infty} C_{\mathrm{ou}}(t)e^{i\omega t}\mathrm{d}t = \frac{2\sigma^2\tau_c}{1 + (\omega\tau_c)^2}. \tag{4.34}$$

11: The above differential equation can be easily discretized, which provides convenient way of generating time series of the noise, provided $w(t_n)$ at each step t_n is drawn from independent Gaussian distribution.

Decoherence factor

As shown in Fig. 4.1, the power of the noise at given frequency (spectral density) is approximately constant up to frequency $1/\tau_c$ at which decay with $1/\omega^2$ starts. For the O-U spectrum one can directly calculate decoherence factor from the correlation function $C_{\mathrm{ou}}(\mathrm{t})$, which due to Gaussian properties, is given by the leading order contribution to dephasing, i.e.

$$\chi_{\mathrm{ou}} \equiv \delta W_\phi(t) = -\frac{\sigma^2}{2}\int_0^t \mathrm{d}t_1 \int_0^t \mathrm{d}t_2 e^{-\frac{|t_1 - t_2|}{\tau_c}} = -\sigma^2\tau_c\left(t + \tau_c[e^{-t/\tau_c} - 1]\right). \tag{4.35}$$

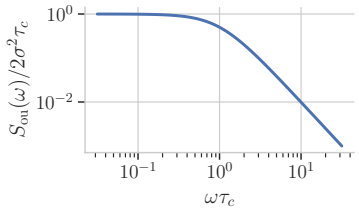

Figure 4.1: Spectral density of Ornstein-Uhlenbeck noise in the double logarithmic scale. Clear transition from flat spectrum into $S(\omega) \propto 1/\omega^2$ is visible at $\omega\tau_c \approx 1$.

We now discuss the limiting cases. Having total power of the noise fixed $\sigma^2 = \text{const}$ one can easily take the limit of quasistatic noise, which amounts to taking $\tau_c \to \infty$. As the τ_c increases, constant power of the noise forces the spectral density $\omega = 0$ to increase since $S_{\text{ou}}(0) = 2\sigma^2\tau_c$. From the above expression for the correlation function one can find, that in the limit of $t/\tau_c \ll 1$, first non-vanishing term gives $\chi_{\text{ou}} \approx \frac{1}{2}\sigma^2 t^2$. This reproduces long-correlation limit from (4.13).

In the second limiting case of fast noise, one has to be extra careful with fixing the total noise power, since taking $\tau_c \to 0$ decreases amplitude of spectral density in the relevant frequency range. This a consequence of keeping the area under the curve constant while making the spectral density flatter. Instead for the white noise limit it is more convenient to vary the correlation time and total noise power, in such a way that flat part of $S(\omega)$ has fixed amplitude[12] , i.e. $S(0) = 2\sigma^2\tau_c = \text{const}$. Note that with fixed $S_{\text{ou}}(0)$ the limit of $\tau_c \to 0$ will provide the noise with the flat spectral density below frequencies $1/\tau_c$ and result in the decoherence factor given by $\chi_{\text{ou}} \approx \sigma^2\tau_c t$ as expected form Eq. (4.13).

12: In such case decreasing correlation time would just move the kink of the spectral density, plotted in Fig. 4.1 towards higher frequencies

Finally the O-U noise can be used to generate the spectrum of the $1/\omega^2$ type, for the frequencies above $1/\tau_c$. Below we show that the sum of many independent O-U process can be used to generate noise processes with $1/\omega^\beta$ spectrum, characterized by a different exponent β.

1/f noise as a sum of Lorentzian fluctuators

We now discuss a highly important example of the environmental classical noise, which often dominates dephasing of solid state qubits. Its name $1/f^\beta$ *noise* generally refers to the process characterized by the spectral density given by the expression[13] :

13: For the reviews on the $1/f^\beta$ noise see [156]

$$S_\beta(\omega) = A_1 \left(\frac{\omega_1}{\omega}\right)^\beta, \quad \text{for} \quad \omega > 0 \tag{4.36}$$

where $\omega_1 = 2\pi/s$ is the angular frequency corresponding to oscillation period $T = 1\text{s}$, i.e. frequency $f_1 = 1\text{Hz}$. With this definition, A_1 stands for the power spectral density of the noise measured at 1Hz, i.e. $A_1 = S(\omega_1)$.

One of the most commonly accepted model of $1/f^\beta$ noise is the ensemble of two-level fluctuators (TLFs) with various characteristic switching rates. We will construct $1/f^\beta$ noise using one of possible models[14] , in which the TLFs can be treated as a source of telegraph noise[15] with the spectral density:

14: The similar derivation can be found in [1, 162]

15: i.e. noise which dynamically changes between two discrete values

$$S_{\text{TLF}}(\omega) = \frac{2\sigma^2\gamma^2}{\gamma^2 + \omega^2}, \tag{4.37}$$

which is identical to spectral density of O-U process with the switching rate $\gamma = 1/\tau_c$. We will be mostly interested in the case where the effective noise $\xi(t)$ originates from sum over multiple, independent TLFs with corresponding rate γ_k, for which the resulting noise can be written as:

$$\xi(t) = \sum_k \xi_k(t) = \int \mathrm{d}\gamma D(\gamma)\xi(t;\gamma), \tag{4.38}$$

where we replaced discrete sum by the integral over density of the fluctuators at given γ, i.e. $D(\gamma)$. If one uses continuous density of fluctuators[16] $D(\gamma) = \frac{N_\beta}{\gamma^\beta}$ the integral above produces desired $1/f^\beta$ spectrum since:

$$S_\beta(\omega) = \int_{-\gamma_{\min}}^{\gamma_{\max}} \mathrm{d}\gamma \frac{N_\beta}{\gamma^\beta} S_{\mathrm{TLF}}(\omega) = \frac{2s_0^2 N_\beta}{\omega^\beta} g(\beta), \tag{4.39}$$

where we introduced normalization constant N_β and dimensionless function

$$g(\beta) = \int_{\gamma_{\min}/\omega}^{\gamma_{\max}/\omega} \frac{\mathrm{d}x}{x^{\beta-1}(1+x^2)} \approx \int_0^{\pi/2} \tan^{1-\beta}(\alpha)\mathrm{d}\alpha. \tag{4.40}$$

The last expression is based on the assumption that for the relevant frequencies $\gamma_{\min} \ll \omega \ll \gamma_{\max}$, the lower and upper limit of the second integral can be set to 0 and ∞ respectively. The function $g(\beta)$ is often of the order of unity with $g(1) = \pi/2$, $g(3/2) = \pi/\sqrt{2}$ as an example. The normalization constant can be set from the comparison between Eqs.(4.36) and (4.39) i.e.

$$N_\beta = \frac{A\omega_1^\beta}{2s_0^2 g(\beta)}, \tag{4.41}$$

where $\omega_1^\beta = (2\pi \text{ Hz})^\beta$. In this way we constructed $1/f^\beta$ spectrum as a superposition of many fluctuators with Lorenzian spectral density. Moreover one can equivalently use O-U or telegraph process, both characterized by the same Lorenzian spectrum, as the non-Gaussian properties of the latter do not matter in the limit of many TLFs[17] . This provides a simple way to numerically simulate $1/f^\beta$ spectrum, using O-U processes.

16: which reflects typical physics of TLFs in the semiconductor device, where the tunneling rate γ_k depends exponentially on the height/width of the barriers, the distribution of which is expected to by approximately float or slowly changing

17: A sum of many RTNs can be often approximated by a Gaussian process. For non-Gaussian effects in small ensembles of TLFs see [163]

Quasistatic noise model

We finally introduce an approximate way in which the slow-fluctuations of the environment will be treated in this thesis. To reflect realistic scenario, we will assume that the dominant contribution to dephasing of freely evolving TLS is due to longitudinal quasistatic noise. As we showed in Eq. (4.23) in such case the dephasing can be expressed by the equation:

$$W'(t) = W(0) \exp\left(-\frac{1}{2}\tilde{\sigma}^2 t^2\right), \tag{4.42}$$

where $\tilde{\sigma}$ is the root-mean-square of the quasistatic fluctuations. In the physical picture the $\tilde{\sigma}$ is determined by the effective strength of environmental fluctuators,[18] which remains approximately constant on the timescale that exceeds experimental time t. For this reason, for the physical noise process which are composed of many independent noise sources the $\tilde{\sigma}(t)$ is time-dependent.

18: Physical entities that fluctuate,

Effective power of quasitatic noise

To estimate power of the effective quasistatic noise we integrate the spectral density of relevant noise process up to frequency related to

experimental time t, i.e. $\omega t < \pi$

$$\tilde{\sigma}^2(t) \equiv \int_{-\pi/t}^{\pi/t} S(\omega)\mathrm{d}\omega. \tag{4.43}$$

As a first relevant example we consider O-U noise for which the quasitatic part of its spectrum $S_{\mathrm{ou}}(\omega)$ from Eq. (4.34) gives:

$$\tilde{\sigma}^2_{\mathrm{ou}}(t) = \int_{-\pi/t}^{\pi/t} \frac{S_{\mathrm{ou}}(\omega)}{2\pi} = \frac{2}{\pi}\sigma^2 \arctan\Big(\frac{\pi\tau_c}{t}\Big). \tag{4.44}$$

From the above one can show that:

$$\tilde{\sigma}^2_{\mathrm{ou}}(t)t^2 \to \begin{cases} 2\sigma^2\tau_c t = S_{\mathrm{ou}}(0)t & \text{for } \tau_c \ll t \\ \sigma^2 t^2 & \text{for } \tau_c \gg t \end{cases} \tag{4.45}$$

which reproduces predictions of Eq. (4.8), where we showed that dephasing is linear function of time for environments with short correlation time and quadratic in the opposite limit.

In contrast to the O-U spectrum the computation of decoherence factor for more realistic $1/f^\beta$ noise,

$$\tilde{\sigma}^2_\beta(t) = A_1\omega_1^\beta \int_0^{\pi/t} \frac{\mathrm{d}\omega}{\pi}\mathrm{sinc}^2\left(\frac{\omega t}{2}\right)\omega^{-\beta}, \tag{4.46}$$

has intrinsic divergence[19] related to ill-defined spectrum as $\omega \to 0$. However the problem of divergence at $\omega = 0$ is never present in any realistic experiment, due to finite data acquisition time T_a, which we define as the time needed to collect data for computation of some observable. In such case, any fluctuators that remains static on the timescale T_a does not contribute to amplitude of the noise. This also means that the lowest possible frequency should be associated with the inverse of data acquisition time, i.e. $\omega_{\mathrm{low}} \approx \pi/T_a$, which allows to write the effective power of quasistatic noise as

$$\tilde{\sigma}^2_\beta(t) = A_1\omega_1^\beta \int_{\pi/T_a}^{\pi/t} \frac{\mathrm{d}\omega}{\pi}\mathrm{sinc}^2\left(\frac{\omega t}{2}\right)\omega^{-\beta}, \tag{4.47}$$

which for $\beta = 1$ reduces to:

$$\tilde{\sigma}^2_1(t) = A_1 \ln(T_a/t) \approx 25A_1, \tag{4.48}$$

where the right hand side corresponds to typical ratio of data acquisition time to evolution time, i.e. $T_a/t \approx 10^{10}$. Note that the dependence on T_a is logarithmic[20] , i.e. the result grows slowly for longer data acquisition time.

In general for any noise process of a large spectral weight in the low-frequencies, we define the effective power of quasistatic noise as:

$$\tilde{\sigma}^2 = \frac{1}{\pi}\int_{\pi/T_a}^{\pi/t} S(\omega)\mathrm{d}\omega. \tag{4.49}$$

We test this approach in Appendix A.

19: Note that in the integral we replaced $\int_{-\infty}^{\infty} \to 2\int_0^{\infty}$ due to symmetry of positive- and negative-frequency of the dephasing spectrum

20: Note that in a different case of $\beta = 2$, effective power of quasistatic noise strongly depends on T_a, since it is given by

$$\tilde{\sigma}^2_2 \approx (A\omega_1^2 T_a)/\pi^2,$$

.

5 Adiabatic drive of the two-level system in presence of environment

In this chapter we consider Landau-Zener drive of the orbital two-level system in the semiconductor quantum dot. In Sec. 5.1 we describe the adiabatic drive of two-level system in absence of the environment. Next in Sec. 5.2 we consider presence of the environment, by including classical fluctuations of the driven Hamiltonian parameters. Next in Sec. 5.3 we derive most common way to deal with dissipative evolution of the driven quantum system in the form of adiabatic Master equation (AME). Finally in Sec.5.4 we discuss the approach used in this thesis to compute effects of longitudinal and transverse couplings in the adiabatic basis.

5.1 Adiabatic drive in absence of environment

We focus now on the adiabatic driving of two-level system (TLS), which will correspond to two lowest lying orbital levels in the Double Quanutm Dot (DQD) system. Following model introduced in Chapter 1 the general charge state of the electron can be represented as:

$$|\psi(t)\rangle = c_L(t)\,|L\rangle + c_R(t)\,|R\rangle\,, \tag{5.1}$$

where $|L\rangle$ and $|R\rangle$ are the ground states of the left and right dot, while $|c_{L(R)}|^2$ corresponds to probability of occupying left (right) dot[1] . The transfer error can be defined in terms of remaining occupation of the initial state, i.e.

$$Q = |c_L(t_f)|^2 = 1 - |c_R(t_f)|^2. \tag{5.2}$$

The transfer of electron charge is made possible by time-dependent modulation of the energy detuning between neighbouring quantum dots $\epsilon(t)$, which for the DQD system gives time-dependent Hamiltonian:

$$\hat{H}_o(t) = \frac{\epsilon(t)}{2}\hat{\sigma}_z + \frac{t_c}{2}\hat{\sigma}_x, \tag{5.3}$$

We assume that in the relevant region of detuning, tunnel coupling can be assumed constant. At any time t the Hamiltonian $\hat{H}_o(t)$ give rise to a pair of *instantaneous states*,

$$\hat{H}_o(t)\,|\pm(t)\rangle = E_\pm(t)\,|\pm(t)\rangle\,. \tag{5.4}$$

1: The basis of dot states $|L\rangle$, $|R\rangle$ is often called *diabatic basis*

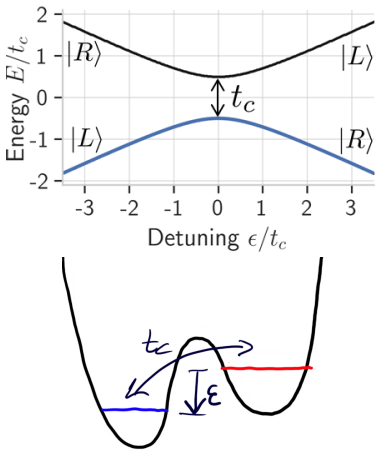

Figure 5.1: The instantaneous energy spectrum of the $\hat{H}_o(t)$ Hamiltonian (top) and sketch of physical realisation of $\hat{H}_o(t)$ in DQD system (bottom) replotted from the Chapter 1.

The states $|\pm(t)\rangle$ give the *adiabatic basis*, while their explicit form read:

$$|+(t)\rangle = \sin\frac{\vartheta(t)}{2}|R\rangle + \cos\frac{\vartheta(t)}{2}|L\rangle$$
$$|-(t)\rangle = \sin\frac{\vartheta(t)}{2}|L\rangle - \cos\frac{\vartheta(t)}{2}|R\rangle\,, \tag{5.5}$$

where we have defined the orbital angle:

$$\mathrm{ctan}\vartheta(t) = \frac{\epsilon(t)}{t_c}. \tag{5.6}$$

Note that sweep of detuning from large and negative $\epsilon(t_i) \ll -t_c$ ($\vartheta(t_i) \approx \pi$) to large and positive values $\epsilon(t_f) \gg t_c$ ($\vartheta(t_i) \approx 0$) moves the ground state from the initial, left dot, i.e. $|-(t_i)\rangle \sim |L\rangle$ to the target, right dot $\left|-(t_f)\right\rangle \sim |R\rangle$. Hence the transfer is successful if the TLS stays in the ground state thought the evolution.

More generally at any time instant, the state of driven TLS can be always written in the adiabatic frame[2] as:

2: which can be related to dot-basis via Eq. (5.5)

$$|\psi(t)\rangle = a_+(t)\,|+(t)\rangle + a_-(t)\,|-(t)\rangle\,. \tag{5.7}$$

For the TLS initialized in the ground state $|\psi(t_i)\rangle = |-(t_i)\rangle$, the *adiabatic evolution* is defined as

$$|a_+(t)|^2 = 1, \quad \text{for any } t, \tag{5.8}$$

Adiabatic frame

In the case of electron transfer, one assumes that for sufficiently large and negative detuning $\epsilon(t_i) \ll -t_c$, the system is initialized in the diabatic state, i.e.

$$|\psi(t_i)\rangle = |-(t_i)\rangle \approx |L\rangle\,, \tag{5.9}$$

while $|+(t_i)\rangle \approx |R\rangle$. Then the instantaneous eigenstate at time t is can be related to initial one via the operator $\hat{S}(t)$, defined through expression

$$|\pm(t)\rangle = \hat{S}(t)\,|\pm(t_i)\rangle \tag{5.10}$$

The operator $\hat{S}(t)$ is time-dependent, however it conveniently removes time-dependence from the states. Note that the arbitrary state can be now expressed as:

$$|\psi(t)\rangle = \hat{S}(t)\Big(a_-(t)\,|-(t_i)\rangle + a_+(t)\,|+(t_i)\rangle\Big) = \hat{S}(t)\,|\Psi(t)\rangle\,, \tag{5.11}$$

where $|\Psi(t)\rangle$ is the state written in the *adiabatic frame*, where only amplitudes $a_\pm(t)$ are time-dependent[3] . In this frame of reference, the Schrodinger equation reads:

3: Since in the adiabatic frame the states are no-longer time-dependent, for brevity we will avoid writing initial time argument, i.e. $|\pm\rangle \equiv |\pm(t_i)\rangle$

$$i\partial_t\,|\Psi(t)\rangle = \Big(\hat{S}^\dagger(t)\hat{H}(t)\hat{S}(t) - i\hat{S}^\dagger(t)\dot{\hat{S}}(t)\Big)\,|\Psi(t)\rangle\,, \tag{5.12}$$

where by definition the transformed Hamiltonian $\hat{S}^\dagger(t)\hat{H}(t)\hat{S}(t)$ is diagonal. In this way we have derived the effective Hamiltonian in the adiabatic frame[4] :

4: We will be using $\mathscr{H}$ and other caligraphic letters to denote quantities in the adiabatic frame.

$$\hat{\mathscr{H}}(t) = \hat{S}^\dagger(t)\hat{H}(t)\hat{S}(t) - i\hat{S}^\dagger(t)\dot{\hat{S}}(t), \tag{5.13}$$

such that effectively $i\partial_t |\Psi(t)\rangle = \hat{\mathscr{H}}(t)|\Psi(t)\rangle$.

For the relevant case of Hamiltonian (5.3) the operator $\hat{S}(t)$ corresponds to rotation around the y-axis of the TLS system and can be explicitly written as:

$$\hat{S}(t) = \exp\left(-i\hat{\varsigma}_y \frac{\vartheta(t)}{2}\right) \tag{5.14}$$

where the orbital angle $\vartheta(t) = \mathrm{ctan}(\epsilon(t)/t_c)$ can be used to generate the instantaneous eigenstates[5] from Eq. (5.5), since $|\pm(t)\rangle = \hat{S}(t)|\pm(t)\rangle$. When definition of $\hat{S}(t)$ is substituted to Eq. (5.13) we obtain Hamiltonian in the adiabatic frame of the form:

$$\hat{\mathscr{H}}(t) = \frac{\Omega(t)}{2}\hat{\varsigma}_z - \frac{\dot{\vartheta}(t)}{2}\hat{\varsigma}_y, \tag{5.15}$$

where we introduced the Pauli matrices in the adiabatic frame i.e. $\hat{\varsigma}_z = |+\rangle\langle+| - |-\rangle\langle-|$ and defined the energy gap between the eigenstates as:

$$\Omega(t) = E_+(t) - E_-(t) = \sqrt{\epsilon^2 + t_c^2}, \tag{5.16}$$

and coherent between them (in the adiabatic frame):

$$\dot{\vartheta}(t) = \frac{\dot{\epsilon} t_c}{\Omega^2(t)}. \tag{5.17}$$

From the above it is clear that evolution is adiabatic, i.e. the electron stays in the ground charge state, if the following condition is fulfilled

$$\text{Evolution is adiabatic} \iff \Omega(t) \gg \dot{\vartheta}(t), \text{ at any } t.$$

Which means that the angular velocity associated with the field rotation $\dot{\vartheta}(t)$ is sufficiently small in comparison to instantaneous splitting $\Omega(t)$.

5: Note that initially $\epsilon(t_i) \ll -t_c$ we have $\vartheta(t_i) \approx \pi$ and $|-(t_i)\rangle \approx |L\rangle$, while at the end of the sweep $\epsilon(t_f) \gg t_c$, $\vartheta(t_f) \approx 0$ and hence $|-(t_f)\rangle \approx -|R\rangle$. We assume here positive value of t_c, such that at zero-detuning, i.e. $\vartheta = \pi/2$ the ground state is an anti-symmetric $|-(0)\rangle = |L\rangle - |R\rangle$, while the excited state is an symmetric $|-(0)\rangle = |L\rangle + |R\rangle$, combination of diabatic orbitals.

Landau-Zener formula

We now relate the DQD system with the Landau-Zener model of avoided crossing[6] , which allows to compute probability of staying in the ground adiabatic state, when the system is driven through avoided crossing, i.e. local minimum of the aidabatic gap $\Omega(t)$. The model Hamiltonian is mathematically identical to $\hat{H}_o(t)$, given by Eq. (5.3), while the detuning between the dots energy levels is assumed to be linear function of time,[7] i.e. $\epsilon = vt$, where v is the detuning sweep rate. For such a system, initialized in the ground state the probability of occupying excited state at the end of the sweep is given by the Landau-Zener Formula

$$Q_{\mathrm{LZ}} = p_1 \approx |a_+(\infty)|^2 = \exp\left(-\frac{\pi}{2}\frac{t_c^2}{v}\right). \tag{5.18}$$

This result can be derived via differential equations using asymptotic expansion of parabolic cylinder function [116, 164]. Here we follow a much simpler approach and compute the limiting cases of almost diabatic and almost adiabatic transition.

6: Although Landau-Zener model assumes the drive is uniaxial and linear in time, it can be applied to broad spectrum of physical systems, in which energy of two energy levels can be tuned into resonance $E_0(\epsilon_0) = E_1(\epsilon_0)$ using some parameter $\epsilon = \epsilon_0$, around which the $\partial_t \epsilon(t) \neq 0$. In presence of a finite coupling between the levels $\langle 0|\hat{H}|1\rangle \equiv t_c$ the degeneracy is lifted and the states hybridized into linear combination of $|0\rangle$ and $|1\rangle$ states split by the energy t_c.

7: Even if the assumption of linear sweep does not hold, the sweep can be usually linearize in vicinity of avoided crossing, the location of which is set to $\epsilon_0 = 0$.

Perturbative derivation of L-Z formula

In the first case we assume the transition is almost diabatic, i.e. we write equations of motion using Hamiltonian $\hat{H}_o(t)$:

$$\dot{c}_R(t_f) = \frac{t_c}{2} e^{i\int_{t_i}^{t_f} \mathrm{d}t' \epsilon(t')} c_L(t), \tag{5.19}$$

In the leading order of perturbation theory we can use the initial condition $c_L(t_i) = 1$, $c_R(t_i) = 0$ and compute first order correction as:

$$\delta c_R(t_f) = \frac{t_c}{2} \int_{t_i}^{t_f} e^{-ivt^2/2} \mathrm{d}t \approx t_c \sqrt{\frac{\pi}{2iv}} = \sqrt{\frac{\pi t_c^2}{2v}} e^{i\alpha}, \tag{5.20}$$

where in the integral we extended the limits to infinity. The $\sqrt{i} = e^{-i\pi/4}$ is largest possible value of so-called Stokes phase α, the additional phase shift acquired by the system during Landau-Zener transition. In many observables including probability of occupying excited state, the Stokes phase is not relevant since such probability is given by:

$$|\delta c_R(t_f)|^2 = \frac{t_c^2 \pi}{2v} \tag{5.21}$$

this result is consistent with the leading order expansion of Q_{LZ} given in Eq. (5.18) for $t_c^2/v \ll 1$.

In the opposite case we use the adiabatic frame, where both the energy gap $\Omega(t) = \sqrt{t_c^2 + \epsilon^2}$ and the coupling between adiabatic states $\dot{\vartheta} = v t_c/\Omega(t)^2$ are time-dependent, and the evolution in the adiabatic frame is governed by the Hamiltonian $\hat{\mathscr{H}}(t)$ given in Eq. (5.15). In such case the equation of motion for the amplitude of ending up in the excited state a_+ is given by:

$$\dot{a}_+(t) = \frac{1}{2} \dot{\vartheta} a_-(t) \exp\left(i \int_{t_0}^{t} \Omega(t') \mathrm{d}t' \right) \tag{5.22}$$

Assuming the evolution starts in the ground energy state, in the leading order we can set $a_-(t) = 1$ and compute first order correction to the occupation of excited state $|\delta a_+(t)|^2$ as:

$$|\delta a_+(t)|^2 = \frac{1}{4} \left| \int_{-\infty}^{t} \dot{\vartheta}(t_1) \exp\left(i \int_{-\infty}^{t_1} \Omega(t') \mathrm{d}t' \right) \right|^2 \tag{5.23}$$

We compute the final occupation of excited state by setting $t \to \infty$ and assuming the relevant evolution takes place around avoided crossing, where $\Omega(t) \approx t_c$. In this way the $\delta a_+(\infty)$ can be approximated by the Fourier transform of angular velocity $\dot{\vartheta}(t)$, evaluated at $\Omega = t_c$, i.e.

$$\delta a_+(\infty) = \frac{1}{2} e^{i\phi_0} \int_{-\infty}^{\infty} \frac{\exp\left[i \frac{t_c^2}{v} \left(\frac{vt}{t_c} \right) \right]}{1 + (\frac{vt}{t_c})^2} \frac{v \mathrm{d}t}{t_c} = \frac{\pi}{2} \exp\left(-\frac{t_c^2}{v} + i\phi_0 \right), \tag{5.24}$$

where ϕ_0 is some complex phase, which does not modify leading order correction to the probability of non-adiabatic transfer:

$$\delta Q_{LZ} = \delta p_0 = |\delta a_+(\infty)|^2 = \frac{\pi^2}{4} \exp\left(-\frac{2t_c^2}{v} \right). \tag{5.25}$$

In Fig. 5.2 we compare Landau-Zener formula against almost-diabatic and almost-adiabatic approximations.

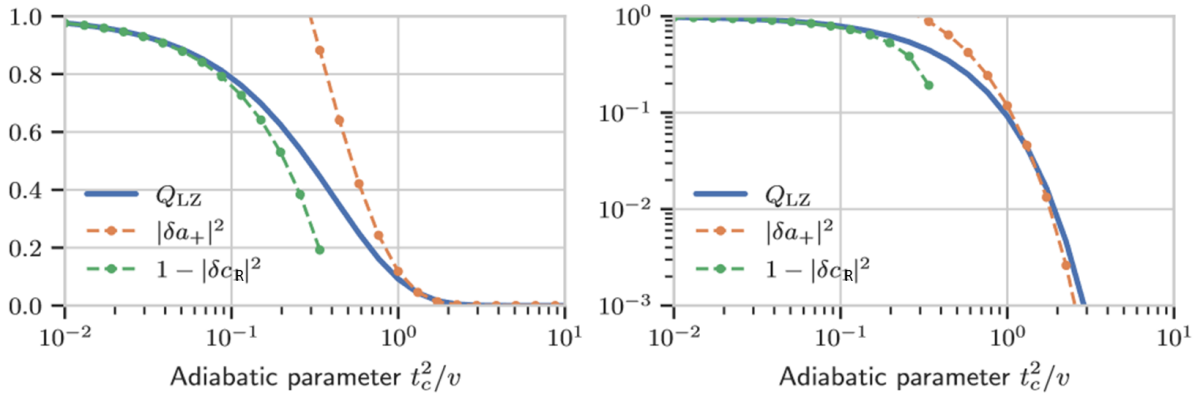

Figure 5.2: Comparison between the Landau-Zener formula $Q_{\mathrm{LZ}} = \exp(-\pi t_c^2/2v)$ [97] (blue line) and parturbative expression in the almost diabatic $t_c^2 \ll v$ (Eq. (5.21) and orange line) and almost adiabatic $t_c^2 \gg 1$ (Eq. (5.25) and green line) limits. We show the result as a function of dimensionless adiabatic parameter t_c^2/v in the linear scale (left) and semi-logarithmic scale (right).

Adiabatic-impulse approximation

For the purpose of the thesis it is convenient to introduce here adiabatic-impulse model, which was formulated in [165], and is equivalent to transfer matrix formalism [166]. In the adiabatic-impulse approach the evolution during L-Z drive is separated into three parts and can be written as:

$$\hat{\mathcal{U}}(-t_i, t_i) = \hat{\mathcal{A}}(t_i, \delta t)\,\hat{\mathcal{T}}\,\hat{\mathcal{A}}(-\delta t, -t_i), \tag{5.26}$$

where the operator:

$$\hat{\mathcal{A}}(t_f, t_i) = \exp\left(-\frac{i}{2}\int_{t_i}^{t_f}\Omega(\tau)\hat{\zeta}_z\right) = \begin{bmatrix} e^{-\frac{i}{2}\int_{t_i}^{t_f}\Omega(\tau)} & 0 \\ 0 & e^{\frac{i}{2}\int_{t_i}^{t_f}\Omega(\tau)} \end{bmatrix}, \tag{5.27}$$

corresponds to the adiabatic part of the evolution, during which the occupation of instantaneous states $|a_\pm|^2$ are constant and the amplitudes undergoes only phase evolution, i.e. $a_\pm(t) = |a_\pm|\exp\{\mp\frac{i}{2}\int\Omega(\tau)\}$. The mixing between the adiabatic states takes place at the avoided crossing,[8] which is modelled by the transfer matrix in the adiabatic frame:

$$\hat{\mathcal{T}} = \begin{bmatrix} i\sqrt{1-Q_{\mathrm{LZ}}}e^{-i\alpha_s} & -\sqrt{Q_{\mathrm{LZ}}} \\ \sqrt{Q_{\mathrm{LZ}}} & -i\sqrt{1-Q_{\mathrm{LZ}}}e^{i\alpha_s} \end{bmatrix}, \tag{5.28}$$

where Q_{LZ} is the Landau-Zener probability of non-adiabatic transition, while α_s is the Stokes phase given by

$$\alpha_s = \pi/4 + \zeta_{\mathrm{LZ}}\ln(\zeta_{\mathrm{LZ}} - 1) + \arg\Gamma(1 - i\zeta_{\mathrm{LZ}}) \tag{5.29}$$

with $\zeta_{\mathrm{LZ}} = t_c^2/4v$, such that $Q_{\mathrm{LZ}} = \exp(-2\pi\zeta_{\mathrm{LZ}})$. In most cases we will concentrate on the nearly adiabatic $\zeta_{\mathrm{LZ}} \gg 1$ or nearly diabatic $\zeta_{\mathrm{LZ}} \gg 1$ transfer, where the Stokes phase reduces to $\alpha_s = 0$ and $\alpha_s = \pi/4$ respectively. Additionally the Stokes phase has a deterministic origin and will be deliberately neglected in all analytical studies of the environmental

8: Note that δt denotes an infinitesimal time before and after avoided crossing.

noise considered in this thesis. It will naturally appear in all numerical integration of equations of motion, which will certify correctness of this approach. The adiabatic-impulse model will be particularity relevant, when we compute correction to adiabatic transfer of the excited spin state (see Chapter 11).

Phase gauge

We finally briefly discuss the phase gauge associated with the transfer matrix $\hat{\mathcal{T}}$. To show its origin we assume adiabatic transition, i.e. set Q_{LZ} to zero. In such case the equal superposition state at $t_i < 0$, i.e. $\frac{1}{\sqrt{2}}(|+\rangle + |-\rangle)$ is transformed into:

$$\hat{\mathcal{T}} \frac{|+\rangle + |-\rangle}{\sqrt{2}} \to i \frac{|+\rangle - |-\rangle}{\sqrt{2}}, \tag{5.30}$$

at the time $t_f > 0$, which introduces relative phase shift between the two states in the superposition equal to $e^{i\pi} = -1$, and the global phase of i which can be ignored. The origin of the former can be understood by looking at the exact form of instantaneous states, since from Eq. (5.5)

$$\begin{aligned} |+(-\infty)\rangle = |R\rangle \to |+(+\infty)\rangle = |L\rangle\,, \\ |-(-\infty)\rangle = |L\rangle \to |-(+\infty)\rangle = -|R\rangle\,, \end{aligned} \tag{5.31}$$

The change of the relative phase between ground and excited state is needed to ensure that the adiabatic transition is unitary.

Complex tunnel coupling

Finally we comment on the phase relation between the terms in Landau-Zener transition. In the typical Landau-Zener model coupling between diabatic states is assumed to be real. This is because in most application phase relation between t_c and ϵ has no direct significance[9] . For instance if detuning is set to be real, and tunnel coupling complex, i.e. $t_c = |t_c|e^{i\theta}$, the θ can be incorporated into additional contribution to Stokes phase, see (5.20). Additionally in this thesis we aim at computing dephasing of the driven systems due to averaging over random evolution, and from this perspective deterministic phases of tunnel coupling and Stokes phase are not essential. Thus for simplicity of the analysis we will treat tunnel coupling as real and cross-check the result with numerical simulation.

9: The complex tunnel coupling might originate from the presence of external magnetic field (Peierls substitution) and become relevant in the case of the electron shuttling in the closed loops [94]

5.2 Classical noise approach

We now introduce the presence of the environment and show how it can modify adiabaticity of the transfer and coherence between the adiabatic levels. For illustration purposes we start this section by considering effects of classical noise in both dots detuning $\delta\epsilon(t)$ and coupling $\delta t_c(t)$, such that the driven Hamiltonian of TLS can be written as:

$$\hat{H}_{\mathrm{o}}(t) = \frac{\epsilon(t) + \delta\epsilon(t)}{2}\hat{\sigma}_z + \frac{t_c + \delta t_c(t)}{2}\hat{\sigma}_x, \tag{5.32}$$

where in contrast to previously considered dephasing effects for undriven case, $\delta\epsilon(t)$ and $\delta t_c(t)$ are time-dependent. Next for each realization of $\delta\epsilon$ and δt_c and at every time-instant we move to adiabatic frame, which similarly to Eq. (5.14) is generated by the operator $\hat{S}(t) = \exp\{-i\hat{\sigma}_y\vartheta(t)/2\}$, where the noise-dependent adiabatic angle is given by the expression:

$$\cot\vartheta(t) = \frac{\epsilon(t) + \delta\epsilon(t)}{t_c + \delta t_c(t)}. \tag{5.33}$$

such that the effective noisy Hamiltonian in the adiabatic frame[10] reads

10: see Eq. (5.13) for definition of adiabatic frame.

$$\mathscr{H}(t) = \frac{1}{2}\Omega(t)\hat{\varsigma}_z - \frac{1}{2}\dot{\vartheta}(t)\hat{\varsigma}_y, \tag{5.34}$$

where the parameters are given by

$$\begin{aligned}\Omega(t) &= \sqrt{(\epsilon[t] + \delta\epsilon[t])^2 + (t_c + \delta t_c[t])^2},\\ \dot{\vartheta}(t) &= \left(\frac{t_c + \delta t_c[t]}{\Omega^2[t]}\right)^2 \frac{\partial}{\partial t}\left(\frac{\epsilon(t) + \delta\epsilon[t]}{t_c + \delta t_c[t]}\right).\end{aligned} \tag{5.35}$$

Let us now investigate in what way fast and slow fluctuations of parameters affects adiabaticity and coherence between the orbital levels.

Weak coupling limit

Using an assumption that we commonly employ in this thesis, the noise contribution is weak in comparison to other deterministic energy scales.[11] This allows us to compute corrections in the first order in $\delta\epsilon, \delta t_c$ i.e. $\Omega(t) = \Omega_0(t) + \delta\Omega(t)$ and $\vartheta(t) = \vartheta_0(t) + \delta\vartheta(t)$ where $\Omega_0(t) = \sqrt{\epsilon^2 + t_c^2}$. Explicitly the leading order corrections read:

11: In particular to t_c, which gives the minimum of $\Omega(t)$.

$$\begin{aligned}\delta\Omega(t) &= \frac{\epsilon(t)\delta\epsilon(t) + t_c\delta t_c(t)}{\Omega_0(t)} = \sin\vartheta_0(t)\delta t_c(t) + \cos\vartheta_0(t)\delta\epsilon(t)\\ \delta\dot{\vartheta}(t) &= -2\dot{\vartheta}(t)\frac{\delta\Omega(t)}{\Omega_0(t)} + \frac{\dot{\epsilon}(t)\delta t_c(t)}{\Omega_0^2(t)} + \sin\vartheta_0(t)\frac{\delta\dot{\epsilon}(t)}{\Omega_0(t)} - \cos\vartheta_0(t)\frac{\delta\dot{t}_c(t)}{\Omega_0(t)},\end{aligned} \tag{5.36}$$

The random modifications of angular velocity $\delta\vartheta(t)$ corresponds to the transverse noise in the instantaneous basis that can cause inelastic transitions between the states $|\pm(t)\rangle$ (see Chapter 3 for dissipation due to transverse noise in undriven case), while the fluctuations of energy gap $\delta\Omega(t)$ can be thought of as the longitudinal noise in the instantaneous basis, which leads to dephasing between the instantaneous states (in analogy to Chapter 4 for undriven case).

Effective non-adiabaticity

First we discuss correction to the occupation probabilities $|\delta a_\pm|^2$, which can be understood as the *effective non-adibaticity*. This can be seen as the analogue of polarization, but in the instantaneous basis[12] , i.e.

12: To be consistent orbital polarization is in the instantaneous basis we will use the written symbol $\mathfrak{L}$

$$\mathfrak{L}(t) = \mathrm{Tr}\{\hat{\varsigma}_z\varrho(t)\}, \tag{5.37}$$

note that if $\mathcal{I}(t) = \text{const}$ the evolution is adiabatic. We will now define effective adiabaticity as:

$$\left|\mathcal{I}(t_f) - \mathcal{I}_o(t_i)\right| \leqslant \delta, \tag{5.38}$$

for sufficiently small $\delta \ll 1$.[13]

13: Note that the effective adiabaticity does not mean that $\mathcal{I}(t)$ was constant during the transfer. In particular, possibility of relaxation-aided transfer can significantly decrease excitation probability obtained using isolated L-Z model.

Low-frequency noise

We concentrate now on the first two contributions to $\delta\dot{\vartheta}(t)$, which contrary to the term involving noise derivative are non-negligible even in the case of slow noise. In contrast to the undriven case, we show here that slow noise in presence of the drive can also modify $\mathcal{I}$.

The first term comes directly from the fluctuations of the gap,[14] ,

$$\frac{v t_c}{(\Omega_0 + \delta\Omega_0)^2} \approx \dot{\vartheta}_0\left(1 - \frac{2\delta\Omega}{\Omega_0}\right). \tag{5.39}$$

14: It can be also understood using a geometrical picture, where coupling between the instantaneous states is interpreted as the angular frequency of rotating magnetic field. In such case modification of the energy (radius) affects angular velocity $\dot{\vartheta}(t)$ even for unchanged sweep rate v

In particular, in vicinity of the avoided crossing,[15] where its value is the largest, it can combined with the second term of Eq. (5.36), which together give:

$$\delta\dot{\vartheta}_{\text{slow}} \approx -\dot{\vartheta}\frac{\delta t_c}{t_c}. \tag{5.40}$$

15: Note that around avoided crossing, we have $\vartheta \approx \pi/2\ \Omega_0 \approx t_c$ and $\delta\Omega \approx \delta t_c$

Clearly the modification of effective non-adiabaticity due to slow noise is related to tunneling fluctuations only, as the slow detuning noise $\delta\epsilon$ amounts to a shift of the initial and final detuning point, that is irrelevant for the adiabatic evolution.

When the fluctuations $\delta t_c(t)$ are slow enough to be considered constant on the timescale at which $\dot{\vartheta}$ is non-negligible, one can compute their effect by directly averaging of Landau-Zener formula over fluctuations of the constant gap, i.e.

$$\langle Q_{\text{LZ}}\rangle = \left\langle \exp\left(-\frac{\pi}{2}\frac{(t_c + \delta t_c)^2}{\hbar v^2}\right)\right\rangle = \sqrt{\frac{1}{\alpha}}\exp\left(-\frac{\pi}{2}\frac{t_c^2}{\alpha v}\right), \tag{5.41}$$

where $\alpha = 1 + \pi\sigma_{\dot{t}_c}^2/v$ is dimensionless constant, which modifies the sweep rate. More involved analysis of the influence of low-frequency noise on the adiabatic transition can be found in [115, 116].

High-frequency noise

We now analyze the last two terms in the expression for $\delta\dot{\vartheta}(t)$, which we relate to dissipative evolution of driven TLS.[16] In the adiabatic frame they can be seen as purely transverse noise $\hat{\mathcal{V}}_\perp(t) = \frac{1}{2}\xi_\perp(t)\hat{\varsigma}_y$, which at each time instant can be written as:

16: The derivation follows the results from [2]

$$\xi_\perp(t) = \frac{\delta\dot{\epsilon}(t)}{\Omega_0(t)}\sin\vartheta_0(t) - \frac{\delta\dot{t}_c(t)}{\Omega_0(t)}\cos\vartheta_0(t). \tag{5.42}$$

Using the above, the equations of motion for the amplitude of being in the excited state is given by:

$$a_+(t_f) = \frac{-i}{2}\int_{t_i}^{t_f} \mathrm{d}t\, \xi_\perp(t) a_-(t) e^{-i\int_{t_i}^{t}\Omega_0(t)+\delta\Omega(t)\mathrm{d}t}. \tag{5.43}$$

In leading order of perturbation theory the occupation of the excited state[17] at time t_f, can be computed by replacing $a_-(t) = 1$ and writing

$$Q = |\delta a_+(t_f)|^2 \approx \frac{1}{4}\int_{t_i}^{t_f}\int_{t_i}^{t_f} \mathrm{d}t_1\mathrm{d}t_2 \langle \xi_\perp(t_1)\xi_\perp(t_2)\rangle e^{-i\int_{t_2}^{t_1}\Omega_0(t)} \tag{5.44}$$

where we have neglected correction to adiabatic gap, as it is a higher order correction. Now we substitute expression for the transverse noise (5.42) and conveniently separate the correction to the occupaiton of the excited state as:

$$\delta Q \approx \delta Q_{\epsilon\epsilon} + \delta Q_{\epsilon t_c} + \delta Q_{t_c\epsilon} + \delta Q_{t_c t_c}, \tag{5.45}$$

where each term is proportional to respective correlation functions of noise derivatives[18] $Q_{xy} \propto \langle \delta\dot{x}\delta\dot{y}\rangle$, where $x, y = \epsilon, t_c$. In terms of spectral density of the noise the corrections read:

$$\delta Q_{xy} = \frac{1}{8\pi}\int_{-\infty}^{\infty} S_{xy}(\omega) F_x(\omega) F_y^*(\omega), \tag{5.46}$$

where the filtering functions are defined as:

$$\begin{aligned} F_\epsilon(\omega) &= \int_{t_i}^{t_f} \sin\vartheta_0 \frac{\omega}{\Omega_0(t)} \exp\left\{ i\omega\tau + i\int_0^\tau \Omega_0(\tau')\mathrm{d}\tau' \right\}\mathrm{d}\tau \\ F_{t_c}(\omega) &= \int_{t_i}^{t_f} \cos\vartheta_0 \frac{\omega}{\Omega_0(\tau)} \exp\left\{ i\omega\tau + i\int_0^\tau \Omega_0(\tau')\mathrm{d}\tau' \right\}\mathrm{d}\tau. \end{aligned} \tag{5.47}$$

We now move the limits of the integral $t_i \to -\infty$ and $t_f \to \infty$, and compute the integral in the leading order of stationary phase approximation[19] as:

$$\begin{aligned} F_\epsilon(\Omega_0) &= 2\frac{t_c}{\Omega_0}\cos(\varphi(\tilde{\tau}) - \pi/4)\sqrt{\frac{2\pi}{v}}\left(1 - \frac{t_c^2}{\Omega_0^2}\right)^{-1/4} \\ F_{t_c}(\Omega_0) &= -2i\frac{v\tilde{\tau}}{\Omega_0}\sin(\varphi(\tilde{\tau}) - \pi/4)\sqrt{\frac{2\pi}{v}}\left(1 - \frac{t_c^2}{\Omega_0^2}\right)^{-1/4}, \end{aligned} \tag{5.48}$$

in which we defined time at which the phase $\varphi(\tilde{\tau}) = \Omega_0\tilde{\tau} + \int_0^{\tilde{\tau}}\Omega_0(\tau')$ is stationary as $\tilde{\tau} = \sqrt{\Omega_0^2 - t_c^2/v^2}$. In the process the frequency became identified with the negative of adiabatic gap[20] i.e. $\omega = -\Omega(\tau)$.

Now in the diagonal contributions we replace rapidly oscillating phase $|F_\epsilon|^2 = \cos^2(\varphi(\tilde{\tau}) - \pi/4) \approx 1/2$ and $|F_{t_c}|^2 \propto \sin^2(\varphi(\tilde{\tau}) - \pi/4) \approx 1/2$ with its average, which allows to rewrite the leading order contribution to effective non-adiabaticity[21] as:

17: Which for the DQD transfer can be identified with the transfer error Q

18: The correlation function of the derivative of the noise can be related to spectral density of the noise, since:

$$S_{\dot{x}\dot{x}}(\omega) = \omega^2 S_{xx}(\omega).$$

and hence

$$\langle \delta\dot{x}(t_1)\delta\dot{y}(t_2)\rangle = \int \frac{\mathrm{d}\omega}{2\pi}\omega^2 S_{xy}(\omega) e^{-i\omega(t_1-t_2)}.$$

19: see the appendix of our work [2] for more detailed derivation

20: Note that the spectrum evaluated at the negative frequence is consistent with Chapter 3, where negative frequency corresponded to absorption of energy quanta.

21: Note that polarization is related to probability of excited state $\delta\mathfrak{X} = 2|\delta a_+|^2$ as a reminder

$$\delta Q_{\epsilon\epsilon} = \frac{1}{2v}\int_{t_c}^{\infty} \frac{S_\epsilon(-\Omega)}{\sqrt{1-t_c^2/\Omega^2}}\left(\frac{t_c^2}{\Omega^2}\right)\mathrm{d}\Omega$$
$$\delta Q_{t_c t_c} = \frac{1}{2v}\int_{t_c}^{\infty} S_t(-\Omega)\sqrt{1-t_c^2/\Omega^2}\mathrm{d}\Omega. \tag{5.49}$$

At this point it is convenient to change the integration variable to time,[22] which results in:

$$\delta Q_{\epsilon\epsilon} = \frac{1}{4}\int_{t_i}^{t_f} S_\epsilon(-\Omega[t])\,\sin^2\vartheta(t)\mathrm{d}t$$
$$\delta Q_{t_c t_c} = \frac{1}{4}\int_{t_i}^{t_f} S_{t_c}(-\Omega[t])\,\cos^2\vartheta(t)\mathrm{d}t, \tag{5.50}$$

22: First one can do it for positive times $t = (\Omega^2 - t_c^2)/v$ and then use the fact that the integral is symmetric under replacing $t \to -t$.

where $\sin\vartheta(t) = t_c/\Omega(t)$ and $\cos\vartheta = \epsilon(t)/\Omega(t)$. In Sec. 5.3 we will use adiabatic Master equation to show that the above result has the structure of the integrated excitation rate, where $\Gamma_{+,\epsilon}(t) = \frac{1}{4}S_\epsilon(\Omega[t])\sin^2\vartheta(t)$ and analogously for $\Gamma_{+,t_c}(t)$. We highlight that level of noise-induced non-adiabaticity δQ is expected to increase for slower sweeps (i.e. smaller v) which can be related to increasing time spent around the avoided crossing where noise-induced accelerations of the sweep rate can occur. This stands in contrast to Landau-Zener model without the noise, where faster sweeps results in more non-adiabatic transfer.

Cross-correlation correction

We finally comment on the cross correlation term, which has the general form:

$$\delta Q_{\epsilon t_c} + \delta Q_{t_c\epsilon} = \frac{1}{2}\int_{-\infty}^{\infty}[S_{\epsilon t_c}(\omega) - S_{t_c\epsilon}(\omega)]F_\epsilon(\omega)F^*_{t_c}(\omega). \tag{5.51}$$

i.e. it vanishes unless $S_{t_c\epsilon}(\omega) \neq S_{\epsilon t_c}(\omega)$ meaning the cross-correlation spectrum has non-zero imaginary part. Non-real spectrum can for instance emerge if the fluctuations in $\delta\epsilon$ and δt_c have causal correlation [151]. However even if this is the case, we stress out that for the non-diagonal correction the rapidly oscillating phase has zero-average $F_\epsilon(\omega)F_{t_c}(\omega) \propto \cos(2\varphi)$, and for this reason is most likely to be negligible.

Dephasing

After considering corrections to effective adiabaticity we discuss now how the relative phase between the instantaneous states can be modified during DQD transition. We assume that the longitudinal noise affects the relative phase only away from avoided crossings, i.e. in the "adiabatic" part of adiabatic-impulse approximation from Sec. 5.1. We concentrate on the relevant case, where the non-zero population of excited state is generated by the transition through avoided crossing, such that the state of the TLS just after avoided crossing reads:

$$|\psi(0+\delta t)\rangle = \sqrt{Q}\,|+(\delta t)\rangle + \sqrt{1-Q}e^{i\phi_0}\,|-(\delta t)\rangle\,, \tag{5.52}$$

with some complex, deterministic phase $e^{i\phi_0}$.[23] Now when detuning sweep continues the probability of occupying instantaneous states remains constant, but the additional phase between ground and excited state is acquired $\phi(t) - \phi_0 = \int_{\delta t}^{t_f} \Omega(t)$, where $\Omega(t) = \Omega_0(t) + \delta\Omega(t)$ with the noise-dependent correction given by the Eq. (5.36).

23: for instance related to Stokes phase introduced in the transfer matrix formalism in Eq. (5.28)

Let us look now on the coherence between ground and excited adiabatic states, averaged over fluctuations of classical noise, which we define as:

$$\mathcal{W}'(t) = 2\,\mathrm{Tr}\{\hat{\xi}_- \varrho'(t)\} = -\mathcal{W}(0)\left\langle \exp\left(-i\int_{\delta t}^{t_f} \delta\Omega(t)\right)\right\rangle. \tag{5.53}$$

Following quasitatic noise approximation from Sec. 4.4, the decrease of $\mathcal{W}'(t)$ can be related to:

$$\left\langle \exp\left(-i\int_0^t \delta\Omega(t)\right)\right\rangle \approx \exp\left(-\frac{1}{2}\Big[\tilde{\sigma}_\epsilon \int_0^{t_f} \cos\vartheta_0\Big]^2 - \frac{1}{2}\Big[\tilde{\sigma}_{t_c}\int_0^{t_f}\sin\vartheta_0\Big]^2\right), \tag{5.54}$$

where we have set $\delta t \to 0$ and used expression for $\delta\Omega(t)$ from Eq. (5.36). The power of quasistatic noise in detuning $\tilde{\sigma}_\epsilon^2$ and tunnel coupling $\tilde{\sigma}_{t_c}^2$ were computed using integral from Eq. (4.43). The integrals are related to the noiseless orbital angle ϑ_0, defined via:

$$\cos\vartheta_0(t) = \frac{\epsilon(t)}{\Omega_0(t)}, \qquad \sin\vartheta_0(t) = \frac{t_c}{\Omega_0(t)}, \tag{5.55}$$

which allows us to compute

$$\begin{aligned}\int_0^{t_f}\cos\vartheta_0 &= \frac{t_c}{v}\left(\sqrt{1+\left(\tfrac{vt_f}{t_c}\right)^2}-1\right)\approx t_f\\ \int_0^{t_f}\sin\vartheta_0 &= \frac{t_c}{v}\mathrm{arctanh}\left(\frac{vt_f}{\Omega(t_f)}\right),\end{aligned} \tag{5.56}$$

where in the first expression we have used the fact that the final detuning is typically much larger then tunnel coupling, i.e. $vt_f/t_c \gg 1$. The above shows that the orbital dephasing is expected to be dominated by the detuning noise. In particular after detuning sweep the coherence between the orbital states can be approximated as:

$$|\mathcal{W}/\mathcal{W}_0| = \left\langle \exp\left(-i\int_0^{t_f}\delta\Omega(t)\right)\right\rangle \approx \exp\left(-\frac{1}{2}\sigma_\epsilon^2 t_f^2\right), \tag{5.57}$$

5.3 Adiabatic master equation

After considering effects of classical noise included in the Landau-Zener Hamiltonian we now turn to a more standard treatment of the open, driven quantum system in the form of adiabatic Master equation (AME) [109–111]. By design such an approach is more suitable to dissipative evolution during adiabatic drive and less for dephasing effects due to low-frequency noise.

Adiabatic Bloch-Redfield equation

We start be deriving the adiabatic version of Bloch-Redfield equation, where to some extent we will follow steps of undriven derivation presented in Sec. 3.2. We concentrate on the orbital drive with the general Hamiltonian

$$\hat{H}(t) = \hat{H}_o(t) + \hat{V}_{oe} + \hat{H}_e. \tag{5.58}$$

24: which in our case corresponds to adiabatically driven DQD system

In the above $\hat{H}_o(t)$ is the Hamiltonian of driven system,[24] $\hat{V}_{oe}$ denotes its coupling to environment while $\hat{H}_e$ is the Hamiltonian of the environment, with the latter assumed to be in equilibrium state $\rho_e = e^{-\beta\hat{H}_e}/\mathcal{Z}$, where $\mathcal{Z} = \mathrm{Tr}\left\{e^{-\beta\hat{H}_e}\right\}$ is the partition function.

We now move to adiabatic, picture using operators $S(t)$ from Eq. (5.10), which diagonalize the driven part of the Hamiltonian:

$$\hat{S}^\dagger \hat{H}_o \hat{S} = \frac{\Omega(t)}{2}\hat{\varsigma}_z \equiv \hat{\mathscr{H}}_0(t), \tag{5.59}$$

where $\hat{\mathscr{H}}_0(t)$ denotes Hamiltonian diagonal in the adiabatic frame, which we express in terms of adiabatic Pauli operators $\hat{\varsigma}_z\,|\pm\rangle = \pm\Omega(t)\,|\pm\rangle$.

Let us now repeat initial steps of the derivation of Bloch-Redfield equation (see Sec. 3.2), this time in the adiabatic frame, in which $\hat{\varrho}_q(t) = \hat{S}(t)\hat{\rho}_q(t)\hat{S}^\dagger(t)$. After Born-Markov approximation (Eq. (3.27)) and in the Schrodinger picture (Eq. 3.29) the equation for density matrix of the driven system is given by:

$$\frac{\partial}{\partial t}\hat{\varrho}_o(t) = -i\left[\hat{\mathscr{H}}(t), \hat{\varrho}_o(t)\right] - \mathrm{Tr}_e\Bigg\{ \left[\tilde{\mathscr{V}}_{oe}(t), \int_0^\infty \mathrm{d}r\, \Big(\hat{\mathscr{U}}_o(t, t-r)\tilde{\mathscr{V}}_{oe}(t-r)\hat{\mathscr{U}}_o^\dagger(t, t-r)\Big)\hat{\varrho}_q(t)\right] + (h.c.)\Bigg\}, \tag{5.60}$$

where $\hat{\mathscr{H}}(t) = \hat{\mathscr{H}}_0(t) - i\hat{S}^\dagger(t)\frac{\partial}{\partial t}\hat{S}(t)$, $\tilde{\mathscr{V}}_{oe}(t) = e^{i\hat{H}_e t}\hat{\mathscr{V}}_{oe}(t)e^{-i\hat{H}_e t}$, with $\hat{\mathscr{V}}_{oe} = \hat{S}^\dagger\hat{V}_{oe}\hat{S}$, being the coupling in the adiabatic frame. The central approximation of AME is related to free-evolution operator inside the dissipative part, which is approximated as:

$$\begin{aligned}\hat{\mathscr{U}}_o(t, t-r) &= \mathscr{T}\exp\left(-i\int_{t-r}^{t}\hat{\mathscr{H}}_0(t') + i\hat{S}(t')\dot{\hat{S}}^\dagger(t')\right) \\ &\approx \exp\left(-i\int_{t-r}^{t}\hat{\mathscr{H}}_0(t')\right) \approx \exp\left(-i\hat{\mathscr{H}}_0(t)\,r\right).\end{aligned} \tag{5.61}$$

This is equivalent to saying that the coupling between adiabatic levels is negligible on the time scale of r which is not larger then the correlation time of the bath. Finally the second approximation assumes, that the on the same timescale r the rotation of the adiabatic frame is negligible, which means that together:

$$\hat{\mathscr{U}}_a(t, t-r)\tilde{\mathscr{V}}_{ae}(t-r)\hat{\mathscr{U}}_a^\dagger(t, t-r) \approx e^{-i\hat{\mathscr{H}}_0(t)\,r}\tilde{\mathscr{V}}_{ae}(t)e^{i\hat{\mathscr{H}}_0(t)\,r} \equiv \tilde{\mathscr{V}}_{ae}(t, -r),$$

where we have treated t as parameter and moved to the interaction picture with respect to approximately constant on the relevant timescale

$\hat{\mathscr{H}}_0(t)$. The above operator can be written explicitly as:

$$\tilde{\mathscr{V}}_{ae}(t,-r) = \sum_{ij} \tilde{V}_e^{'ij}(t)\,|i\rangle\langle j|\,e^{i\Omega_{ij}(t)r}, \tag{5.62}$$

where $\Omega_{ij}(t) = E_i(t) - E_j(t)$ are the energies of adiabatic states $|i(t)\rangle$, $|j(t)\rangle$ and $\tilde{V}_e^{'ij}(t)$ it is the operator in the interaction picture with respect to bath Hamiltonian, that acts in the environmental degrees of freedom. Up to this moment the above derivation can be used for general dimensions of the driven system.

Two-level system

We concentrate now on the two-level system coupled to environment via the two-axis coupling[25] :

$$\hat{V}_{oe} = \frac{1}{2}\left(\hat{V}_x\hat{\sigma}_x + \hat{V}_z\hat{\sigma}_z\right). \tag{5.63}$$

25: The lack of $\hat{V}_y$ is chosen to reflect previously considered fluctuations of tunnel coupling and detuning between DQD system

In contrast to previously used TLS-environment transverse coupling Eq. (2.12), for the illustration proposes we used here Pauli matrices instead of ladder operators, however one can always translate between two representations using identities $\hat{V}_x = \frac{1}{2}(\hat{V}_+ + \hat{V}_-)$ with $\hat{V}_+ = \hat{V}_-$, such that $\hat{V}_y = \frac{1}{2i}(\hat{V}_+ - \hat{V}_-) = 0$. We additionally assume each coupling is statistically independent[26] and hence $\mathrm{Tr}_e\{\hat{V}_k(s)\hat{V}_l(0)\rho_e\} = \delta_{kl}C_{kl}(s)$. With the approximations above, the Bloch-Redfield AME have the form:

26: Such independence can be caused by different physical origin of the couplings. Also, as we showed in Sec. 5.2 the cross-term between $\hat{V}_x$ and $\hat{V}_z$ is typically much weaker then the auto-correlation terms

$$\dot{\rho}_o(t) = -i\left[\hat{\mathscr{H}}(t), \hat{\rho}_o(t)\right] - \sum_{k=x,z}\left[\hat{S}^\dagger(t)\hat{\sigma}_k\hat{S}(t), \hat{\mathscr{R}}_k\varrho_q(t)\right] + h.c. \tag{5.64}$$

where we have defined the adiabatic version of Bloch-Redfield tensor (vector) as:

$$\hat{\mathscr{R}}_k(t) = \frac{1}{4}\int_0^\infty \left(e^{-i\mathscr{H}_0(t)r}\hat{S}^\dagger(t)\hat{\sigma}_k\hat{S}(t)e^{i\mathscr{H}_0(t)r}\right)C_k(r)\mathrm{d}r, \tag{5.65}$$

with $C_k(r) = \mathrm{Tr}_e\{\hat{V}_k(r)\hat{V}_k(0)\rho_e\}$.

We finally apply the above to the previously considered Landau-Zener drive of orbital states defined by the driven Hamiltonian $\hat{H}_o(t)$ from Eq. (5.3). In such a case the transformation to adiabatic frame amounts to rotation around single axis $\hat{S} = \exp\left\{-i\frac{\vartheta(t)}{2}\hat{\sigma}_y\right\}$. As a result one can easily compute the transformation to adiabatic frame of reference for each Pauli operator as:

$$\begin{aligned}\hat{S}^\dagger(t)\hat{\sigma}_x\hat{S}(t) &= \hat{\varsigma}_x\cos\vartheta(t) + \hat{\varsigma}_z\sin\vartheta(t)\\ \hat{S}^\dagger(t)\hat{\sigma}_z\hat{S}(t) &= \hat{\varsigma}_z\cos\vartheta(t) - \hat{\varsigma}_x\sin\vartheta(t)\end{aligned} \tag{5.66}$$

where we used $\hat{\varsigma}_i$ to highlight that the operators in the right hand side are given in the adiabatic frame, e.g. $\hat{\varsigma}_x = |+\rangle\langle -| + |-\rangle\langle +|$ and used trigonometric function of time-dependent orbital angle $\vartheta(t)$ defined via $\cos\vartheta(t) = \epsilon(t)/\Omega(t)$ and $\sin\vartheta(t) = t_c/\Omega(t)$.

Adiabatic Master equation in the Linblad form

27: see discussion of standard Master equation Sec. 3.2

Let us apply the secular approximation,[27] i.e. leave only the energy-conserving terms proportional to $\hat{\varsigma}_\pm\hat{\varsigma}_\mp$. Next, we neglect the zero-frequency contribution $\propto \hat{\varsigma}_z$, which will be included by averaging over slow fluctuations of classical noise and finally omit the deterministic Lamb-shift terms. As a result the remaining terms can be represented as:

$$\sum_{j=x,z}\left[\hat{\sigma}_j(t),\hat{\mathcal{R}}_j(t)\hat{\rho}_q(t)\right]=\frac{1}{2}\Gamma_-(t)\left[\hat{\varsigma}_-,\hat{\varsigma}_+\hat{\rho}_q\right]+\frac{1}{2}\Gamma_+(t)\left[\hat{\varsigma}_+,\hat{\varsigma}_-\hat{\rho}_q\right], \tag{5.67}$$

where:

$$\Gamma_\mp(t)=\frac{1}{4}\Big(S_x(\pm\Omega[t])\cos^2\vartheta(t)+S_z(\pm\Omega[t])\sin^2\vartheta(t)\Big), \tag{5.68}$$

which was expressed in terms of spectral densities of the operators $\hat{V}_x$, $\hat{V}_z$ i.e.

$$S_i(\Omega[t])=\int_{-\infty}^{\infty}\mathrm{Tr}\{\hat{V}_i'(s)\hat{V}_i'(0)\hat{\rho}_e\}e^{i\Omega[t]s}\mathrm{d}s\ \text{ for } i=x,z. \tag{5.69}$$

The commutator (5.67) together with its Hermitian conjugate and the unitary terms $\hat{\mathscr{H}}(t)=\frac{1}{2}\Omega(t)\hat{\varsigma}_z-\frac{1}{2}\dot{\vartheta}(t)\hat{\varsigma}_y$ produces adiabatic Master equation (AME) in the Linbladian form:

$$\begin{aligned}\dot{\hat{\varrho}}_o(t)=&-i\left[\frac{\Omega(t)}{2}\hat{\varsigma}_z-\frac{\dot{\vartheta}(t)}{2}\hat{\varsigma}_y,\hat{\varrho}_o(t)\right]\\&-\sum_{k=\pm}\left(\hat{L}_k(t)\hat{\varrho}_q(t)\hat{L}_k^\dagger(t)-\frac{1}{2}\left\{\hat{L}_k^\dagger(t)\hat{L}_k(t),\hat{\varrho}_o(t)\right\}\right),\end{aligned} \tag{5.70}$$

with time-dependent Linbladians defined in terms of Eq. (5.68):

$$\hat{L}_+(t)=\sqrt{\Gamma_+(t)}\hat{\varsigma}_+,\qquad \hat{L}_-(t)=\sqrt{\Gamma_-(t)}\hat{\varsigma}_-. \tag{5.71}$$

We highlight that contrary to the undriven case, the unitary part of the AME is non-diagonal and contains the coupling between the adiabatic states. The presence of the coupling makes the resulting equations motion difficult to solve analytically, hence later in the thesis some approximate methods will be used.

Excited state occupation

We first consider occupation of excited state, i.e. $Q(t)=\langle+|\,\varrho(t)\,|+\rangle$ in the adiabatic limit, where $\dot{\vartheta}(t)\ll\Omega(t)$. In such a case the AME produces the differential equation:

$$\dot{Q}(t)=\Gamma_+(t)-Q(t)\big(\Gamma_-(t)+\Gamma_+(t)\big). \tag{5.72}$$

For the initial condition $Q(t)=Q_0$, the above can be solved analytically, i.e.

$$Q(t_f)=Q_0e^{-\chi(t_i,t_f)}+\int_{t_i}^{t_f}\mathrm{d}t'\Gamma_+(t')e^{-\chi(t',t_f)}, \tag{5.73}$$

where the relaxation factor has been defined as:

$$\chi(t_1, t_2) = \int_{t_1}^{t_2} \mathrm{d}t' \big(\Gamma_+(t') + \Gamma_-(t')\big). \tag{5.74}$$

Note that for the case of initially ground state $Q_0 = 0$ and using first order perturbation theory[28] we can reconstruct the classical noise result from Eq. (5.50), i.e.

28: for the differential equation (5.72)

$$\delta Q(t_f) = \int_{t_i}^{t_f} \Gamma_+(t'). \tag{5.75}$$

5.4 Dephasing and dissipation in the time-dependent basis

We conclude this section by discussing the approach used in the thesis to treat dissipative and dephasing evolution of the driven quantum system. For the remainder of this thesis we will concentrate on the coupling between the DQD system and the environment of the form:

$$\hat{V}_{oe} = \frac{\hat{V}_x}{2}\hat{\sigma}_x + \frac{\hat{V}_z}{2}\hat{\sigma}_z, \tag{5.76}$$

which is written in the basis of DQD two-level system, i.e. $\hat{\sigma}_z = |L\rangle\langle L| - |R\rangle\langle R|$, and hence the couplings correspond to fluctuations of the tunnel coupling and dots detunings $\hat{V}_x$ and $\hat{V}_z$ respectively.

Transverse coupling

For time-dependent instantaneous states $|+(t)\rangle, |-(t)\rangle$ of the TLS Hamiltonian one can define the instantaneous transverse coupling as:

$$\hat{V}_\perp = \langle +(t)|\, \hat{V}_{oe}\, |-(t)\rangle + \text{h.c} = (d_{\perp,x}(t)\hat{V}_x + d_{\perp,z}(t)\hat{V}_z) + \text{h.c.} \tag{5.77}$$

where for convenience we defined the *transverse dipole moments* with respect to tunnel coupling (x) and detuning (z) fluctuations as:

$$d_{\perp,x}(t) = \langle +(t)|\, \hat{\sigma}_x\, |-(t)\rangle = \cos\vartheta(t) \tag{5.78}$$

$$d_{\perp,z}(t) = \langle +(t)|\, \hat{\sigma}_z\, |-(t)\rangle = -\sin\vartheta(t). \tag{5.79}$$

With their help in Sec. 5.3 we showed that the time-dependent relaxation rates can be computed as:

$$\Gamma_\pm(\Omega[t]) = \frac{1}{4}\Big(|d_{\perp,x}(t)|^2 S_x(\pm\Omega[t]) + |d_{\perp,z}(t)|^2 S_z(\pm\Omega[t])\Big), \tag{5.80}$$

where we neglected typically small correlations between the operators $\hat{V}_x$ and $\hat{V}_z$, and used their respective spectral densities evaluated at the instantaneous energy gap (See Eq. (5.69)). As a result of the above in the remaining chapters we will concentrate on the modeling of the relaxation rates corresponding to the tunnel coupling and detuning fluctuations in the realistic DQD systems, which can be used as an input for the AME from Eq. (5.70).

Longitudinal coupling

Similarly we present the effective approach to dephasing caused by the longitudinal coupling in the instantaneous basis of the TLS system $|+(t)\rangle, |-(t)\rangle$. In analogy to the above coupling can be written as:

$$\hat{V}_\phi = \langle +(t)| \hat{V}_{oe}(t) |+(t)\rangle - \langle -(t)| \hat{V}_{oe}(t) |-(t)\rangle = (d_{\phi,x}(t)\hat{V}_x + d_{\phi,x}(t)\hat{V}_z), \tag{5.81}$$

where we defined *longitudinal dipole moments*:

$$\begin{aligned} d_{\phi,x}(t) &= \langle +(t)| \hat{V}_x |+(t)\rangle - \langle -(t)| \hat{V}_x |-(t)\rangle = \sin\vartheta(t) \\ d_{\phi,z}(t) &= \langle +(t)| \hat{V}_z |+(t)\rangle - \langle -(t)| \hat{V}_z |-(t)\rangle = \cos\vartheta(t), \end{aligned} \tag{5.82}$$

As long as the dipole moment have non-zero average, the dephasing due to low-frequency noise can be modeled by the quasistatic approximation as it was done in Eq. (5.57). As a result in the leading order the phase error in the orbital degrees of freedom can be written as:

$$\langle \delta\varphi^2 \rangle \approx \tilde{\sigma}_\epsilon^2 \left[\int_0^t d_{\phi,z}(t')\mathrm{d}t' \right]^2 + \tilde{\sigma}_{t_c}^2 \left[\int_0^t d_{\phi,x}(t')\mathrm{d}t' \right]^2, \tag{5.83}$$

where $\tilde{\sigma}_\epsilon, \tilde{\sigma}_{t_c}$ are RMS of the quasistatic fluctuations of the tunnel coupling and the detuning, which can be computed using methods from Sec. 4.4.

In fact, in this thesis we will be not directly interested in the phase relation between the orbital (charge) degrees of freedom. Instead in Chapter 12 we will show how in the presence of correlation between spin and charge degree of freedom, the coherence of spin qubit can be also affected by the tunnel coupling and detuning noise. In language of the above it would mean that the spin-qubit temporally acquires non-zero longitudinal dipole moment with respect to one of the noise sources, which can be computed in analogy to Eq. (5.82) as

$$d_{\phi,i}^{\mathrm{spin}}(t) = \langle \tilde{\uparrow}(t)|\hat{V}_i|\tilde{\downarrow}(t)\rangle \neq 0, \tag{5.84}$$

where the states $|\tilde{\uparrow}(t)\rangle, |\tilde{\downarrow}(t)\rangle$ corresponds to the instantaneous spin states, which for the adiabatic transition might be partly correlated with the charge degree of freedom (see Eq. (9.20) for an example). We discuss possibility of using this approach for probing spatial correlation of the noise in the outlook.

Numerical simulations

We conclude this chapter by describing the approach use to numerically simulate the interdot transition in presence of both low-frequency and high-frequency environmental noise. Using realistic models of the environment we will compute the relaxation rates between the instantaneous states of the double quantum dot system as a function of detuning (energy gap). Following Eq. (5.80) the relaxation rates will be used as the input for adiabatic Master equation in the Linblad form written in Eq. (5.71). The resulting equations of motions will be averaged numerically over multiple realisations of the quasistatic noise in detuning $\delta\epsilon$ and tunnel

29: and eventually the fluctuations of the Zeeman splitting δE_z, when spin degree of freedom will be considered in Part III.

coupling δt_c,[29] each of them drawn from the independent Gaussian distribution with the effective RMS and zero average. To prove validity of such approach in the Appendix A we numerically test the *averaged adiabatic Master equation* method against numerical average of Schrodinger equation over classical noise process.

II. Charge transfer of spin qubit

6 The orbital states of a confined electron

In many realizations of the qubits the computational states used for quantum information processing are not the only accessible discrete levels. As a relevant example in this thesis we consider the electron spin-qubit in the quantum dot, where apart from the spin degree of freedom used for quantum computation, the presence of confinement potential introduces orbital degrees of freedom. The orbital states in semiconductor spin qubit are associated with the charge degree of freedom and due to electrostatic nature of the potential defining the quantum dots they will be sensitive to fluctuations of electric field. We will show that the electric drive of orbital state, i.e. time-dependent modification of electrostatic potential can be in principle used to move the spin-qubit. In this thesis we focus on semiconductor quantum dot spin qubit, but it should kept in mind that such external degrees of freedom can be found in many other realizations of the qubits[1] . In this chapter we first define a model of the wavefunction of the electron, confined in a semiconductor quantum dot (Sec. 6.1) and double quantum dot (Sec. 6.2). Then in Sec. 6.3 we propose and discuss three models of the Double Quantum Dot (DQD) systems corresponding to Si/SiGe, SiMOS, and GaAs devices.

1: for instance vibrational modes for trapped ions [167]

6.1 Single quantum dot

In order to perform quantum information processing on the electron spin, one has to first be able to trap a single electron in a finite element of space. A natural example of bound electron state is the hydrogen atom, where electron is bound to a single proton via electrostatic attraction. For this reason, artificially created containers for single electrons known as the quantum dots (QD) are often called artificial atoms [168]. However contrary to hydrogen atom, the electron confinement inside the QD is not isotropic, but depends on the method of the confinement used.

One way to generate the bound state of the electron is to use its non-zero electric charge, sensitive to electric potential generated by classical electronics. However the state of the trapped electron not only depends on the confinement shape, but it is also affected by the crystal structure of the semiconductor material and in particular the shape of conduction band, that the electron occupies. Below we briefly discuss[2] the influence of crystalline potential on the state of the spin qubit in *gate-defined quantum dots*.[3]

2: We use standard textbook knowledge. More detailed derivations and in-depth discussion can be found in [169, 170]

3: As mentioned before we will not consider here alternative ways of trapping the electron in other semiconductor nanostructures, which include: point defects [50], shallow donors [51] or self-assembled QDs [52]

Crystalline potential

The quantum states of non-interacting electrons in periodic external potential are the Bloch states,

$$\psi_{n,\mathbf{k}}(\mathbf{r}) = u_{n,\mathbf{k}}(\mathbf{r})e^{i\mathbf{kr}}, \tag{6.1}$$

where index n is the band index, $\mathbf{k}$ is the quasi-momentum and the function $u_{n,\mathbf{k}}(\mathbf{r})$ have the same periodicity as the crystal. At zero temperature, the electrons fill the states labeled by n and $\mathbf{k}$ with energy not larger then the Fermi energy. For the an undoped semiconductors the Fermi energy lies between two bands known as the conduction band (first empty one) and the valence band (the last filled one). As a result the semiconductors are insulating at zero temperature, as all quasi-momentum states are filled and no net motion of charge carriers (no electric current) is possible. However the current can flow if finite number of the electrons are injected to the otherwise empty conduction band, where all the momentum states are available[4] .

4: The process of injecting electron is related to absorption of energy quanta equal to the bandgap, which is typically of the order of $\Delta \sim 1\mu$eV. Alternatively the activation energy is reduced by doping the semiconductor with the impurities.

Envelope function approximation (EFA)

A quantum dot allows for trapping a single electron at the bottom of the conduction band, which leads to a distinct characteristic features of electron wavefunction for GaAs and Si devices considered in this thesis, as these materials have qualitatively different structure of relevant parts of the conduction band. Quite generally however electron confinement in the QD is varying slowly in comparison to crystalline unit cell a, i.e.

$$V(\mathbf{r})/\boldsymbol{\nabla} V(\mathbf{r}) \gg a. \tag{6.2}$$

This directly leads to separation of scales between the atomic-scale oscillations, the Bloch functions $u_{\mathbf{k}}(\mathbf{r})e^{i\mathbf{kr}}$ and the slowly varying (on the length scale of lattice constant) component $F(\mathbf{k})$, using which the wavefunction of the electron reads:

$$\psi(\mathbf{r}) = \sum_{\mathbf{k}} F(\mathbf{k})e^{i\mathbf{kr}}u_{\mathbf{k}}(\mathbf{r}) \rightarrow u_{\mathbf{k_0}}(\mathbf{r})F(\mathbf{r}), \tag{6.3}$$

where in the above we have used single band approximation, and concentrated on the $\mathbf{k}_0$ corresponding to the a single minimum of the conduction band[5] , which allowed us to replace $u_{\mathbf{k}}(\mathbf{r}) \rightarrow u_{\mathbf{k_0}}(\mathbf{r})$ and $\sum_{\mathbf{k}} F(\mathbf{k})e^{i\mathbf{kr}} = F(\mathbf{r})$ as a consequence.

5: as we will discuss below, the case of a single minimum corresponds to GaAs, while in Si we have six degenerated minima

Effective mass approximation

A single electron trapped inside the quantum dot, occupies a minimum of otherwise empty conduction band at $\mathbf{k} = \mathbf{k}_0$. The modeling of electron wavefunction follows effective mass approximation, in which we expand the energy dispersion of the conduction band up to a second order in $\mathbf{k}$. For the isotropic dispersion relation we have:

$$E_{\mathbf{k}} = E_0 + \frac{(\mathbf{k}-\mathbf{k}_0)^2}{2}\frac{\partial^2 E}{\partial k^2}\bigg|_{k=k_0} \equiv E_0 + \frac{(\mathbf{k}-\mathbf{k_0})^2}{2m^*}. \tag{6.4}$$

In this approach the influence of crystalline potential is modeled by the modification of kinetic energy, done by introducing renormalized mass m^*. The effective mass is isotropic if the conduction band minimum is at $\mathbf{k} = 0$ point ($m^*_{\mathrm{GaAs}} = 0.067m_e$), however in many cases it becomes anisotropic with the prominent example of silicon where the longitudinal effective mass $m^*_{\mathrm{Si},\parallel} = 0.92m_e$ is different from the transverse effective mass $m^*_{\mathrm{Si},z} = 0.19m_e$, where m_e is the mass of free electron. One should bear in mind, that some important phenomena, that are sensitive to band mixing or atomistic effects like spin-orbit coupling or microscopic calculation of valley splitting are beyond EMA. Their microscopic description can be obtained using multiband envelope function approximation or tight-binding methods.

Valleys in Si-based devices

Important example of phenomena sensitive to the atomistic effects but still describable in terms of EFA is the presence of valley states[6] in the group IV semiconductors (Si, Ge), where the conduction band minimum is not situated in the Γ-point with $\mathbf{k} = 0$. In such case the minimum (hence the name valley) has n-fold degeneracy following from crystal symmetry. For the example of silicon relevant here, the minimum of conduction band occurs at so-called X-point at $\mathbf{k}_x = (\pm k_0, 0, 0)$, $\mathbf{k}_y = (0, \pm k_0, 0)$, $\mathbf{k}_z = (0, 0, \pm k_0)$, where $k_0 = 0.85\pi/a$ [20], which due to cubic symmetry of bulk silicon has six-fold symmetry. However during the formation of quantum dots due to effects of strain, confinement and electric field, four of those minima corresponding to X-Y valleys are significantly higher in energy.[7]

6: The valley states are absent in the group III-V nanostructures, where conduction band minimum is at non-degenerate Γ-point, with prominent example of GaAs/AlGaAs quantum dots.

We thus concentrate on two remaining valleys, and assume the wavefunction of the electron occupies single quantum dot is the linear combination of $z_\pm$ valleys, characterized by the wavevector $\mathbf{k}_\pm = (0, 0, \pm k_0)$, i.e.

$$\psi(\mathbf{r}) = \sum_{\nu=\pm} \alpha_\nu e^{i\nu k_0 z} u_{\mathbf{k}_\nu}(\mathbf{r}) F_\nu(\mathbf{r}) = \sum_{\nu=\pm} \alpha_v \psi_\nu(\mathbf{r}). \tag{6.5}$$

7: In typical experiments generated splitting is much larger then thermal energy $k_B T$ and hence carriers can populate only low-energy $z_\pm$ valleys.

Because the electron state is bound, i.e. it does not propagate along any of directions, the coefficients $|\alpha_+| = |\alpha_-| = 1/\sqrt{2}$, such that a standing wave is created. Hence the only degree of freedom is their relative phase. The valley splitting emerges as a result of the interface presence [171, 172].

In this thesis we will not directly model influence of valley degree of freedom on the adiabatic transfer of spin-qubit between two quantum dots. However we highlight that to some extent developed theory can be also used for the valley states[8] , as we have done in context of coherent electron transfer in the moving quantum dot [3]. We briefly discuss the connection in the outlook. Also in the outlook we comment how the valley degree of freedom can modify spin coherence in interdot transfer.

8: which can be seen as another internal two-level states of the electron

Confinement potential of single dot

A single electron injected into conduction band can be made immobile by confining its motion in all three dimensions. One method of doing it is generating spatially-varying electric field, with local minima that electron

can occupy[9] . However generating 3D electrostatic potential is difficult to realize experimentally. For this reason the motion of the electron is first restricted to two dimensions by formation of two-dimensional electron gas (2DEG) [30, 33]. Confinement in the two remaining dimensions is realized by the electrostatic potential generated by the metallic gates fabricated above 2DEG, hence the name gate-defined quantum dots. Fabrication of metallic gates with few-nanometer precision allows for formation of many quantum dots, with respective electrochemical potential controlled by the plunger gates (gates directly above QD) and the barrier gates responsible for formation and coupling between the neighbouring QDs.

9: We mean here minima of negative potential

In general the orbital states defined by the confinement potential can be modeled by the position- and in principle time-dependent Hamiltonian:[10]

$$\hat{H}_o(\mathbf{r},t) = \frac{\hat{\mathbf{p}}^2}{2m^*} + \hat{V}_{xy}(x,y,t) + \hat{V}_z(z), \tag{6.6}$$

10: when the voltages on the gates are made time-dependent

where we assumed that the transverse potential $\hat{V}_z(z)$ formed by the quantum well is independent of the planar potential $\hat{V}_{xy}(x,y,t)$ formed by the electronic gates[11] .

11: The time-dependence of the planar potential will be later used to change stationary qubit into a moving one

Transverse along the z axis

We discuss the confinement in the direction perpendicular to 2DEG, characterized by confinement length scale $L_z = 2-5$nm much tighter then the planar confinement $L_{xy} = 10-40$nm. For this reason the energy of the first excited state of the transverse confinement lies high above excited state of the planar confinement, since for simple square well model $E \sim L^{-2}$. Thus we restrict our low-energy analysis to the lowest-lying transverse, orbital state only. The exact shape of the wavefunciton in the z-direction in most devices is modified by the electric field, which makes the potential well triangular, i.e.

$$\hat{V}_z(z) = V_0(z) + eFz, \tag{6.7}$$

where F is the electric field and e is the elementary charge. For this reason the typically used wavefunction is the so-called modified Fang-Howard variational wave function [173]. However since its exact shape will be not relevant for studies conducted in this thesis, we assume the wavefunction is Gaussian with the characteristic length-scale $L_z = \sqrt{1/m^* E^{(z)}_{\text{orb}}} \sim 5$nm, i.e.

$$\psi_z(z) \approx \frac{1}{(\pi L_z^2)^{1/4}} \exp\left(-\frac{z^2}{2L_z^2}\right). \tag{6.8}$$

The value of confinement length L_z will be relevant for calculations of phonon induced transitions.

12: In this section we possibility of time-dependent modulation of the potential

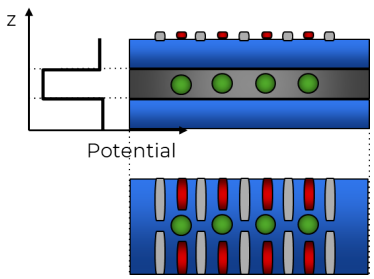

Figure 6.1: Sketch of typical geometry of the gate-defined quantum dots in the semiconductor heterostructure. The potential well confines the electron in the z-direction (out-of-plane). The in-plane potential is generated by the metallic gates.

Planar confinement

As argued above the planar confinement, realized by electric field is expected to be less tight than transverse one, mostly due to distance between then 2DEG and the gates that generate the planar potential $V_{xy}(x,y)$[12] . To show the geometry of the system we illustrate the typical quantum dot system in Fig. 6.1

If the potential minimum of $V_{xy}(x,y)$ is deep enough to host a bound electronic state it becomes the quantum dot. In many applications it is sufficient to expand the potential up to the second order around the minimum $\mathbf{r}_0$. If the quantum dot is located at $\mathbf{r}_0 = (x_0, 0, 0)$, it gives rise to harmonic potential:

$$\hat{V}_{\mathrm{xy}}(x,y) = m^* E_{\mathrm{orb}}^2 \left[(x-x_0)^2 + y^2\right], \tag{6.9}$$

where E_{orb} is the energy gap between the ground and first excited energy level[13] . For the assumed here harmonic potential the ground state is Gaussian in both directions, i.e.

$$\psi_{\mathrm{o},0}(x,y) = \frac{1}{(\pi L^2)^{1/4}} \exp\left(-\frac{(x-x_0)^2}{2L^2}\right) \frac{1}{(\pi L^2)^{1/4}} \exp\left(-\frac{y^2}{2L^2}\right), \tag{6.10}$$

where $L = \sqrt{1/m^* E_{\mathrm{orb}}}$ is the confinement length scale or simply *size of QD*, which in the Si-devices predicts $L \approx 20$nm for $E_{\mathrm{orb}} \approx 1$meV.[14]

In this thesis we will choose the axis x as the shuttling direction, and develop effectively 1D model for which the ground state reads:

$$\psi_{\mathrm{o},0}(x) = \frac{1}{(\pi L^2)^{1/4}} \exp\left(-\frac{(x-x_0)^2}{2L^2}\right). \tag{6.11}$$

In the analysis we will also include first excited orbital state, which in agreement with harmonic potential approximation for the effective 1D model is characterized by the wavefunction:

$$\psi_{\mathrm{o},1}(x) = \frac{1}{(\pi L^2)^{1/4}} \sqrt{\frac{2x^2}{L^2}} \exp\left(-\frac{(x-x_0)^2}{2L^2}\right). \tag{6.12}$$

Due to a relatively large energy gap between the orbital states[15] , we will take into account the two lowest-lying orbital state, which will allow us to compute effect of environment using language of Part I.

13: Note that in the units where $\hbar$ is explicitly written

$$\hat{V}_{\mathrm{xy}}(x,y) = m^*(E_{\mathrm{orb}}/\hbar)^2\left[(x-x_0)^2 + y^2\right]$$

14: The same orbital splitting results in $L \approx 35$nm in GaAs due to smaller effective mass.

15: As mentioned above, in the typical quantum dot the orbital splitting is of the order of $E_{\mathrm{orb}} \sim 1$meV which is well above other relevant in this thesis energy scales

Matrix elements

Let us highlight that there is non-zero dipole matrix element between ground and excited orbital state, i.e.

$$\langle 0|\, \hat{x} - x_0 \,|1\rangle = \frac{L}{\sqrt{2}} \tag{6.13}$$

while $\langle 0|\, \hat{x} - x_0 \,|0\rangle = \langle 1|\, \hat{x} - x_0 \,|1\rangle = 0$. This means the coupling between the orbital states is possible in the first order expansion of the position-dependent field $V_{\mathrm{env}}(\hat{x})$ (see Sec. 7.1 for the analysis). One can also relate the position matrix element to momentum matrix element[16] , i.e.

$$\langle 0|\, \hat{p} \,|1\rangle = \frac{L}{\sqrt{2}}\, i m^* E_{\mathrm{orb}}, \tag{6.14}$$

while $\langle 1|\, \hat{p} \,|0\rangle = -\langle 0|\, \hat{p} \,|1\rangle$ and $\langle n|\, \hat{p} \,|n\rangle = 0$ for any n. This will be relevant for spin-orbit coupling (see Sec. 9.2).

16: This can be done via the commutation relation $[\hat{x}, \hat{p}] = i$, using which the commutator $\left[\hat{H}_o, \hat{x}\right] = -i\hat{p}/m^*$, where $\hat{H}_o = \frac{\hat{p}^2}{2m^*} + m^* E_{\mathrm{orb}}(\hat{x} - x_0)^2$. Now since $\hat{H}_o\,|n\rangle = E_n\,|n\rangle$, we have

$$\langle n|\, \hat{p} \,|n'\rangle = i\,\langle n|\, \hat{x} \,|n'\rangle\, m^*(E_n - E_{n'})$$

6.2 Double quantum dot

Relaxation between the orbital states can be significantly limited if the relevant orbital states are located in a different dots. We now consider the system of two dots in close proximity to each other, which induces small overlap between the wavefunctions.

Tunnel coupling and dots detuning

First we consider the ground states of two quantum dots $|L\rangle$ and $|R\rangle$, with their respective energies given by E_L and E_R. The probability amplitude of the tunneling event between them, enters the Hamiltonian written in the $|L\rangle$, $|R\rangle$ basis as:

$$\hat{H}_{\mathrm{DQD}} = \begin{bmatrix} E_L & \frac{1}{2}t_c \\ \frac{1}{2}t_c^* & E_R \end{bmatrix}, \tag{6.15}$$

where $\frac{1}{2}t_c = \langle L|\, \hat{H}_{\mathrm{DQD}}\, |R\rangle$. Without losing generality, we will mostly consider real and positive tunnel coupling $t_c = t_c^* > 0$, which amounts to proper rotation of the Hamiltonian Eq. (6.15). It is convenient to introduce the energy detuning between the dots, i.e.

$$\epsilon = E_L - E_R, \tag{6.16}$$

such that the Hamiltonian can be rewritten in a form:

$$\hat{H}_{\mathrm{DQD}} = \frac{\epsilon}{2}\hat{\sigma}_z + \frac{t_c}{2}\hat{\sigma}_x. \tag{6.17}$$

In particular at the resonance, i.e. when $\epsilon_L = \epsilon_R$ the eigenstates of the Hamiltonian (6.15) are given by the symmetric and anti-symmetric combination of the dot eigenstates:

$$|\pm(\epsilon = 0)\rangle = \tfrac{1}{\sqrt{2}}\big(\, |L\rangle \pm |R\rangle \,\big), \tag{6.18}$$

which is in full analogy to molecular-orbital states from quantum chemistry, while the corresponding energies are given by $E_\pm = \pm t_c/2$, and hence t_c can be seen as the gap between hybridised states[17] . This shows that the possibility of electron tunneling between the dots is lowering the energy of the ground state as it is expected from the position-momentum uncertainty principle[18] .

In many calculations the tunnel coupling is assumed to be constant and independent of the detuning ϵ. However as we know from the WKB theory the tunnel coupling element between the levels on two sides of the barrier depends on the energy detuning between them [174]. The simplest model used in literature [57, 175] to reconstruct experiments conducted in the semiconductor devices, is the Gaussian decay of the tunnel coupling as a function of dots detuning, i.e.

$$t_c(\epsilon) = t_c \exp\!\left(-\frac{\epsilon^2}{2w_\epsilon^2}\right), \tag{6.19}$$

where $w_\epsilon \sim 100 t_c$. Although in this thesis we will never directly use the above formula, we use it as the indicator of the finite range of tunnel

17: Note that in quantum dot community the gap between the states if sometimes given by $2t_c$. An example: [88].

18: From $\Delta x \Delta p \sim \hbar$, we see that the typical energy of the system (kinetic part) scales as $E \sim \hbar^2/\Delta x^2$, which means that larger uncertainty in position should result in lowering the energy.

coupling, which allows us to assume that for large enough detuning $\sim$ 1meV the t_c effectively goes to zero.

We point out that the Hamiltonian derived above constitutes direct realization of the Landau-Zener Hamiltonian for the orbital states given by Eq. (5.3). The other remaining element is the detuning sweep, understood as the act of making dots detuning time-dependent, i.e. $\epsilon = \epsilon(t)$. For the consistency with L-Z model the detuning sweep rate is assumed constant[19] and hence $\epsilon(t) = vt$, As showed in the analysis of many experimental papers, such model is often sufficient to recreate the observed behaviour of DQD system [98, 101, 118].

19: Note that if $\epsilon(t)$ is not linear, one can use the linear term in the expansion of the sweep around $\epsilon = 0$, i.e.

$$v = \left.\frac{\partial \epsilon(t)}{\partial t}\right|_{\epsilon=0}. \tag{6.20}$$

Hund-Mulliken wavefunctions

In the previous section we have used the states $|L\rangle$, $|R\rangle$, which can be related to the isolated orbital states $|L_0\rangle$, $|R_0\rangle$ via simple procedure of orthogonalization. We follow here [2, 176, 177] and assume that the effective orbitals $|L\rangle$ $|R\rangle$ are expressed as a linear combination of bare, single-dot orbitals $|L_0\rangle$ and $|R_0\rangle$, i.e.

$$|L\rangle = \mathcal{N}(|L_0\rangle - g\,|R_0\rangle), \quad |R\rangle = \mathcal{N}(|R_0\rangle - g\,|L_0\rangle), \tag{6.21}$$

where $|N\rangle$ is the normalization constant. For the left and the right dot located at position $x_L = -d/2$ and $x_R = d/2$ respectively their bare wavefunctions are given by $\langle x|L_0\rangle = \psi^{(g)}_{\text{dot}}(x - x_L)$, $\langle x|R_0\rangle = \psi^{(g)}_{\text{dot}}(x - x_R)$, where $\psi^{(g)}_{\text{dot}}$ was given by the Eq. (6.11). Note that the integral between the bare waveunciton is not necessary zero, which we denote by $l = \langle L_0|R_0\rangle$.[20]
.

20: Since the wavefunctions are assumed real, the l is real as well

We now enforce orthogonality of the target orbitals, i.e.

$$0 = \langle L|R\rangle = \mathcal{N}^2(l - 2g + lg^2), \tag{6.22}$$

from which $g = (1 - \sqrt{1 - l^2})/l$. For typically small $l \ll 1$ it reduces to $g = l/2$. Up to leading order in l we have:

$$1 = \langle L|L\rangle = \mathcal{N}^2(1 - 2gl + g^2) \approx \mathcal{N}^2, \tag{6.23}$$

which altogether gives:

$$|L\rangle \approx |L_0\rangle - \tfrac{1}{2}\langle L_0|R_0\rangle\,|R_0\rangle\,, \quad |R\rangle \approx |R_0\rangle - \tfrac{1}{2}\langle L_0|R_0\rangle\,|L_0\rangle\,. \tag{6.24}$$

Finally for the assumed wavefuncitons separated by d, the overlap between the bare wavefunctions is given by:

$$\langle L_0|R_0\rangle = \exp\left(-d^2/4L^2\right). \tag{6.25}$$

As DQD Hamiltonian is identical to Landau-Zener one, which has been analyzed in Sec. 5.1, the eigenstates of the double dot as a function of adiabatic angle defined via relation $\cot\vartheta = -\epsilon/t_c$ are given by the states from Eq. (5.5). By combining their definition with the formula for $|L\rangle$ and $|R\rangle$ states from Eq. (6.24), in the Fig. 6.2 we illustrate the wavefunction of DQD ground and excited state as a function of ϑ for two separations between the dots $d = 2.5, 5$L.

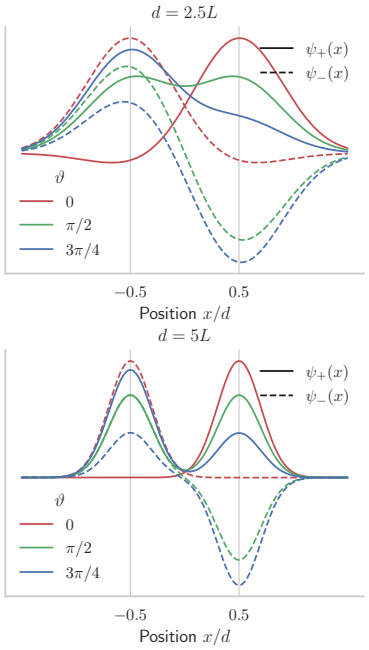

Figure 6.2: The wavefunctions of the ground (solid line) and excited (dashed) states of the DQD system within Hund-Mulliken approximation for two different separations of the dots d, expressed in the units of dot size L. We plot the wavefunctions for three different orbital angles $\vartheta = 0, \pi/2, 3\pi/4$ (colors). See Eq. (5.6) for definition of ϑ.

6.3 Si- and GaAs-based quantum dots

In this section we briefly compare most relevant representatives of group IV and III-V semiconductors used to fabricate quantum dots, that host spin qubis.

GaAs quantum dots

We start by historically first important example of semiconductor nanostructure used to realized spin qubits, the GaAs/AlGaAs heterostructure which we will refer to as *GaAs*. Due to small effective mass, the size of GaAs devices are relatively large [30], which allowed for easier fabrication. However as a member of III-V group, the GaAs does not have any naturally existing spin-less isotope, and thus random magnetic field generated by slow evolution of nuclear spins leads to dephasing of electron spin in the $T_2^* \approx 10$ns time [55, 64]. With possibility of active driving via dynamical decoupling the qubit coherence can be prolonged up to $T_2 \approx 1\mu$s [28, 64, 65]. Also dissipation of energy in GaAs quantum dot is expected to be relatively fast due to phonons. This is due to large mass of the nuclei, which translates to strong spin-orbit coupling [178]. Additionally the polar structure of the alloy, means that lattice vibrations are associated with the fluctuations of electric field, which couples the orbital states via piezoelectric coupling. On the good side, the presence of piezoelectric coupling allowed for demonstration of coherent electron spin shuttling using surface accosting waves [93]. Altogether technology developed for GaAs spin qubit in connection to relatively easy fabrication makes it an important testbed for quantum computer development. However the inevitable presence of nuclear spins, and strong spin-orbit interaction points towards group IV semiconductors, with the prominent example of Si (below) and Ge [24].

Silicon quantum dots

We now concentrate on Si-based quantum dots, which are recently most promising group IV semiconductor for further development of dot-based quanutm computation. In contrast to group III-V, for the natural Si only 5% of the nuclei have nonzero spin [20]. Additionally this number can be further reduced by orders of magnitude in the process of isotopic purification, leading to identifying Si-based nanostructures as the semiconductor vacuum (no nuclear spins) [31].

21: As a consequence of indirect energy gap (see below)

The Si-based devices have much smaller spin-orbit interaction,[21] which reduces coupling of spin to phonons and minimizes coupling between isolated spin qubit and fluctuations of electric field. As a result the coherence time of the electron spin-qubit in isotopically purified Silicon can be as long as $T_2^* = 10\,\mu$s [32, 43, 63]. Another important asset is the existing transitor technology, which can be reused for the purpose of building relatively similar in size quantum dots. This also provides a natural interface to connect the qubit to classical electronic including the transistor-based unit processing classical information.

However on the downside, typically for group IV semiconductor the Si has indirect bandgap, which means the location of valence and conduction

band are not in the same place of Brillouin zone. In particular the minimum of conduction band of the electron is not at the Γ point, which introduces fast oscillations of electron wavefunction in the quantum dot. Due to crystal symmetries it also means, that its state is six-fold degenerate in the bulk case, and two-fold degenerate (due to strain) in a typical quantum dot architecture. Although degeneracy is also lifted by the presence of interface, the typically small and sensitive to microscopic disorder, value of the valley splitting hinders many Si spin qubit experiments [36, 67, 172]. On top of this fabricating devices is not straightforward due to their small size, forced by the larger than in GaAs effective mass.

Si/SiGe and SiMOS devices

We briefly discuss the difference between two most popular architectures of Si-based quantum dots. In the case of Si/SiGe the out-of-plane confinement is realised by inserting the Si layer between the SiGe layers. As a result the conduction band offset allows for trapping the electron. In the SiMOS devices electrons are trapped at the Si-oxide interface, for which such offset is much larger and allows for applying stronger electric fields. This minimizes the distance between the formed quantum dots and the metallic gates, typically tighter confinement and possibly larger tunnel couplings then in Si/SiGe devices. However the proximity of the gates, and glass like structure of the oxide might induce higher amplitude of the charge noise felt by the electrons.

Models of the DQDs system

Following the above analysis we define here three models of the dots. Two of them would correspond to Si-based devices with relatively small and large distance between the dots, which would correspond to $d = 50$nm and $d = 100$nm. We will associate the first one with the *SiMOS* and the second with the Si/SiGe device or *SiGe* for short, however the rest of the parameters will be assumed common for both of them. In particular we will use the amplitude of intrinsic spin-orbit interaction and the amplitude of the charge noise from the experiments performed in the SiMOS devices, which can be seen as the upper bound for the Si/SiGe device [179]. We assume both devices are isotopically purified[22] with $0.01\%\mathrm{Si}^{29}$ which allow us to connect the devices to the typically measured coherence time $T_2^* \sim 10\mu$s. Finally for comparison we add GaAs/AlGaAs double quantum dot system, which we will refer to as *GaAs*. Due to much larger effective mass the quantum dots are expected to be larger and more separated in space. We have included all relevant parameters used in the numerical simulation in Tab. 6.1.

22: see Sec.9.3 for the discussion of the nuclear spins

Table 6.1: Parameters of the three effective models of double quantum dot systems, which will be used throughout the analysis. Parameters based on [2] and references therein.

Model name	SiMOS	SiGe	GaAs
Effective mass (m^*/m_e)	0.19		0.063
Dots distance d (nm)	50	100	150
Dot size L (nm)	20	20	40
Quantum well width $2L_z$ (nm)	5	5	20
Tunnel coupling t_c (μeV)	$10, 20, 60$		
Spin orbit coefficients $(\alpha + \beta)/2$ (m/s)	50		10^3
Zeeman splittings E_z (μeV)	$2, 120$		
Shear deformation potential Ξ_u(eV)	5×10^6		0
Dilatation deformation potential Ξ_d (eV)	8.77×10^6		7×10^6
Piezoelectric constant χ_p (eV/m)	0		1.4×10^6
Longitudinal speed of sound c_L (m/s)	9.15×10^3		5.3×10^3
Transverse speed of sound c_T (m/s)	5×10^3		2.5×10^3
Crystal density ϱ (kg/m^3)	2.3×10^3		5.3×10^3

7 Non-unitary evolution of orbital two-level system

We now compute the consequences of coupling between the orbital states and the spatially dependent environmental field. As an relevant example we consider fluctuations of electric field caused by the lattice vibrations (phonons) and the charge noise. In 7.1 we briefly discuss their physics and also analyze relation between the wavefunction of the TLS and its non-unitary evolution due to their presence. In particular we show that protection against dephasing is possible only when wavefunctions for ground and excited state are alike, or their shape matches symmetries of the noise. In contrast, protection against dissipation is possible if the wavefunctions of the ground and excited states have negligible overlap. However as a counterexample, lack of the overlap of the wavefunctions would lead to vanishing tunnel coupling between double quantum dot system and hinder possibility of using it for coherent communication. In the next Sec. 7.2 and 7.3 we compute the relaxation rates between the orbital TLS in the DQD system due to the phonons and the charge noise respectively.

7.1 Non-unitary evolution due to spatially dependant field

Both phonons and the charge noise are the examples of position dependent field,[1] , which in the Fourier space can be represented as:

$$\hat{V}_{\mathrm{fld}}(\hat{\mathbf{r}}) = \sum_{\mathbf{k}} \hat{V}_{\mathbf{k}} e^{i\mathbf{k}\hat{\mathbf{r}}}. \tag{7.1}$$

As a result the coupling between the field and the TLS depends on the wavfunctions of the latter and in particulair, the position matrix element between its eigenstates[2] .

Spatial degree of freedom

We concentrate now on the general discussion of orbit-environment coupling that originates from spatially varying field $\hat{V}_{\mathrm{fld}}(\hat{x})$.[3] It affects the orbital states by modulating confinement potential. As summarized in Sec. 5.4, for a pair of instantaneous states of the TLS $|\pm\rangle$, one can define the instantaneous: transverse and longitudinal coupling and relate them to relaxation and dephasing times respectively.

1: more specifically different forms of electric field that modifies electron confinement.

2: see Eq. (6.13), where we computed non-vanishing dipole matrix elements between two orbital states in a single quantum dot $\langle 0|\,\hat{x}\,|1\rangle = L/\sqrt{2}$,

3: which in this section we treat as effectively one-dimensional,

Transverse coupling

For the position-dependant operator $\hat{V}_{\text{fld}}(\hat{x})$ the transverse coupling in the basis of $|\pm\rangle$ states can be written as:

$$\hat{V}_{\perp} = \langle +| \hat{V}_{\text{fld}}(\hat{x}) |-\rangle + \text{h.c.} = \int \mathrm{d}x \psi_{+}^{*}(x) \hat{V}_{\text{fld}}(x) \psi_{-}(x) + \text{h.c} \tag{7.2}$$

where $\psi_{-}(x)$ and $\psi_{+}(x)$ corresponds to the wavefunction of ground and excited state of the TLS respectively and $\hat{V}_{\text{fld}}(x)$ acts on the environmental degrees of freedom only. From the above, we see that the operator $\hat{V}_{\perp}$ is non-zero only if absolute value squared of the wavefunctions has common support[4] . It means the interaction is expected to be weaker if the spatial separation between the wavefunctions is larger, which will be particularly relevant for the double-dot case. Also when wavefunctions have a different symmetry, for instance ground state is symmetric while the excited anti-symmetric with respect to certain point, the coupling between them should be also anti-symmetric such that the integral is non-zero. This is typically the case for the excited and ground state of the orbital levels in the single dot and two the double quantum dot at zero detuning[5] . Finally a good indicator of the coupling between two levels is the position matrix element between the eigenstates:

4: the overlap between the probability distributions is non-zero $\int |\psi_e(x)|^2 |\psi_g(x)|^2 \neq 0$,

5: when the eigenstates are molecular combinations of the dot states, i.e. $|\pm\rangle \propto |R\rangle \pm |L\rangle$,

$$x_{+-} = \langle +| \hat{x} |-\rangle \tag{7.3}$$

If $x_{+-} \neq 0$ it means the coupling is non-zero at the leading order of the expansion $\hat{V}_{\text{fld}}(\hat{x}) \approx \hat{x}\partial_x \hat{V}(x)|_{x_0}$. As an example, for the DQD system position matrix element between the eigenstates is largest at $\epsilon = 0$, when:

$$\langle +(0)| \hat{x} |-(0)\rangle = \frac{1}{2}\big(\langle L| + \langle R| \big)\hat{x}\big(|L\rangle - |R\rangle \big) \approx d, \tag{7.4}$$

where d is the distance between the dots, and we have omitted the small correction due to H-M wavefunctions from (6.24). As an relevant example the non-zero position matrix element between DQD states has been used to realise coherent spin-photon coupling in DQD systems [85].

From the above analysis a certain trade-off behaviour is observed. On one hand the energy dissipation between similar wavefunctions is suppressed due to small position matrix element. On the other hand, large spatial separation between excited and ground state, reduces the overlap between the probability densities, and makes the relaxation slow. This means that the fastest energy dissipation is expected between the wavefunctions of the similar support but opposite symmetry with the prominent example of ground and excited state in the single quantum dot or lowest-lying states in the DQD at the resonance. In the second case the relaxation is expected to be suppressed for sufficiently large detuning, i.e. when the ground and excited states are located in a different dot.

Longitudinal coupling

Let us now write the longitudinal coupling, which is typically associated with the dephasing of the TLS. In the instantaneous basis of the TLS it

can be written as:

$$\hat{V}_\phi = \langle + | \hat{V}_{\text{fld}}(\hat{x}) | + \rangle - \langle - | \hat{V}_{\text{fld}}(\hat{x}) | - \rangle = \int \mathrm{d}x \hat{V}_{\text{fld}}(x) \Big(|\psi_+(x)|^2 - |\psi_-(x)|^2 \Big). \tag{7.5}$$

Analogously to the dissipation case, the relatively similar wavefunctions allows to minimize effect of environment and in this way extend coherence time between the levels. However in contrast to energy dissipation, the dephasing of the superposition located at two different positions with zero support, i.e. $\int |\psi_+|^2 |\psi_-|^2 = 0$ is generally strong, unless the operator $\hat{V}_{\text{fld}}(\hat{x})$ averaged by two different probability densities $|\psi_\pm(x)|^2$ is effectively the same. The last observation shows the relevance of spatial correlations of the field which we discuss in context of charge noise in Sec. 7.3.

Lattice vibrations - phonons

We now discuss physics of environmental electric field, starting with the one due to lattice vibrations. The phonons can influence the TLS by creating typically small electric field due to motion of charge atoms in the crystal. This takes place either on the atomistic scale (deformation) or in a more global way via piezoelectric mechanisms. The latter one is present only in polar materials like GaAs and does not occur in the centrosymmetric crystals like Si.[6] For both cases the phonon-electron coupling can be written as [169]:

$$\hat{V}_{\text{el-ph}}(\mathbf{r}) = \sum_{j,\mathbf{k},\lambda=L,T} \sqrt{\frac{|\mathbf{k}|}{2\varrho c_\lambda V}}\, v^{(j)}_{\mathbf{k},\lambda} \big(\hat{b}_{\mathbf{k},\lambda} + \hat{b}^\dagger_{-\mathbf{k},\lambda} \big) e^{i\mathbf{k}\mathbf{r}} \,, \tag{7.6}$$

where we used material constants: ϱ – crystal density, V – crystal volume, and c_λ – the speed of λ-polarized phonons[7] . The $v^{(j)}_{\mathbf{k},\lambda}$ stands for the coupling constant, which for piezoelectric ($j = p$) and deformation potentials ($j = d$), are given by the explicit formulas:

$$v^{(\text{p})}_{\mathbf{k},\lambda} = \frac{\chi_p}{k}, \quad v^{(\text{d})}_{\mathbf{k},L} = \Xi_d + \Xi_u \left(\frac{k_z}{k} \right)^2, \quad v^{(\text{d})}_{\mathbf{k},T} = -\Xi_u \frac{k_{xy} k_z}{k^2}. \tag{7.7}$$

The values of piezoelectric constant χ_p and dilatation (shear) deformation potentials $\Xi_d (\Xi_u)$ for the GaAs and Si-based quantum dots are given in Tab. 6.1.

Phonons are responsible for most dissipation inside typical semiconductor nanostructure. In comparison to other sources of non-unitary evolution the phonon bath has relatively short correlation time. As discussed in Chapter 3, it means the phonons are causing dissipative evolution. The relaxation rates due to phonons are computed in Sec. (7.2). The lack of purely dephasing contribution, can be associated with the low density of state of acoustic phonons (spectral density) at the small energies (frequencies).

6: In particular piezoelectric coupling can be used in GaAs to shuttle the electron using Surface Acoustic Waves (SAW) [92–95].

7: for numerical values corresponding to Si- and GaAs-based quantum dots see Tab. 6.1

Charge noise

In the quantum dot system the orbital states are defined by the confinement potential realized by the electrostatic potential. For this reason random fluctuations of the electric field will directly couple to the orbital states. We use here empirical approach and use experimentally measured spectral density of the charge noise in QD and DQD systems to infer the expected values of relaxation rates and the amplitude of dephasing noise for the typical GaAs- and Si-based quantum dot.

$1/f^\beta$ noise

We start by the noise, which dominates at low-frequencies. The name $1/f^\beta$ noise reflects commonly measured in the semiconductor device shape of spectral density.[8] . The measured values of the spectral density of the $1/f^\beta$ noise measured at 1Hz falls into region of $A_1 = 0.1^2 - 2^2\mu\text{eV}^2/\text{Hz}$ [179], with the exponent β varying between the different semiconductor materials. Although this feature hints at some universal physical mechanism, the microscopic origin of 1/f noise remains not obvious. As discussed in [136], it is commonly related to two-level fluctuators (TLF).[9] As we showed in Sec. 4.4 superposition of such TLFs successfully reproduces $1/f^\beta$ spectrum.[10]

Due to high spectral weight at the low-frequencies the 1/f noise dominates dephasing of TLSs, the splitting of which is sensitive to electric field fluctuations, i.e. charge qubit or spin-qubits in presence of magnetic field gradient [6, 156]. Following analysis of the 1/f noise feature, we highlight that dephasing noise gets larger if data acquisition time increases, which can be understand as increasing number of TLFs, which changes during averaging process [11] . For the same reason, apart from modifying coherence during single experimental averaging, low-frequency charge noise causes drift of the device parameters on the macroscopic timescale,[12] which introduces the need of recalibration.

In this thesis we will be not only interested at low-frequency part of 1/f spectrum, but also analyze influence of its tail on the incoherent transition between orbital levels. Although as we will see the dissipation mediated by the 1/f noise is likely to be overshadowed by the phonon induced relaxation in a single quantum dot,[13] the situation might be reversed at the smaller energy scales, which corresponds to the tunnel coupling or the Zeeman splitting. For this reason it is important to provide a model for the tail of 1/f noise spectrum at the GHz frequencies (Energy of μeV). However the high-frequency shape of the noise from TLFs is far from universal. In particular, theoretical model from [136] predicts that at the finite frequency lying between MHz-GHz (depends on microscopic details) one should expect transition to $1/f^2$ shape. At even higher frequency transition to flat and then to Ohmic spectrum $S(\omega) \propto \omega$ are expected. On the other hand recently measured charge noise in the single-triplet TLSs, where the $1/f$ and $1/f^{0.7}$ in Si/SiGe [27] and Si-MOS [183] nanostructures showed no sign of such transitions up to 100MHz ($\sim 0.4\mu$eV). On top of this, the predicted flat/Ohmic shape of spectral density from TLFs becomes indistinguishable from Johnson-Nyquist noise, which is expected to become dominant in the same regime of frequencies (see section below).

8: Note that this type of the noise process was previously introduced in context of classical noise processes in Sec. 4.4. We remind that the shape of spectral density reads

$$S_\beta = A_1(\omega_1/\omega)^\beta, \tag{7.8}$$

where $\omega_1 = 2\pi/\text{Hz}$ and A_1 is its amplitude at 1Hz.

9: Its role is expected to be played by the local defects in the insulating layer, which acts as the electric monopoles or dipoles [180]. In the glassy materials, like SiMOS the character of the fluctuating TLS might be less local, i.e. the system can switch between pairs of collective electrons state [181, 182].

10: The $1/f^\beta$ shape was obtained by considering quantum noise caused by an ensemble of TLF coupled to thermal bath, where the exact shape of $1/f^\beta$ spectrum was showed to depend on the microscopic details of these fluctuators [136]

11: Up to this date no intrinsic low-frequency cut-off was detected in the semiconductor devices.

12: for instance days or weeks.

13: Due to typically large energy scale

Johnson-Nyquist noise

As another source of charge noise, which is relevant at high frequencies can be attributed to reservoir of the electrons in the nearby circuits [184]. At sufficiently low temperature its quantum[14] spectral density has a form [90, 185]:

$$S_J(\omega) = \frac{\mathrm{Re}\{Z\}}{R_q}\frac{\omega}{1-e^{-\beta\omega}} \tag{7.9}$$

where R_q is the inverse of conductance quantum, i.e. $R_q = \pi/e^2 = 13k\Omega$ and Z is the impedance of noise source. The temperature dependence follows the Bose-Einstein distribution $n(\omega) = 1/(e^{\beta\omega}-1)$ for positive $\omega > 0$ and negative $\omega < 0$ frequencies corresponding to relaxation and excitation respectively. For simplicity we will assume the noise is caused by the $Z = 50\Omega$ ideal resistor, for which the spectrum is flat at $\beta\omega \ll 1$ and Ohmic $S_J(\omega) \propto \omega$ at $\beta\omega \gg 1$.[15] .

The Johnson noise is expected to be relevant for dissipative evolution only, due to its high-frequency character.[16]

14: i.e. asymmetric,

15: For the typical temperature of $T = 100$mK the crossover energy can be estimated as $k_B T \sim 8\mu$eV (2GHz)

16: For dephasing physics the has classical form $S(\omega) \approx (R/R_q)k_B T$, which allow to compute its effective power of quasistatic noise as:

$$\sigma_J^2 \approx \int_{\pi/T_a}^{\pi/t}\frac{\mathrm{d}\omega}{\pi}\frac{R}{R_q}k_B T \leq \frac{0.02}{t[ns]}\mu\mathrm{eV}^2. \tag{7.10}$$

which shows that dephasing due to Johnson noise for $t \gg$ns is not expected to be relevant.

7.2 Phonon induced relaxation between the orbital states

We now compute relaxation rate for two-lowest lying orbital states of a single and double quantum dot. We assume that due to typically small energy-scale $\Omega \leq 1$meV the relaxation is caused only by the acoustic phonons, for which the dispersion relation reads $\Omega = c_\lambda k$, where $k = |\mathbf{k}|$. In such case the zero-temperature relaxation rate, can be obtained by introducing phonon-electron interaction Eq. (7.6) into the Fermi-Golden rule, which gives:

$$\Gamma^{(0)}_{\mathrm{ph},-}(\Omega) = 2\pi\sum_{j,\mathbf{k},\lambda=L,T}\frac{k}{2\varrho c_\lambda V}|v_{\mathbf{k},\lambda}|^2\,|\langle -|\,e^{i\mathbf{kr}}\,|+\rangle|^2\,\delta(\Omega - c_\lambda k), \tag{7.11}$$

where the temperature dependence can be incorporated by introducing an additional factor

$$\Gamma^{(\beta)}_{\mathrm{ph},-}(\Omega) = \frac{\Gamma^{(0)}_{\mathrm{ph},-}(\Omega)}{1+e^{-\beta\Omega}}, \tag{7.12}$$

such that for negative frequencies $\Omega < 0$ (TLS excitation by energy absorbtion), the excitation rate is proportional to number of phonons that has the resonant energy Ω, i.e. Bose-Einstein distribution[17] . As a consequence of detailed balance condition $\Gamma_+ = \Gamma_- e^{-\beta\Omega}$, the relaxation is proportional to $\Gamma_-(\Omega) \propto \langle n(\Omega)\rangle + 1$, which together for positive and negative Ω gives a factor $(1+e^{-\beta\Omega})^{-1}$.

We replace the sum over large density of phonon modes by the integral[18] over phonon density of states, and integrate over length of the wavevector $k_\lambda = \Omega/c_\lambda$, such that only the integral over solid angle $A_{\mathbf{k}} = \mathrm{d}\theta_{\mathbf{k}}\mathrm{d}\varphi_{\mathbf{k}}\sin\theta_{\mathbf{k}}$ is left:

$$\Gamma^{(0)}_{\mathrm{ph},-}(\Omega) = \sum_{\lambda,j}\frac{\Omega^3}{8\pi^2\varrho c_\lambda^5}\int \mathrm{d}A_{\mathbf{k}}\left|v^{(j)}_{\mathbf{k}_\lambda,\lambda}\right|^2|F(\mathbf{k}_\lambda)|^2. \tag{7.14}$$

17:

$$\Gamma_+(\Omega) \propto \langle n(\Omega)\rangle = \frac{1}{e^{\beta\Omega}+1}. \tag{7.13}$$

18: $\Sigma_{\mathbf{k}} = \int \mathrm{d}\mathbf{k}\frac{V}{(2\pi)^3}$

Above we introduced form factor $F(\mathbf{k}) = \langle -| e^{i\mathbf{kr}} |+\rangle$, evaluated at resonant wavevector of the length $k_\lambda = \Omega/c_\lambda$.

Single quantum dot

We now compute relaxation from excited to the ground state of harmonic potential, which represents the electronic potential of the QD. Following model of the wavefunction from Sec. 6.1 we assume that the ground and excited orbital state have the wavefunctions:

$$\psi_-(x) = \psi_{o,0}(x)\psi_{o,0}(y)\psi_z(z), \qquad \psi_+(x) = \psi_{o,1}(x)\psi_{o,0}(y)\psi_z(z) \quad (7.15)$$

the functional form of the ground states $\psi_{o,0}(x), \psi_{o,0}(y)$ is given by Eq. (6.10), the excited state $\psi_{o,1}(x)$ by (6.12)), while $\psi_z(z)$ by Eq. (6.8). Using the above model the form factor reads:

$$\langle 0| e^{i\mathbf{kr}} |1\rangle = \mathcal{N} \int_{-\infty}^{\infty} \mathrm{d}\mathbf{r} \frac{x}{L} e^{i\mathbf{kr}} e^{-\frac{x^2+y^2}{4L^2} + \frac{z^2}{4L_z^2}} e^{i\mathbf{kx}} = i\, k_x L e^{-\frac{k_{xy}^2 L^2 + k_z^2 L_z^2}{4}}. \quad (7.16)$$

We now evaluate the above formula for the resonant wavevector $\mathbf{k}_\lambda$ with length $k_\lambda = \Omega/c_\lambda$, and express the form factor $F(\mathbf{k}_\lambda)$ in terms of polar and azimuth angles, i.e.

$$|F(\mathbf{k}_\lambda)|^2 = \frac{\Omega^2}{c_\lambda^2} L^2 \sin^2\theta_{\mathbf{k}} \cos^2\varphi_{\mathbf{k}} B_\lambda(\Omega, \theta_{\mathbf{k}}), \quad (7.17)$$

where the last term is respondible for so-called *bottleneck* effect, and is explicitly given by:

$$B_\lambda(\Omega, \theta_{\mathbf{k}}) = \exp\left(-\frac{\Omega^2}{2c_\lambda^2}(L_z^2 \cos^2\theta_{\mathbf{k}} + L^2 \sin^2\theta_{\mathbf{k}})\right). \quad (7.18)$$

Substituting the above to the expression for the relaxation rates allows to integrate over polar angle $\varphi_{\mathbf{k}}$, and write the relaxation between the orbital levels as:

$$\Gamma^{(0)}_{-,\mathrm{def}} = \frac{\Omega^5 L^2}{4\pi\varrho}\left(\frac{I_0\Xi_d^2 + 2I_2\Xi_d\Xi_u + I_4\Xi_u^2}{c_L^7} + \frac{J\Xi_u^2}{c_T^7}\right),$$
$$\Gamma^{(0)}_{-,\mathrm{piez}} = \frac{\Omega^3 L^2}{4\pi\varrho}\chi_p^2\left(\frac{1}{c_L^5} + \frac{1}{c_T^5}\right) I_0, \quad (7.19)$$

where we separated the contributions into deformation and piezoelectric coupling respectively, and defined the relevant integrals as:

$$I_n = \int_0^\pi \mathrm{d}\theta_{\mathbf{k}} \sin^3\theta_{\mathbf{k}} \cos^n\theta_{\mathbf{k}} B_\lambda(\Omega, \theta_{\mathbf{k}})$$
$$J = \int_0^\pi \mathrm{d}\theta_{\mathbf{k}} \sin^5\theta_{\mathbf{k}} \cos^2\theta_{\mathbf{k}} B_\lambda(\Omega, \theta_{\mathbf{k}}) \quad (7.20)$$

In Fig. 7.1 we plot relaxation rate as a function of the energy Ω for the GaAs and Si-based devices using the parameters from Tab. 6.1. As it can be seen the lifetime of the excited orbital state in the typical Si dot with $E_{\mathrm{orb}} \approx 1\mathrm{meV}$ reads $1/\Gamma_- \approx 0.1\mathrm{ns}$ and hence it is expected to

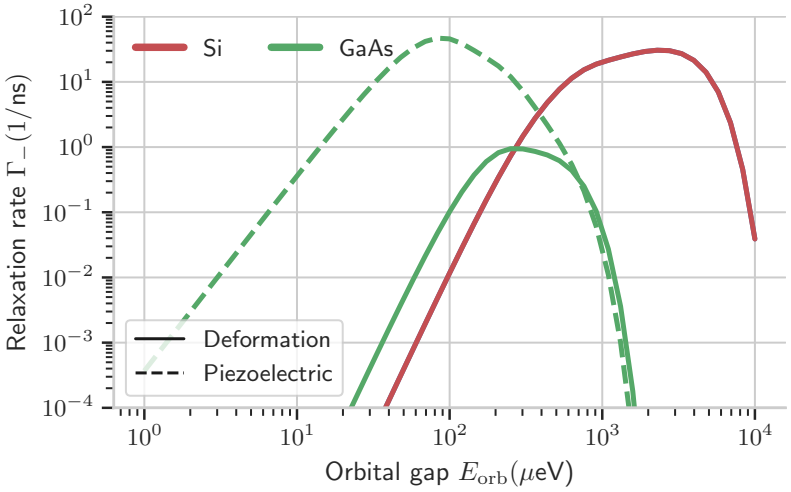

Figure 7.1: Relaxation rates due to lattice vibrations (phonons) in the single Si (red) and GaAs (green) quantum dots as a function of the energy gap between ground and excited state E_{orb}. The solid line is the ralaxation due to deformation potential, while the dashed line is due to piezoelectric coupling in the GaAs. The device parameters are summarized in Tab. 6.1.

dominate the other sources of the non-coherent evolution. In contrast the relaxation time in the GaAs at $E_{\mathrm{orb}} \approx 1\mathrm{meV}$ is two-orders of magnitude longer $1/\Gamma_- \approx 10\mathrm{ns}$, which is caused by the bottleneck effect caused by the exponential attenuation of the transition rate above the energy $\Omega = L/c$ (See Eq. (7.18)). Due to different sizes of the QD this happens at $\Omega \approx 100\,\mu\mathrm{eV}$ in GaAs and at more then an order of magnitude larger Ω in Si.

Double quantum dot

We now move to double quantum dot case, in which the relaxation of between two-lowest lying orbital states are expected to be lower[19] . Similarly to the previous case we start by computing the form factor, this time using instantaneous ground and excited states $|+\rangle = |+(\theta)\rangle$ and $|-\rangle = |-(\theta)\rangle$ of double dot potential derived previously using Hund-Mulliken approximation (See Eq. (6.24)). Up to the first order in the overlap between the bare wavefunctions, the form factor reads:

$$\begin{aligned}\langle -(\theta)|\, e^{i\mathbf{kr}}\, |+(\theta)\rangle \approx \frac{1}{2}\sin\theta\Big(\langle L_0|\, e^{i\mathbf{kr}}\, |L_0\rangle - \langle R_0|\, e^{i\mathbf{kr}}\, |R_0\rangle\Big) \\ + \cos\theta\Big(\langle L_0|\, e^{i\mathbf{kr}}\, |R_0\rangle - g\big(\langle L_0|\, e^{i\mathbf{kr}}\, |L_0\rangle + \langle R_0|\, e^{i\mathbf{kr}}\, |R_0\rangle\big)\Big),\end{aligned} \tag{7.21}$$

where $g = \langle L_0|R_0\rangle = \exp\left(-d^2/4L^2\right)$ for assumed in Sec. 6.1 model of the ground state of the uncoupled quantum dots $|L_0\rangle$, $|R_0\rangle$ with

$$\psi_{L_0}(x) = \psi_{o,0}(x+d/2)\psi_{o,0}(y)\psi_z(z),\;\; \psi_{R_0}(x) = \psi_{o,0}(x-d/2)\psi_{o,0}(y)\psi_z(z). \tag{7.22}$$

Using the above the form factor separates into two contributions:

$$\langle -(\theta)|\, e^{i\mathbf{kr}}\, |+(\theta)\rangle = \cos\theta F_x(\mathbf{k}) - i\sin\theta F_z(\mathbf{k}), \tag{7.23}$$

which can be related to the transitions between dot-like states F_x and molecular-orbital states F_z.[20] Their explicit form read:

19: As the overlap between absolute value squared of the wave-function is small for large detuning

20: Note that the form factor is dominated by the $F_x(\mathbf{k})$ at $\theta = 0, \pi$, where the eigenstates have dot-like character, and becomes dominated by $F_z(\mathbf{k})$ at $\theta = \pi/2$, where the ground and excited states are symmetric and antisymmetric combination of orbitals, i.e. $|\pm(\pi/2)\rangle = (|L\rangle \pm |R\rangle)/\sqrt{2}$

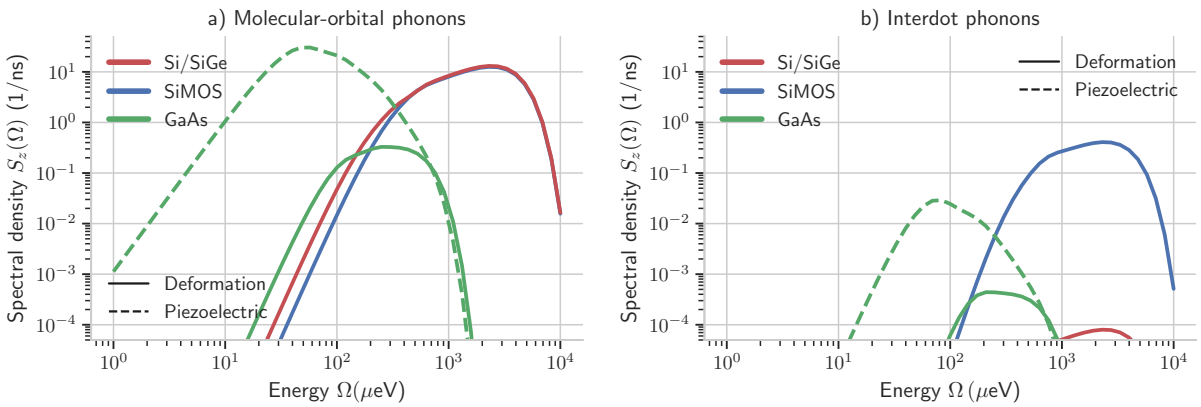

Figure 7.2: Spectral density of the phonons in three models of DQD system: SiGe (red), SiMOS (blue) and GaAs (green) as a function of the orbital energy $\Omega = \sqrt{\epsilon^2 + t_c^2}$. In a) we plot the spectrum of the phonons that causes the relaxation between molecular-orbital levels $|L\rangle \pm |R\rangle$ due to $\hat{V}_z$ operator and in b) for the phonons that causes the transitions between the dot levels $|L\rangle, |R\rangle$ due to $\hat{V}_x$ operator (See Fig. 8.5 for illustration of the difference between the interdot/molecular-orbital transitions). For GaAs devices we separately plot contribution from deformation phonons (solid line) and piezoelectric phonons (dashed line). The remaining parameters of the model are given in Tab. 6.1.

$$F_x(\mathbf{k}) = \exp\left(-\frac{k_{xy}^2 L^2 + k_z^2 L_z^2}{4}\right) \exp\left(-\frac{d^2}{4L^2}\right)\left(1 - \cos\left(\frac{k_x d}{2}\right)\right)$$
$$F_z(\mathbf{k}) = \exp\left(-\frac{k_{xy}^2 L^2 + k_z^2 L_z^2}{4}\right) \sin\left(\frac{k_x d}{2}\right). \tag{7.24}$$

We now substitute the form factor into the relaxation rate, and evaluate the rate at the resonant wavevector $|\mathbf{k}_\lambda| = \Omega/c_\lambda$. As a result the relaxation rate between double dot orbital states reads:

$$\Gamma^{(0)}_{\text{ph},-}(\Omega) = \frac{1}{4}\sin^2\theta S_z(\Omega) + \frac{1}{4}\cos^2\theta S_x(\Omega), \tag{7.25}$$

where we defined the spectral density of the phonon bath:

$$S_i^{(\text{ph})}(\Omega) = \sum_{\lambda,j} \frac{\Omega^3}{2\pi^2 \varrho c_\lambda^5} \int \mathrm{d}\Omega_{\mathbf{k}} \left|v^{(j)}_{\mathbf{k}_\lambda,\lambda}\right|^2 |F_i(\mathbf{k}_\lambda)|^2, \tag{7.26}$$

Note that the spectral density is insensitive to the tunnel coupling, i.e. its value determines the relaxation by defining the transition energy $\Omega(t) = \sqrt{\epsilon(t)^2 + t_c^2}$ and the orbital angle $\tan\theta(t) = -\epsilon(t)/t_c$. Below in Fig. 7.2 we plot spectral densities of the molecular-orbital phonons $S_z(\Omega)$ (a) and the interdot phonons $S_x(\Omega)$ (b) as a function of the energy Ω using parameters corresponding to the DQD devices from Sec. 6.3. We point out that the spectral densities of the phonons in the DQD systems are only slightly modified in comparison to spectral density of the phonon bath in the case of single quantum dot, which we have plotted in Fig. 7.1. In particular the spectral density of the interdot phonons from Fig. 7.2b) is attenuated by a factor which can be related to the overlap between the dots wavefunctions, i.e. $|\langle L_0|R_0\rangle|^2 = e^{-d^2/2L^2}$. As it can be seen such attenuation is the weakest in SiMOS (blue) where $d \approx 2.5L$. In all considered cases, a clear bottleneck effect is visible. In GaAs the piezoelectric coupling to phonons (green dashed line in all plots) has the largest spectral density in the region of $\Omega \approx 50\mu$eV, which commensurate with the typical values of the tunnel couplings $t_c \approx 50\mu$eV. Note that in the same range of energies, the phonons in Si are effectively absent. This will play an important role in the non-adiabatic transitions around the avoided crossing.

Finally we discuss the possibility of phonon-assisted relaxation to the ground state at relatively large detuning $\epsilon \gg t_c$, which can be used for the inelastic transition between the dots. Due to large dot-size and hence fast bottlenecking, the piezoelectric phonons in the regime of $\Omega > 100\mu$eV are expected to rapidly fall as Ω increases. This means they would provide fast transition rates only for $t_c < 100\mu$eV. Next, despite large spectral density at $\epsilon \approx 1$meV, the relaxation rate of molecular-orbital phonons in Si (blue/red lines in Fig. 7.1a)) is attenuated by the factor of t_c^2/Ω^2 factor, which means it is non-negligible only for very large $t_c > 100\mu$eV. Finally, significant relaxation at large detuning is expected due to interdot phonons in SiMOS (blue line in Fig. 7.1b)). This happens due to close proximity of the dots (large overlap), however as we discussed above such overlap is expected to decrease for strongly detuned dots, i.e. for $\Omega \approx \epsilon \approx 1$meV.

7.3 Charge noise in double quantum dot

Above the relaxation rate between the orbital states was computed directly from the microscopic Hamiltonian. Here we present a different approach and compute dephasing and dissipation of the DQD orbital states[21] by reconstructing longitudinal and transverse spectral densities of the charge noise from the experimental observations. As discussed in Sec. 5.4 we aim at computing relaxation rate, related to the transverse spectral density of detuning and tunnel coupling noise:

21: We do not consider here single dot TLS as its evolution is dominated by coupling to phonons

$$\Gamma_{-}^{(\mathrm{ch})}(\Omega) = \frac{1}{4}\left(\sin^2\theta S_\epsilon(\Omega) + \cos^2\theta S_{t_c}(\Omega)\right), \tag{7.27}$$

and the rms of the quasistatic fluctuations of them, i.e. $\tilde{\sigma}_{t_c}$ and $\tilde{\sigma}_\epsilon$ related to integral of the spectral density $S_i(\Omega)$ (see Eq. (4.49)).

Noise in detuning

Dephasing

Most commonly measured effect of charge noise is the low-frequency noise in detuning, that is dominated by the $1/f$, using which the effective variance of detuning fluctuations reads:

$$\tilde{\sigma}_\epsilon^2(t) = \int_{\pi/T_a}^{\pi/t} S_{1/f}(\omega)\mathrm{d}\omega. \tag{7.28}$$

The spectrum of $1/f$ noise $S_{1/f}(\omega)$ was given in Eq. (4.36). The commonly measured values of the spectral density at $\omega_1 = 2\pi$Hz, i.e. $A_1 \approx 0.1^2 - 2^2\mu\mathrm{eV}^2/\mathrm{Hz}$ translates to $\tilde{\sigma}_\epsilon^2 \approx 0.5 - 10^2\mu\mathrm{eV}^2$ for typical ratio of data acquisition time to experiment time $T_a/t \approx 10^{10}$.

Dissipation

For the dissipative effect of the detuning noise we take the combination of Johnson noise and extrapolate the spectrum of $1/f$ noise using its

amplitude from low-frequency measurements, i.e.

$$S_\epsilon(\Omega) = S_{1/f}(\Omega) + S_{\text{Joh}}(\Omega). \tag{7.29}$$

The spectral density of Johnson noise was given in Eq. 7.9. It included scaling with temperature and respected detailed balance condition for the negative frequencies.[22] One can estimate that at zero-detuning[23] the relaxation rate due to Johnson noise is given by:

$$\Gamma^{(\text{Joh})}_{\epsilon,-}(t_c)[1/\text{ns}] \approx 10^{-3} t_c[\mu\text{eV}]. \tag{7.30}$$

where as a source of Johnson noise we took the resistance of $Z = 50\Omega$, and assumed that the tunnel coupling is larger then thermal energy that corresponds to typical $T = 100$mK, i.e. $t_c > 10\mu$eV. In comparison the relaxation rate due to extrapolated 1/f noise can be estimated as:

$$\Gamma^{(1/\text{f})}_{\epsilon,-}(t_c)[1/\text{ns}] \approx 10^{9(1-\beta)} \frac{A_1[\mu\text{eV}^2/\text{Hz}]}{t_c^\beta[\mu\text{eV}]}. \tag{7.31}$$

Note that from the above the crossover between 1/f and Johnson noise is expected to be present around $t_c \approx 1 - 100\mu$eV.[24]

22: which gives the relation between relaxation and excitation rates $\Gamma_+/\Gamma_- = e^{-\beta\Omega}$

23: i.e. when $\theta = \pi/2$

24: Which is typical order of magnitude of tunnel coupling in realistic double quantum dot structure.

Model of 1/f noise

In the above considerations we assumed that 1/f noise continues from low-frequencies up to frequencies corresponding to typical tunnel coupling, i.e. $\omega \approx 2\pi/\text{ns}$ with a constant exponent $\beta = 1$. This approach should extrapolate the behaviour of the noise, the character of which is expected to change first to $1/f^2$ and then to flat spectrum [136]. The estimations were conducted for the typical temperature of quantum dot system, which is usually estimated as $T = 100$mT. Although it is not clear how the noise of 1/f noise would change if the temperature is changed, in general one can expect $A(T)$ to be not decreasing function of T. Direct measurement of dephasing process due to 1/f noise in the quantum dots provide the linear scaling of its amplitude with temperature, i.e. $A(T) \propto T$ [27, 157], which is consistent with the classical considerations on the 1/f noise in semiconductors [186]. However in many other experiments either negligible [160, 179] or quadratic [158] scaling with T was observed. As we are dealing with temperatures in the close vicinity of 100mK we will use the linear order correction:

$$A_1(T) = A_1 \frac{T}{T_{100}}, \tag{7.32}$$

where $T_{100} = 100$mK and A_1 is typically measured in experimental realizations[25] amplitude of the noise at $\omega = 2\pi$Hz.

25: Conducted at nominal temperature of the fridge $T_{\text{fridge}} = 20$mT, which at QD position translates to $T \approx 100$mT.

Model of spatial correlations of the noise

We now use a simple model, to describe the possible relation between the detuning noise, tunnel coupling noise and spatial correlations of electric field fluctuations. To do so we assume that the slow-fluctuations of the environment are caused by spatially varying quasistatic classical

field $\hat{V}_{\text{fld}}(x) \to \xi(x)$. We additionally assume the exponential correlation function, characterized by the correlation length x_c, i.e.

$$\langle \xi(x_1)\xi(x_2)\rangle = \sigma_x^2 e^{-|x_1-x_2|/x_c}, \tag{7.33}$$

where σ_x^2 is the power of spatially varying field.

Single dot energy fluctuations

For the single dot the small correction to the ground state energy due to $\xi(x)$ can be computed as $\delta E = \langle \psi_g|\xi(\hat{x})|\psi_g\rangle$, where $\left|\psi_g\right\rangle$ is the ground state of an isolated dot. From this model the variance of such corrections can be computed by averaging over realisations of the noise $\xi(x)$, i.e. $\sigma_E^2 = \langle \delta E^2\rangle$, which gives:

$$\sigma_E^2 = \int \langle \xi(x_1)\xi(x_2)\rangle |\psi_g(x_1)|^2 |\psi_g(x_2)|^2 = \int \frac{d\mathrm{k}}{2\pi} S_x(k)|F_g(k)|^2, \tag{7.34}$$

where we introduced spectral density of the stationary, spatially varying noise $S_x(k) = \int \mathrm{d}x \langle \xi(x)\xi(0)\rangle e^{-ikx} = \frac{2\sigma_x^2 x_c}{1+(kx_c)^2}$ and the Fourier transform of electron probability density $F_g(k) = \int \mathrm{d}x |\psi_g(x)|^2 e^{-ikx}$. For the Gaussian model of dots wavefunction from Eq. (6.10) with a typical size of L we have:

$$\sigma_E^2 \approx \sigma_x^2 \begin{cases} x_c/L, & \text{for} \quad x_c \ll L \\ 1 - \frac{L}{x_c}, & \text{for} \quad x_c \gg L, \end{cases} \tag{7.35}$$

which shows that the fluctuations of the dot ground state is expected to increase with larger correlation length x_c.[26]

26: Outside of the limiting cases, the variance of dot energy can be written in terms of Gaussian error function i.e.

$$\sigma_E^2 = \sigma_x^2 \exp\left(\frac{L^2}{2x_c^2}\right)\left(1 - \operatorname{erf}\left[\frac{L}{\sqrt{2}x_c}\right]\right). \tag{7.36}$$

Noise in detuning

We now repeat the analysis for the detuning noise, which is defined by the difference between the ground state energies of the left and the right dot, i.e. $\delta\epsilon = \delta E_L - \delta E_R$. From the above analysis we can write:

$$\sigma_\epsilon^2 = \int \frac{\mathrm{d}k}{2\pi} S_x(k)|F_L(k) - F_R(k)|^2, \tag{7.37}$$

where in general we use the Fourier transform of Hund-Mulliken orbital from Eq. 6.24:

$$F_L(k) = \int \mathrm{d}x \left(|\psi_{L_0}|^2(x) - \langle L_0|R_0\rangle\, \psi_{L_0}(x)\psi_{R_0}(x) + \frac{\langle L_0|R_0\rangle^2}{4}|\psi_{R_0}(x)|^2 \right) e^{-ikx}. \tag{7.38}$$

However in detuning considerations, we can neglect the correction due to typically small $\langle L_0|R_0\rangle \ll 1$, and arrive at the result:

$$\sigma_\epsilon^2 \approx 2\int \frac{\mathrm{d}k}{2\pi} S_x(k)\big[1 - \cos(kd)\big] \exp\left(-\frac{k^2L^2}{2}\right). \tag{7.39}$$

For the long correlation length, i.e. $x_c \gg d > L$ we have:

$$\sigma_\epsilon^2 \approx \sigma_x^2 \frac{d^2}{x_c\, L} = \frac{d^2}{x_c^2}\sigma_E^2 \qquad \text{for } x_c \gg d, \tag{7.40}$$

which contrary to single dot case from Eq. (7.35), predicts that in the limit of long correlation length the detuning noise is expected to decrease[27] . In the opposite limit of $x_c \ll L < d$ we have:

$$\sigma_\epsilon^2 \approx 2\sigma_x^2 \frac{x_c}{L}\left[1 - \exp\left(-\tfrac{d^2}{2L^2}\right)\right] \leqslant 2\sigma_E^2, \quad \text{for } x_c \ll L, \tag{7.41}$$

27: Since two dots effectively feels common noise

This result follows the intuition that the variance of the sum/difference of two uncorrelated noise processes equals the sum of their variances.

Tunnel coupling noise amplitude

We now move the the similar calculations for the tunnel coupling noise. By definition the coupling noise δt_c is longitudinal in the instantaneous basis around the avoided crossing, where the eigenstates are symmetric and anti-symmetric combination of dots orbitals. In particular using H-M wavefunctions from Eq. (6.24), at $\epsilon = 0$ for the ground and excited state::

$$\psi_\pm(x) \approx \tfrac{1}{\sqrt{2}}(\psi_{\mathrm{L}_0}(x) \pm \psi_{\mathrm{R}_0}(x))(1 - \tfrac{1}{2}\langle L_0|R_0\rangle), \tag{7.42}$$

which substituted to the definition of tunnel coupling noise, caused by spatially varying field, allows to write

$$\delta t_c = \int \xi(x)(|\psi_+(x)|^2 - |\psi_-(x)|^2)\mathrm{d}x. \tag{7.43}$$

We now follow calculations analogous to detuning noise, namely compute the power of tunnel coupling noise $\sigma_{t_c}^2 = \langle \delta t_c^2 \rangle$ by moving to a Fourier space, which in leading order in the dots overlap $\langle L_0|R_0\rangle = e^{-d^2/4L^2} \ll 1$ allows to write:

$$\sigma_{t_c}^2 = 4\exp\left(-\frac{d^2}{2L^2}\right)\int \frac{\mathrm{d}k}{2\pi} S_x(k)\left(1 - \cos\tfrac{kd}{2}\right)^2 e^{-k^2L^2/2} = \sigma_{t_c,0}^2 \exp\left(-\frac{d^2}{2L^2}\right). \tag{7.44}$$

In the above we defined the normalized power of the tunnel coupling fluctuations $\sigma_{t_c}^2$, representing the fluctuations in the limit of large dot overlap $d \ll L$. Despite slightly modified oscillating factor we assume that such fluctuations should have similar amplitude as the detuning noise $\sigma_{t_c,0}^2 \approx \sigma_\epsilon^2$. To confirm above predictions in Fig. 7.3 we plot effective power of quasistatic noise σ_ϵ^2 (blue) and compare against normalized amplitude of tunnel coupling noise $\sigma_{t_c,0}^2$ (red). The result plotted for two dot spacings of $d = 3L$ (solid line) and $d = 5L$ (dashed line) confirms that both σ_ϵ^2 and $\sigma_{t_c}^2$ are proportional to x_c in the limit of $x_c \ll L$ and inversely proportional to x_c in the opposite limit. The maximum amplitude of the noise is expected, when the correlation length is of the same order as the dot size L.

Model of tunnel coupling noise

We conclude the analysis by describing our effective treatment of the tunnel coupling noise due to charge noise. We assume both low-frequency (dephasing) and high-frequency (dissipation) fluctuations of the tunnel coupling noise to have the same form as the detuning noise, however

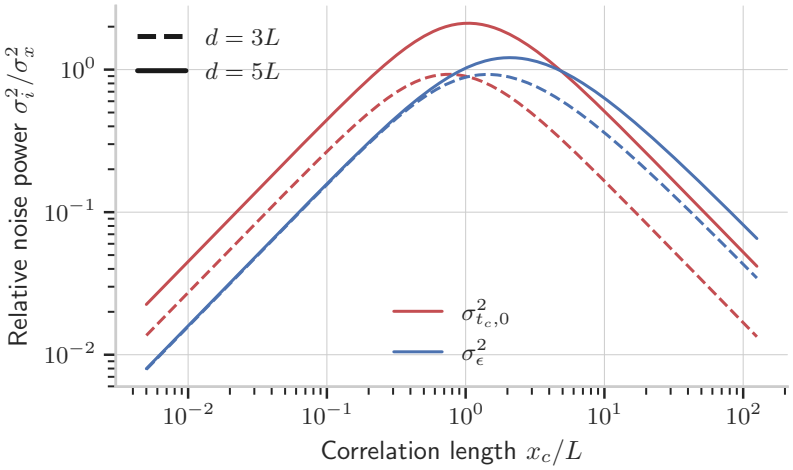

Figure 7.3: Comparison between the power of the quasistaic noise in detuning (blue) and tunnel coupling (red) caused by the spatially varying classical field $\xi(x)$, for two separations between the quantum dots $d = 3L$ (dashed line) and $d = 5L$ (solid line), where L is the dot size, as a function of the correlation length of the environmental field x_c. For the tunnel coupling noise we plot its normalized power, i.e. $\sigma^2_{t_c} = \sigma^2_{t_c,0} e^{-d^2/2L^2}$.

but with significantly lower amplitude. The scaling factor is extrapolated from the analysis of spatial correlations (above), and set to:

$$\alpha = \frac{\sigma^2_{t_c}}{\sigma^2_\epsilon} \approx e^{-d^2/2L^2} = 10^{-2}, \tag{7.45}$$

which corresponds to the short distance between the dots $d \approx 3L$ and should be treated as the upper bound for noise in tunnel coupling. As a result we set:

$$S_{t_c}(\Omega) = \alpha S_\epsilon(\Omega), \quad \sigma^2_{t_c} = \alpha \sigma^2_\epsilon, \tag{7.46}$$

while the amplitude of detuning noise is assumed to be approximately the same as the fluctuations of single dot ground state energy, i.e.

$$\sigma^2_\epsilon \approx \sigma^2_E. \tag{7.47}$$

Hence according Eq. (7.41) we assume small, but finite correlation of the charge noise between two dots, which has been confirmed experimentally for low-frequency noise in the Si-DQD system [187].

8 Application to charge transfer between the dots

We finally directly apply the developed theory to the transfer of electron charge between GaAs- and Si-based quantum dots. Firstly in Sec. 8.1 we reduce the multilevel structure of interdot transition in the semiconductor quantum dot to the two-level system and define the problem in terms of relevant parameters. Next in Sec. 8.2 we follow our work [1] and consider classical noise in detuning, which leads to non-monotonic function of the charge transfer error as a function of detuning sweep and show numerical equivalence between classical simulation of 1/f noise and adiabatic Master equation predictions. In the next Sec. 8.3 we present results of [2], where we moved to the experimentally relevant low-temperature limit in which relaxation and excitation rate are related by a non-trivial Boltzmann factor. In particular we show that the charge transfer error eventually vanishes for sufficiently slow sweep. From this perspective we discuss difference between the interdot charge transfer in GaAs and Si-based devices and show that additional minimum of the error as a function sweep rate is expected for the latter.

8.1 The model

In general transfer of spin qubit between two-quantum dots constitutes a multilevel adiabatic problem [1] . However from the perspective of the coherent transport of quantum information, in the minimal model one could first concentrate on the adiabatic evolution of lowest-lying adiabatic state[2] . The coherent communication is naturally impossible if the charge transfer fails.

1: which will be considered in the last Part III.

2: As it is necessary condition of coherent shuttling of quantum information. See Chapter 1 for discussion.

Two state reduction

We illustrate the typical energy spectrum for Si-DQD system in the Fig. 8.1, where the states relevant for this chapter are marked using blue line (ground) and red lines (excited).

In the figure we plot all the eight levels corresponding to the Hilbert space spanned by the valley, spin and DQD degrees of freedom[3] . In such an extended space we assume that the initial state for large negative detuning is given by:

$$|\psi(t_i)\rangle = |L,\downarrow,v_-\rangle \equiv |L\rangle\,, \tag{8.1}$$

i.e. the electron occupies the left dot, in the ground spin and valley state. In the closed quantum system, purely adiabatic dynamics due to slow enough detuning sweep results in the electron state being always in the ground state of instantaneous Hamiltonian (i.e. following the blue line in Fig. 8.1). Otherwise the initial spin-down electron is either left in the

3: In GaAs the valley degree of freedom is absent, see Chapter 6

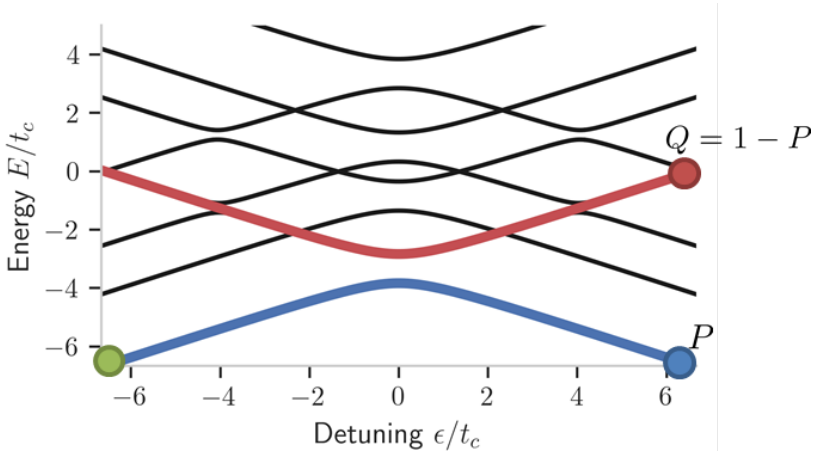

Figure 8.1: The typical instantaneous energy spectrum of the system of spin, valley and charge degrees of freedom during interdot transition as a function of dots detuning ϵ. By the blue line we marked the state relevant for our analysis in this chapter, which corresponds to the simultaneous ground state of valley, spin and charge degree of freedom. By the red line we marked an effective excited state. We define Q as the probability of not occupying lowest lying energy state at the end of the transition.

initial dot or ends up in the excited valley or spin state. The probability of this event can be computed as:

$$Q = 1 - \left|\left\langle \psi_-(t_f)\middle|\psi(t_i)\right\rangle\right|^2, \tag{8.2}$$

where the target state, localized in the right dot has an explicit form:

$$\left|\psi_-(t_f)\right\rangle = |R,\downarrow,v_-\rangle \equiv |R\rangle\,. \tag{8.3}$$

Note that in this way we approximately reduced multilevel problem to minimal problem of charge transfer between two orbital states[4] .

Reduction to two-level system allow us to use previously derived treatment of driven orbital TLS, the unitary evolution of which is defined in terms of Landau-Zener Hamiltonian

$$H_{\mathrm{DQD}}(t) = \frac{\epsilon(t)}{2}\hat{\sigma}_z + \frac{t_c}{2}\hat{\sigma}_x. \tag{8.4}$$

We attempt to model charge transfer in the realistic devices, where influence of the environment cannot be neglected.

4: As mentioned above add spin degree of freedom in Part III. For the analogous problem of excited spin state transfer see Chapter 11. For the dephasing between spin components see Chapter 12. Finally for the perspective on the role of valley degree of freedom see brief discussion in the outlook

8.2 Classical noise limit (high temperature)

We start by considering classical noise in the parameters of time-dependent Landau-Zener Hamiltonian

$$H_{\mathrm{DQD}}(t) = \frac{\epsilon(t) + \delta\epsilon(t)}{2}\hat{\sigma}_z + \frac{t_c + \delta t_c(t)}{2}\hat{\sigma}_x. \tag{8.5}$$

Noise in detuning

First we explicitly concentrate on the 1/f charge noise in detuning with the parameters reflecting experimental reality. We ignore fluctuations of the tunnel coupling as they are typically much weaker in amplitude.[5] This means that the analysis in this section will be more relevant for Si-based devices, where influence of phonons in many cases can be neglected, as we will show later in this chapter. As discussed in Sec. 5.2, the leading order correction due to classical noise of $1/f^{\beta}$ with the spectral density

5: See analysis in Sec.7.3, where we estimated than relative power of the noise is at most given by the factor $\alpha = 10^{-2}$, also the classical noise limit, where $\beta\Omega \ll 1$ is most likely to work in the regime where the gap is smallest, i.e. around avoided crossing. In this region the transitions are dominated by the detuning noise.

$S_\beta(\omega) = A_1(\omega_1/\omega)^\beta$ can be computed from the expression derived in Eq. (5.50), which for $1/f^\beta$ noise reads

$$\delta Q_{\epsilon\epsilon} = \frac{A_1 x \omega_1}{2v} \int_{t_c}^{\infty} \mathrm{d}\Omega \frac{t_c^2}{\Omega^{2+\beta}\sqrt{1-t_c^2/\Omega^2}} = \frac{A_1 \omega_1^\beta}{2v} t_c^{1-\beta} h(\beta), \tag{8.6}$$

where the $h(\beta)$ function can be represented as:

$$h(\beta) = \int_1^\infty \frac{dx}{x^{\beta+1}\sqrt{x^2-1}} = \int_0^{\pi/2} \cos^\beta(\alpha)\mathrm{d}\alpha = \frac{\sqrt{\pi}}{2}\frac{\Gamma(\frac{\beta+1}{2})}{\Gamma(\frac{\beta}{2}+1)}, \tag{8.7}$$

with $\Gamma(x)$ representing Γ function[6] . The function $h(\beta)$ decreases monotonically with β, and its typical values read $h(1) = 1$, $h(3/2) \approx 0.87$.

6: $\Gamma(z) = \int_0^\infty x^{z-1}e^{-z}\mathrm{d}x$

$\beta = 1$ case

We now compute the transfer error as a function of detuning sweep rate v for the typically measured amplitudes of the charge noise, characterize by the exponent $\beta = 1$. In such case, the analytical formula for the leading order correction Eq. (8.6) predicts that:

$$\delta Q_{\epsilon\epsilon,1} = \frac{A_1\omega_1}{2v}, \tag{8.8}$$

which is independent of tunnel coupling[7] .

7: For the reminder $A_1 = S(\omega_1)$ is the value of spectral density measured at $\omega_1 = 2\pi(1/\mathrm{s})$

This surprising result can be physically understood using simple model from the introductory chapter, i.e. since the relaxation rate at the zero-detuning reads $\Gamma_-(t_c) \propto S_\epsilon(-\omega)/4 = A_1\pi/2t_c$, while for linear sweep typical time spent in the vicinity of the avoided crossing can be estimated as $2t_{\mathrm{LZ}} \approx 2t_c/v$. Together we have

$$\delta Q_{\epsilon\epsilon,\beta} \approx \tfrac{1}{4}A_\beta(t_c)\frac{2t_c}{v} = \frac{A_1\omega_1^\beta}{2v}t^{1-\beta}, \tag{8.9}$$

which exactly recreates result of the integral for $\beta = 1$. In particular such probability of excitation can be given in the typical units as:

$$\delta Q_{\epsilon\epsilon,1} \approx 5\frac{A_1[\mu\mathrm{eV}^2/\mathrm{Hz}]}{v[\mu\mathrm{eV/ns}]}, \tag{8.10}$$

which predicts the 5% error for $A_1 = 1\,\mu\mathrm{eV}^2/\mathrm{Hz}$ and $v = 100\,\mu\mathrm{eV/ns}$.

We confirmed the above prediction by direct comparison against numerical simulation, in which we average the adiabatic evolution over realisations of $1/f$-noise in detuning with different amplitude A_1. In Fig. 8.2 we plot the probability of successful transfer $P = \langle|a_-|^2\rangle = 1 - Q$ as a function of sweep rate v for different values of tunnel couplings $t_c = 5, 15, 25\,\mu\mathrm{eV}$. By a different colors we denote different amplitude of the noise, the symbols denote results the averaging over realisations of the classical noise, the dashed lines are leading order predictions $\delta Q_{\epsilon\epsilon,1}$ while the solid line are the exponential fit to the formula[8] $Q = \frac{1}{2}(1 - e^{-2\delta Q_{\epsilon\epsilon,1}})$.

8: The origin of exponential will become natural when adiabatic Master equation is used in Sec. 8.3

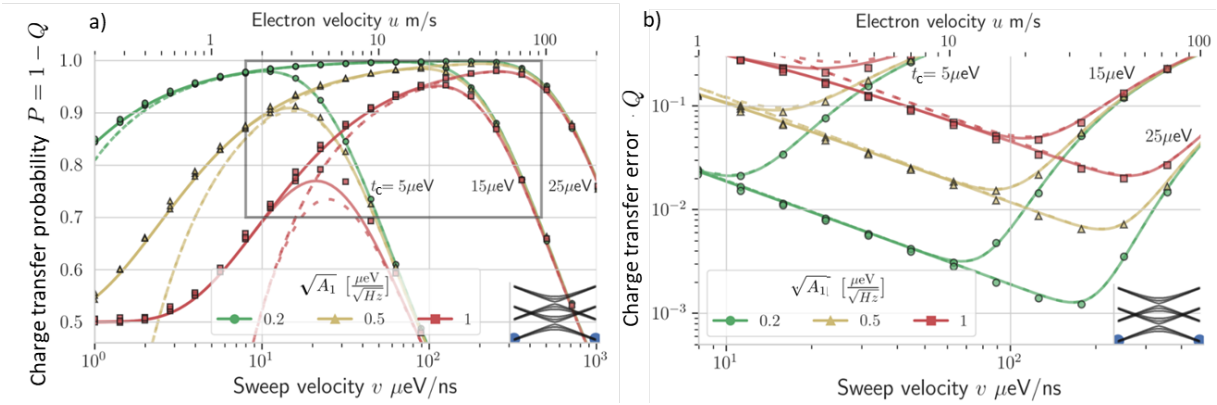

Figure 8.2: The charge transfer in presence of 1/f classical noise in detuning. a) The semi-log plot of the probability of charge transfer $P = 1 - Q$ as a function of sweep rate for three different amplitudes of 1/f noise (colors). In the right, the same but for the charge transfer error Q. The results marked by the symbols are obtained by averaging the driven evolution over 1000 realisations of the 1/f noise. The dashed line is the leading order correction $\delta Q_{\epsilon\epsilon,1}$ from Eq. (8.9). The solid line is the exponential fit $Q = \frac{1}{2}(1 - e^{-2\delta Q_{\epsilon\epsilon,1}})$. Adapted from [1]

As it can be seen from Fig. 8.2a), for the fast sweeps the transfer error is given by the Landau-Zener formula, where the shape of the transfer probability as a function of v depends on the value of tunnel coupling only. In the opposite regime of slow sweeps the transfer probability depends only on the amplitude of the noise $\sqrt{A_1}$, and as predicted is independent of the tunnel coupling.

To show that the noise dominated error is initially inversely proportional to the sweep rate, in Fig. 8.2b) we plot the transfer error $Q = 1 - P$ in the full logarithmic scale. We concentrate on the low-error part of Fig. 8.2a), which is denoted by a red rectangle. As shown in Fig. 8.2b) for the relatively small[9] error, the $Q \propto 1/v$ trend is visible in the regime where Landau-Zener probability of non-adiabatic transition is exponentially small, i.e. the transfer error does not depend on the tunnel coupling. As one can see, the interplay between Landau-Zener and charge noise non-adiabaticity, results in the optimal sweep rate at which the transfer error Q is minimal. For considered parameters the minimal error is predicted to be as low as $Q = 10^{-3}$ for $t_c = 25\,\mu$eV and $\sqrt{A_1} = 0.2\ \mu\text{eV}/\sqrt{\text{Hz}}$.

9: But still relevant for quantum information processing

$\beta \neq 1$ case

In the above analysis we have shown that for $\beta = 1$ case the noise induced non-adiabaticity, resulting in transfer error does not depend on the tunnel coupling. We now confirm that this is not the case for other exponents, as the predicted leading order correction gives $Q_{\epsilon\epsilon} \propto t_c^{1-\beta}$. In particular since the error only depends on the spectral density at $\Omega = t_c \gg 1$Hz, it means that the error is expected to be larger for $\beta < 1$ and smaller for $\beta > 1$ then for the $\beta = 1$ case[10] . Let us now assume the $\beta = 1$ and $\beta \neq 1$ spectra are equal not at $\omega_1 = 1$Hz but at some high-frequency ω_h[11] , i.e.

$$A_1(\omega_h) = A_\beta(\omega_h), \tag{8.11}$$

the relative error depends now on the relation between ω_h and tunnel coupling t_c. In particular the error for the $\beta \neq 1$ noise can be related to

10: naturally when $1/f^\beta$ noise has the same power at 1Hz, i.e. $A_1 = A_\beta$

11: which we set to $\omega_h \approx 15\,\mu$eV to reflect typical tunnel coupling value

the transfer error for $\beta = 1$ as

$$\delta Q_{\beta\neq 1} = \delta Q_{\beta=1} \left(\frac{t_c}{\omega_h}\right)^{1-\beta} h(\beta). \tag{8.12}$$

Note that from the above formula the error for $\beta \neq 1$ at $\omega_h = t_c$ is expected to be larger for $\beta < 1$ and smaller then for $\beta > 1$, since $h(\beta)$ is monotonically decreasing function of β. We confirm this analysis by plotting in Fig. 8.3 the transfer probability $1-Q$ averaged over numerically generated realizations of $1/f^{1.5}$ noise.

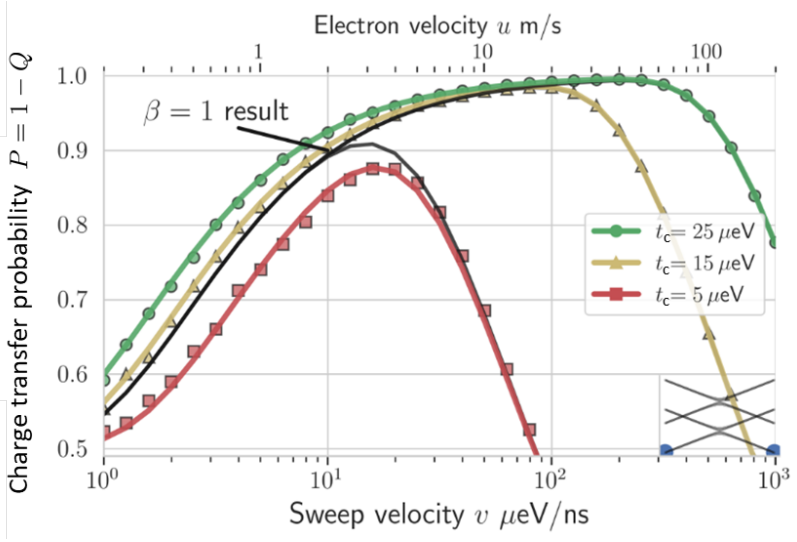

Figure 8.3: Charge transfer probability $P = 1 - Q$ as a function of sweep rate v in presence of $1/f^{1.5}$ noise for three different values of tunnel couplings (colors). The symbols corresponds to a numerically averaged 100 realizations of the classical noise. Solid lines are the exponential $Q = \frac{1}{2}(1 - e^{-2\delta Q_{\epsilon\epsilon,1}})$. The black line is the result for $1/f$ noise. We use the calibration described in Eq. (8.11), in which $S_1(\omega_h) = S_{1.5}(\omega_h)$, where $\omega_h = 15\,\mu$eV. Adapted from [1]

The result in Fig. (8.3) is plotted for different tunnel couplings t_c (colors) and compared against $\beta = 1$ noise (black line). We calibrate both noise spectra at $\omega_h = 15\,\mu$eV, and as expected the transfer probability at $t_c = 15\,\mu$eV for $\beta = 1.5$ case is above $\beta = 1$ case, since $h(1.5)/h(1) = 0.87$. Physically it means that there is less power spectral densities in the frequencies above $\Omega > 15\,\mu eV$. For the same reason the result for large tunnel coupling $t_c = 25\,\mu$eV, lies above the $\beta = 1$ case. In the opposite regime of $t_c = 5\,\mu$ eV, the spectral weight of $1/f^{1.5}$ is larger, and hence the error increases.

High temperature regime

The above analysis has been developed using the assumption of the classical fluctuations in detuning, for with the relaxation and excitation rates are equal, i.e. $\Gamma_+ = \Gamma_-$. This can be associated with the relatively high temperature[12] in comparison to relevant energy scales, i.e. tunnel coupling t_c. We now attempt to estimate range of parameters, in which classical noise approach can be applied.

12: more precisely thermal energy $k_B T$

Significance of high temperature

As a motivation we take the recently considered possibility of quantum computation using spin qubits at relatively high temperature of $T = 1$K. Achieving this task is expected to be beneficial from the perspective of saving resources[13] and enabling integration to classical control electronic

13: in particular to significantly limit the energy consumption,

inside the qubit array [188, 189]. For this reason we set the temperature to $T = 1\text{K}$, which corresponds to thermal energy of $k_B T \approx 100\,\mu\text{eV}$.

Prediction of adiabatic Master equation

We now compute predictions of adiabatic Master equation in the limit of high temperature, i.e. $\Gamma_+ = \Gamma- \equiv \Gamma$. As usually in this thesis we assume here that the electron is initially in the ground state, i.e. $Q_0 = 0$, which from the Eq. (5.73) allows to write the final error as

$$Q_{\text{cl}}(t_f) = \int_{t_i}^{t_f} \mathrm{d}t \Gamma(t) e^{-2\int_t^{t_f} \Gamma(t')\mathrm{d}t'}. \tag{8.13}$$

We now expand the limits to infinity and compute the integral analytically[14] , which gives

14: Using substitution $\chi(t) = 2\int_t^\infty \Gamma(t')\mathrm{d}t'$

$$Q_{\text{cl}} = \frac{1}{2}\left(1 - e^{-2\int_{-\infty}^{\infty}\Gamma(t)}\right), \tag{8.14}$$

and shows that in the limiting case of $\int_{-\infty}^{\infty}\Gamma(t) \gg 1$, i.e. strong coupling or relatively long evolution time, we obtain $Q_{\text{cl}} = 1/2$. Note that when both detuning and tunnel coupling noise are considered, the relaxation rate reads:

$$\Gamma(t) = \frac{1}{4}\left[S_\epsilon(\Omega[t])\cos^2\vartheta(t) + S_{t_c}(\Omega[t])\sin^2\vartheta(t)\right], \tag{8.15}$$

Numerical simulation

Motivated by the above we now move to numerical simulation, which aims at reproducing classical noise approach at $T = 1\text{K}$. To keep the orbital gap below thermal energy we set initial and final detuning to $\epsilon = \pm 100\,\mu\text{eV}$. We consider here both 1/f and Johnson charge noise. For the 1/f noise we use the $A_1(1K) = (1.5)^2\,\mu\text{eV}^2/\text{Hz}$, which using linear scaling with temperature from Eq. (7.32) can be related to $A_1(0.1K) = (0.5)^2\,\mu\text{eV}^2/\text{Hz}$. Since in the considered regime of temperatures, the Johnson noise is effectively flat[15] , for numerical simulation we model Johnson noise by the white Gaussian Noise with the spectrum $S_j(\omega) = (0.3)^2\,\mu\text{eV}^2/\text{Hz}$. For completeness we add also the fluctuations of tunnel-coupling, which for both 1/f and Johnson noise spectra are reduced by a factor of 10^{-2}, i.e. $S_{t_c}(\omega) = 10^{-2}S_\epsilon(\omega)$.

15: See definition of spectral density for $\omega \ll k_B T$

In fig. (8.4) we plot the transfer error Q as numerical averages over realization of the Johnson (filled dots) and 1/f (hollow dots) noise processes in tunnel coupling and detuning. We plot the results for different tunnel couplings (colors). The numerically averaged result confirms predictions of adiabatic Master equation (AME) fed by the spectral densities of the corresponding noise processes. The AME results are plotted using solid lines for the noise in detuning, and dashed lines for the noise in tunnel coupling.

First we see that in the limit of fast sweeps, the error is dominated by the L-Z process. In the opposite limit noise-dominated error for 1/f noise is independent of tunnel coupling for both fluctuations of tunnel coupling and detuning as expected. The independence of t_c is approximately true

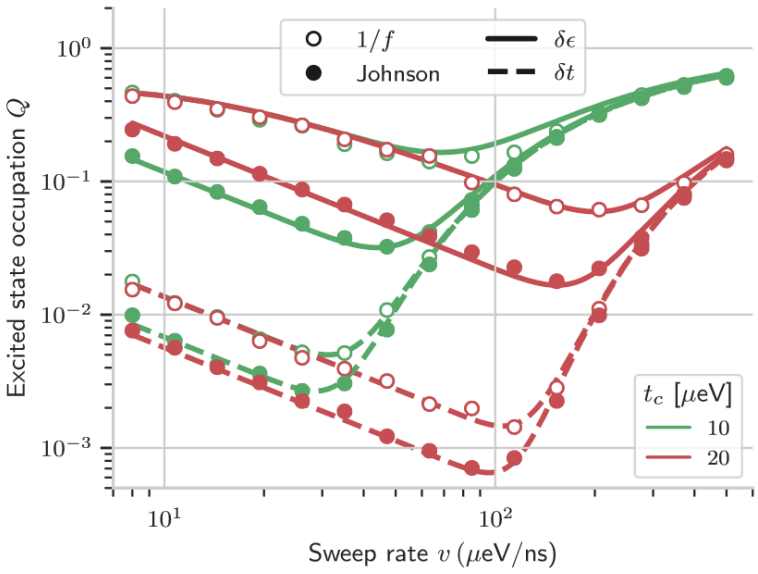

Figure 8.4: Charge transfer error as a function of sweep rate, plotted separately for the evolution in presence of only 1/f noise (hollow dots) or only Johnson noise (filled dots), in the detuning (solid lines) or tunnel coupling (dashed lines) for two tunnel couplings $t_c = 10, 20\,\mu$eV. We compare the direct averaging over realisation of the noise (symbols) versus the results of the adiabatic Master equation (lines) with suitable spectral densities. Adapted from [2].

for the white noise in tunnel coupling and untrue for the white noise in detuning. As the spectral density of white noise does not depend on the energy gap, the difference can be understood from considerations on amount of time during which, detuning and tunnel coupling noise are transverse in the orbital basis. The detuning noise can be considered transverse in vicinity of avoided crossing, for approximate time period of $\sim 2t_c/v$. On the other hand the tunnel coupling noise is transverse away from avoided crossing for the time period $2\epsilon(t_f)/v - 2t_c/v \approx 2\epsilon(t_f)/v$, which for large detuning sweep range $2\epsilon(t_f) \gg t_c$ weakly depends on tunnel coupling. We finally conclude that difference between the error caused by the white and 1/f noise is slightly larger for detuning noise. This is because the relaxation due to detuning noise takes place around avoided crossing, where less energy transfer is needed in comparison to relaxation due to coupling noise, which takes place at larger energies at which $1/f$ spectrum has less weight.

Overall we conclude this section by stating that in the limit of high-, but still relevant for some applications temperature, the classical noise and Master equation approaches predict equivalent transfer errors due to typical amplitudes of charge noise. We now move to the low-temperature limit, that is relevant for most ongoing experiments. In this limit the classical noise approach is expected to fail, since the excitation rates are thermally suppressed in comparison to relaxation.

8.3 Quantum noise limit

The end-goal of our analysis is the estimation of fidelity of coherence electron transfer for the μm distance. For the transfer realised using consecutive DQD transitions, it will require hundreds of pre-defined quantum dots. The sequential structure of the transfer means that in most likely scenario the transfer might be limited by a weak link, e.g. pair of quantum dots, with low value of tunnel coupling. For this reason we now concentrate on the limit when tunnel coupling is comparable to typical thermal energy of $k_B T \sim 10\,\mu$eV. In this limit, although excitation

rate is suppressed by the Boltzmann factor,[16] i.e. $\Gamma_+ = \Gamma_- e^{-\beta\Omega}$, it cannot be completely neglected[17] . In particular it suggest finite probability of excitation around avoided crossing, where the gap between ground and excited orbital state is minimal.

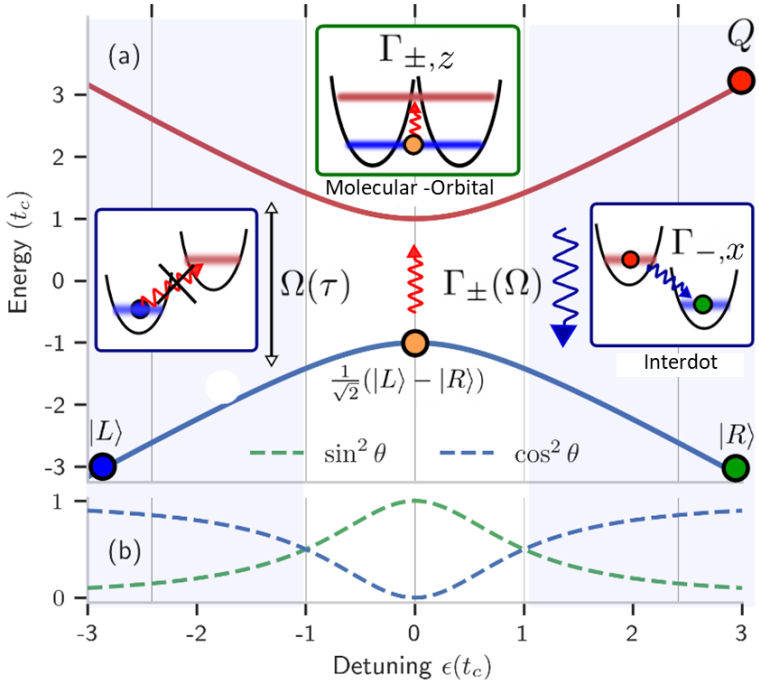

Figure 8.5: The schematic picture of the interdot transition in presence of the high-frequency environmental noise that causes inelastic transitions between the levels. In a) we plot the instantaneous spectrum of the DQD charge transfer, together with the insets which show most relevant processes in a given regime. We illustrate the that at typical temperatures most excitations takes place around the avoided crossing, where the levels have molecular-orbital character (inset), while the relaxation takes place between the dot-like states (interdot) at larger detuning. In b) we show the composition of the instantaneous states which can be related to dot-like states (blue dashed line) and molecular-orbital (green-dashed line). Adapted from [2]

We illustrate the typical scenario in Fig. 8.5a), where the energy spectrum of the DQD transition is showed as a function of dots detuning. We schematically show the physical picture, in which for the initially occupied ground state, the evolution is expected to be adiabatic up to the moment where $e^{-\beta\Omega}$ is not negligibly small, which takes place around avoided crossing. It is the place where most excitations takes place. For large, positive detunings typically the relaxation process dominates, which allow to recover some of the occupation of the ground state that is being transferred to the target dot. Note that around avoided crossing the transition between the instantaneous state are mostly caused by the detuning noise $\Gamma_{\pm,z}(\mp\Omega[t]) \propto S_z(\mp\Omega[t])\sin^2\theta$, while the relaxation at large detuning is caused by noise in tunnel coupling $\Gamma_{-,x}(\Omega[t]) \propto S_x(\Omega[t])\cos^2\theta$. To illustrate dynamically change character of transverse noise in Fig. 8.5b we plot the value of the $\sin^2\theta$ and $\cos^2\theta$ as a function of detuning.

Coherent and incoherent evolution

In the limit of fast sweep we expect the error to be dominated by the physics of the Landau-Zener transition, associated with the coherent transition from ground to excited state. The probability of occupying excited state due to such coherent coupling, was previously given as:

$$Q_{\mathrm{LZ}} = \exp\left(-\frac{\pi}{2}\frac{t_c^2}{2v}\right), \tag{8.16}$$

16: i.e. which prevent analysis using classical noise approach.

17: In recent demonstration of charge transfer between two quantum dots, the value of tunnel coupling strongly exceeded thermal energy, i.e. $t_c > 100\,\mu$eV [100, 101], and in this way effectively suppressed any thermal excitations. We expect such regime would be difficult to achieve in the limit of long quantum array.

which shows that the Landau-Zener error is suppressed exponentially for sufficiently slow sweep rate v.

It also means that there exists the adiabatic regime, where $t_c^2/v \gg 1$ and coherent coupling between adiabatic levels $\dot{\vartheta}$ in the Master equation can be neglected[18] . In such case, the loss of occupation of the ground state Q due to presence of environment has the analytical form:

$$Q_{\text{env}} = \int_{-\infty}^{\infty} \mathrm{d}\tau \Gamma_+(\tau) \exp\left(-\int_{t_i}^{t_f} \Gamma_+(\tau') + \Gamma_-(\tau')\mathrm{d}\tau'\right). \tag{8.17}$$

Since the general treatment of the nested integral might be complicated for time-dependent relaxation rate, below we present a few approximate treatment for noise induced charge error.

18: See Eq. (5.70) for the exact form of adiabatic Master equation in the Linblad form

Single Excitation Approximation Limit

We continue with one of the simplest approaches, in which w assume that at most a single transition from ground to excited state is possible. In such case the equations of motion, from the Master equation can be solved perturbatively, leading to a result in Single Excitation Approximation Limit (SEAL)

$$Q_{\text{SEAL}} = \int_{t_i}^{t_f} \Gamma_+(\Omega[t]), \tag{8.18}$$

where the excitation rate is evaluated at avoided crossing. The above approach is applicable only if the typical $Q_{\text{SEAL}} \ll 1$, since otherwise relaxation process has to be considered[19]

19: As we will show this approach would be more suitable to electron transfer between Si-based quantum dot, where timescale needed for inelastic transition is much longer.

We now take into account the time-dependence of the excitation rate, which result from dynamically changing: orbital gap $\Omega(t)$ and the composition of adiabatic states. In particular in typical situation where the detuning noise dominates over the noise in tunnel coupling, i.e. $S_\epsilon(\Omega) \gg S_{t_c}(\Omega)$ most transitions takes place at the avoided crossing, when multiplicity factor of $\sin^2\theta \approx 1$. In such a case the integral in Q_{SEAL} can be computed in the approximate manner, by assuming that the relaxation rate around avoided crossing is approximately constant and given by $\Gamma_+(t_c)$ and the excitation takes place in a finite finite time-window Δt, i.e.

$$Q_{\text{SEAL}} \approx \Gamma_+(t_c)\Delta t \tag{8.19}$$

In particular as we have showed in the classical noise considerations, in high temperature limit the time-window is just given by the time spent in vicinity of avoided crossing[20] $\Delta t = 2t_c/v$ i.e.

20: which we estimated by the time during which the orbital gap $\Omega = \sqrt{t_c^2 + \epsilon(t)^2}$ is dominated by the tunnel coupling

$$Q_{\text{SEAL}}^{(\beta t_c \ll 1)} = \Gamma_-(t_c)\frac{2t_c}{v}, \tag{8.20}$$

For the lower temperature the excitation window Δt is expected to be smaller due to exponential suppression by the Boltzmann factor. To find its effective width we expand the gap around $\epsilon = 0$, i.e.

$$\Omega(\tau) \approx t_c + \frac{1}{2}\frac{(vt)^2}{t_c}. \tag{8.21}$$

Single Excitation Limit Approximation (SEAL)

The resulting Gaussian integral in Eq. (8.19) can be computed by expanding integration limits of to infinity. In such case we obtain:

$$Q_{\mathrm{SEAL}}^{(\beta t_c \gg 1)} = \frac{\sqrt{2\pi}}{v} \sqrt{k_{\mathrm{B}} T t_c}\, \Gamma_+(t_c), \tag{8.22}$$

Both in high- and low-temperature regimes we have showed that the probability of the excitation at the avoided crossing is inversely proportional to the sweep rate $Q_{\mathrm{SEAL}} \propto 1/v$, which together with Landau-Zener probability, for which the Q_{LZ} increases with higher v, predicts a trade-off behaviour and the existence of optimal velocity. Below we will show that this is further modified by possibility of ground state recovery.

Healed Excitation Approximation Limit

Healed Excitation Limit Approximation (HEAL)

The effect of subsequent transitions is encapsulated by the exponential function in Eq. (5.73), however its exact computation might be complicated for realistic $\Gamma_\pm(\Omega[t])$. We proceed with an approximate way of taking account relaxation process. We assume the excitation can take place only once[21] , in the vicinity of the avoided crossing, i.e. $\Gamma_+(\Omega[t]) = Q_{\mathrm{SEAL}}\delta(t)$, where $\delta(t)$ is the dirac delta. Consequently

$$Q_{\mathrm{HEAL}} = Q_{\mathrm{SEAL}}^{(\beta t_c \gg 1)} \exp\left(-\int_0^{t_f} \Gamma_-(\tau')\right), \tag{8.23}$$

where $Q_{\mathrm{SEAL}}^{(\beta t_c \gg 1)}$ have been given by Eq. (8.22).

21: Naturally this approach is suitable in low-temperature, in which relaxation rate $\Gamma_- \gg \Gamma_+$.

Relaxation-aided transfer

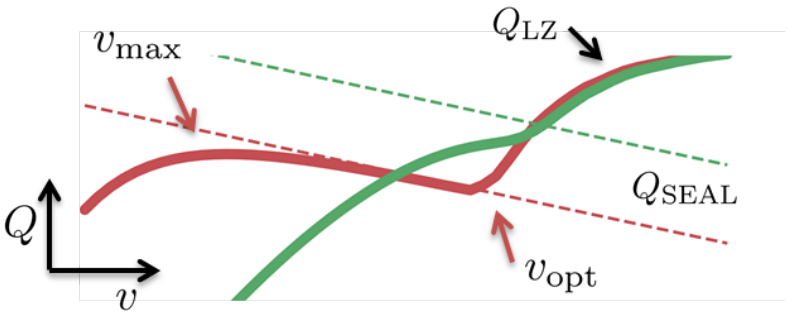

Figure 8.6: Sketch of the charge transfer error as a function of sweep rate. For weakly coupled case (red line), we expect to local extrema: The local minimum at v_{opt} at which $Q_{\mathrm{LZ}}(v_{\mathrm{opt}}) = Q_{\mathrm{SEAL}}(v_{\mathrm{opt}})$ (See Eq. (5.18) and Eq. (8.22) respectively), and the local maximum at $v_{\max}$ at which $\int_0^{t_f} \Gamma_-(t) = 1$ (note that $v = \epsilon(t_f))/t_f$. For the stronger coupling to environment (green line), similar estimation gives $v_{\max} > v_{\mathrm{opt}}$ and hence result in the monotonic behaviour of $Q(v)$.

We now use the above formulas to discuss the additional effects due to relaxation process, which can recover some occupation of the ground state. In the limit of fast sweeps, which can be related to short transition times $2t_f$[22] . In such a case, the relaxation is often too slow to affect the error dominated by the exponential form of the Landau-Zener excitations, that scales as $Q_{\mathrm{LZ}} \propto e^{-At_f}$. For slower sweeps, at some point the error becomes dominated by the single transitions from ground to excited state which however is proportional to transfer time $Q_{\mathrm{SEAL}} \propto 1/v \propto t_f$. Finally when the transfer time becomes comparable with some effective relaxation time $\tilde{\Gamma}_-$, i.e.

$$\chi_{\mathrm{HEAL}} = \int_0^{t_f} \Gamma_-(t) \approx \tilde{\Gamma}_- t_f \sim 1, \tag{8.24}$$

22: which for constant detuning sweep range can be related to $t_f \propto 1/v$

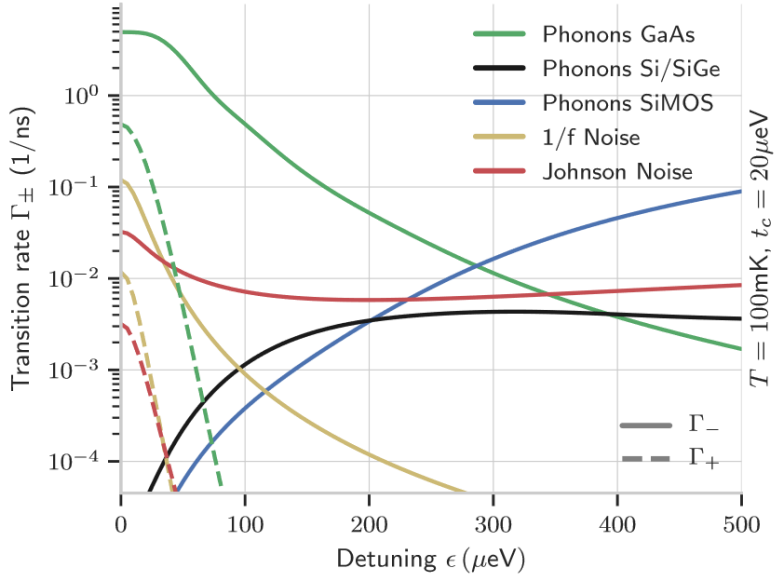

Figure 8.7: Transition rates in the DQD systems. We plot Relaxation (solid lines) and excitation (dashed) rates in the double quantum dot systems as a function of dots detuning at $t_c = 20\,\mu$eV and $T = 100$mK, using models developed in Chapter 7. We separately plot contributions from 1/f noise (yellow line), Johnson noise (red), and phonons in the three DQD models from Sec. 6.3: GaAs (green), Si/SiGe (black) and SiMOS (blue). Adapted from [2].

the occupation of excited state becomes exponentially suppressed $Q_{\text{HEAL}} \propto e^{-2\tilde{\Gamma}_- t_f}$, which means the error start to decrease for slower sweeps[23] . The illustration of the expected non-monotonic behaviour of $Q(v)$ is showed in Fig. 8.6, where we denote the location of local minimum as v_{max}[24] and location of local maximum as v_{opt}[25] .

Note that the non-monotonic pattern is present only if $v_{\text{max}} < v_{\text{min}}$. Otherwise the $Q(v)$ is a monotonically increasing function of v, which is a typical situation in the case of sufficiently fast relaxation rate.

23: Similarly to Q_{LZ}

24: which we define via the relation

$$\chi_{\text{HEAL}} \sim 1$$

25: which we define via

$$Q_{\text{LZ}}(v_{\text{opt}}) = Q_{\text{SEAL}}(v_{\text{opt}})$$

Relaxation rates for realistic DQD devices

To prepare the ground for computing probability of charge transfer, now in Fig. 8.7 we compute the values of relaxation (solid lines) and excitation (dashed lines) rates due to phonons (Sec. 7.2) and charge noise (Sec. 7.3), computed for three DQD devices from Sec. 6.3. We assume the charge noise weakly depends on the dots geometry[26] and separately plot 1/f, Johnson and phonon transition rates for each of the considered devices using different colors. We use parameters from the ballpark of relevant experiments, i.e. $t_c = 20\,\mu$eV and $T = 100\,$mK for which $\Gamma_+(t_c)/\Gamma_-(t_c) \approx 0.1$

26: Which might not be the case in presence of non-negligible spatial correlation of the noise. See Sec. 7.3 for discussion

We start with GaAs-based device for which piezoelectric phonons dominate both relaxation and excitation. In this case we see relatively fast relaxation rate in vicinity of avoided crossing, with translates to excitation timescale at the avoided crossing $1/\Gamma_+^{(\text{GaAs})}(t_c) \approx 2$ns and similar value of typical relaxation time $1/\tilde{\Gamma}_-^{(\text{GaAs})} \approx 1$ns.[27] This means that any sweep that leads to ns-time spent in the vicinity of the avoided crossing would leads to high probability of occupying the excited state[28] . As discussed above for sufficiently slow sweeps the fast relaxations is expected to bring the qubit to thermal equilibrium value of

$$Q_{\text{eq}}(\Omega) \approx \frac{\Gamma_+(\Omega)}{\Gamma_+(\Omega) + \Gamma_-(\Omega)} \approx e^{-\beta\Omega}, \tag{8.25}$$

27: as it ranges from $1/\tilde{\Gamma}_-^{(\text{GaAs})}(t_c) = 0.2\,$ns to $1/\tilde{\Gamma}_-^{(\text{GaAs})}(200\,\mu\text{eV}) = 20\,$ns

28: One can estimate that for $v = 10\,\mu$eV and $t_c = 20\,\mu$eV the time spend around $\epsilon = 0$ is $t_c/v \sim 2\,$ns.

which for considered parameters gives $Q_{\mathrm{eq}}(t_c) = 0.1$ at the avoided crossing. Note that away from the avoided crossing the equilibrium occupation is decreasing exponentially, which means that for sufficiently slow sweep rate v the transfer is expected to be ideal provided $\int \Gamma_-(\Omega[t])\mathrm{d}t$ is sufficiently large.

We now move to the case of Si-based device, in which the excitations around the avoided crossing are dominated by charge noise. Note that the predicted amplitude of 1/f and Johnson noise are comparable and estimate excitation timescale as low as $1/\Gamma_+^{(\mathrm{SiGe})}(t_c) = 100$ns. This shows that for the same sweep v probability of transition from ground to excited state is lower then in GaAs. However the weak coupling between the electron and the environment also means that the relaxation aided transfer is less probable, meaning that the speed at which relaxation allows for significant recovery of the ground state is expected to be much lower. In particular, relaxation aided transfer in SiGe devices requires transfer time of the order of $t_f \approx 1/\tilde{\Gamma}_- \sim 100\,\mathrm{ns}$ (red line). The situation might slightly improve in the SiMOS devices where smaller distance between the dots allows for faster interdot phonon relaxation, which gives $1/\tilde{\Gamma}_- \sim 10\,\mathrm{ns}$ but only at large detunings (blue line)[29] .

29: In theory it would allow to park the electron at sufficiently large detuning and wait for the relaxation to take place. However as we will show in the Chapter 12 this most likely would lead to spin dephasing of shuttled electron

We conclude that typical GaAs device represent the limit of strong coupling, where possibly multiple transitions between the adiabatic levels are expected. In contrast both Si-based devices show weak coupling, which limits exciations around avoided crossing but prevent their subsequent recovery away from avoided crossing.

Results and discussions

We finally use the above to compute and analyze electron charge transfer. In Fig. 8.8 we compute charge transfer error Q as a function of sweep rate for various tunnel couplings $t_c = 10, 20\,\mu$eV and the sweep range $\Delta\epsilon = 1$meV for the DQD devices from Sec. 6.3. For each tunnel coupling and DQD system we compute transition rates $\Gamma_\pm(\tau)$ using methods from Chapter 7. In the figure we compare exact solution of adiabatic Master equation (AME, filled and hollow squares) against approximate solutions, i.e. Q_{SEAL} (dashed line) and Q_{HEAL} (solid line). By hollow squares we denote results obtained beyond the expected limits of validity of AME in the Linblad form[30] . Additionally we plot bare Landau-Zener probability using dotted black line. Below we discuss separately results of GaAs- and Si-based nanostructures.

30: As it was pointed out in [111]

Si-based devices

We start with the analysis of Si-based devices, which shows relatively weaker coupling to environmental fluctuations. The picture is similar for SiMOS (blue) and SiGe (red) devices, however in the former case, the error in the relaxation dominated region[31] is smaller thanks to larger role of interdot phonons.

31: i.e. in the region of small v, where $\int \Gamma_-(t)$ is not negligible,

Commonly for both SiGe and SiMOS we observe the non-monotonic structure of the charge transfer error $Q(v)$ as a function of sweep rate. For slowest sweeps $v < v_{\max}$ the error increases with v, since the electron

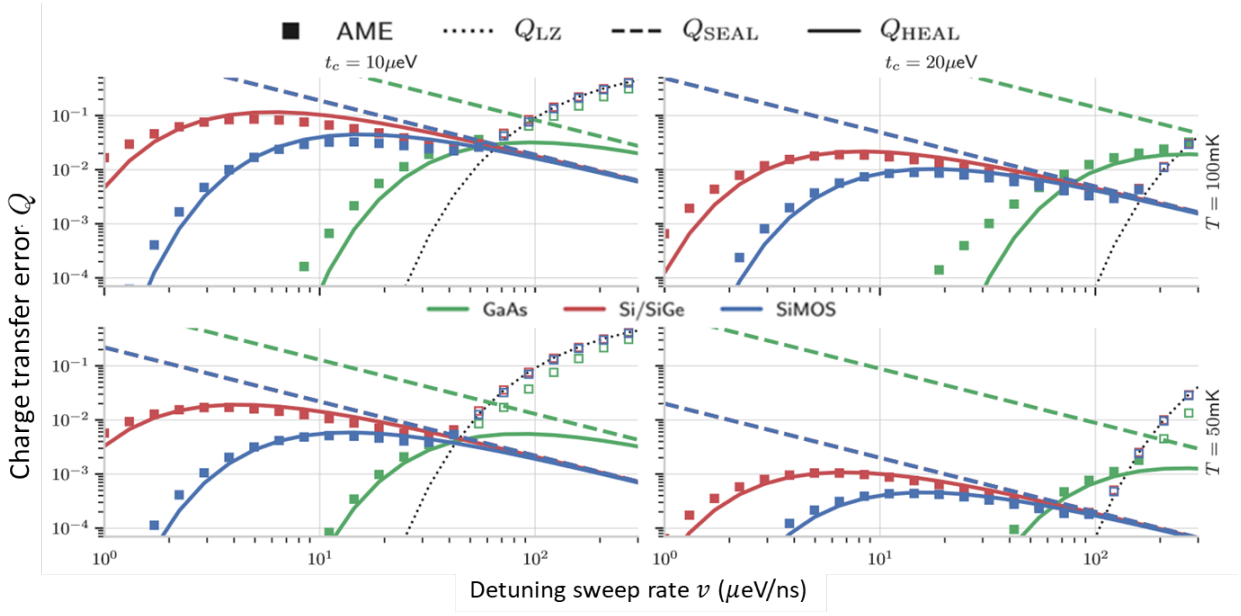

Figure 8.8: Charge transfer error during interdot transition Q for $t_c = 10, 20\,\mu$eV and $T = 50, 100$mK. Using different colors we plot the results for the GaAs (green), Si/SiGe (red) and SiMOS (blue) devices from Sec. 6.3. The dashed lines are the predictions of the Q_{SEAL} from Eq. (8.22). The solid lines are the predictions of the Q_{HEAL} from Eq. (8.23). Symbols shows the result of the adiabatic Master equations. Hollow symbols shows the regime where Landau-Zener transition (black dotted line) dominates. Adapted from [2].

has less time to relax from the excitation that took place around avoided crossing. Next the character of the curve changes at $v > v_{\max}$, where $\chi_{\mathrm{HEAL}} < 1$, and hence ground state recovery is inefficient. In this limit, dominated by $Q \sim Q_{\mathrm{SEAL}} \sim 1/v$, the slower sweeps leads to more time spent around avoided crossing where unaided excitations take place.[32] Finally at the fastest sweeps $v > v_{\mathrm{opt}}$ the error start to increase due to coherent excitations described by the Landau-Zener model.

32: Hence the error decreases for faster sweeps

Note that this picture is common for all $t_c = 10, 20\,\mu$eV and $T = 50, 100$mK, where however the Q_{HEAL} formula works best for $t_c = 20\,\mu$eV and $T = 100$mK limit, where the time-window for relaxation is the smallest. Also the location of v_{opt} and $v_{\max}$ is modified, however their location is consisted with the predictions based on the transition rates. Note that based on the computed rates from Fig. 8.7, for $t_c = 20\,\mu$eV and $T = 100$mK, typical relaxation rate in Si $\tilde{\Gamma}_- \sim 0.01\,\mathrm{ns}^{-1}$ one can estimate[33] $v_{\mathrm{opt}} \approx 10\,\mu\mathrm{eV/ns}$, which agrees with numerical data.

33: from the equation $\tilde{\Gamma}_- \frac{\Delta\epsilon}{v_{\mathrm{opt}}} \sim 1$

GaAs device

The non-monotonic structure of $Q(v)$ is absent in GaAs-based device, where relatively stronger coupling to piezoelectric phonons is present. This is indicated by at least order of magnitude stronger Q_{SEAL}, which shows how much larger probability of excitation at avoided crossing in GaAs is in comparison to Si. In fact when its square becomes comparable to unity $Q^2_{\mathrm{SEAL}} \approx 1$, we expect more than a single excitation from ground to excited state, which means that the Q_{HEAL} approximation is no longer expected to work[34] . The absence of the local maximum can be attributed to estimated value of $v_{\max} > 100\,\mu\mathrm{eV/ns}$ which is larger or at least comparable to the intersection of Q_{LZ} and Q_{SEAL}.

34: As it can be seen from $t_c = 20\,\mu$eV, $T = 100$mK case from Fig. (8.8)

Although higher probability of excitations at avoided crossing leads to possibly larger error in the vicinity of $v \approx 100\,\mu$eV/ns, where Q_{LZ} becomes dominated by the incoherent contribution, orders of magnitude faster relaxation allows for much lower transfer error for slower sweeps in comparison to Si-based devices. In particular the charge transfer error is expected to be $Q < 10^{-4}$ for $v < 10\,\mu$eV/ns in all the considered cases.

Larger tunnel coupling

We move to larger tunnel coupling. We take $t_c = 40\,\mu$eV,[35] and similarly to before in Fig. 8.9 plot charge transfer error as a function of v. For $T = 100$mK, previously described difference between the Q for Si- and GaAs-based devices is even more visible: the charge transfer in the former is better at faster sweeps and worse in the slower sweeps where in principle relaxation processes can be used for the recovery of the ground state occupation.

35: which corresponds to reported value of tunnel coupling used to demonstrate charge transfer in the array of 9 quantum dots [98]

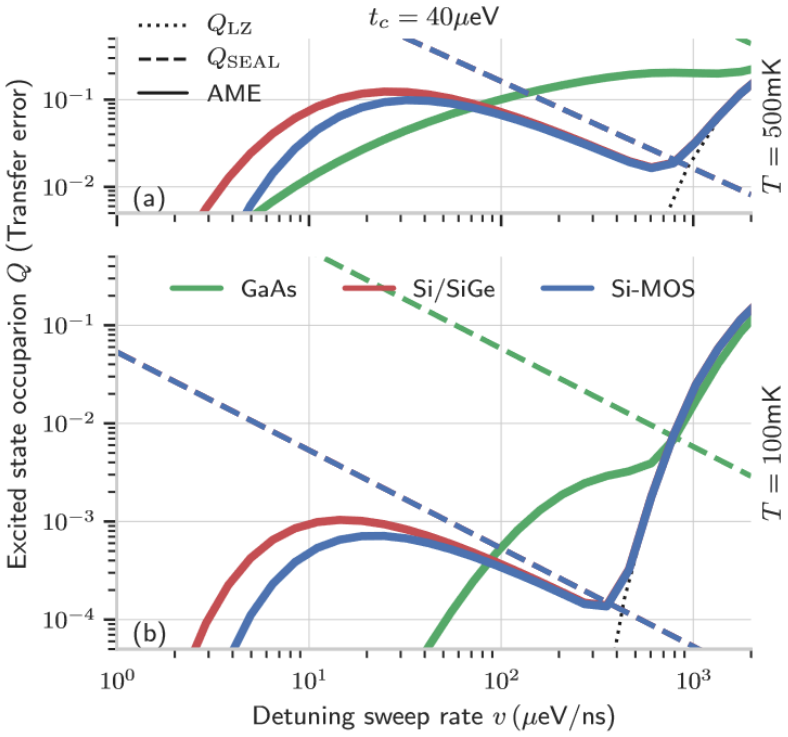

Figure 8.9: Charge transfer error during interdot transition Q for $t_c = 40\,\mu$eV and two different temperatures $T = 500$mK (a) and $T = 100$mK (b). With different colors we plot the results for the GaAs (green), Si/SiGe (red) and SiMOS (blue) devices from Sec. 6.3. The solid lines are the predictions of the Q_{HEAL} from Eq. (8.23). The black dotted line is the Landau-Zener formula. Adapted from [2].

Note that larger tunnel coupling generally allows for faster transfer, i.e. the $v_{\mathrm{opt}} = 400\,\mu$eV for Si-based devices, which translates to much more practical few-ns transfer. In this regime the error for GaAs device is more then order of magnitude larger then for Si-based devices, for which it becomes close to $Q = 10^{-4}$ at v_{opt}. We highlight that such transfer error could easily allow for shuttling over $N \sim 10$ dots ($L \sim 1\,\mu$m), but might become above 1% for $N > 100$dots ($L > 10\,\mu$m) since $100Q > 10^{-2}$.[36]

36: See the discussion in the Sec. 13.2.

To analyze possibility of electron shuttling at higher temperatures we include here also result for the temperature of $T = 0.5K$. In this case the probability of excitation naturally increases, but the position of the v_{max} and v_{opt} for Si remains approximately the same. The difference is much bigger for the GaAs-based device for which higher temperature hinders

relaxation-aided transfer[37] , which is visible by making the $Q(v)$ line less steep and much more comparable to Si at low v.

37: Increased equilibrium occupation of the excited state

III. Spin degree of freedom during charge transfer

9 Spin qubit in semiconductor quantum dot

We now focus on the electron internal degree of freedom, the spin, which is used as a carrier of quantum information in quantum dot-based quantum devices. We start in Sec. 9.1 by introducing undriven spin qubit in a single quantum dot. We first define its Hamiltonian and show that in absence of spin-orbit coupling the source of non-unitary evolution are the nuclear spins. We discuss the nuclear-induced dephasing and discuss most important difference between the spin qubit in GaAs- and Si-based devices. Next in Sec. 9.2 we discuss the intrinsic and synthetic spin-orbit coupling and show how it leads to correlation between spatial and spin degrees of freedom. We finally in Sec. 9.3 argue that in presence of such a correlation spin qubit inherits from the charge qubit sensitivity to environmental fields, previously discussed in context of orbital states of DQD.

9.1 Electron spin qubit

From the analysis of the coupling between orbital TLS and environmental fields from Sec. 7.1, one can infer that the influence of the environment can be minimized if the quantum information is encoded in an internal degree of freedom (such as spin), characterized by similar wavefunction. Thus, natural candidate for the quantum information precessing using electron trapped in the semiconductor quantum dot is the electron spin. In presence of external magnetic field $\mathbf{B}$, the states associated with intrinsic angular momentum splits into two levels known as spin-up and spin-down, i.e. $\hat{H}_{\text{spin}}|\uparrow\rangle = E_z/2\,|\uparrow\rangle$ and $\hat{H}_{\text{spin}}|\downarrow\rangle = -E_z/2\,|\downarrow\rangle$, where E_z is called the Zeeman splitting. The general Hamiltonian of the electron occupying quantum dot can be written as:

$$\hat{H}_{\text{spin}}(t) = \frac{1}{2}(\hat{\boldsymbol{\sigma}} \cdot \mathbf{b}(t)), \tag{9.1}$$

where $\hat{\sigma}$ are the Pauli operators in some basis, which in general is not the eigenbasis of $\hat{H}_{\text{spin}}$. Such Hamiltonian generates precession around instantaneous effective magnetic field $\mathbf{b}(t)$, which at any time can be related to external magnetic field $\mathbf{B}$ by the equation:

$$\mathbf{b}(t) = \mu_B \hat{\mathbf{g}}(t)\mathbf{B}(t), \tag{9.2}$$

where $\hat{\mathbf{g}}(t)$ is the so-called g-factor tensor,[1] that translates external magnetic field $\mathbf{B}(t)$ into the precession axis $\mathbf{b}(t)$. Due to much stronger confinement in the transverse direction the external magnetic field is usually applied in-plane,[2] i.e.

$$\mathbf{B}_0 = B_0(\cos\varphi_B, \sin\varphi_B, 0), \tag{9.4}$$

1:
$$\hat{\mathbf{g}} = \begin{bmatrix} g_{xx} & g_{xy} & g_{xz} \\ g_{yx} & g_{yy} & g_{yz} \\ g_{zx} & g_{yz} & g_{zz} \end{bmatrix} \tag{9.3}$$

2: Which allows to minimize corrections from the electron cyclotron motion [30]

where the angle φ_B donates angle with respect to x-axis defined here as [110] crystallographic axis.

For the isolated electron the g-factor is isotropic[3] , i.e. $g_{ii} = g$ and $g_{i\neq j} = 0$ with $g = -2.002319$ [169], while for the electron confined in the quantum dot, the g-factor tensor is often significantly anisotropic due to: cubic symmetry of the crystal lattice, presence of spin-orbit interaction, and anisotropic shape of the quantum dot, all of which reduces SU(2) symmetry of the spin in vacuum [30].

3: and negative as a consequence of electron negative charge. We will use the convention in which only absolute value of g factor matter, i.e. adjust the direction of external magnetic field such that $E_z > 0$ for both considered materials.

In most application, the Zeeman splitting is caused by the to external magnetic field. They can by related by Eq. (9.2), i.e. $E_z = |\mathbf{b}|$, using which the Hamiltonian of isolated spin reads

$$\hat{H}_{\text{spin,iso}} = \frac{1}{2} E_z \hat{s}_z , \tag{9.5}$$

where $\hat{s}_z$ Pauli operator, points along direction of $\mathbf{b}_0 = \mu_B \hat{\mathbf{g}} \mathbf{B}_0$.

Spin-qubit control

The possibility of modulating magnetic field of the g-factor tensor in time allows for coherent control of electron spin qubit. In the basis of $\hat{H}_{\text{spin,iso}}$ the control is realized by the the perpendicular component, i.e.

$$\hat{H}_{\text{spin,ctrl}} = \frac{1}{2} \left(b_\perp(t) \hat{s}_+ + b_\perp^*(t) \hat{s}_- \right) , \tag{9.6}$$

where $\hat{s}_\pm = (\hat{s}_x \pm \hat{s}_y)/2$. It is often used to drive Rabi rotations, which can be achieved if $b_\perp(t) \approx A \cos(\omega t)$, where $\omega \approx E_z$ and $A \ll |\omega - E_z|$. Two most popular methods uses time-dependent magnetic field known as electron spin resonance and time-dependent electric field,[4] known as Electric dipole spin resonance (EDSR) [190]. We highlight that in view of building quantum computer the second method allows to significantly improve scalability and the speed of the coherent control. However it requires a creation of finite effective electric dipole moment of the electron. This is usually done by coupling the electron spin to orbital degree of freedom, which by design makes the spin qubit sensitive to environmental electric fields[5] .

4: that couples to spin degree of freedom due to presence of spin-orbit interaction

5: This includes uncontrolled fluctuations of electric field (charge noise) and lattice vibrations.

9.2 Spin-orbit coupling

We now discuss origin of the interaction between the two lowest-lying in energy, bound states of the electron in the quantum dot and its internal spin states used for quantum information processing. We continue to use here an effectively 1D model, within which general form of the spin-orbit Hamiltonian reads:

$$\hat{V}_{\text{so}}(\hat{x}, \hat{p}_x) = \frac{1}{2} \left(\mathbf{b}_{\text{so}} \cdot \hat{\mathbf{s}} \right) = \frac{1}{2} \left(\delta b_\parallel^{(\text{so})}(\hat{x}, \hat{p}_x) \hat{s}_z + \delta b_\perp^{(\text{so})}(\hat{x}, \hat{p}_x) \hat{s}_x \right) , \tag{9.7}$$

where we introduced position $\hat{x}$ and momentum operator $\hat{p}_x$ along relevant axis and the spin Pauli operators $\hat{s}_i$. In general we assume that the spin-orbit coupling is weak, such that the orbital wavefunctions introduced in Sec. 6.1 can be used as the basis for perturbative expansion.

Below we explicitly specify contribution from the intrinsic and synthetic spin-orbit coupling and then show how they influence wavefunctions of the spin qubit states.

Intrinsic spin-orbit coupling

Physically the intrinsic spin-orbit interaction is related to the motion of the electron. When electron is moving, relativistic transformation to the frame co-moving with it transforms part of electric field in the stationary frame to magnetic field in moving frame.[6] Many gate-defined quantum dots, including relevant for this thesis GaAs- and Si-based ones, have a C_{2v} point-group symmetry, which is the same as H_2O molecule [191]. As a result of symmetry considerations[7] the planar part of the general spin-orbit Hamiltonian has a form:

$$\hat{V}_{\text{so,xy}} \sim A\hat{p}_x\hat{s}_{c,y} + B\hat{p}_y\hat{s}_{c,x} = \hat{V}_{\text{so},D} + \hat{V}_{\text{so},R}, \tag{9.9}$$

where the spin Pauli operators defined with respect to crystallographic axes, i.e. $\hat{s}_{x,c}$ generates rotation around $\hat{x} \sim [110]$ while $\hat{s}_{y,c}$ around $\hat{y} \sim [\bar{1}10]$. The above formulation is commonly expressed in terms of separated parameters $A = (\alpha + \beta)/2$ and $B = (\alpha - \beta)/2$ and in this way the Dresselhaus $H_{\text{so},D} = \beta(\hat{p}_x\hat{s}_{c,y} + \hat{p}_y\hat{s}_{c,x})$ and Rashba (or Bychkov-Rashba) terms $H_{\text{so},R} = \alpha(\hat{p}_x\hat{s}_{c,y} - \hat{p}_y\hat{s}_{c,x})$ are defined. In this thesis we assume shuttling takes place along $x-$axis, which allows us to neglect contribution from $\hat{p}_y$.

We now briefly discuss microscopic origin of Rashba and Dresselhaus contribution. The Rashba spin-orbit mechanism $\hat{H}_{\text{so}}$ originates from the lack of symmetry between the structure above and below the quantum dot[8] . Such structure inversion asymmetry (SIA) is common for both GaAs- and Si-based nanostructures. The second, Dresselhaus term $\hat{H}_{\text{so},D}$ is caused by the lack of inversion symmetry of the crystal and is typical for zincblende lattice like GaAs (group III-V) semiconductor. In principle it should be absent in group IV semiconductors like Si. However its non-zero value of $\beta \sim 50\text{m/s}$ measured in Si-based quantum dots [192] is caused by the interface, which effectively breaks the inversion symmetry of the QD. The commonly assumed parameters of intrinsic spin-orbit interaction for the devices related to previously introduced models of GaAs, SiGe and SiMOS QD are given in Tab. 6.1.

For the in-plane magnetic field is applied at the angle φ_B with respect to x-axis (See Eq. (9.4)), the Pauli operators can be rotated $\hat{s}_{c,y} = -\sin\varphi_B\hat{s}_x + \cos\varphi_B\hat{s}_y$, such that in the basis of spin-qubit the components of intrinsic spin-orbit field reads:

$$\begin{aligned}\delta b_{\parallel}^{(\text{so-int})}(\hat{p}_x) &= -\sin\varphi_B\frac{\alpha+\beta}{2}\hat{p}_x \\ \delta b_{\perp}^{(\text{so-int})}(\hat{p}_x) &= \cos\varphi_B\frac{\alpha+\beta}{2}\hat{p}_x,\end{aligned} \tag{9.10}$$

note that the rotation of magnetic field allows to switch between longitudinal and transverse contribution from the intrinsic spin-orbit coupling [193].

6: For the spherical symmetry the spin-orbit coupling reduces to

$$\hat{H}_{\text{so}} \propto \hat{\mathbf{L}} \cdot \hat{\mathbf{S}}. \tag{9.8}$$

i.e. the inner product between orbital and intrinsic (spin) angular momentum operators. The gate-defined dots in semiconductor are not spherically symmetric.

7: Such that the spin-orbit Hamiltonian has to share the same symmetry as the dots, i.e. transforms under the same symmetry operations

8: This can be caused by the presence of electric field along z axis, or the fact that materials on two sides of heterointerface are different.

Synthetic spin-orbit coupling

Another physical way to induce coupling between spin and orbital state is the application of a magnetic field gradient. In the materials, where the intrinsic spin-orbit coupling is relatively weak introducing such gradient might be the only way to allow for all-electrical control of electron spin state. We assume that the relevant part of the gradient is applied only along x-axis,[9] which allows to write

$$\begin{aligned}\delta b_{\parallel}^{(\text{so-syn})}(\hat{x}) &= a_{\parallel}\hat{x}\\ \delta b_{\perp}^{(\text{so-syn})}(\hat{x}) &= a_{\perp}\hat{x},\end{aligned} \tag{9.11}$$

where

$$\begin{aligned}a_{\parallel} &= \cos\varphi_B \tfrac{\partial \delta b_x(x)}{\partial x} - \sin\varphi_B \tfrac{\partial \delta b_y(x)}{\partial x},\\ a_{\perp} &= \sin\varphi_B \tfrac{\partial \delta b_x(x)}{\partial x} + \cos\varphi_B \tfrac{\partial \delta b_y(x)}{\partial x}.\end{aligned} \tag{9.12}$$

We will assume that on the scale of few quantum dots the gradient can be assumed constant, i.e. terms $\frac{\partial \delta b_i(x)}{\partial x}$ and hence the gradients a_i do not depend on x.

9: Note that in general $\nabla \cdot \mathbf{B} = 0$, however in vicinity of DQD the change can effectively along single direction

9.3 Non-unitary evolution of stationary spin qubit

We conclude this chapter by discussing non-unitary evolution of the undriven spin qubit in a single quantum dot.

Nuclear spins

We start by introducing a model of interaction between electron spin-qubit and the nuclear spins, which constitutes the only source of non-unitary evolution in absence of spin-orbit coupling. Due to relatively large extend of the electrically-defined quantum dot, the electron-nuclear spin interaction is dominated by the Fermi contact interaction [194], which for the kth nuclear spin interacting with the electron has the form:

$$\hat{H}_{\text{el-nuc},k} = A_k \hat{\mathbf{I}}_k \cdot \hat{\mathbf{S}}, \tag{9.13}$$

where $\hat{\mathbf{I}}_k$ is the spin operator of kth nucleus, $\hat{\mathbf{S}}$ denotes electron spin operator, while $A_k \propto |F(r_k)|^2$ is the coupling constant, proportional to the overlap squared between the envelope function of the electron in the dot (see Sec. 6.1), evaluated at the position of the nucleus [195]).

In typical experiments, which do not involve spin echo or dynamical decoupling sequence the dynamics of nuclear spins is much slower than the dynamics of the qubit. In particular, the state of nuclear bath is hardly changing on the timescale of typical free evolution experiment. For this reason the influence of nuclear spins is conveniently described in terms of classical, quasistatic noise[10] . In particular, this means that for each realization of the experiment we expect slightly modified nuclear field,

10: The effect of which on two-level system was discussed in Sec.4.3

known as the *Overhauser field*, which is added to external magnetic field. The Overhauser field can be effectively modelled as

$$\left(\sum_{k}^{N} A_k \hat{\mathbf{I}}_k\right) \rightarrow g\mu_b \delta \mathbf{B}_n \equiv \delta \mathbf{b}_n. \tag{9.14}$$

Now due to slow character of the noise and typically much stronger constant magnetic field[11] the transverse component can be neglected[12] , which means that effective influence of the nuclear spins can be encapsulated by the pure-dephasing Hamiltonian:

$$\hat{V}_\phi \approx \frac{1}{2}\delta b_{n,z}\hat{s}_z. \tag{9.15}$$

11: The typical root-mean square of random component of magnetic field $\delta b \approx m$T and orders of magnitude less in Si, depending on the level of isotopic purification. See discussion below.

12: In such case the transverse component induces tilt of quantization axis. The shift of the qubit splitting is given by $\tilde{E}_z = \sqrt{(E_z + \delta b_{n,z})^2 + \delta b_{n,\perp}^2}$, i.e. is quadratic in transverse component

$$\tilde{E}_z - E_z \approx \frac{\delta b_{n,z}}{E_z} + \frac{\delta b_{n,\perp}^2}{2E_z^2}$$

. This is consistent with the initial assumption that we neglect the renormalizaiton of the energy gap due to typically weak in magnitude transverse noise.

13: We highlight that expected correlation length of the Overhauser field $x_c \ll d$ might be different from the correlation length of the charge noise. Recently weak correlation between the dephasing noise in two quantum dots has been measured in Si/SiGe device [187].

Spatial correlation

Thanks to its contact interaction origin, the Overhauser field is expected to have relatively short correlation length. In particular, in case of double quantum dot the random contribution to Larmor Frequency in the left $\delta E_{z,L}$ and in the right dot $\delta E_{z,R}$ are expected to be uncorrelated[13] , such that the fluctuation of the average reads:

$$\langle \overline{E}_z^2 \rangle = \left\langle \left(\frac{E_{z,L} + E_{z,R}}{2} \right)^2 \right\rangle \approx \tfrac{1}{4}\left(\langle E_{z,L}^2\rangle + \langle E_{z,R}^2\rangle\right) \approx \tfrac{1}{2}\langle \delta b_{n,z}^2 \rangle. \tag{9.16}$$

Note that in comparison to fluctuations of the Zeeman splitting in a single dot, the fluctuations of the average $\overline{E}_z$ are reduced as a result of short correlation length of the Overhauser field. The continuous version of this phenomenon is known as the motional narrowing. Similarity for the difference between the fluctuations of spin-splitting in each dot reads:

$$\langle \Delta E_z^2 \rangle = \langle E_{z,L} - E_{z,R} \rangle \approx \tfrac{1}{2}\left(\langle E_{z,L}^2\rangle + \langle E_{z,R}^2\rangle\right) \approx \langle \delta b_{n,z}^2 \rangle. \tag{9.17}$$

From the above we also conclude that $\langle \overline{E}_z \Delta E_z \rangle = 0$.

Dephasing time due to nuclear spins

As discussed above, the nuclear spins are the source of typically slowly varying, random magnetic field, which in absence of active electron control modifies the spin coherence by averaging over random magnetic field. Hence the coherence can be written as:

$$W(t) = W_0 e^{-iE_z t}\langle e^{-i\delta b_{n,z} t}\rangle_{\delta b_{n,z}} = W_0 e^{-iE_z t} e^{-\left(t/T_2^*\right)^2}, \tag{9.18}$$

where the dephasing time is defined in terms of variance of the longitudinal component of nuclear field $\delta b_{n,z}$ as:

$$T_2^* = \frac{\sqrt{2}}{g\mu_B\sqrt{\langle \delta b_{n,z}^2\rangle}} \equiv \frac{\sqrt{2}}{\sigma_N}, \tag{9.19}$$

where using the electron g-factor g and Bohr magneton μ_B and we have related the measured T_2^* to the effective power of quasistatic noise due to nuclear spins σ_N^2 analogous to the noise from Sec. 4.4.

We comment on the typical magnitude of $\delta b_{n,z}$. First its value is proportional to the magnetic field measured for ideally polarized nuclear bath, which for GaAs was measured to be $\delta b_{n,\max} = 5T$ [33, 196]. For the unpolarized case the statistical fluctuations follows rule for large numbers and gives typical $\delta b_{n,z} \propto \delta b_{n,\max}/\sqrt{N}$ where N denotes number of spinful nuclei. Now if some fraction x of the nuclear spins has zero spin, which is true for natural Si for which $x = 0.95$, the magnitude of Overhauser field is reduced by a factor of $\sqrt{1-x}$, since both maximum field and N are reduced by $1 - x$.

Numerical parameters

We apply the above analysis to the Si- and GaAs-based devices from Sec. 6.3. We assume both Si-devices are isotopically purified such that only 0.01%^{29}Si is left. From the [194] this means about 10 nuclei remains in each dot, which result in $T^*_{2,\mathrm{Si}} \sim 5\mu$s. This can be compared with experimentally measured values of $T^*_{2,\mathrm{Si}} \approx 10\mu$s. When translated to power of quasistatic noise, it gives $\sigma_{N,\mathrm{Si}} \approx 0.1$neV.

In contrast in the GaAs devices number of spinful nuclei is orders of magnitude larger, and can be estimated as 10^6, which translates into relatively short $T^*_{2,\mathrm{GaAs}} = 10$ns and as a consequence into $\sigma_{N,\mathrm{GaAs}} \approx 0.1\mu$eV. Note that the amplitude of the Overhauser field is three orders of magnitude above the value for isotopically purified Si. This not only limits the coherence of spin-qubit in GaAs but also affect the interference pattern during spin qubit transition between two quantum dots, as we describe in Chapter 11.

Coupling to random electric fields

As another source of spin qubit non-unitary evolution we identify finite coupling between the spin and orbital degrees of freedom. We will show that its dephasing and dissipation can be caused by environmental electric fields.

Wavefunction of spin qubit in single quantum dot

We start by showing how the wavefunciton of single dot spin qubit is affected by the presence of the spin-orbit interaction of the form $\hat{V}_{\mathrm{so}}(\hat{x}, \hat{p}_x)$, given previously by Eq. (11.4).

For the illustration purpose we assume here the spin qubit occupies a single quantum dot[14] . Typically the orbital splitting of the dot is much larger then the Zeeman splitting, i.e. $E_{\mathrm{orb}} \gg E_z$, which allow us to use the first order perturbation theory for the correction to the instantaneous spin states:

14: The DQD case will be considered in next Chapter 10

$$
\begin{aligned}
|\tilde{\uparrow}\rangle &\approx |0,\uparrow\rangle + \sum_{n>0}\left(\frac{\langle n,\uparrow|\,\hat{V}_{\mathrm{so}}\,|0,\uparrow\rangle}{E_n}\,|n,\uparrow\rangle + \frac{\langle n,\downarrow|\,\hat{V}_{\mathrm{so}}\,|0,\uparrow\rangle}{E_n - E_z}\,|n,\downarrow\rangle\right)\\
|\tilde{\downarrow}\rangle &\approx |0,\downarrow\rangle + \sum_{n>0}\left(\frac{\langle n,\downarrow|\,\hat{V}_{\mathrm{so}}\,|0,\downarrow\rangle}{E_n}\,|n,\downarrow\rangle + \frac{\langle n,\uparrow|\,\hat{V}_{\mathrm{so}}\,|0,\downarrow\rangle}{E_n + E_z}\,|n,\uparrow\rangle\right).
\end{aligned}
\tag{9.20}
$$

where for brevity we omitted the arguments of spin-orbit Hamiltonian $\hat{V}_{\rm so} = \hat{V}_{\rm so}(\hat{x}, \hat{p}_x)$ from Eq. (11.4) and E_n is the energy between nth orbital state $|n\rangle$ with respect to ground orbital state $|0\rangle$. We take into account only the first excited state[15] , and compute modification of the spin states as

$$
\begin{aligned}
|\tilde{\uparrow}\rangle &\approx |0,\uparrow\rangle + \frac{\Delta E_z}{4E_{\rm orb}}|1,\uparrow\rangle - \frac{1}{2}\frac{t_{01}}{E_{\rm orb}-E_z}|1,\downarrow\rangle \\
|\tilde{\downarrow}\rangle &\approx |0,\downarrow\rangle - \frac{\Delta E_z}{4E_{\rm orb}}|1,\downarrow\rangle - \frac{1}{2}\frac{t_{01}}{E_{\rm orb}+E_z}|1,\uparrow\rangle\,.
\end{aligned}
\tag{9.21}
$$

where we have defined the difference in orbit-dependent Zeeman splitting as ΔE_z, and the coupling between ground and excited orbital state with a spin-flip as t_{01}, i.e.

$$
\begin{aligned}
\Delta E_z &= \langle 1|\, b_{\parallel}(\hat{x},\hat{p}_x)\,|1\rangle - \langle 0|\, b_{\parallel}(\hat{x},\hat{p}_x)\,|0\rangle \\
t_{01} &= \langle 1|\, b_{\perp}(\hat{x},\hat{p}_x)\,|0\rangle\,,
\end{aligned}
\tag{9.22}
$$

which are expressed in terms of $\hat{b}_{\parallel}$ and $\hat{b}_{\perp}$ corresponding to the components of spin-orbit field $\mathbf{b}_{\rm so}$ from Eq. (11.4) along and perpendicular to the external magnetic field $\mathbf{B}_0$ from Eq. (9.4).

As we showed the spatial wavefunction corresponding to lower and higher energy spin state are shifted in space. As showed below such correlation between spin and position degree of freedom exposes the spin qubit to fluctuations of electric fields.

15: Such that the only non-vanishing matrix elements read $\langle 0|\,\hat{x}\,|1\rangle = L/\sqrt{2}$ and $\langle 0|\,\hat{p}_x\,|1\rangle = im^* E_{\rm orb} L/\sqrt{2}$

Spin relaxation

We start by computing spin-relaxation due to transverse field. Following Fermi Golden rule from Eq. (3.6), we first calculate transverse coupling in the spin basis as:

$$
\hat{V}_{\perp,\rm spin} = \langle\tilde{\downarrow}|\hat{V}_{\rm fld}(\hat{x})|\tilde{\uparrow}\rangle + \text{h.c.} \approx -t_{01}\int \mathrm{d}x\,\hat{V}_{\rm fld}(x)\left(\frac{\psi_0\psi_1}{E_{\rm orb}-E_z} + \frac{\psi_0\psi_1}{E_{\rm orb}+E_z}\right)
\tag{9.23}
$$

where we used real-valued wavefunctions. If we neglect small quadratic term $(E_z/E_{\rm orb})^2$, it can be written as:

$$
\hat{V}_{\perp,\rm spin} = \langle\tilde{\downarrow}|V_{\rm fld}(\hat{x})|\tilde{\uparrow}\rangle \approx -\frac{t_{01}}{E_{\rm orb}}\hat{V}_{\perp,\rm orb}\,,
\tag{9.24}
$$

where $\hat{V}_{\perp,\rm orb} = \langle 0|\,\hat{V}_{\rm fld}(\hat{x})\,|1\rangle$ + h.c is the transverse component of the environmental field in the orbital basis. Since the relaxation rate is proportional to spectral density of transverse noise,[16] which is quadratic in the $\hat{V}_{-,\rm orb}$ operator, the spin-relaxation rate can be expressed in terms of orbital relaxation rate as

16: see analysis in Chapter 3,

$$
\Gamma_{-,\rm spin} = \frac{|t_{01}|^2}{4E_{\rm orb}^2}S_{\perp}(E_z),
\tag{9.25}
$$

where $S_{\perp}(E_z) = \int \mathrm{Tr}\{\hat{V}'_{\perp,\rm orb}(t)\hat{V}'_{\perp,\rm orb}(0)\hat{\rho}_e\}e^{-iE_z t}\mathrm{d}t$ is the spectral density of the environment, coupled transversly in the orbital basis, which is evaluated at the Zeeman splitting E_z.

Dephasing due to charge noise

Similarly in the leading order, the dephasing of spin qubit due to spatially varying field is proportional to the square the longitudinal coupling in the spin basis $\hat{V}_{\phi,\text{spin}}$[17] . Such coupling can be written as:

17: See Sec. 5.4 for discussion

$$\hat{V}_{\phi,\text{spin}} = \int \mathrm{d}x \left(\hat{V}_{\text{fld}}(x) \left(|\psi_{\tilde{\uparrow}}(x)|^2 - |\psi_{\tilde{\downarrow}}(x)|^2 \right) \right) \approx$$
$$\approx \frac{\Delta E_z}{2E_{\text{orb}}} \text{Re}\left\{ \langle 0| \hat{V}_{\text{fld}}(\hat{x}) |1\rangle \right\} = \frac{\Delta E_z}{2E_{\text{orb}}} \hat{V}_{x,\text{orb}}, \quad (9.26)$$

where $\hat{V}_{x,\text{orb}} = \hat{V}_{+,\text{orb}} + \hat{V}_{-,\text{orb}}$ and we neglected terms quadratic in typically small $(E_z/E_{\text{orb}})^2$. The means that in leading order, the spin-dephasing is caused by the environmental field transverse in the orbital basis. At the same time the decoherence of spin qubit remains insensitive to the fluctuations longitudinal in the orbital basis. In particular, this means that the power of the spin-longitudinal noise, that causes spin dephasing[18] is related to slow, transverse noise in the orbital basis via

18: For the spin-qubit the coherence reads

$$W_{\text{spin}}(t) = \exp\left(-\frac{1}{2} \sigma_{\text{spin}}^2 t^2 \right),$$

or equivalently

$$T_2^* = \sqrt{2}/\sigma_{\text{spin}}$$

.

$$\tilde{\sigma}^2_{\text{spin}} = \frac{\Delta E_z^2}{4E_{\text{orb}}^2} \tilde{\sigma}^2_{\perp,\text{orb}}, \quad (9.27)$$

which according to effective quasistatic noise model from Sec. 4.4 can be computed from:

$$\tilde{\sigma}^2_{\perp,\text{orb}} = 2 \int_{\pi/T_a}^{\pi/t} \mathrm{d}\omega S_\perp(\omega) \mathrm{d}\omega. \quad (9.28)$$

Note that in the crucial for dephasing low-frequency range we have $S_\perp(\omega) = S_\perp(-\omega)$. In this way we showed additional source of the spin qubit dephasing, which is activated by non-zero spin-orbit coupling. As mentioned above the finite correlation between the spin and charge degrees of freedom leads to the sensitivity of the former to the environmental electric fields (which are transverse in the orbital basis).

10 Spin qubit in double quantum dot as an open quantum system

In this chapter we consider the electron in a double quantum dot (DQD), that undergoes interdot L-Z transition. First in Sec. 10.1 we show effects of spin-orbit coupling in absence of the environment. Next in Sec. 10.2 we show these effects in the adiabatic frame and in the final Sec. 10.3 we couple the system to the environment. In particulair we derive there the Lindblad form of adiabatic Master equation, that will be used in the subsequent chapters to produce numerical results.

10.1 Closed but driven qubit-orbit system

Model Hamiltonian

Uncoupled spin states

We start by introducing the model of the system. We consider the system of two-lowest lying levels of DQD, that undergoes a Landau-Zener transition, i.e.

$$\hat{H}_o(t) = -\frac{\epsilon(t)}{2}\hat{\sigma}_z + \frac{t_c}{2}\hat{\sigma}_x, \tag{10.1}$$

where $\hat{\sigma}_z = |L\rangle\langle L| - |R\rangle\langle R|$, while $|L\rangle$, $|R\rangle$ are Hund-Mulliken orbitals localized in the left and right dots respectively[1] . We now add spin degree

1: see Eq. 6.24 for definition of Hund-Mulliken states

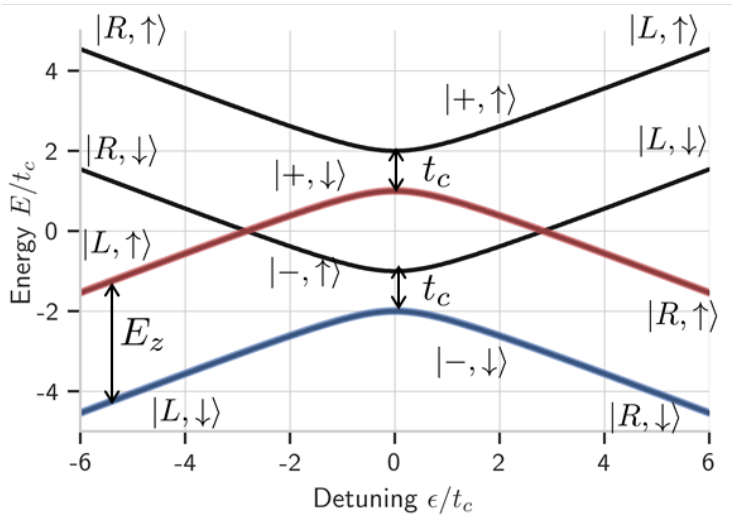

Figure 10.1: Instantaneous energy spectrum of the Hamiltonian $\hat{H}_{so}(t) = \hat{H}_o(t) + \hat{H}_s$ that corresponds to the electron in the DQD with internal degrees of freedom (spin) in absence of spin-orbit coupling. Using colored lines, we show adiabatic path corresponding to the ground orbital state corresponding to spin-up $|-,\uparrow\rangle$ (red) and spin-down $|-,\downarrow\rangle$ (blue). We also denote qubit splitting E_z and tunnel coupling t_c and show the dot composition of the instantaneous states at large negative and large positive detunings.

of freedom, the Hamiltonian of which is written as:

$$\hat{H}_s = \frac{E_z}{2}\hat{s}_z, \tag{10.2}$$

where $\hat{s}_z = |\uparrow\rangle\langle\uparrow| - |\downarrow\rangle\langle\downarrow|$ are the Pauli operator in the spin basis $|\uparrow\rangle$, $|\downarrow\rangle$ and $E_z \equiv \overline{E}_z$ is the orbit-average Zeeman splitting. In Fig. 10.1 we plot the instantanous energy spectrum of qubit-orbit Hamiltonian

$$\hat{H}_{so}(t) = \hat{H}_o(t) + \hat{H}_s, \tag{10.3}$$

as a function of ϵ. By the thicker lines we denote ground orbital eigenstates corresponding to spin-up (red) and spin-down (blue).

Consequence of spin-orbit coupling

We now introduce weak coupling between the electron spin and its charge degree of freedom. Similarly to the single dot analysis, for the semiconductor system it originates from the artificial or synthetic spin-orbit interaction.[2] The effect of $\hat{V}_{\rm so}(\hat{x}, \hat{p}_x)$ can be encapsulated by the Hamiltonian in the basis of $|L\rangle$, $|R\rangle$ states as:

2: See analysis in Sec.9.1

$$\hat{V}_{so} = \frac{\Delta E_z}{4}\hat{s}_z\hat{\sigma}_z + \frac{t^{(\rm int)}_{\rm flip}}{2}\hat{s}_y\hat{\sigma}_y + \frac{t^{(\rm syn)}_{\rm flip}}{2}\hat{s}_x\hat{\sigma}_z, \tag{10.4}$$

where we define the difference in dot-dependent spin-splitting as:

$$\Delta E_z = \langle R|\, b_{\parallel}(\hat{x}, \hat{p}_x)\,|R\rangle - \langle L|\, b_{\parallel}(\hat{x}, \hat{p}_x)\,|L\rangle\,, \tag{10.5}$$

the contribution from transverse magnetic field gradient[3] :

3: we assume that the gradient is symmetric with respect to dots, i.e. $\delta b_x(d/2) = -\delta b_x(-d/2)$.

$$t^{(\rm syn)}_{\rm flip} = \langle R|\, \hat{b}^{(\rm syn)}_{\perp}(\hat{x})\,|R\rangle - \langle L|\, \hat{b}^{(\rm syn)}_{\perp}(\hat{x})\,|L\rangle \equiv a_{\perp} d, \tag{10.6}$$

and finally spin-flip contribution from intrinsic spin-orbit coupling as

$$t^{(\rm int)}_{\rm flip} = \langle L|\, \hat{b}^{(\rm int)}_{\perp}(\hat{p}_x)\,|R\rangle\,, \tag{10.7}$$

which in contrast to synthetic contribution is associated with the tunneling between the dots[4] . We assume the spin-orbit coupling is weak in comparison to both average Zeeman splitting E_z and the gap between ground and excited charge state $\Omega(t)$, the minimum of which is set by the tunnel coupling t_c. In Fig. 10.2 we plot the instantaneous energy spectrum of the combined Hamiltonian

4: Note that the for consider wavefunctions $\langle L|\,\hat{x}\,|R\rangle = \langle R|\,\hat{x}\,|L\rangle$, while $\langle L|\,\hat{p}_x\,|R\rangle = -\langle R|\,\hat{p}_x\,|L\rangle$

$$\hat{H}(t) = \hat{H}_{so}(t) + \hat{V}_{\rm so}(t), \tag{10.8}$$

as a function of detuning. In the figure we illustrate the way in which parameters of spin-orbit coupling: ΔE_z, and

$$|t_{\rm ff}| = \sqrt{[t^{(\rm int)}_{\rm flip}]^2 + \left[\tfrac{t_c}{E_z} t^{(\rm syn)}_{\rm flip}\right]^2} \tag{10.9}$$

affect the instantaneous spectrum.

Numerical values

We quickly estimate orders of magnitude associated with the coupling between the spin and charge degree of freedom in the typical semiconductor devices. For the typical gradients of $\Delta b_x/\Delta x \sim 1$ mT/nm, which

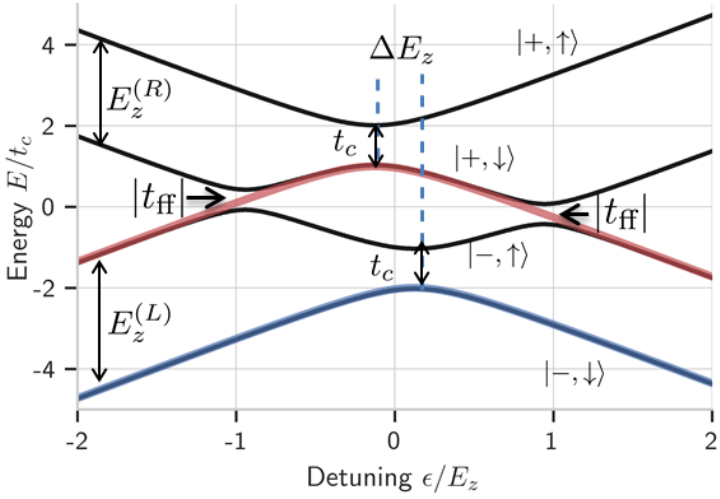

Figure 10.2: Instantaneous energy spectrum of the Hamiltonian $\hat{H}(t) = \hat{H}_o(t) + \hat{H}_s + \hat{V}_{\rm so}$ corresponding to the electron in the DQD with internal degrees of freedom (spin), in presence of spin-orbit coupling. Using colored lines, we show adiabatic path corresponding to the ground orbital states corresponding to spin-up $|-,\uparrow\rangle$ (red) and spin-down $|-,\downarrow\rangle$ (blue). The different spin spitting in the left and right dot give rise to $\Delta E_z = E_z^{(L)} - E_z^{(R)}$ and shifts the spin-up and spin-down transitions with respect to each other. The tunnel coupling with the spin-flip $t_{\rm flip}$ give rise to additional avoided crossings between the flip-flop states $|+,\downarrow\rangle$ and $|-,\uparrow\rangle$. The size of the energy gap at such crossing is given by $t_{\rm ff}$ (See Eq. (10.9)).

corresponds to

$$a_{\parallel} \approx \frac{0.1\mu\text{eV}}{nm} \tag{10.10}$$

the contribution from synthetic spin-orbit interaction for $d = 100$nm distance between the dots is expected to be of the order of magnitude:

$$t_{\rm flip}^{(\rm syn)} \approx 10\,\mu\text{eV} \gg \Delta E_z^{(\rm syn)}. \tag{10.11}$$

Above we used the fact that gradient is usually oriented in the transverse direction[5] such that ΔE_z can be safely assumed to be much smaller. We now estimate the contribution from intrinsic spin-orbit coupling, for which the operators $b^{(\rm int)}$ have been given explicitly in Eq. (9.10). We ignore the factor coming from the orientation of magnetic field and estimate the order of magnitude. We start with estimating momentum matrix element between the left and right dot. We use a toy model in which we treat DQD system as a single dot with size $L_{\rm dqd} = d \approx 100$nm. Next we concentrate at the zero-detuning point at witch the symmetric state $|+\rangle = (|L\rangle + |R\rangle)/\sqrt{2}$ and anti-symmetric state $|-\rangle = (|L\rangle - |R\rangle)/\sqrt{2}$ can be treated as ground and excited state of large dot with effective splitting t_c. In such a case the element $\langle -|\,\hat{x}\,|+\rangle \approx d$ and the momentum element $|\,\langle -|\,\hat{p}_x\,|+\rangle\,| \approx d\,m^* t_c$. Finally we use this toy model to estimate:

$$\langle L|\,\hat{p}_x\,|R\rangle \approx d\,m^* t_c \approx 10^{-27}\text{kg m/s} \tag{10.12}$$

for typical $t_c \approx 10\,\mu$eV, $d = 100\,$nm and $m^* = 0.2m_e$, where we use the fact that $|L\rangle = (|+\rangle + |-\rangle)/\sqrt{2}$ and $|R\rangle = (|+\rangle - |-\rangle)/\sqrt{2}$. We now multiply the typical momentum operator times the combination of Rashba and Dresselhaus parameters, which for the SiMOS reads $(\alpha_{\rm Si} + \beta_{\rm Si})/2 \approx 50$m/s [2][6] . Together this allows to estimate the flipping element as:

$$t_{\rm flip,Si}^{(\rm int)} \sim 0.1\mu\text{eV}, \tag{10.13}$$

For the GaAs devices we expect the momentum matrix element to be comparable, as a result of typically larger dinstance between the dots and smaller effective mass. However due to typically larger spin-orbit coefficients $\alpha_{\rm GaAs}$ given by $(\alpha_{\rm GaAs} + \beta_{\rm GaAs})/2 \approx 10^3\,$m/s [193] we can

5: to provide the coherent control of the spin-qubit from Sec. 9.1

6: often spin-orbit coupling in Si/SiGe devices is expected to be smaller, however we will assume their value to be the same as in SiMOS

estimate:

$$t^{(\mathrm{int})}_{\mathrm{flip,GaAs}} \sim 1\mu\mathrm{eV}. \tag{10.14}$$

We highlight that the above estimations lies close to directly measured electron tunneling with a spin flip, which provides the energy splitting between the singlet and triplet two-electron state close to their degeneracy point [178, 193, 197].

10.2 Adiabatic frame

Diagonal spin-orbit coupling

We now represent the total Hamiltonian in the basis of the instantaneous states, which have been introduced in Eq. (5.1). We define the diagonal terms of the combined Hamiltonian as:

$$\left[\hat{H}_{\mathrm{so}}(t) + \hat{V}_{\mathrm{so}}\right]_{\mathrm{diag}} = \frac{\epsilon(t) + \frac{1}{2}\Delta E_z \hat{s}_z}{2}\hat{\sigma}_z + \frac{t_c}{2}\hat{\sigma}_x, \tag{10.15}$$

which allows to introduce the spin-dependent detuning $\epsilon_s = \epsilon(t) + \frac{\sigma_s}{2}\Delta E_z$ leading to spin-dependent orbital angle:

$$\vartheta_s(t) = \mathrm{ctan}\left(\frac{\epsilon(t) + \frac{\sigma_s}{2}\Delta E_z}{t_c}\right), \tag{10.16}$$

for $\sigma_\uparrow = 1$ or $\sigma_\downarrow = -1$. We now move to the spin-dependent adiabatic basis using the transformation,

$$\hat{S}(t) = \sum_{s=\uparrow,\downarrow} \exp\left(-i\frac{\vartheta_s}{2}\hat{\varsigma}_y\right)|s\rangle\langle s|, \tag{10.17}$$

using which the Hamiltonian in the adiabatic frame reads:

$$\begin{aligned}\hat{\mathscr{H}} = \hat{S}^\dagger(t)\left(\left[\hat{H}_{\mathrm{so}}(t) + \hat{V}_{\mathrm{so}}\right]_{\mathrm{diag}}\right)\hat{S}(t) - i\hat{S}^\dagger(t)\dot{\hat{S}}(t) = \\ = \frac{E_z}{2}\hat{s}_z + \sum_{s=\uparrow,\downarrow}\left(\frac{\Omega_s(t)}{2}\hat{\varsigma}_z - \frac{\dot{\vartheta}_s(t)}{2}\hat{\varsigma}_y\right)|s\rangle\langle s|\end{aligned} \tag{10.18}$$

where we have used Pauli operators in the adiabatic basis, i.e. $\hat{\varsigma}_z = |+\rangle\langle+| - |-\rangle\langle-|$ and

$$\begin{aligned}\Omega_s(t) &= \sqrt{(\epsilon + \tfrac{\sigma_s}{2}\Delta E_z)^2 + t_c^2}, \\ \vartheta_s(t) &= \frac{v t_c}{\Omega_s(t)},\end{aligned} \tag{10.19}$$

where $\sigma_s = \pm 1$ for $s = \uparrow$ and $\downarrow$ respectively. This means that the non-zero difference between dot-dependent Zeeman splitting $\Delta E_z \neq 0$ leads to a delay in transitions of spin-up and spin-down components. In particular, it is convenient to define difference in spin-dependent orbital splittings,

and difference in spin-dependent orbital angle as

$$\begin{aligned}\Delta\Omega(t) &= \Omega_\uparrow(t) - \Omega_\downarrow(t),\\ \Delta\vartheta(t) &= \vartheta_\uparrow(t) - \vartheta_\downarrow(t).\end{aligned} \tag{10.20}$$

Orbital adiabatic limit

In general the assumption of weak coupling, means that the effects of environment will be visible only for sufficiently slow sweeps. This is visible in the analysis of charge transfer in realistic DQD systems (for instance in Fig. 8.9), where the evolution in the limit of fast sweeps, was well approximated by the Landau-Zener formula. This means that in the analytical analysis of the environmental effect we might as well neglect the term responsible for coherent mixing between the charge levels[7] , i.e. off-diagonal term $\propto \dot{\vartheta}_s$. This effectively means that in the adiabatic limit,[8] the dynamics of the uncoupled spin-orbit system is given by the Hamiltonian that is diagonal in the adiabatic frame:

$$\hat{\mathscr{H}}_0 = \frac{\overline{E}_z}{2}\hat{s}_z + \frac{1}{2}\left(\overline{\Omega}(t) + \tfrac{1}{2}\Delta\Omega(t)\hat{s}_z\right)\hat{\varsigma}_z. \tag{10.21}$$

7: This statement will be proved in a numerical simulation where $\dot{\vartheta}_s\hat{\varsigma}_y$ is kept.

8: i.e. when Landau-Zener probability $Q_{\mathrm{LZ}} \ll 1$ is neglegibley small

Off-diagonal spin-orbit coupling

We now apply the same transformation to the non-diagonal coupling between the spin and charge states, i.e.

$$\begin{aligned}\hat{\mathscr{V}}_{so}(t) = \hat{S}^\dagger(t)\big([\hat{V}_{so}]_{\text{non-diag}}\big)\hat{S}(t) &= \frac{t_{\text{flip}}^{(\text{int})}}{2}\left(\sin\frac{\Delta\vartheta(t)}{2}\hat{s}_x + \cos\frac{\Delta\vartheta(t)}{2}\hat{s}_y\hat{\varsigma}_y\right)\\ &+ \frac{t_{\text{flip}}^{(\text{syn})}}{2}\left(\cos\overline{\vartheta}(t)\hat{s}_x\hat{\varsigma}_z - \sin\overline{\vartheta}(t)\hat{s}_x\hat{\varsigma}_y\right),\end{aligned} \tag{10.22}$$

where additionally we defined average of spin-dependent orbital angle $\overline{\vartheta}(t) = \vartheta_\uparrow(t) + \vartheta_\downarrow(t)$.

Secular approximation for spin-orbit coupling

We finally simplify the off-diagonal interaction $\hat{\mathscr{V}}_{so}(t)$ using secular approximation, i.e. use the fact that weak coupling leads to mixing between the levels only in the limit of sufficient long evolution time, in which strongly nonresonant transitions are suppressed[9] . In analogy to undriven case we move here to the interaction picture with respect to adiabatic Hamiltonian, diagonal in the adiabatic basis,

$$\hat{\mathscr{V}}'_{so}(t) = \hat{\mathscr{U}}_0^\dagger(t)\hat{\mathscr{V}}_{so}\hat{\mathscr{U}}_0(t), \tag{10.23}$$

9: see Sec. 3.2 for the analysis of secular approximation in the undriven case

where the evolution operator in the adiabatic picture[10] , reads:

$$\hat{\mathscr{U}}_0(t) = \sum_{s=\uparrow,\downarrow}\exp\left(-\tfrac{i}{2}\int_{t_i}^{t}(\hat{\varsigma}_z\Omega_s(t') + \sigma_s E_z)\mathrm{d}t'\right)|s\rangle\langle s|\,, \tag{10.24}$$

10: and without mixing between charge levels

where $\sigma_s = \pm$ for spin-up and spin-down respectively. Due to dynamical drive we argue that some terms will be secular only locally, i.e. when

two eigenstates of Hamiltonian $\hat{\mathcal{H}}_0$ from Eq. (10.21) become close in energy. In particular, this will happen in vicinity of the point at which $\Omega(t) = E_z > 0$.

We now argue that the only, locally secular term is the flip-flop term $\hat{\varsigma}_\pm \hat{s}_\mp$, since in the interaction picture with respect to adiabatic basis it reads:

$$\hat{\mathcal{U}}_0^\dagger(t)\hat{\varsigma}_\pm\hat{s}_\mp\hat{\mathcal{U}}_0(t) = \hat{\varsigma}_\pm\hat{s}_\mp e^{\pm i\int_{t_i}^{t}(\Omega(t')-E_z)\mathrm{d}t'}. \tag{10.25}$$

As showed previously in Eq. (5.47), any time integral of the above expression would be dominated by the stationary point of the phase, which takes place at $\Omega(\tilde{t}) = E_z$. Note that due the fact that both $E_z > 0$ and $\Omega(t) > 0$ the stationary phase is absent in the remaining terms of $\hat{\mathcal{V}}_{so}(t)$. Also the presence of stationary phase, and hence effective coupling between the qubit and charge states requires that $t_c < E_z$, since otherwise $\Omega(t) \neq E_z$ at all times.[11]

The above analysis allows us to use secular form of transverse spin-orbit coupling in the adiabatic basis, which reads:

$$\hat{\mathcal{V}}_{so}^{(\mathrm{sec})}(t) = \frac{t_{\mathrm{ff}}(t)}{4}\hat{\varsigma}_+\hat{s}_- + h.c, \tag{10.26}$$

where we have defined the complex flip-flop term, which reads:

$$t_{\mathrm{ff}}(t) = t_{\mathrm{flip}}^{(\mathrm{int})}\cos\frac{\Delta\vartheta(t)}{2} - it_{\mathrm{flip}}^{(\mathrm{syn})}\sin\Big(\overline{\vartheta}(t)\Big). \tag{10.27}$$

Effective Hamiltonian

Above considerations of the weak spin-orbit coupling allows us to write the qubit-orbit Hamiltonian in the adiabatic basis as:

$$\mathcal{H}_0(t) + \mathcal{V}_{\mathrm{so}}^{(\mathrm{sec})} \approx \frac{\Omega_0(t) + \frac{1}{2}\Delta\Omega(t)\hat{s}_z}{2}\hat{\varsigma}_z + \frac{E_z}{2}\hat{s}_z + \frac{t_{\mathrm{ff}}\hat{\varsigma}_+\hat{s}_- + h.c}{2}, \tag{10.28}$$

where we additionally assumed that the spin-average orbital splitting is effectively indepedent of spin-orbit coupling i.e.

$$\overline{\Omega}(t) \approx \Omega_0(t) = \sqrt{\epsilon^2 + t_c^2}, \tag{10.29}$$

In spin basis, the longitudinal contribution is related to difference in the orbital splittings for spin-up and spin-down given by:

$$\Delta\Omega(t) = \sqrt{\big(\epsilon + \tfrac{\Delta E_z}{2}\big)^2 + t_c^2} - \sqrt{\big(\epsilon - \tfrac{\Delta E_z}{2}\big)^2 + t_c^2} \tag{10.30}$$

while the coupling between the spins enters via the flip-flop term,

$$t_{\mathrm{ff}} = t_{\mathrm{flip}}^{(\mathrm{int})} - i\frac{t_c}{E_z}t_{\mathrm{flip}}^{(\mathrm{syn})}. \tag{10.31}$$

Note that by definition $|t_{\mathrm{ff}}|$ gives the gap between the avoided crossing between $|+,\downarrow\rangle$ and $|-,\uparrow\rangle$ states, as it was illustrated in Fig. 10.2.

11: Alternatively one can consider perturbative corrections to $|\pm, s\rangle$ states due to presence of $\hat{\mathcal{V}}_{so}$. In the simplest approach we use t as the parameter and compute time-independent corrections to the state $|-,\downarrow\rangle$ as:

$$\tilde{|-,\downarrow\rangle} = |-,\downarrow\rangle + \sum_{d=\pm}\frac{\langle d,\uparrow|\hat{\mathcal{V}}_{so}|-,\downarrow\rangle}{\Delta E_d(t)}|d,\uparrow\rangle,$$

where $\Delta E_-(t) = -E_z$ for $|-,\uparrow\rangle$ correction and $\Delta E_+(t) = -E_z - \Omega(t)$ for $|+,\uparrow\rangle$. Which means that corrections scales as $t_{\mathrm{flip}}/E_z \ll 1$ for all couplings. On the contrary for the spin-up state $|-,\uparrow\rangle$ we have

$$\tilde{|-,\uparrow\rangle} = |-,\uparrow\rangle + \sum_{d=\pm}\frac{\langle d,\downarrow|\hat{\mathcal{V}}_{so}|-,\uparrow\rangle}{\Delta E_d(t)}|d,\downarrow\rangle,$$

where $\Delta E_+(t) = E_z$ for admixture with $|+,\uparrow\rangle$, but $\Delta E_-(t) = E_z - \Omega(t)$ due to coupling with $|+,\downarrow\rangle$, Which shows that for sufficiently large $t_c > E_z$, there exist a time instant at which $E_z - \Omega(t)$ and the states $|+,\downarrow\rangle, |-,\uparrow\rangle$ hybridize even for weak t_{flip}. This justifies why the terms $\hat{\varsigma}_\mp\hat{\sigma}_\pm$ are kept

Avoided crossing between the flip-flop states

The regime of $E_z > t_c$ is relevant for the long-range shuttling, in which tunnel couplings are expected to be relatively low. In this regime the additional avoided crossings take place at:

$$\Omega(t_\pm) = E_z \implies t_\pm \approx \pm\frac{E_z}{v}. \tag{10.32}$$

Additionally these crossings involves the flip-flop states $|+,\downarrow\rangle$, $|-,\uparrow\rangle$, which in the limit $E_z \gg t_c$ can be treated as the *diabatic basis* for the flip-flop avoided crossing. We illustrate such crossing schematically in Fig. 10.3.

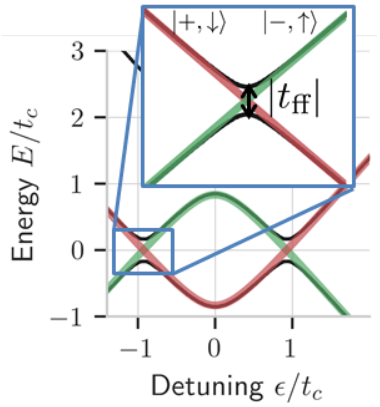

Figure 10.3: Spin-flip avoided crossing. The scheme of the avoided crossing between adiabatic levels $|+,\downarrow\rangle$ (red) and $|-,\uparrow\rangle$ (green), the size of which is given by $|t_{\rm ff}|$.

To prove the above point, we assume now that the evolution is adiabatic in the charge degrees of freedom and concentrate on the two flip-flop states. In their basis the Hamiltonian $\hat{\mathscr{H}}_0(t) + \hat{V}_{so}^{(\rm sec)}(t)$ reduces to:

$$\hat{\mathscr{H}}_{\rm ff}(t) = -\frac{\Omega(t) - E_z}{2}\hat{\sigma}_z^{(\rm ff)} + \frac{t_{\rm ff}}{2}\hat{\sigma}_x^{(\rm ff)} = \begin{bmatrix} -\Omega(t) + E_z & t_{\rm ff}(t) \\ t_{\rm ff}^*(t) & \Omega(t) - E_z \end{bmatrix}, \tag{10.33}$$

where we introduced flip-flop Pauli matrices, e.g. $\sigma_z^{(\rm ff)} = |-,\uparrow\rangle\langle-,\uparrow| - |+,\downarrow\rangle\langle+,\downarrow|$. The above Hamiltonian produces double Landau-Zener passage with the avoided crossings located at the points $t_\pm$. Its effective detuning sweep rate in the $E_z \gg t_c$ limit coincides with v since:

$$\partial_t(\Omega(t) - E_z)\Big|_{t=t_\pm} = \frac{v\epsilon}{\sqrt{t_c^2 + \epsilon^2}}\Big|_{t=t_\pm} = v\,\frac{\sqrt{E_z^2 - t_c^2}}{E_z} \approx v. \tag{10.34}$$

The effective tunnel coupling between the flip-flop levels as:

$$t_{\rm ff} \equiv t_{\rm ff}(t_\pm) \approx t_{\rm flip}^{(\rm int)} - i\frac{t_c}{E_z}t_{\rm flip}^{(\rm syn)} = |t_{\rm ff}|e^{i\phi_{\rm ff}}, \tag{10.35}$$

where we evaluated the off-diagonal term in $\mathscr{H}_{\rm ff}(t)$ at the vicinity of flip-flop crossings, where $\Delta\vartheta(t_\pm) \ll 1$ and $\sin\vartheta(t_\pm) \approx \sin\vartheta_0(t_\pm) = t_c/\Omega(t_\pm) \approx t_c/E_z$, while the complex phase reads:

$$\phi_{\rm ff} = -\arctan\left(\frac{\frac{t_c}{E_z}t_{\rm flip}^{(\rm syn)}}{t_{\rm flip}^{(\rm int)}}\right). \tag{10.36}$$

We finally conclude that the probability of the non-adiabatic transition through flip-flop avoided crossing, which corresponds to staying in the same flip-flop state, e.g. $|-,\uparrow\rangle \to |-,\uparrow\rangle$ is given by:

$$Q_{\rm ff} = \exp\left(-\frac{\pi}{2}\frac{|t_{\rm ff}|^2}{v}\right) \approx 1 - \frac{\pi}{2}\frac{|t_{\rm ff}|^2}{v}, \tag{10.37}$$

where the expansion assumed that $|t_{\rm ff}|^2/v \ll 1$, i.e. the probability of spin-flip is relatively small. We will show that this regime is typical for realistic devices. Note however that in contrast to charge adiabaticity, where unwanted adiabaticity scales exponentially with v, here probability of spin-flip falls as $1/v$, which makes it difficult to avoid.

10.3 Coupling to environment

Orbit-environment coupling in the adiabatic basis

We now include the interaction between the environment and the charge states, of the form:

$$\hat{V}_{oe} = \frac{\hat{V}_x}{2}\hat{\sigma}_x + \frac{\hat{V}_z}{2}\hat{\sigma}_z, \tag{10.38}$$

which originate from fluctuations the of tunnel coupling $\hat{V}_x$ and the detuning $\hat{V}_z$ due to electron-phonon coupling and the charge noise.

We first express the above coupling in the adiabatic basis. We assume that the fluctuations of detuning and tunnel coupling are weakly correlated[12] , such that the cross-terms $\mathrm{Tr}\{\hat{V}_x\hat{V}_z\hat{\rho}_e\}$ can be neglected[13] . We write the interaction in the form:

$$\hat{\mathcal{V}}_{oe} = \frac{1}{2}\left(\hat{V}_x\hat{\Sigma}_x(t) + \hat{V}_z\hat{\Sigma}_z(t) + \hat{\mathcal{V}}_\phi(t)\hat{\varsigma}_z\right), \tag{10.39}$$

where we separated the dissipative terms $\Sigma_i(t)$ and the dephasing-like term $\hat{\mathcal{V}}_\phi(t)$, which can be written explicitly as

$$\begin{aligned}
\hat{\Sigma}_x(t) &= \hat{\varsigma}_x \cos\hat{\vartheta} \\
\hat{\Sigma}_z(t) &= -\hat{\varsigma}_x \sin\hat{\vartheta}, \\
\hat{\mathcal{V}}_\phi(t) &= \hat{V}_z \cos\hat{\vartheta} + \hat{V}_x \sin\hat{\vartheta}.
\end{aligned} \tag{10.40}$$

In the above, for brevity we introduced the spin-diagonal operator:

$$\hat{\vartheta}(t) = \sum_{s=\uparrow,\downarrow} \vartheta_s(t)\,|s\rangle\langle s|\,, \tag{10.41}$$

where $\vartheta_s(t)$ was given in Eq. (10.16).

Non-dissipative evolution

Following previously considered cases, we assume that the non-dissipative part of system-environment coupling $\hat{V}_\phi$ can be safely treated using classical noise approximation, i.e.

$$\hat{\mathcal{V}}_\phi(t) = \delta\epsilon\cos\hat{\vartheta} + \delta t_c \sin\hat{\vartheta}, \tag{10.42}$$

where we assume that $\delta\epsilon$ and δt_c are effectively quasistatic noise with their power computed using methods from Sec. 4.4.

Dissipative evolution - adiabatic master equation

We now discuss the method to treat disispative evolution of spin-charge system expressed in terms of the operators,

$$\hat{\Sigma}_j(t) = \sum_j c_{j,s}(t)(\hat{\varsigma}_{-,s} + \hat{\varsigma}_{+,s}), \tag{10.43}$$

where we have introduced the spin-diagonal, orbital ladder operator $\hat{\varsigma}_{-,s} = \hat{\varsigma}_-\,|s\rangle\langle s|$, with the real coefficients $c_{j,s}(t)$, that can be read from

12: This would be the typical case if each contributions comes from uncoupled or sufficiently weakly coupled environmental fluctuators.

13: where $\hat{\rho}_e$ is the density matrix of the environment at thermal equilibrium with its Hamiltonian, i.e. $\hat{\rho}_e \propto e^{-\beta\hat{H}_e}$

Eq. (10.40), i.e. $c_{x,s}(t) = \cos\vartheta_s(t)$, while $c_{z,s}(t) = -\sin\vartheta_s(t)$ for s = ↑ and ↓.

Adiabatic-Bloch-Redfield equation

We will now start from the form of Adiabatic-Bloch-Redfield equation, derived previously in Eq. (5.64), i.e.

$$\dot{\varrho}(t) = -i\big[\hat{\mathscr{H}}(t) + \hat{\mathscr{V}}_{so}(t), \hat{\varrho}(t)\big] - \sum_{j=x,z}\big[\hat{\Sigma}_j(t), \hat{\mathscr{R}}_j(t)\varrho(t)\big] + h.c. \quad (10.44)$$

where we assume that the unitary part includes the complete Hamiltonian $\hat{\mathscr{H}}(t)$, given by Eq. (10.18) and spin-orbit coupling $\hat{\mathscr{V}}_{so}(t)$ given by Eq. (10.22), in the adiabatic frame. The non-unitary part is generated by the Bloch-Redfield adiabatic tensor of the form:

$$\begin{aligned}\hat{\mathscr{R}}_j(t) &= \frac{1}{4}\int_0^\infty e^{-i\hat{\mathscr{H}}_0(t)r}\hat{\Sigma}_j(t)e^{i\hat{\mathscr{H}}_0(t)r}C_j(r)\mathrm{d}r \\ &= \frac{1}{4}\sum_{s=\uparrow,\downarrow} c_{j,s}(t)\int_0^\infty \big(\hat{\varsigma}_{-,s}e^{i\Omega_s r} + \hat{\varsigma}_{+,s}e^{-i\Omega_s r}\big)C_j(r)\mathrm{d}r \end{aligned} \quad (10.45)$$

We now introduce spectral density of the environment defined as $S_j(\omega_s) = \int_{-\infty}^{\infty} C_j(r)e^{i\omega_s r}\mathrm{d}r$ and ignore the deterministic Lamb shift (see Sec. 3.2 for analogous derivation and discussion). As a result each commutator can be written as:

$$\begin{aligned}&\big[\hat{\Sigma}_j, \hat{\mathscr{R}}_j(t)\hat{\varrho}\big] = \\ &= \frac{1}{8}\sum_{s,s'} c_{j,s}c_{j,s'}\Big(\Big[\big(\hat{\varsigma}_{-,s} + \hat{\varsigma}_{+,s}\big), \big(\hat{\varsigma}_{-,s'}S_j(\Omega_{s'}) + \hat{\varsigma}_{+,s'}S_j(-\Omega_{s'})\big)\hat{\varrho}\Big].\end{aligned} \quad (10.46)$$

Local secular approximation

We now attempt at performing secular approximation, which amounts to neglecting terms with rapidly oscillating phase factors[14] . This would naturally allow to keep spin-diagonal terms of the form $\hat{\varsigma}_{\pm,s}\varsigma_{\mp,s}$. However, in view of analysis coherence between the spins states we keep the terms

$$\hat{\varsigma}_{+,\uparrow}\hat{\varsigma}_{-,\downarrow}, \quad \text{and} \quad \hat{\varsigma}_{-,\uparrow}\hat{\varsigma}_{+,\downarrow}, \quad (10.47)$$

as they are associated with the relatively small phase $\propto \int_{t_i}^{t}\Delta\Omega(t')\mathrm{d}t'$. We term this operation local-secular approximation [138] as we neglect terms which do not conserve the energy in the orbital subspace, i.e. $\hat{\varsigma}_{\pm,s}\hat{\varsigma}_{\pm,s'}$.

14: In the interaction picture with respect to $\hat{\mathscr{H}}(t) = \sum_s \Omega_s\,|s\rangle\langle s|$

After local secular approximation the commutator reads:

$$\begin{aligned}\big[\hat{\Sigma}_j(t), \hat{\mathscr{R}}_j(t)\varrho(t)\big] = \frac{1}{8}\sum_{s,s'=\uparrow,\downarrow} c_{js}c_{js'}\big[\hat{\varsigma}_{-,s}, \hat{\varsigma}_{+,s'}S_j(-\Omega_{s'})\hat{\varrho}(t)\big] \\ + \big[\hat{\varsigma}_{+,s'}, \hat{\varsigma}_{-,s}S_j(\Omega_s)\hat{\varrho}(t)\big],\end{aligned} \quad (10.48)$$

Linblad form

We now write equations of motion for the blocks of density matrix, i.e. $\varrho_{ss'} \equiv \langle s| \hat{\varrho} |s'\rangle$:

$$\begin{aligned}\frac{\partial}{\partial t}\hat{\varrho}_{ss'} = &-i(\hat{\mathscr{H}}_s\hat{\varrho}_{ss'} - \hat{\varrho}_{ss'}\hat{\mathscr{H}}_{s'}) - i\langle s|\left[\hat{\mathscr{V}}_{\mathrm{so}}(t), \hat{\varrho}\right]|s'\rangle + \\ &+\frac{1}{8}\sum_{j=x,z}\Big(-c_{js}^2\left(\hat{\varsigma}_-\hat{\varsigma}_+\hat{\varrho}_{ss'}S_j(-\Omega_s) + \hat{\varsigma}_+\hat{\varsigma}_-\hat{\varrho}_{ss'}S_j(\Omega_s)\right) \\ &\quad - c_{js'}^2\left(\varrho_{ss'}\hat{\varsigma}_-\hat{\varsigma}_+S_j(-\Omega_{s'}) + \hat{\varrho}_{ss'}\hat{\varsigma}_+\hat{\varsigma}_-S_j(\Omega_{s'})\right) \\ &\quad + c_{js}c_{js'}\left(\hat{\varsigma}_+\hat{\varrho}_{ss'}\hat{\varsigma}_-\left[S_j(-\Omega_s) + S_j(-\Omega_{s'})\right]\right) \\ &\quad + c_{js}c_{js'}\left(\hat{\varsigma}_-\hat{\varrho}_{ss'}\hat{\varsigma}_+\left[S_j(\Omega_s) + S_j(\Omega_{s'})\right]\right)\Big). \end{aligned} \tag{10.49}$$

where we have defined the spin-diagonal part

$$\hat{\mathscr{H}}_s \equiv \langle s|\hat{\mathscr{H}}|s\rangle = \frac{\Omega_s}{2}\hat{\varsigma}_z - \frac{\dot{\vartheta}_s}{2}\hat{\varsigma}_y. \tag{10.50}$$

Note that the only coupling between the blocks $\hat{\varrho}_{ss'}$ is provided by the transverse spin-orbit coupling $\hat{\mathscr{V}}_{so}(t)$ defined by Eq. 10.22.[15] We conclude that the first two terms in dissipative evolution can be directly related to the charge excitation and relaxation rates since

15: Note that in the numerical we do not perform any approximations to $\hat{\mathscr{V}}_{so}(t)$

$$\Gamma_{j,\mp}(\Omega_s) = \frac{1}{4}c_{js}^2 S_j(\pm\Omega_s) \tag{10.51}$$

However last two lines involves cross-terms, which cannot be directly related to $\Gamma_\pm(\Omega_s)$ unless $c_{jq} = c_{jq'}$, which makes this formula difficult to represent using Linblad form analogous to Eq. (5.70). However if only the the arithmetic average of spectral densities is replaced by the geometric one, i.e.

$$\frac{S_j(\pm\Omega_q) + S_j(\pm\Omega_{q'})}{2} \to \sqrt{S_j(\pm\Omega_q)S_j(\pm\Omega_{q'})} \tag{10.52}$$

the dissipative evolution can be generated by the Linblad form of Master equation given by Eq. (5.70), with time-dependent Linbladians:

$$\begin{aligned}\hat{L}_{j,+} &= \hat{\varsigma}_+\sum_{s=\uparrow,\downarrow}\sqrt{\Gamma_{j,+}(\Omega_s)}\,|s\rangle\langle s| \\ \hat{L}_{j,-} &= \hat{\varsigma}_-\sum_{s=\uparrow,\downarrow}\sqrt{\Gamma_{j,-}(\Omega_s)}\,|s\rangle\langle s|\,, \end{aligned} \tag{10.53}$$

for $j = x, z$. We highlight that transition to a Linblad form of Master equation will not modify the spin-diagonal evolution, since for $s = s'$ the two averages are equal. Also in the elements corresponding to orbital coherence $\langle\pm|\hat{\varrho}_{ss'}|\mp\rangle$ modified cross-terms are absent. The only possibly modified elements are the coherences in the ground and excited instantaneous states, which we define as:

$$W_\pm(t) = \langle\pm|\hat{\varrho}_{\uparrow\downarrow}(t)|\pm\rangle\,. \tag{10.54}$$

Naturally the effect of modification introduced in (10.52) depends on the shape of spectral density and difference between spin-dependent orbital gap $\Delta\Omega$, however for typically flat spectrum and in weak coupling limit

the difference is expected to be negligible. For instance, for the spectrum of the form $S(\Omega) \propto \Omega^{\alpha}$ the relative rate between arithmetic and geometric average of the spin-dependent spectrum reads:

$$\frac{S(\Omega_\uparrow) + S(\Omega_\downarrow)}{2\sqrt{S(\Omega_\uparrow)S(\Omega_\downarrow)}} - 1 \approx \frac{\alpha^2}{2}\frac{\Delta E_z^2}{\Omega^2} \leq 0.05, \tag{10.55}$$

where the equlity holds for the extreme case of $\alpha = 3$ (deformation phonons), $\Omega = 10\,\mu$eV and $\Delta E_z = 1\,\mu$eV. In reality the ratio is expected to be orders of magnitude smaller since at the small orbital splitting the spectrum is flatter[16] . For this reason we find the Linblad form of adiabatic Master equation for composite spin-charge system sufficient to describe the physics of spin qubit shuttling between two tunnel-coupled quantum dots.

16: See Fig. 8.7 for the typical relaxation rates as a function of sweep rate

Equations of motion

Using Linblad equation one can find the equations of motion for the coherences at time t, i.e.

$$\begin{aligned}\dot{W}_\pm(t) = -i\,\langle \pm,\uparrow|\left[\hat{\mathscr{H}}(t) + \hat{\mathscr{V}}_{so}(t), \hat{\varrho}(t)\right]|\pm,\downarrow\rangle + \\ + \sum_{j=x,z}\sqrt{\Gamma_{j,\pm}(\Omega_\uparrow)\Gamma_{j,\pm}(\Omega_\downarrow)}W_\mp(t) - \frac{\Gamma_{j,\mp}(\Omega_\uparrow)+\Gamma_{j,\mp}(\Omega_\downarrow)}{2}W_\pm(t).\end{aligned} \tag{10.56}$$

Crucially in the limit where the coherent coupling between the spins and the orbital states can be neglected, i.e. $\hat{\mathscr{H}} + \hat{\mathscr{V}}_{so}(t) \to \hat{\mathscr{H}}_0$, the above differential equations involve only $W_\pm(t)$ terms, i.e.

$$\begin{aligned}\dot{W}_\pm(t) \approx -i\frac{\Delta\Omega}{2}W_\pm(t) + \sum_{j=x,z}\sqrt{\Gamma_{j,\pm}(\Omega_\uparrow)\Gamma_{j,\pm}(\Omega_\downarrow)}W_\mp(t) + \\ - \frac{\Gamma_{j,\mp}(\Omega_\uparrow)+\Gamma_{j,\mp}(\Omega_\downarrow)}{2}W_\pm(t),\end{aligned} \tag{10.57}$$

which will be used in Sec. 12.3 for the analytical analysis.

11 Shuttling of the excited spin state

Let us now compute the probability of a successful interdot transfer of an electron in an excited spin state, i.e. we consider the initial state given by

$$|\psi(t_i)\rangle = |-,\uparrow\rangle \approx |\uparrow\rangle \otimes |L\rangle\,, \tag{11.1}$$

and analyze the loss of occupation of the ground adiabatic spin-up state, during adiabatic transition from the left to the right dot. Thus the figure of merit is defined by the observable:

$$Q_\uparrow = 1 - P_\uparrow. \tag{11.2}$$

where the probability of successful spin-up transfer $P_\uparrow$ has an explicit form:

$$P_\uparrow = |\left\langle -(t_f),\uparrow\right| \hat{\varrho}(t_f) \left|-(t_f),\uparrow\right\rangle|^2, \tag{11.3}$$

where $\left|-(t_f),\uparrow\right\rangle \approx |R,\uparrow\rangle$. In Sec. 11.1 we compute $Q_\uparrow$ in absence of the environment. In Sec. 11.2 we show how the low-frequency noise can affect $Q_\uparrow$. Next in Sec. 11.3 we include also high-frequency noise. In particulair we propose there an experimental realizaiton of the Elitzur-Veidman bomb testing. In the final Sec. 11.4 we compute $Q_\uparrow$ for the realistic DQD devices from Sec. 6.3.

11.1 Transfer in absence of an environment

We start by neglecting the presence of environment and computing coherent evolution generated by the Hamiltonian:

$$\hat{H}(t) = \hat{H}_o(t) + \hat{H}_s(t) + \hat{V}_{so}(t), \tag{11.4}$$

where $\hat{H}_o = \frac{1}{2}(\epsilon(t)\hat{\sigma}_z + t_c\hat{\sigma}_x)$, $\hat{H}_s(t) = \frac{1}{2}E_z\hat{s}_z$ and the coupling between spin and orbital degree of freedom $\hat{V}_{\rm so}$ was given in Eq. (10.4). We consider two regimes: that of low ($E_z < t_c$) and high ($E_z > t_c$) magnetic field.

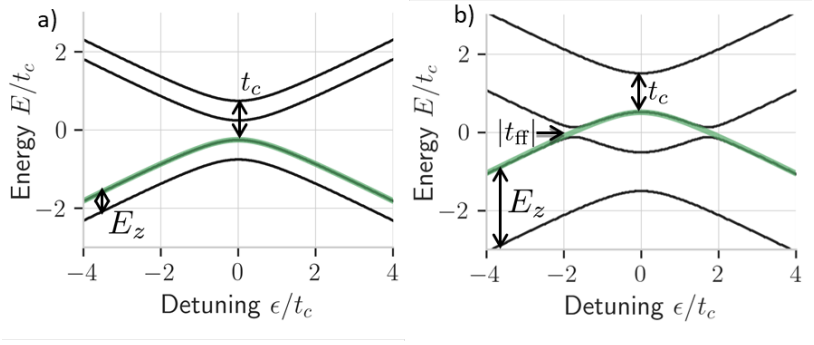

Figure 11.1: Instantaneous energy spectrum of the total Hamiltonian $\hat{H}(t)$ from Eq. (11.4), a) in the regime of large magnetic field $E_z > t_c$ and b) small magnetic field $E_z < t_c$. Green line corresponds to the energy of the ground orbital spin-up state $|-(t),\uparrow\rangle$. The main difference is the absence of the spin-flip avoided crossing in the $E_z < t_c$ case. We highlight however that finite mixing between the $|+,\uparrow\rangle$ (green) and $|+,\downarrow\rangle$ due to spin-orbit coupling will lead to possibility of spin-relaxation (See Fig. 11.6).

As it can be seen from the instantaneous energy spectrum drawn in Fig. 11.1a), in the first case $E_z < t_c$ the adiabatic evolution of spin-up state in absence of environment should be similar to Landau-Zener model (see Sec. 5.1). In the second case shown in Fig. 11.1b), the $E_z > t_c$ large gives rise to additional avoided crossings, due to presence of non-negligible spin-orbit interaction. It leads to repulsion of instantaneous orbital states $|+,\downarrow\rangle, |-,\uparrow\rangle$ at times $t_\pm \approx E_z/v$, where the gap between the hybridized states[1] at avoided crossing is given by:

$$|t_{\text{ff}}| = \sqrt{\left[t_{\text{flip}}^{(\text{int})}\right]^2 + \left[\tfrac{t_c}{E_z} t_{\text{flip}}^{(\text{syn})}\right]^2}, \tag{11.5}$$

where $t_{\text{flip}}^{(\text{int})}$ and $t_{\text{flip}}^{(\text{syn})}$ are related to intrinsic and synthetic spin-orbit interaction defined in Eq. (10.7) and Eq. (10.6) respectively.

1: of the form $|\psi_\pm\rangle \propto |+,\downarrow\rangle \pm |-,\uparrow\rangle$

LZSM interferometer

Since each of the avoided crossings can be treated as a Landau-Zener crossing, adiabatic evolution through both of them leads to Landau-Zener-Stuckelberg-Majorana interference [97]. As a result, the final population of target $|-,\uparrow\rangle$ state, defined as $P_\uparrow$, will depend on the phase difference ϕ_{int} for the two paths of the interferometer denoted in Fig. 11.2 using green and red lines[2] .

2: In a different context, an analogy between adiabatic transitions, two-slit experiment and LZSM interferometer was analyzed in [198]

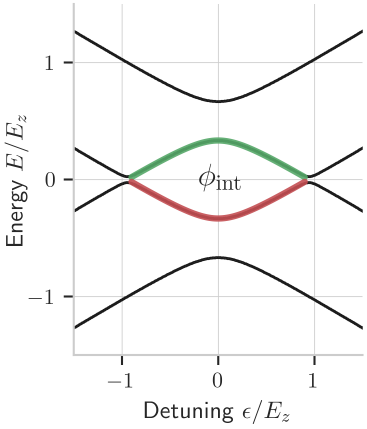

Figure 11.2: The spin-flip interferometer. In the relevant region of ϵ, we denoted the energy of the $|-,\uparrow\rangle$ state using green and the energy of the $|+,\downarrow\rangle$ state using red line. They gives the upper and lower path of the spin-flip interferometer respectively. We plotted the colored lines using expression for the energy of the orbital adiabatic states from Eq. (11.6), which agrees with the instantaneous spectrum of total Hamiltonian $\hat{H}(t)$ for typical regime of $t_{\text{ff}} \ll t_c$. We symbolically illustrated the relative phase between the paths as ϕ_{int}.

Adiabatic-impulse approximation

We now treat the interferometer using adiabatic-impulse approximation (see Sec. 5.1), assuming the avoided crossings take place at t_+ and t_-. We assume the modification of the energy due to small spin-orbit coupling can be ignored, and hence the adiabatic evolution amounts to integral over energy of the instantaneous orbital states,

$$\begin{aligned} E_{\pm,\uparrow}(t) &= \frac{\overline{E}_z}{2} \pm \frac{1}{2}\sqrt{(vt + \tfrac{\Delta E_z}{2})^2 + t_c^2} \\ E_{\pm,\downarrow}(t) &= -\frac{\overline{E}_z}{2} \pm \frac{1}{2}\sqrt{(vt - \tfrac{\Delta E_z}{2})^2 + t_c^2}. \end{aligned} \tag{11.6}$$

Assuming orbital adiabaticity[3] and absence of environment the evolution can be computed in the flip-flip subspace, i.e. the evolution operator reads:

$$\hat{U}_{\text{ff}}(t_f, t_i) = \hat{A}_{\text{ff}}(t_f, t_+ + \delta t)\hat{T}_{\text{ff}}^\dagger \hat{A}_{\text{ff}}(t_+ - \delta t, t_- + \delta t)\hat{T}_{\text{ff}}\hat{A}_{\text{ff}}(t_- - \delta t, t_i), \tag{11.7}$$

which is in full analogy to Eq. (5.26)[4] . We assume $\delta t \to 0$ and hence the adiabatic evolution matrix reads:

$$\hat{A}_{\text{ff}}(a,b) = \begin{bmatrix} e^{i\int_a^b E_{+,\downarrow}(t)\mathrm{d}t} & 0 \\ 0 & -e^{-i\int_a^b E_{-,\uparrow}(t)\mathrm{d}t} \end{bmatrix}, \tag{11.8}$$

where we included the relative shift of $e^{i\pi} = -1$ generated by adiabatic transition across different branches of orbital avoided crossing[5] . The

3: No coherent transtitions between $|\pm, s\rangle$ states

4: Note that the Hermitian conjugate here is due to the fact that the second transition is a mirror image of the first

5: Note that the $|+,\downarrow\rangle$ goes through upper branch of spin-down orbital crossing, while $|-,\uparrow\rangle$ goes across lower branch of spin-up orbital crossing

transfer matrix for the spin-flip avoided crossing $\hat{T}_{\rm ff}$ reads:

$$\hat{T}_{\rm ff} = \begin{bmatrix} \sqrt{Q_{\rm ff}} & \sqrt{1-Q_{\rm ff}}e^{i\alpha_{s,\rm ff}} \\ -\sqrt{1-Q_{\rm ff}}e^{-i\alpha_{s,\rm ff}} & \sqrt{Q_{\rm ff}} \end{bmatrix}, \tag{11.9}$$

where $Q_{\rm ff} = \exp\left(-\frac{\pi}{2}\frac{|t_{\rm ff}|^2}{2v}\right)$. Note that the above form of the transfer matrix is different from $\hat{\mathcal{T}}$, previously introduced in Eq. (5.28). There we wrote the transfer matrix in the basis of adiabatic states $|\pm\rangle$ with respect to considered avoided crossing. Here the transition matrix was written in the flip-flip basis of the states $|+,\downarrow\rangle$, $|-,\uparrow\rangle$, i.e. the diabatic levels for the spin-flip avoided crossing (see Fig. 11.3).

As before we have included the deterministic Stokes phase[6] . We expect the AIA to be a reliable method for computing effects of spin-flip avoided crossing, since in the limit of weak coupling the widths of the crossings[7] are small in comparison to other energy scales.

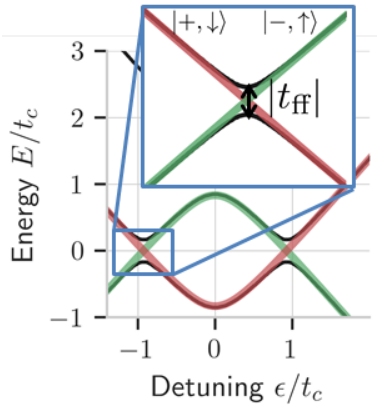

Figure 11.3: Spin-flip avoided crossing. The scheme of the avoided crossing between orbital adiabatic levels $|+,\downarrow\rangle$ (red) and $|-,\uparrow\rangle$ (green), the size of which is given by $|t_{\rm ff}|$. This time we highlight that the orbital adiabatic states $|+,\downarrow\rangle$ and $|-,\uparrow\rangle$ can be seen as the diabatic states of the spin-flip avoided crossing as it was plotted using green and red lines in the inset. The true instantaneous states around the spin-flip avoided crossing are the linear combinations of the above and their energy spectrum is plotted using black lines.

Interference pattern

We now compute the loss of occupation of the target $|-(t_f),\uparrow\rangle$ state using AIA, i.e.

$$Q_\uparrow(t_f) = 1 - \left|\langle -(t_f),\uparrow|\,\hat{U}_{\rm ff}(t_f,t_i)\,|-(t_i),\uparrow\rangle\right|^2 = 4(1-Q_{\rm ff})Q_{\rm ff}\cos^2(\tfrac{\phi_{\rm int}}{2}) \tag{11.10}$$

where the relative phase $\phi_{\rm int}$ can be written as:

$$\phi_{\rm int} = \int_{t_-}^{t_+}[E_z - \overline{\Omega}(t)]{\rm d}t, \tag{11.11}$$

in which $\overline{\Omega}(t) = \frac{1}{2}[\Omega_\uparrow(t)+\Omega_\downarrow(t)] \approx \sqrt{v^2t^2+t_c^2}$ is the average orbital splitting. Note that in the AIA the dependence on ΔE_z is not present for the symmetry reasons. In the limit of $E_z \gg t_c$ the interference phase can be computed as:

$$\phi_{\rm int} = \frac{2E_z^2}{v} - \frac{t_c}{v}\left(E_z\sqrt{1+\frac{E_z^2}{t_c^2}} + t_c\ln\left(E_z/t_c + \sqrt{E_z^2/t_c^2+1}\right)\right) \approx \frac{E_z^2}{v}, \tag{11.12}$$

where we have neglected a logarithmic correction. This shows that the phase is expected to be sensitive to the fluctuations of E_z[8] .

Numerical result

We now numerically test the above prediction and show that the origin of spin-orbit interaction[9] introduces only non-relevant phase-shift of quickly changing interference pattern. In Fig. (11.4) we plot the loss of occupation of the spin-up state $Q_\uparrow$ as a function of dimensionless sweep rate v/t_c^2. In the figure we use $t_c = 2E_z = 50|t_{\rm ff}| = 10\Delta E_z$, which would be typical ballpark of parameters in the semiconductor quantum dots. In the figure we compare the results for $t_{\rm ff} = t_{\rm flip}^{\rm (int)}$ (blue) and $t_{\rm ff} = -i\frac{t_c}{E_z}t_{\rm syn}$ (red), which enters the simulation via the full spin-orbit interaction $\hat{V}_{so}(t)$, given by Eq. (10.4). In the figure we see the black lines corresponding to the

6: which for mosty non-adiabatic spin-flip crossing will be close to $\alpha_{s,\rm ff} \approx \pi/4$. Note that the value is consistent with perturbation theory given by Eq. (5.20), since $[1,0]\hat{T}_{\rm ff}[0,1]^T \approx \sqrt{it_c^2\pi/2v}$

7: Region of ϵ for which two spin-flip states hybridises.

Spin-flip interference

8: which in our case are attributed to presence of nuclear spins

9: intrinsic versus synthetic spin-orbit contribution to $t_{\rm ff}$ from Eq. (10.35)

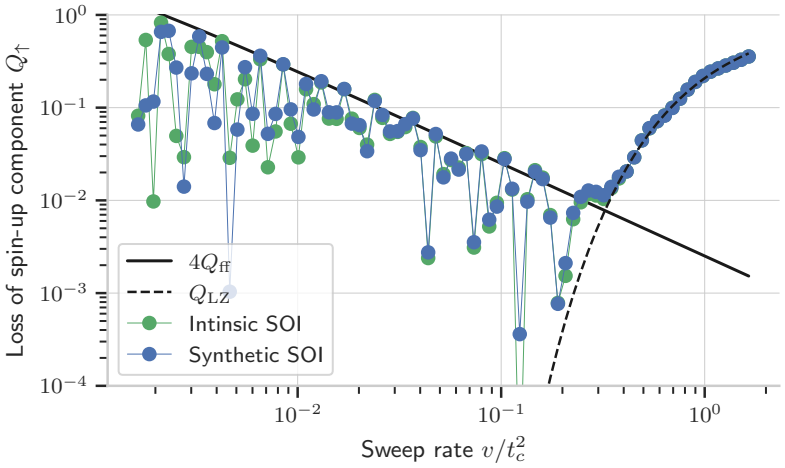

Figure 11.4: Probability of losing the occupation of the orbital ground state corresponding to spin-up component during interdot electron transition $Q_\uparrow$, as a function of dimensionless sweep rate v/t_c^2. We use $t_c = 2E_z = 50|t_{\mathrm{ff}}| = 10\Delta E_z$ parameters and plot the numerical simulation of the unitary dynamics in presence of: intrinsic (green) and synthetic (blue) spin-orbit interaction leading to the same value of $|t_{\mathrm{ff}}| = t_c/50$. With dashed black line we plot Q_{LZ}, and with a solid black line $4Q_{\mathrm{ff}}$. The latter is the upper bound on the spin-flip interference effect.

probability of Landau-Zener orbital transition $Q_{\mathrm{LZ}} = \exp\left(-\frac{\pi}{2}\frac{t_c^2}{2v}\right)$(dashed line) and predicted in Eq. (11.10) upper limit of the $Q_\uparrow(t_f)$ (solid line), which for $Q_{\mathrm{ff}} \ll 1$ can be approximated as:

$$Q_{\uparrow,\max}(t_f) = 4Q_{\mathrm{ff}}, \tag{11.13}$$

where $Q_{\mathrm{ff}} = \exp\left(-\frac{\pi}{2}\frac{|t_{\mathrm{ff}}|^2}{2v}\right)$. In the limit of fast sweeps the loss of spin-up occupation can be related to coherent transitions to the $|+,\uparrow\rangle$ state,which can be seen by agreement between numerical simulations and the Landau-Zener curve. For slower sweeps the probability of Q_{ff} becomes non-negligible which results in the interference pattern, with rapidly oscillating phase ϕ_{int}. The upper limit of the oscillation is approximately given by $4Q_{\mathrm{ff}}$. The significant difference between the synthetic and intrinsic spin-orbit coupling is visible only for the slowest sweeps, where the two interference patterns are slightly shifted[10] . Due to the rapidly oscillating phase we will not aim here at defining optimal sweep rate at which the destructive interference of $Q_\uparrow$ takes place. Instead we aim at discovering how the envelope of the oscillation is modified by the presence of environment.

Thus for the rest of thesis we will assume that t_{ff} is a real parameter. Its value will be chosen to be of a typically measured order of magnitude.[11]

10: This can be related to the different time-dependence of two spin-orbit coupling in vicinity of spin-flip avoided crossing. See Eq. (10.22)

11: We expect the intrinsic SOI to be dominant in the GaAs-based devices, and synthetic in Si

11.2 Transfer in presence of quasistatic noise

We now consider the influence of low-frequency noise, which we model by the quasistatic noise in the parameters of the Hamiltonian (11.4), in the form of detuning and tunnel coupling noise caused by the charge noise and fluctuations of Zeeman splitting δE_z due to presence of nuclear spins[12] :

$$\epsilon' = \epsilon(t) + \delta\epsilon, \qquad t_c' = t_c + \delta t_c, \qquad E_z' = E_z + \delta E_z. \tag{11.14}$$

In principle the above fluctuations might affect Q_{ff} via slow modification of t_{ff} or dynamical noise in detuning. However we highlight that in the

12: This would be particularly relevant for GaAs device

considered regime of almost-diabatic transition both can be neglected, as we have shown in Eq. (5.41) where polynomial correction to Landau-Zener probability due to slow fluctuation of tunnel coupling was shown, and in Chapter 8 where we showed that Landau-Zener excitation should dominate the noise-induced corrections.

With the assumptions above, from Eq. (11.10) $Q_\uparrow$ depends now only on the value of $\phi_{\rm int}$, an expression for which is given in Eq. (11.11). We now evaluate the $Q_\uparrow$, averaged over realizations of the low-frequency noise, which gives:

$$\langle Q_\uparrow\rangle = 4(1-Q_{\rm ff})Q_{\rm ff}\left\langle \cos^2\left(\tfrac{\phi_{\rm int}^{(0)}+\delta\phi_{\rm int}}{2}\right)\right\rangle \approx \overline{Q}_\uparrow \frac{1+\cos(\phi_{\rm int}^{(0)})\langle e^{i\delta\phi_{\rm int}}\rangle}{2}, \tag{11.15}$$

where $\delta\phi_{\rm int}(\delta\epsilon, \delta t_c, \delta E_z)$ is the zero-average correction to deterministic phase $\phi_{\rm int}$. As it can be seen in the limit of strong fluctuations $Q_\uparrow$ averaged realizations of the noise tends to the incoherent limit

Dephased spin-flip interference

$$\overline{Q}_\uparrow = 2(1-Q_{\rm ff})Q_{\rm ff}, \tag{11.16}$$

which corresponds to completely random interference phase $\phi_{\rm int}$ for which $\langle\cos^2(\phi_{\rm int})\rangle \to 1/2$. Below we compute the central quantity $\langle e^{i\delta\phi_{\rm int}}\rangle$ for each of the independent contributions.

Noise in detuning

We first consider noise in detuning $\delta\epsilon$ which affects the spin-averaged splitting, i.e. in the leading order in ΔE_z and $\delta\epsilon$ reads

$$\overline{\Omega}(t) \approx \Omega_0(t)\cos\vartheta_0(t)\delta\epsilon + \sin\vartheta_0^2(t)\frac{\delta\epsilon^2}{\Omega_0}, \tag{11.17}$$

where $\cos\vartheta_0(t) = vt/\Omega_0(t)$ and $\sin\vartheta_0(t) = t_c/\Omega_0(t)$ with $\Omega_0(t) = \sqrt{v^2t^2+t_c^2}$. With these definitions the random contribution to phase is related to the quadratic term[13] , i.e.

13: Due to symmetric limits of integrations

$$\delta\phi_{\rm int}(\delta\epsilon) = \delta\epsilon^2 t_c^2\int_{-E_z/v}^{E_z/v}\Omega_0^{-3} = \frac{2\delta\epsilon^2}{v}, \tag{11.18}$$

which averaged over realizations of the noise gives only polynomial correction:

$$\langle e^{i\delta\phi_{\rm int}}\rangle_{\delta\epsilon} = \left(1-i\frac{4\sigma_\epsilon^2}{v}\right)^{-1/2}. \tag{11.19}$$

Noise in tunnel coupling

We now move to the noise in tunnel coupling, for which the modification to average orbital splitting is non-vanishing already in the first order, i.e.

$$\overline{\Omega}(t) \approx \Omega_0(t) + \sin\vartheta_0(t)\delta t_c, \tag{11.20}$$

which translates into fluctuation of the phase, given by:

$$\delta\phi_{\text{int}}(\delta t_c) = t_c \delta t_c \int_{-E_z/v}^{E_z/v} \sin\vartheta_0(t)\mathrm{d}t = \frac{t_c \delta t_c}{v} \ln\left(\frac{4E_z^2}{t_c^2}\right), \tag{11.21}$$

and as a consequence leads to the averaged phase:

$$\langle e^{i\delta\phi_{\text{int}}}\rangle_{\delta t_c} = \exp\left(-\tfrac{1}{2}\left[\frac{\sigma_{t_c} t_c}{v}\ln\left(\frac{4E_z^2}{t_c^2}\right)\right]^2\right). \tag{11.22}$$

Fluctuations of spin splitting

We finally consider fluctuations of the Zeeman splitting. In sec 9.1, we discussed that in most cases the fluctuations in the left and right dot can be treated as independent. We use here the direct estimation of the interference phase $\phi_{\text{int}} \approx E_z^2/v$, using which the modification of Zeeman splitting $E_z \to E_z + \delta E_z$ introduces phase shift,

$$\delta\phi_{\text{int}}(\delta E_z) = \frac{2E_z \delta E_z}{v}, \tag{11.23}$$

which translates into the averaged phase:

$$\langle e^{i\delta\phi_{\text{int}}}\rangle_{\delta E_z} = \exp\left(-2\frac{E_z^2}{v^2}\sigma_{E_z}^2\right). \tag{11.24}$$

11.3 Transfer in presence of high-frequency noise

We now consider corrections to fidelity of spin-up transfer in presence of high-frequency noise, which as shown in Sec. 5.3 introduces inelastic transitions between the instantaneous levels.

Interference pattern at high magnetic fields

We start with the limit of $E_z > t_c$, where the spin-flip avoided crossings are created. We assume that probability of inelastic transitions before the first spin-flip avoided crossing located at $t_- = -E_z/v$ is negligible. Just after the avoided crossing the general state can be written as:

$$|\psi(t_+ + \delta t)\rangle = \sqrt{Q_{\text{ff}}}\,|-,\uparrow\rangle + e^{i\phi_0}\sqrt{1-Q_{\text{ff}}}\,|+,\downarrow\rangle\,, \tag{11.25}$$

where we have included some initial phase[14] $e^{i\phi_0}$. With such an initial condition we now use the AME from Sec. 5.3 to compute evolution in-between the spin-flip anticrossings, i.e. $t \in (t_-, t_+)$. Note that with spin-diagonal coupling to environment, and away from spin-flip avoided crossing we can treat the dynamics of each superposition component separately.

For sufficiently slow sweeps[15] , probability of occupying each of the

14: we can corresponds to Stokes phase for instance

15: such that coherent, L-Z coupling between spin-diagonal state can be neglected

instantaneous states can be computed from the differential equation:

$$\dot{P}_{\pm,s} = -\Gamma_{\pm}(\Omega_s)P_{\pm,s} + \Gamma_{\mp}(\Omega_s)P_{\pm,s}, \tag{11.26}$$

where the excitation and relaxation rates $\Gamma_{\pm}(\Omega_s[t])$ are in general time-dependent. For initial conditions $p_{-,\uparrow} = Q_{\text{ff}}$, $p_{+,\downarrow} = 1 - Q_{\text{ff}}$ and $p_{-,\downarrow} = p_{+,\uparrow} = 0$, the above equation can be solved as:

$$\begin{aligned} P_{-,\uparrow} &= Q_{\text{ff}}\left(e^{-\int_{t_-}^{t_+}\Gamma_+ + \Gamma_-} + \int_{t_-}^{t_+}\Gamma_-(t')e^{-\int_{t'}^{t_+}\Gamma_+ + \Gamma_-}\right) \\ P_{+,\downarrow} &= (1 - Q_{\text{ff}})\left(e^{-\int_{t_-}^{t_+}\Gamma_+ + \Gamma_-} + \int_{t_-}^{t_+}\Gamma_+(t')e^{-\int_{t'}^{t_+}\Gamma_+ + \Gamma_-}\right). \end{aligned} \tag{11.27}$$

In the low-temperature limit,[16] the probability of excitation can be neglected, which means

16: in which $\int_{t_-}^{t_+}\Gamma_+ \ll 1$

$$\begin{aligned} P_{-,\uparrow} &\approx Q_{\text{ff}} \\ P_{+,\downarrow} &\approx (1 - Q_{\text{ff}})\exp\left(-\int_{t_-}^{t_+}\Gamma_-(t')\mathrm{d}t'\right). \end{aligned} \tag{11.28}$$

The above result shows that the amplitude of excited orbital state with flipped spin $|+,\downarrow\rangle$ is more likely to decay. Note that the described above leakage from mostly lower branch of interferometer[17] bounds transfer of the spin-up state, since $P_{\uparrow} \leqslant P_{-,\uparrow} + P_{+,\downarrow}$, or equivalently

17: Note that in principle relaxation process can recover part of irrelevant in low-temperature leakage to $|+,\uparrow\rangle$ state

$$Q_{\uparrow} \geqslant \left(1 - Q_{\text{ff}}\right)\left(1 - e^{-\int_{t_-}^{t_+}\Gamma_-(t')\mathrm{d}t'}\right). \tag{11.29}$$

Elitzur-Veidman bomb

The above formula takes into consideration averaging over many runs of the experiment. However one can imagine a situation in which the emission of energy quanta[18] in a single realization could be detected by measuring the state of transferred electron. For instance we take a situation in which the interference term is fined-tuned towards the constructive one with $\phi_{\text{int}} = 2k\pi$, while the sweep rate is slow enough so that $Q_{\text{ff}} \approx 1/2$. In such case the the probability of the excited spin state staying in the initial dot, would be close to unity

18: for instance the phonon

$$Q_{\uparrow,\text{constr}} = 4Q_{\text{ff}}(1 - Q_{\text{ff}}) \approx 1. \tag{11.30}$$

This means that in absence of the environment the spin-up electron is guaranteed to stay in the initial dot. Now in presence of the relaxation from the lower branch of the interferometer, the electron would also stay in the initial dot, unless the relaxation takes place.

To show this is the case we consider a single realization of the experiment, which is schematically plotted in Fig. 11.5. After first spin-flip crossing, for $Q_{\text{ff}} = 1/2$ the electron state reads:

$$|\psi(t_- + \delta t)\rangle = \frac{1}{\sqrt{2}}\left(|+(t_-),\downarrow\rangle + e^{i\phi}\,|-(t_-),\uparrow\rangle\right). \tag{11.31}$$

If phonon is not emitted, the electron continues the evolution and as a

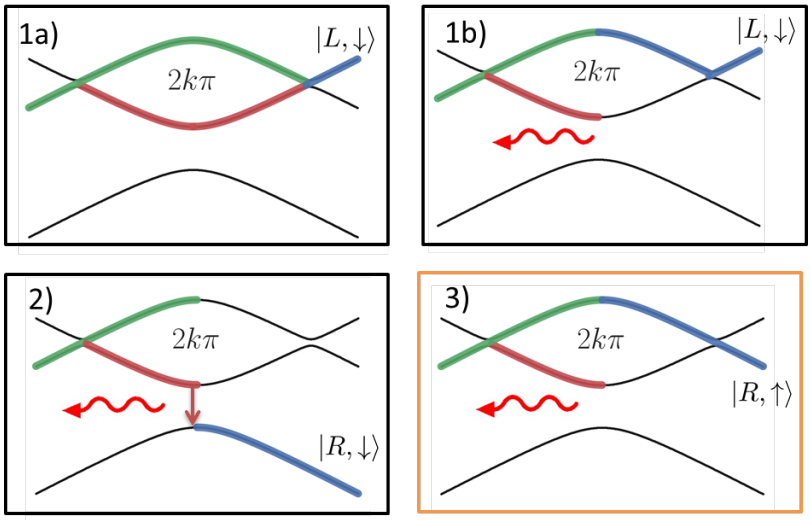

Figure 11.5: Realization of Elitzur–Vaidman bomb testing experiment from [199]. Four possible quantum paths of the spin-up evolution during interdot transition. In the 1a) we plot evolution in absence of the environment, where initial state $|-,\uparrow\rangle$ (green) becomes first superimposed with $|+,\downarrow\rangle$ (red), and then ends up in the $|L,\downarrow\rangle$ (blue) as a result of constructive interference i.e. $\phi_{\text{int}} = 2k\pi$ for $k \in \mathfrak{Z}$ and $Q_{\text{ff}} = 1/2$. In the remaining cases a phonon is emitted from the lower branch (red) around the avoided crossing (wavy red line). In 2) case, the superposition "collapses" into the ground energy state and ends up in $|R,\downarrow\rangle$ state. In cases 1b) and 3) the superposition "collapses" into the upper branch of the interferometer and with equal probability ends in the states $|L,\downarrow\rangle$ or $|R,\uparrow\rangle$. In the most interesting case 3) (orange box), the emission of the phonon was detected, without physical relaxation of the electron.

result of the constructive interference ends up in $|L,\downarrow\rangle$ state (1a option in Fig. 11.5). If however the phonon emission takes place at time t_r, the superposition state from (11.31) "collapses" with probability $1/2$ to $|-,\uparrow\rangle$ state and relaxes with probability $1/2$ to the ground energy state $|-,\downarrow\rangle$, where the probabilities are given by the absolute values squared of the amplitudes in Eq. (11.31). In the first option, the electron arrives at the second spin-flip avoided crossing in a single branch, from which with probability $Q_{\text{ff}} = 1/2$ ends up in the $|+(t_f),\downarrow\rangle \approx |L,\downarrow\rangle$ state (1b) and with probability $1 - Q_{\text{ff}} = 1/2$ ends up in the state $|-,\uparrow\rangle = |R,\uparrow\rangle$ (2). If however the second option is realized, i.e. the electron relaxes to $|-,\downarrow\rangle$ state, it ends up in the $|R,\downarrow\rangle$ state (3).

We now discuss now all possible outcomes of the single realization of the experiment, together with the conditional probabilities, $p(|\text{state}\rangle\,|\text{ph}\rangle$:[19] . Thus, if the electron was detected in the state:

1. $|L,\downarrow\rangle$ (Left dot, flipped spin). This could mean that either phonon was not emitted (a), i.e.

$$p(|L,\downarrow\rangle\,|0) = 1$$

   or was emitted (b), in case of which probability to end up at $|L,\uparrow\rangle$ equals

$$p(|R,\uparrow\rangle\,|1) = 0.5(1 - Q_{\text{ff}}) = 0.25$$

2. $|R,\downarrow\rangle$ (Right dot, flipped spin). This means the phonon was emitted and the electron relaxed to the ground state. This gives conditional probability:

$$p(|R,\downarrow\rangle\,|1) = 0.5$$

3. $|R,\uparrow\rangle$ (Right dot, unflipped spin). This means that although relaxation took place (phonon was emitted), the electron did not move to the lowest lying level. This is possible with conditional probability:

$$p(|-,\uparrow\rangle\,|1) = 0.5Q_{\text{ff}} = 0.25.$$

Note that the third outcome can be seen as the apparent contradiction to

19: where $|\text{state}\rangle$ denotes measured state and ph = 1 if phonon was emitted and ph = 0 if it was not emitted

the conservation of the energy, and is a consequence of the phenomenon of the quantum superposition. In the original proposal of Elitzur-Veidman [199], the emission of phonon would be associated with the active bomb, while the lack of emission means inactive bomb (a dud). The original proposal states that a similar setup[20] can be used to distinguish the active bomb from the dud. In particular when the third scenario is realised, an active bomb has been detected without its physical detonation. This phenomenon was called in [199] interaction-free measurement.

20: Using optical interferometers

Spin relaxation in low magnetic fields

In the limit of sufficiently low magnetic field, i.e. $E_z < t_c$, the spin-flip avoided crossing is absent, however presence of the environment can induce the transition from $|-,\uparrow\rangle$ to $|-,\downarrow\rangle$ around the avoided crossing, where the mixing between the spin states due to $\hat{\mathcal{V}}_{so}$ is non-negligible.[21] This process is schematically illustrated in Fig. 11.6.

21: see Eq. (10.4) for the expression for $\hat{\mathcal{V}}_{so}$

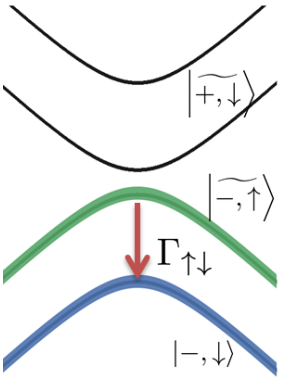

Figure 11.6: Schematic picture showing the process of losing of occupation of the dressed spin-up state $|\widetilde{-,\uparrow}\rangle$ due to relaxation to the ground state $|\widetilde{-,\downarrow}\rangle$. This process is activated by the non-zero tunnel coupling with the spin flip t_{flip}, See Eq. (11.34).

Time-independent approach

We first use the fact that around the avoided crossing the orbital splitting is approximately constant and equal to $\Omega(0) \approx t_c$. In this analysis we neglect ΔE_z as its exact value does not matter as long as $\Delta E_z \ll t_c$. We concentrate on the initially populated state $|-(t),\uparrow\rangle$ and its composition at the avoided crossing, i.e. for $t = 0$. Similarly to Eq. (9.20), we compute perturbative modification of the spin-up state as:

$$|\widetilde{-(0),\uparrow}\rangle \approx |-(0),\uparrow\rangle + \frac{\langle +(0),\downarrow|\,\mathcal{V}_{so}(0)\,|-(0),\uparrow\rangle}{t_c - E_z}\,|+(0),\downarrow\rangle\,, \tag{11.32}$$

which shows that the around the avoided crossing the initially occupied spin-up state becomes mixed with $|+(0),\downarrow\rangle$ state.

Although the above-derived admixture is temporary[22] it exposes the electron to spin-diagonal relaxation to lowest-lying state $|-(0),\downarrow\rangle$. In particular, we use an approach similar to that from Eq. (9.25) to show that the spin relaxation[23] around avoided crossing $\Gamma_{\uparrow\downarrow}$ can be related to the relaxation between the states $|-(0),\uparrow\rangle$ and $|-(0),\downarrow\rangle$, i.e.

$$\Gamma_{\uparrow\downarrow}(t_c) \approx |\,\langle +(0),\downarrow|\,\widetilde{-(0),\uparrow}\rangle|^2\Gamma_{-}(t_c) = \frac{|\,\langle +(0),\downarrow|\,\hat{\mathcal{V}}_{so}(0)\,|-(0),\uparrow\rangle\,|^2}{(t_c - E_z)^2}\Gamma_{-}(t_c), \tag{11.33}$$

where $\Gamma_{-}(t_c)$ is the spin-diagonal relaxation rate computed in Chapter 7. The matrix element can be directly related to the secular term $\hat{\mathcal{V}}_{so}(0)$, given previously in Eq. (10.26). This together with the limit of $t_c \gg E_z$ gives:

$$\Gamma_{\uparrow\downarrow}(t_c) \approx \frac{|t^{(\text{int})}_{\text{flip}} - i t^{(\text{syn})}_{\text{flip}}|^2}{4t_c^2}\Gamma_{-}(t_c). \tag{11.34}$$

Note that in the above formula the suppression of the synthetic contribution by a factor of t_c/E_z, that was present in $t^{(\text{syn})}_{\text{flip}}$ is missing. This makes the synthetic spin orbit interaction (magnetic field gradient) relatively more relevant.

22: i.e. in the absence of the environment it would vanish away from avoided crossing

23: understood as the relaxation rate between $|\widetilde{-(0),\uparrow}\rangle$ and the $|-(0),\downarrow\rangle$ states

Let us now estimate the loss of population from the adiabatic spin-up state during adiabatic transfer. We assume the rate can be treated as constant in the vicinity of avoided crossing, which has a typical width of $t_{LZ} = 2t_c/v$[24] . In such case the spin-up transfer error reads:

$$Q_\uparrow \approx \Gamma_{\uparrow\downarrow}(t_c)\frac{2t_c}{v} = \frac{|t^{(\mathrm{int})}_{\mathrm{flip}} - it^{(\mathrm{syn})}_{\mathrm{flip}}|^2}{2vt_c}\Gamma_-(t_c). \tag{11.35}$$

Next if we assume that

$$|t^{(\mathrm{int})}_{\mathrm{flip}} - it^{(\mathrm{syn})}_{\mathrm{flip}}| \approx 1\,\mu\mathrm{eV} \tag{11.36}$$

which would correspond to $\Delta B/\Delta x = 0.1\mathrm{mT/nm}$[25] or relatively large intrinsic spin-orbit interaction[26] result in

$$Q_\uparrow \sim \frac{\Gamma_-(t_c)[1/\mathrm{ns}]}{2t_c[\,\mu\mathrm{eV}]v[\,\mu\mathrm{eV}/ns]}, \tag{11.37}$$

which gives $Q_\uparrow \approx 10^{-2}$ at $v = 25\,\mu\mathrm{eV/ns}$ and $t_c = 20\,\mu\mathrm{eV}$ (see Fig. 11.9 for confirmation).

11.4 Application to spin qubit shuttling

We finally use the above example to analyze numerical simulations of the spin-up electron transfer between realistic semiconductor quantum dots. We consider here three models of DQD systems, which correspond to model GaAs, SiGe and SiMOS quantum dots from Sec. 6.3.

Parameters used

In the analysis we we will start with the published result on the effect on the interference pattern of nuclear spins purification in Si at relatively small $t_c = 10\,\mu\mathrm{eV}$. Later for two tunnel couplings of $t_c = 20, 60\,\mu\mathrm{eV}$ at $T = 100\mathrm{mK}$, we will compute the error loss of occupation of the spin-up ground state $Q_\uparrow$. We will use corresponding relaxation rates from Chapter 7, which we replot together with the relaxation rates for $t_c = 60\,\mu\mathrm{eV}$ in Fig. 11.7 below.

As the difference between SiGe and SiMOS is not expected to be significant we concentrate on the first of them and compare against the GaAs device.[27] For both we consider the quasistatic fluctuations of detuning, tunnel coupling and Zeeman splitting. The first two originates from $1/f$ charge noise, with the amplitude $A_1 = 1^2\,\mu\mathrm{eV}^2/\mathrm{Hz}$, that we translate to effective RMS of quasistatic noise $\tilde{\sigma}_{1/f} = 5\,\mu\mathrm{eV}$.[28] For the noise in Zeeman splittings we take $\sigma_N = 0.1$ neV for the Si-based devices [29] and $\sigma_N = 1$ neV for the GaAs-device [194].

We highlight that without spin-flip tunnel coupling t_{ff} the transfer of spin-up and spin-down component can be computed using methods previously developed in Chapter 8 for the spin-down transfer. For this reason we consider here a non-zero value of spin-flip tunnel coupling, which is commonly set to $|t_{\mathrm{ff}}| = 0.1\,\mu\mathrm{eV}$. It reproduces measured value in SiMOS devices [197], a rather optimistic case in GaAs, where $|t_{\mathrm{ff}}| = 0.5\,\mu\mathrm{eV}$

24: see Eq. for similar assumption leading to correct estimation of charge transfer error

Spin relaxation at the avoided crossing

25: see estimation around Eq. (10.11)

26: $t^{(\mathrm{int})}_{\mathrm{flip}}$, which would rather correspond to GaAs then Si.

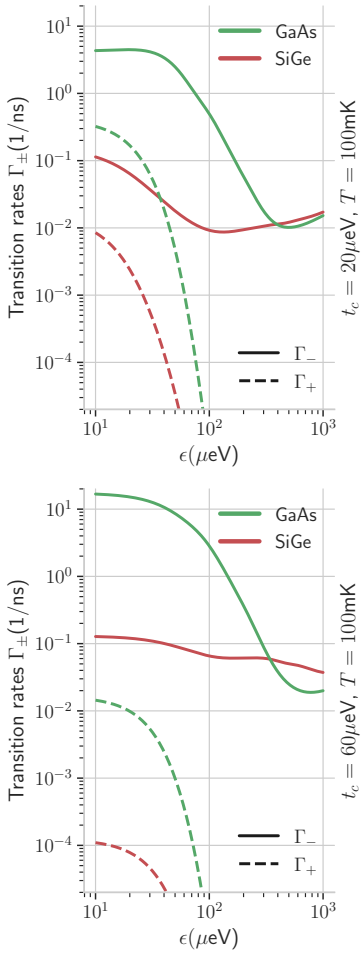

Figure 11.7: Relaxation rates for the DQD computed using methods from Chapter 7 using parameters from Tab. 6.1.

27: For the parameters of DQD models see Sec. 6.3

28: assuming around $N = 10000$ experimental shots. See Eq. (4.48) for connection between power of the 1/f noise and data acquisition time

29: which corresponds to 0.01% abundance of Si^{29}

Model name	Si	GaAs
Tunnel coupling t_c (μeV)	20, 60	
Detuning range ϵ (μeV)	(−500, 500)	
RMS of quasistatic detuning noise $\tilde{\sigma}_\epsilon$ (μeV)	5	
RMS of Overhauser field σ_N (neV)	0.1	100
Average zeeman splitting E_z (μeV)	2, 120	
G-factor difference between the dots $\Delta g/g$	10^{-3}	
Tunnel coupling with a spin-flip t_{ff} (μeV)	0.1	
Temperature T (mK)	100	

Table 11.1: Parameters describing the model of the environment of the DQD system, which we have used in the simulations of the averaged adiabatic Master equation.

was measured [57], and a rather pessimistic prediction for SiGe model, where effects of t_{ff} have not been directly observed yet. On top of this, we consider two values of average Zeeman splittings $\overline{E}_z = 120, 2\,\mu$eV, which in Si-based devices approximately corresponds to magnetic fields[30] of $B_{\text{Si}} \approx 1, 0.02$T. Finally we assume that the difference in dot-dependent Zeeman splittings ΔE_z is dominated by the g-factor difference between the dots $\Delta g/g = 10^{-3}$, and hence is proportional to the constant magnetic field $\Delta E_z = 0.12, 0.002\,\mu$eV for $\overline{E}_z = 120, 2\,\mu$eV respectively. Introduced parameters are summarized in Tab. 11.1.

30: Note that due to approximately 5-times smaller g-factor in GaAs devices, the same selection of Zeeman splittings $\overline{E}_z = 120, 2\,\mu$eV corresponds to $B_{\text{GaAs}} \approx 5, 0.1$ T.

Nuclear spin content in Si

We start by discussing the effect of decreasing number of spinful nuclei on the interference pattern, generated by the spin-flip avoided crossings from Sec. (11.1). In Fig. (11.8) we plot the fidelity of spin-up transfer, i.e. $P_\uparrow = \text{Tr}\{|-(t_f),\uparrow\rangle\langle-(t_f),\uparrow|\hat{\varrho}(t_f)\}$ as a function of sweep rate. We use

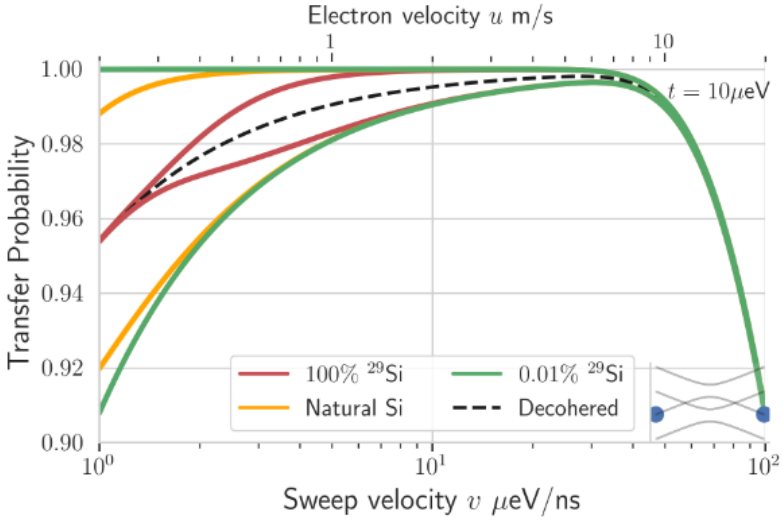

Figure 11.8: Probability of successful spin up transfer in presence of nuclear spins in Si. Due to fast oscillations we plot only their envelopes. Using different colors we plot the results for the Natural Si (yellow), 100%^{29}Si (red) and relevant for this thesis 0.01%^{29}Si (yellow) content of spinful nuclei. We show how they converge to the decohered result of the spin-flip interference (black dashed line) from Eq. (11.16). Adapted from [1].

different colors to plot result of interference for various concentration of spinful Si^{29} isotope, and due to rapidly oscillating interference pattern (see Fig. 11.4) we plot only the envelope of the oscillations. In particular we show how the amplitude shrinks towards completely dephased result $\overline{Q}_\uparrow = 2Q_{\text{ff}}(1 - Q_{\text{ff}})$ (dashed black line) at slowest sweep rates. In the plot we use tunnel coupling of $t_c = 10\,\mu$eV, $E_z = 120\,\mu$eV and $t_{\text{ff}} = 0.1\,\mu$eV. We use the analysis above to show that isotopically purified Si-devices with 0.01%^{29}Si allows for maximum contrast of the interference pattern

even at the sweep rate of $v = 1\,\mu$eV/ns. This level of purification typically translates to $T_2^* \approx 10\,\mu$s and will used in the remainder of the thesis.

Numerical results

Small tunnel coupling

We start by showing the result for relatively small $t_c = 20\,\mu$eV and compare the prediction for large and small magnetic fields, i.e. $E_z = 120\,\mu\text{eV} \gg t_c = 20\,\mu\text{eV}$ and $E_z = 2\,\mu\text{eV} \ll t_c$ respectively. In Fig. 11.9 we plot the loss of occupation of the spin-up state $Q_\uparrow$ as a function of sweep rate.

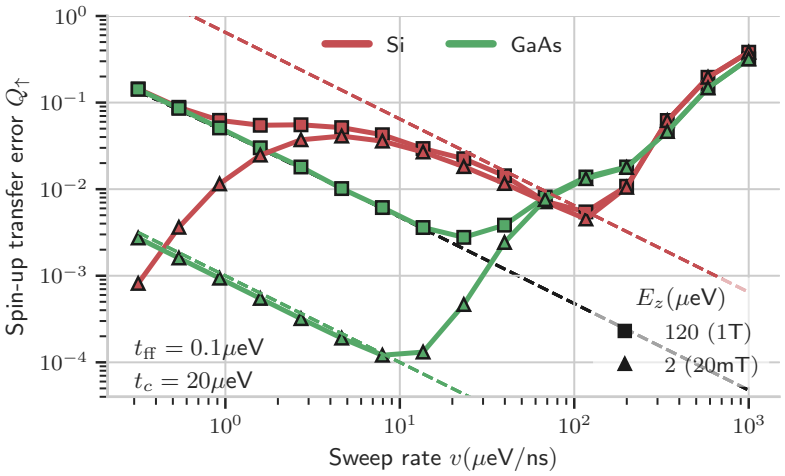

Figure 11.9: Probability of losing occupation of $|-(t),\uparrow\rangle$ state, $Q_\uparrow$ as a function of sweep rate for the spin-flip coupling of $t_{\text{ff}} = 0.1\,\mu$eV, tunnel coupling of $t_c = 20\,\mu$eV and two Zeeman splittings $E_z = 120, 2\,\mu$eV, which for Si-device corresponds to $B = 1, 0.02\,$T, drawn using squares and triangles respectively. Two colors correspond to GaAs (green) and SiGe (red) devices from Tab. 6.1. By dashed lines we plot theoretical predictions: for Si single-excitation approximation limit from Eq. (8.22) (red), for GaAs spin-relaxation around avoided crossing from Eq. (11.35) (green) and for both decohered interference pattern from Eq. (11.16) (black). For both numerical simulations and analytical predictions we used relaxation rates from Fig. (11.7) and parameters from Tab. 11.1. In numerical results (symbols and lines for guidance) we averaged over $N = 100$ realizations of slow noise using averaged Master equation method from Appendix A.

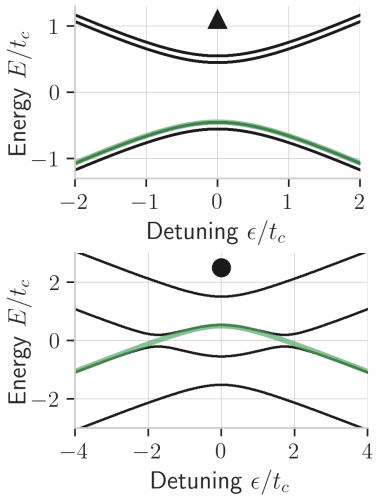

Figure 11.10: The instantaneous energy spectra of total Hamiltonian from Eq. (12.1) in two regimes of magnetic field used in this chapter. The $E_z = 2\,\mu\text{eV} < t_c$ (top) and $E_z = 120\,\mu\text{eV} > t_c$ (bottom)

As it can be seen from Fig. 11.9, for the fast sweeps, the transfer of spin-up for both devices is limited by the Landau-Zener transitions from the ground $|-,\uparrow\rangle$ to the excited $|+,\uparrow\rangle$ orbital states. Next around $v \approx 100\,\mu$eV/ns the result is identical to $Q_\downarrow$, i.e. the Si device shows smaller error due to weaker coupling to the environment. In particular for the slower sweeps the Si device (red symbols) follows a single excitation line, which can be seen by the proximity between numerically simulated symbols and the red dashed line, which represents $Q_{\text{SEAL}} \propto 1/v$ given previously in Eq. (8.22). At slower sweeps the result for large and small magnetic field starts to differ, since the case of $E_z > t_c$ (squares), suffers from the spin-flip interference in both GaAs (red squares) and SiGe (green squares) at slowest sweeps, the error converges to the completely dephased result of the interference (black dashed line), given by $\overline{Q} = 2(1 - Q_{\text{ff}})Q_{\text{ff}}$ from Eq. (11.16).

In contrast, the case of weaker magnetic field, i.e. $E_z < t_c$ (triangles), avoids creation of spin-flip avoided crossings and in Si (red triangles) benefits from relaxation aided transfer, which resembles Q_{HEAL} mechanism from Eq. (8.23). This also proves that due to relatively slow relaxation in Si, $\Gamma_-(t_c) \sim 0.1\,\text{ns}^{-1}$, the spin-relaxation mechanism due to admixture of spin states around avoided crossing from Eq. (11.35) is not effective. The result is different for the GaAs device (green triangles), where for the

small magnetic field the relaxation decreases the error only in the regime of $v > 10\,\mu$eV/ns. For slower sweeps the transfer gets worse as the time spent in vicinity of avoided crossing increases. This agrees well with the formula for spin-relaxation around avoided crossing (Eq. (11.35)), which for relatively fast relaxation rate in $\Gamma_- \sim 5\,\text{ns}^{-1}$ is plotted using green dashed line.

Large tunnel coupling

We now move to the case of relatively large tunnel coupling of $t_c = 60\,\mu$eV, for which using models from Chapter 7 we compute the modified transition rates and plot them in Fig. 11.7. The remaining parameters from Tab. 11.1 are kept unchanged. In the Fig. 11.7 one can observe that the relaxation (solid line) and the excitation (dashed) rates in the Si device are weakly dependant on the detuning, which can be attributed to the dominant role of the Johnson charge noise, the spectrum of which grows linearly with energy $S(\omega) \propto \omega$, but at the same time falls t_c^2/Ω^2 due to dominant role of detuning noise[31] . The corresponding value of typical relaxation, i.e. $\Gamma_{-,\text{Si}} \approx 0.1\text{ns}^{-1}$ gives excitation rate at avoided crossing $\Gamma_{+,\text{Si}}(t_c) \approx 10^{-4}\text{ns}^{-1}$. In GaAs the dominant role of phonons allows to leads to rapid decay of the relaxation rate away from avoided crossing. However its relatively large value of $\Gamma_{-,\text{GaAs}}(t_c) \approx 10\text{ns}^{-1}$ translates to non-negligible excitation rate $\Gamma_{+,\text{GaAs}}(t_c) \approx 10^{-2}\text{ns}^{-1}$.

31: for the analysis see Sec. 7.3

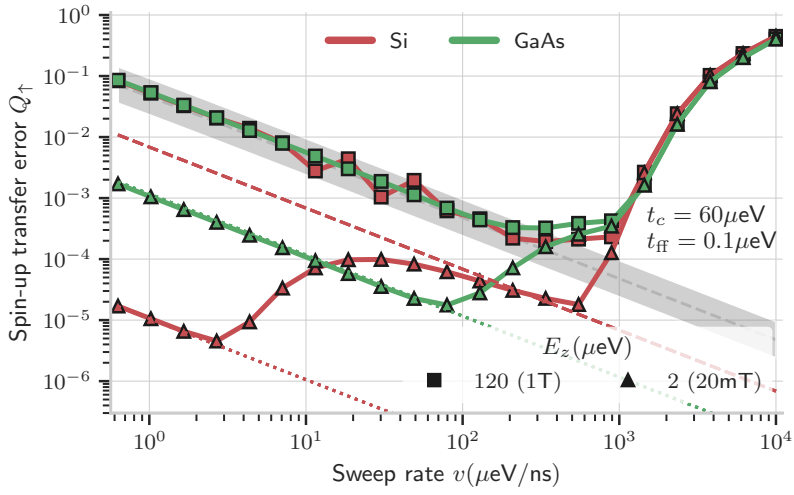

Figure 11.11: Probability of losing occupation of $|-(t),\uparrow\rangle$ state, $Q_\uparrow$ as a function of sweep rate for $t_{\text{ff}} = 0.1\,\mu$eV, $t_c = 60\,\mu$eV and $E_z = 120, 2\,\mu$eV, drawn using squares and triangles respectively. Two colors correspond to GaAs (green) and SiGe (red) devices from Tab. 6.1. We plot the analytical result of spin-flip interference using gray color, i.e. upper bound represents constructuve interference $4Q_{\text{ff}}$ and solid gray line is the dephased result from Eq. 11.35. The red dashed line is the effect of single-excitation approximation limit from Eq. (8.22) in Si. The dotted lines represent the effect of spin relaxation at avoided crossing from Eq. (11.35) for the GaAs (green) and Si (red). For both numerical simulations and analytical predictions we used relaxation rates from Fig. (11.7) and parameters from Tab. 11.1. In numerical results (symbols and lines for guidance) we averaged over $N = 100$ realizations of slow noise using averaged Master equation method from Appendix A.

In Fig. 11.11 we plot $Q_\uparrow$ as a function of v for $t_c = 60\,\mu$eV. Similarly to the result for smaller tunnel coupling, the error for fast sweeps is limited by Q_{LZ}. The biggest difference is the result for large magnetic field $E_z > t_c$, for which the transfer in both Si and GaAs is limited by the spin-flip interference pattern, which we illustrate using gray shaded region. For the GaAs much stronger fluctuations of E_z lead to faster convergence towards decohered result of $\overline{Q_\uparrow}$, which corresponds to dashed line in the middle of the shaded region. For Si the oscillations are visible up to $v \approx 10\,\mu$eV/ns, below which mostly the fluctuations of E_z and t_c leads to the same result. Note however that the oscillations of $Q_\uparrow$ are generally contained below

result of constructive interference $Q_\uparrow = 4Q_{\rm ff}(1-Q_{\rm ff})$, which corresponds to upper limit of shaded region. For the low magnetic field regime of $E_z = 2\,\mu$eV$\ll t_c$, the error is generally smaller in comparison to result illustrated in Fig. 11.9 due to larger t_c in comparison to $k_{\rm B}T$. Another difference can come from the slight modification of the relaxation rates as a function of ϵ (See comparison of relaxation rates in Fig. 11.7). The results in both devices can be reproduced by the spin relaxation around avoided crossing from Eq. (11.35) (dotted lines).

Note that the charge transfer in Si, shows two local minima. First around $v = 10^3\,\mu$eV/ns due to interplay between the coherent and incoherence excitation to the higher energy level $|+,\uparrow\rangle$. The second at $v \approx 1\,\mu$eV/ns due to interplay between the recovery of ground state occupation via the relaxation from $|+,\uparrow\rangle$ to $|-,\uparrow\rangle$ states and the spin-flip relaxation from ground spin-up $|-,\uparrow\rangle$ to ground spin-down state $|-,\downarrow\rangle$. As we will show in the next Chapter 12 the second minimum will be modified by the spin dephasing due to slow environmental noise.

12 Spin coherence during spin-qubit shuttling

We finally arrive at computing the spin coherence of the electron that underwent interdot transfer. As mentioned in Chapter 1, such transfer constitutes a single building block, which in principle can allow for coherent communication between distant registers in semiconductor-based quantum processor. However to achieve this task, the transfer of both spin components, together with low enough phase error.

12.1 The model

Similarly to the previous chapters we consider here the Hamiltonian the spin-dot system:

$$\hat{H}(t) = \hat{H}_o(t) + \hat{H}_s + \hat{V}_{so}, \tag{12.1}$$

where $\hat{H}_o(t) = \frac{1}{2}\epsilon(t)\hat{\sigma}_z + \frac{1}{2}t_c\hat{\sigma}_x$, $\hat{H}_s = \frac{1}{2}E_z\hat{\sigma}_z$ and the form of spin-orbit interaction $\hat{V}_{\rm so}$ is given in Eq. (10.4). As a result of linear sweep of interdot detuning the character of the ground state changes, from the one localized in the left dot $|-(t_i)\rangle \sim |L\rangle$ to the one localized in the right dot $\left|-(t_f)\right\rangle \sim |R\rangle$. Thus the for us a figure of merit is the spin coherence in the ground state, which is given by the off-diagonal element of the density matrix

$$W_-(t_f) = 2\,\mathrm{Tr}\left\{\left|-(t_f),\downarrow\right\rangle\!\left\langle-(t_f),\uparrow\right|\hat{\varrho}(t_f)\right\}, \tag{12.2}$$

where $\hat{\varrho}(t_f)$ is the density matrix of the composite spin-dot-environment system. Note that for electron initialized in a spin superposition in the left dot

$$|\psi(t_i)\rangle = |-(t_i)\rangle \otimes \frac{|\uparrow\rangle + |\downarrow\rangle}{\sqrt{2}}, \tag{12.3}$$

we have $W_-(t_i) = 1$. It is convenient to consider the influence of the environment that is modeled as a classical noise. In such case the density matrix of the spin-orbit system should be averaged over realization of the noise, i.e. the coherence in the ground state can be defined equivalently to expression from Eq. (12.2) as:

$$W_-(t_f) = 2\left\langle-(t_f),\uparrow\right|\hat{\varrho}(t_f)\left|-(t_f),\downarrow\right\rangle = 2\left\langle|c_{-,\uparrow}(t_f)||c^*_{-,\downarrow}(t_f)|e^{i\phi}\right\rangle, \tag{12.4}$$

where the coefficients are the complex amplitudes corresponding to the pure states $|-,s\rangle$, i.e. $c_{-,s} = \langle-,s|\psi(t)\rangle$, ϕ is the complex phase difference between them and $\langle\ldots\rangle$ denotes classical averaging. In this analysis we are mostly interested in the limit of small error, defined as the

$$\delta W_-(t_f) \equiv 1 - |W_-(t_f)| < 10^{-1}, \tag{12.5}$$

which is still relevant for the future quantum computers, working at the quantum error correction threshold. In the small error limit the loss of

coherence can be written as:

$$\delta W_-(t_f) \approx \tfrac{1}{2}(Q_\uparrow + Q_\downarrow + \langle \delta\phi^2 \rangle). \tag{12.6}$$

which means that in the leading error the loss of spin coherence can be related to the sum of three contributions[1] . The first two of them are associated with the failure of occupying adiabatically transferred state associated with spin-up and spin-down components $Q_\downarrow$ and $Q_\uparrow$, which have been extensively analyzed in Chapter 8 and Chapter 11 respectively. In this chapter we concentrate on the remaining component $\langle \delta\phi^2 \rangle$, which is related to the non-deterministic phase due to presence of uncontrolled environment.

In Sec. 12.2 we analyze the loss of coherence due low-frequency transverse noise affecting the orbital degree of freedom, which influences the qubit via the non-zero correlation between spin and spatial degree of freedom due to non-zero ΔE_z. We analyze also loss of coherence due to slow fluctuations of nuclear spins, which leads to spin dephasing independent of the orbital drive. Next in Sec. 12.3 we move to the random phase evolution activated by the transition between the adiabatic levels, and in particular show how the random phase can be introduced by temporal occupation of the excited state. Finally in Sec. 12.4 we describe the numerically computed loss of coherence against theoretical predictions for the realistic problem of electron transfer between models of GaAs- and Si-based DQD system from Sec. 6.3.

1: This result can be obtained from Eq. (12.4) by considering leading order corrections to the probability of occupying spin-up and spin-down state i.e.

$$P_s = |c_{-,s}|^2 = \tfrac{1}{2} + \delta P_s$$

for $s = \uparrow, \downarrow$ from which $|c_{-,s}| \approx (1 + \delta P_s)/\sqrt{2}$. Next we consider random contribution to a phase $\phi = \phi_0 + \delta\phi$ with $\langle \delta\phi \rangle = 0$, which together allows to write:

$$W_-(t_f) \approx e^{i\phi_0}\Big\langle (1 + \delta P_\uparrow + \delta P_\downarrow) \times (1 - i\delta\phi - \tfrac{\delta\phi^2}{2}) \Big\rangle \tag{12.7}$$

We now compute the average by taking only leading order in small parameters, such that the loss of coherence $\delta W_- = 1 - |W_-(t_f)|$ can be written as

$$|\delta W_-| \approx \tfrac{1}{2}\langle \delta\phi^2 + 2\delta P_\uparrow + 2\delta P_\downarrow \rangle, \tag{12.8}$$

where finally we can associate change in occupation probability with previously computed probability of losing occupation of particular spin state, i.e. $Q_s = \delta P_s / P_{s,0}$, where initial occupation $P_{s,0} = 1/2$ for both spin components.

12.2 Dephasing due to low-frequency noise

Quasistatic charge noise

We start by considering non-dissipative operator in the adiabatic basis, i.e.

$$\hat{\mathcal{V}}_\phi(t) = \sum_s \left(\hat{V}_z \cos\hat{\vartheta}_s(t) + \hat{V}_x \sin\hat{\vartheta}_s(t)\right) |s\rangle\langle s| \,, \tag{12.9}$$

where $\operatorname{ctan}(\vartheta_s(t)) = -\frac{\epsilon(t) + \sigma_s \Delta E_z/2}{\Omega_0(t)}$ with $\sigma_s = \pm 1$ for $s = \uparrow, \downarrow$ respectively[2] . Following Chapter 4 we assume dephasing is caused by the classical noise, and as such we replace the operators $\hat{V}_z$ and $\hat{V}_x$ by classical fluctuations of detuning $\delta\epsilon(t)$ and $\delta t_c(t)$ respectively. With this identification a single realization of the noise produces a phase

$$\begin{aligned}\delta\phi &= \int_{t_i}^{t_f} \langle -,\uparrow| \hat{\mathcal{V}}_\phi(t) |-,\uparrow\rangle - \langle -,\downarrow| \hat{\mathcal{V}}_\phi(t) |-,\downarrow\rangle \, \mathrm{d}t \\ &= \frac{1}{2}\int_{t_i}^{t_f} \Big(\delta t_c(t)[\sin\vartheta_\uparrow(t) - \sin\vartheta_\downarrow(t)] + \delta\epsilon(t)[\cos\vartheta_\uparrow(t) - \cos\vartheta_\downarrow(t)] \Big) \mathrm{d}t,\end{aligned} \tag{12.10}$$

This shows that the random phase vanishes if $\vartheta_\uparrow = \vartheta_\downarrow$, which is the case for $\Delta E_z = 0$. Otherwise we compute the integrals using quasistatic approximation from Sec. 4.4, i.e. by assuming $\delta\epsilon$, δt_c are constant on the time scale of single evolution (i.e. $t = t_f - f_i$). This amounts to integration of functions of the orbital angle, i.e. $\sin\vartheta_s = t_c/\Omega_s$ and $\cos\vartheta_s = \epsilon/\Omega_s$

2: As a reminder $\Omega_0(t) = \sqrt{\epsilon^2(t) + t_c^2}$ with $\epsilon(t) = vt$

where $\Omega_s = \sqrt{(\epsilon - \sigma_s \Delta E_z/2)^2 + t_c^2}$. In the integrand we use the weak coupling limit, i.e. assume $\Delta E_z \ll t_c$ using which

$$\sin\vartheta_\uparrow(t) - \sin\vartheta_\downarrow(t) \approx -\frac{\Delta E_z}{2\Omega_0}\sin(2\vartheta_0(t))$$
$$\cos\vartheta_\uparrow(t) - \cos\vartheta_\downarrow(t) \approx \frac{\Delta E_z}{\Omega_0}\sin^2(\vartheta_0(t)), \tag{12.11}$$

where $\vartheta_0 = vt/\Omega_0$. For the quasistatic noise and in the symmetric limits, i.e. $t_i = -t_f$, the contribution from δt_c noise vanishes for the symmetry reasons, while the term multiplying $\delta\epsilon$ gives the random contribution:

$$\delta\phi \approx \frac{\Delta E_z}{v}\delta\tilde{\epsilon}, \tag{12.12}$$

where we have evaluated the integral by extending the limits to infinity $-t_i = t_f \to \infty$. As a result the variance of random phase, which contributes to loss of spin coherence is given by:

Dephasing due low-frequency detuning noise

$$\langle\delta\phi^2\rangle = \left(\frac{\Delta E_z}{v}\right)^2 \tilde{\sigma}_\epsilon^2, \tag{12.13}$$

where σ_ϵ^2 is the power of quasistatic noise in detuning[3] .

3: See Eq. (4.48) for the formula for the effective power of quasistatic noise in case of 1/f noise

An alternative derivation

We now present an alternative derivation of the above result, which uses the result of Eq. (9.27), in which we have shown that in presence of longitudinal spin-orbit coupling ΔE_z the power of spin dephasing noise for the spin-qubit occupying its ground orbital state is related to the fluctuations, that are transverse in the orbital basis.

First we assume $\epsilon \ll t_c$, in case of which the ground and excited orbital states are given by:

$$|\pm(0)\rangle \approx \frac{1}{\sqrt{2}}\left(|L\rangle + |R\rangle\right), \tag{12.14}$$

The splitting between two levels is given by $\Omega(0) = t_c$. We now assume the presence of the classical noise in detuning and tunnel coupling, i.e.

$$\hat{H}_{\rm noise} = \frac{\delta\epsilon}{2}\hat{\sigma}_z + \frac{\delta t_c}{2}\hat{\sigma}_x, \tag{12.15}$$

where the Pauli operators are written in the dot basis, i.e. $\hat{\sigma}_z = |R\rangle\langle R| - |L\rangle\langle L|$. We now express the above Hamiltonian in the basis of $|\pm(0)\rangle$ states, such that the

$$\hat{H}_{\rm noise} = \frac{\delta\epsilon}{2}\hat{\sigma}_\perp + \frac{\delta t_c}{2}\hat{\sigma}_\parallel, \tag{12.16}$$

where $\hat{\sigma}_\parallel = |+(0)\rangle\langle+(0)| - |-(0)\rangle\langle-(0)|$ and $\hat{\sigma}_\perp = |+(0)\rangle\langle-(0)| + |-(0)\rangle\langle+(0)|$. One can directly check that $\langle+(0)|\,\hat{H}_{\rm noise}\,|-(0)\rangle = \delta\epsilon/2$, and hence $\delta\epsilon$ is transverse in the basis of orbital states $|\pm(0)\rangle$.

We now add the spin degree of freedom. We initialize the electron in the ground orbital state, at zero detuning, in the spin superposition, such

that the initial state reads:

$$|\psi(t_i)\rangle = |-(0)\rangle \otimes \frac{1}{\sqrt{2}}\left(|\uparrow\rangle + |\downarrow\rangle\right). \tag{12.17}$$

To show how orbital fluctuations affect spin coherence we add coupling between orbital and spin degrees of freedom $\Delta E_z = \langle R|\hat{V}_{\rm so}|R\rangle - \langle L|\hat{V}_{\rm so}|L\rangle$, where the spin-orbit interaction $\hat{V}_{\rm so}$ was given in Eq. (10.4). In analogy to Eq. (9.20) we write the correction to the ground orbital state $|-(0), s\rangle$ as:

$$\widetilde{|-(0), s\rangle} = |-(0), s\rangle + \sigma_s \frac{\Delta E_z}{4t_c}|+(0), s\rangle. \tag{12.18}$$

One can easily show that the effectively longitudinal noise in the spin basis reads:

$$\xi_{\phi,\rm spin} = \widetilde{\langle -(0),\uparrow|}\hat{H}_{\rm noise}\widetilde{|-(0),\uparrow\rangle} - \widetilde{\langle -(0),\downarrow|}\hat{H}_{\rm noise}\widetilde{|-(0),\downarrow\rangle} = \frac{\Delta E_z}{2t_c}\delta\epsilon, \tag{12.19}$$

from which the variance of spin-dephasing noise reads:

$$\tilde{\sigma}^2_{\rm spin} = \left(\frac{\Delta E_z}{t_c}\right)^2 \tilde{\sigma}^2_\epsilon. \tag{12.20}$$

Now if the evolution goes from large negative to large positive detuning in the form $\epsilon(t) = vt$, one can estimate that the spin-qubit spends $t_{\rm LZ} \approx 2t_c/v$ time around the avoided crossing, where detuning noise is transverse in the adiabatic basis. As a result the dephasing of spin superposition, during the adiabatic transfer of electron charge reads:

$$\delta W(t) \approx 1 - e^{-\frac{1}{2}\sigma^2_{\rm spin} t^2_{\rm LZ}} \approx \frac{1}{2}\sigma^2_\epsilon \left(\frac{\Delta E_z}{t_c}\right)^2 \left(\frac{t_c}{v}\right)^2 = \frac{1}{2}\left(\frac{\Delta E_z}{v}\right)^2 \sigma^2_\epsilon, \tag{12.21}$$

which reconstructs the result of Eq. (12.13).

Nuclear spins

The dephasing due to slow charge noise should be compared with that caused by nuclear spins. As discussed in Sec. 9.3, we expect the Overhauser field to be uncorrelated between two dots, which allows to use the T_2^* time as the upper bound for coherent transfer time. In particular the spin dephasing due to nuclei depends on the transfer time $\Delta t = \frac{\Delta\epsilon}{v}$, where $\Delta\epsilon$ is the sweep range. For $\Delta\epsilon = 1$meV sweep, and $\sigma^2_N = (\sqrt{2}/T_2)^2$ reads:

Dephasing due nuclear spins

$$\langle\delta\phi^2\rangle = \left(\frac{\Delta\epsilon}{v}\right)^2 \sigma^2_N = \begin{cases} \left(\frac{10^2}{v[\,\mu\text{eV/ns}]}\right)^2, & \text{for GaAs} \\ \left(\frac{10^{-1}}{v[\,\mu\text{eV/ns}]}\right)^2, & \text{for Si} \end{cases} \tag{12.22}$$

. which shows that for GaAs $v > 100\,\mu$eV/ns is required for significantly coherent transfer, while orders of magnitude lower $v \approx 0.1\,\mu$eV/ns would allow to neglect the effects of nuclear spins in isotopically purified Si.

12.3 Dephasing due to high-frequency noise

We now show that inelastic transitions between the orbital states in presence non-zero longitudinal coupling ΔE_z can also lead to spin dephasing.

We use the adiabatic Master equations in which we neglect coherent coupling between the adiabatic orbital levels $\dot{\vartheta}_s(t)$ and the coupling between the spin-components possibly leading to spin-flip avoided crossing t_{ff}. Additionally we assume the difference between spin-up and spin-down relaxation rates are negligible and use equations of motion for the coherence in the ground and excited states $W_\pm = \langle \pm | \hat{\varrho}_{\uparrow\downarrow} | \pm \rangle$, previously derived in Eq. (10.57). In the rotating frame[4] they read:

4: i.e. $W'_\pm(t) = W_\pm e^{\mp \frac{i}{2}\Delta\Omega(t)}$

$$\begin{aligned}\dot{W}'_+(t) &= -\Gamma_-(t)W'_+(t) + \Gamma_+(t)W'_-(t)e^{-i\int \Delta\Omega(t)} \\ \dot{W}'_-(t) &= -\Gamma_+(t)W'_-(t) + \Gamma_-(t)W'_+(t)e^{i\int \Delta\Omega(t)}.\end{aligned} \tag{12.23}$$

The main source of dephasing, activated by the high-frequency noise, are inelastic transitions between two energy levels of possibly different Zeeman splittings. For non-zero value of ΔE_z, the time spent in the state with spin splitting different that the one corresponding to perfectly adiabatic evolution, will lead to additional phase between two spin components. Due to the stochastic nature of the inelastic transition, this time period and hence the phase become random. As a result the averaging of such random phase over many realisation of the experiment will lead to non-negligible dephasing. We now show a few relevant examples.

Dephasing during excitation

We start with the computing contribution to a random phase acquired during excitation taking place around the avoided crossing. We follow the SEAL approximation from Eq. (8.22), in which we assumed most exciations are taking place in the vicinity of the avoided crossing, i.e. $|\epsilon| \ll t_c$ where we have $\Omega_s(t) \approx t_c + \frac{v^2 t^2}{2t_c}$, $\Gamma_+(t) = \Gamma_-(t_c)e^{-\beta\Omega_s(t)}$ and the difference between the orbital splitting can be approximated[5] as:

5: Since $\Delta\Omega = \sqrt{(vt + \Delta E_z/2)^2 + t_c^2} - \sqrt{(vt - \Delta E_z/2)^2 + t_c^2}$

$$\Delta\Omega \approx \frac{vt\Delta E_z}{t_c}. \tag{12.24}$$

We use the initial state

$$|\psi(0)\rangle = \frac{|\uparrow\rangle + |\downarrow\rangle}{2} \otimes |-(t_i)\rangle\,, \tag{12.25}$$

which corresponds to initial condition $W_-(0) = 1$ and $W_+(0) = 0$, and using Eq. (12.23) in the leading order of perturbation theory we obtain $W'_-(t) \approx e^{-\Gamma_+(t_c)t}$ and as a consequence:

$$W'_+(t) \approx \Gamma_-(t_c)e^{-\beta t_c}\int_0^t \mathrm{d}t\, \exp\left[\left(i\frac{v\Delta E_z}{2t_c} - \frac{\beta v^2}{2t_c}\right)t^2 - \Gamma_+(t_c)t\right]. \tag{12.26}$$

In the relevant regime the excitation rate in the exponent can be omitted, which allows to compute the loss of coherence during a single transition

Dephasing during excitation

from ground to excited state as:

$$W'_{+}(t) = \Gamma_{-}(t_c)e^{-\beta t_c}\sqrt{\frac{t_c}{v}}\frac{1}{\sqrt{\beta v - i\Delta E_z}}, \tag{12.27}$$

where we moved the limit of integration $t \to \infty$. This means that for $v \gg \Delta E_z k_B T$ the loss of coherence $\delta W_+ \propto 1/v$, while at slower sweep rates $\delta W_+ \propto 1/\sqrt{v}$.

Dephasing during relaxation

We now move to the relaxation process and compute the loss of coherence during recovery of the ground state occupation. We consider the situation in which the electron occupies an excited orbital state, i.e. $W_+(0) = 1$ and $W_-(0) = 0$. In such case, analogously to the excitation process the coherence in the ground state after the relaxation can be computed as:

$$W'_{-}(t) = \int_0^t \mathrm{d}t'\, \Gamma_{-}(\Omega[t'])\, e^{i\int_0^{t'} \Delta\Omega(t'') - \Gamma_{-}(\Omega[t''])\mathrm{d}t''}. \tag{12.28}$$

We assume the relaxation rate is relatively flat as a function of transferred energy Ω and takes place in the detunned regime where $\Delta\Omega \approx \Delta E_z$. Hence we treat the variables as time-independent and compute the integral as:

$$W'_{-}(t) = \frac{\Gamma_{-}}{\Gamma_{-} - i\Delta E_z}\left(1 - e^{(i\Delta E_z - \Gamma_{-})t}\right) \to \frac{\Gamma_{-}}{\Gamma_{-} - i\Delta E_z}, \tag{12.29}$$

where the final expression was taken in the limit of $\Gamma_- t \gg 1$, i.e. in the limit when the qubit is transferred from excited to the ground state. We conclude that during the relaxation process the spin coherence acquires a phase shift, which in the limit of $\Delta E_z \gg \Gamma_-$ reads $e^{i\pi/2}$. Additionally the absolute value of the coherence left in the ground state is reduced since:

Dephasing during relaxation

$$|W_-| = \frac{\Gamma_-^2}{\sqrt{\Gamma_-^2 + \Delta E_z^2}} \approx 1 - \frac{1}{2}\left(\frac{\Delta E_z}{\Gamma_-}\right)^2, \tag{12.30}$$

where the last expression was written in the limit of $\Delta E_z \ll \Gamma_-$.

This shows that fast orbital relaxation allows for conservation of spin coherence. Note that the obtained coherence error reconstructed result of Eq. (1.27), where dephasing during relaxation was related to the variance of random phase $\langle \delta\phi^2 \rangle = (\Delta E_z/\Gamma_-)^2$.

Two-way transitions

We finally consider the case where both relaxation and excitation are active. For illustration purposes we assume the transition rates and difference in orbital-dependent spin splitting can be treated as time-independent. This corresponds to the case of stationary qubit or the case where the rates $\Gamma_\pm(t)$ and $\Delta\Omega$ are approximately constant on the timescale set by $1/\Gamma_\pm$.

For the static case we solve differential equation from Eq. (12.23), using the initial state of the electron $|\psi\rangle = |-\rangle \otimes (\frac{1}{\sqrt{2}}|\uparrow\rangle + |\downarrow\rangle)$, for which we have

$$\begin{aligned} W_+ &= 2e^{-\frac{1}{2}a^*t}\frac{\Gamma_+}{A}\sinh\left(\tfrac{A^*t}{2}\right) \\ W_- &= e^{-\frac{1}{2}at}\left\{\cosh\left(\tfrac{At}{2}\right) + \frac{(a-2\Gamma_+)}{A}\sinh\left(\tfrac{At}{2}\right)\right\}, \end{aligned} \tag{12.31}$$

where $a = \Gamma_+ + \Gamma_- - i\Delta\Omega$ and $A = \sqrt{a^2 + 4i\Gamma_+\Delta\Omega}$. Note that for $\Gamma_+ = 0$, we have $|W_-| = 1$, i.e. the dephasing is activated by a non-negligible excitation rate.

We now compute ground state coherence in two relevant regimes of fast and slow relaxation rate in comparison to $\Delta\Omega$, where in both cases we will assume that $\Gamma_+ \ll \Gamma_-$. In each of the regimes we will expand the parameter A in the corresponding small parameter.[6] Firstly for $\Gamma_- \gg \Delta\Omega$, the ground state coherence reads:

$$W_-(t) \approx \frac{\Gamma_- - i\Delta\Omega}{\Gamma_+ + \Gamma_- - i\Delta\Omega} e^{i\frac{\Delta\Omega\Gamma_+}{\Gamma_-}t} e^{-\frac{\Delta\Omega^2\Gamma_+}{\Gamma_-^2}t}, \tag{12.32}$$

which in the limit of $\Gamma_- \gg \Delta\Omega$, can be expressed as:

$$W_-(t) \approx e^{i\phi_0(t)} \exp\left(-\frac{\Delta\Omega^2}{\Gamma_-^2}\Gamma_+ t\right), \text{ for } \Gamma_- \gg \Delta\Omega \tag{12.33}$$

where we have introduced the phase factor $\phi_0(t)$. This shows that spending too much time in the regime, in which the excitation rate is non-negligible would lead to spin dephasing. The above can be applied to the adiabatic transition, where in the simplest model we assume that the excitation rate is only non-negligible for $t = t_{\mathrm{LZ}} = 2t_c/v$ time around the avoided crossing. However in such case $\Delta\Omega(t) \approx -vt\Delta E_z/t_c$ becomes the function of time. To compute the effective dephasing we overestimate the excitation rate by setting $\Gamma_+(\Omega) = \Gamma_-(t_c)e^{-\beta t_c}$, assume constant relaxation rate $\Gamma_- = \Gamma_-(t_c)$, such that only $\Delta\Omega(t)$ is remaining function of time. In such case dephasing during transition across the avoided crossing can be estimated as:

$$|W_-(t)| = \exp\left(-\frac{v^2\Delta E_z^2}{t_c^2\Gamma_-}e^{-\beta t_c}\int_{-t_c/v}^{t_c/v} t^2 \mathrm{d}t\right) = \exp\left(-\frac{2\Delta E_z^2}{3\Gamma_-}\frac{t_c}{v}e^{-\beta t_c}\right), \tag{12.34}$$

from which the loss of coherence in the leading order can be written as:

$$\delta W_- = 1 - |W_-(t)| \approx \frac{\Delta E_z^2}{3\Gamma_-}\frac{t_c}{v}e^{-\beta t_c}. \tag{12.35}$$

Dephasing due to many inelastic transitions

We now show that the additional dephasing is absent in the opposite case of slow relaxation $\Gamma_- \ll \Delta\Omega$. One can show that in leading order the expression for coherence reads:

$$W_-(t) \approx e^{i\phi_0(t)} \exp\left(-\left[1 + \frac{\Gamma_-^2}{\Delta\Omega^2}\right]\Gamma_+ t\right) \propto e^{i\phi_0(t)}e^{-\Gamma_+ t}, \text{ for } \Gamma_- \ll \Delta\Omega \tag{12.36}$$

which shows that in this case the loss of coherence is dominated by the charge error.

6: In particular in the limit of fast relaxation $\Gamma_- \gg \Delta\Omega$ we expand:

$$\begin{aligned} A &= \sqrt{(\Gamma_+ + \Gamma_- - i\Delta\Omega)^2 + 4i\Delta\Omega\Gamma_+} \\ &\approx \Gamma_+ + \Gamma_- + i\Delta\Omega - 2i\frac{\Delta\Omega\Gamma_+}{\Gamma_-} - 2\frac{\Delta\Omega^2\Gamma_+}{\Gamma_-^2}, \end{aligned}$$

while in the limit of slow relaxation $\Gamma_- \ll \Delta\Omega$ we have:

$$\begin{aligned} A &= \sqrt{(\Gamma_+ - \Gamma_- + i\Delta\Omega)^2 + 4\Gamma_-\Gamma_+} \\ &\approx \Gamma_+ - \Gamma_- + i\Delta\Omega - 2i\frac{\Gamma_+\Gamma_-}{\Delta\Omega} - 2\frac{\Gamma_-^2\Gamma_+}{\Delta\Omega^2} \end{aligned}$$

.

12.4 Application to spin qubit shuttling

We now head towards the final results of the thesis, which concern the loss of spin coherence during transfer of electron in spin superposition between two realistic quantum dots in GaAs and Si-based devices.

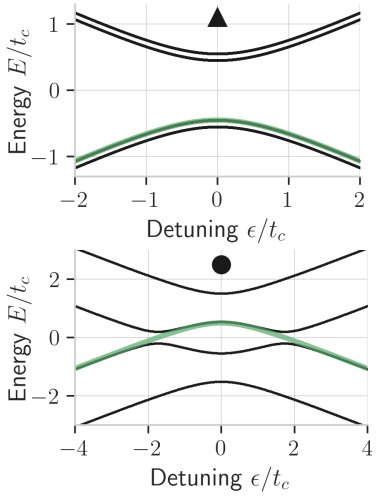

Figure 12.1: The instantaneous energy spectra of total Hamiltonian from Eq. (12.1) in two regimes of magnetic field used in this chapter. The $E_z < t_c$ (top) and $E_z > t_c$ (bottom)

7: The absence of low-frequency noise may correspond to some active control of the qubit during shuttling, which works analogously to spin echo. Alternatively effective fluctuation of detuning noise can be suppressed by spatial correlations of the charge noise see Sec.. 7.1

Parameters used

To large extent we use here parameters from Tab. 11.1, which were introduced in the analysis of spin-up state transfer. We compute the loss of spin coherence δW_- with and without additional averaging over slow noise due to nuclei and low-frequency contribution for $1/f$ charge noise.[7] We concentrate here on sweep rates $v > 2\,\mu$eV/ns, as for slower sweeps the phase error due to presence of nuclear spins, even in isotopically purified silicon with 0.01 % ^{29}Si is expected to be significant, $\langle\phi^2\rangle > 10^{-3}$, see Eq. (12.22).

Small tunnel coupling

We start with the analysis of $t_c = 20\,\mu$eV. In Fig. 12.2 we plot the loss of spin coherence in the ground orbital state, δW_-, as a function of sweep rate for two different Zeeman splittings $E_z = 120, 2\,\mu$eV, which correspond to $\Delta E_z = 0.12, 0.002\,\mu$eV.

In Fig. 12.2a, in which results obtained in absence of slow fluctuations are plotted, we can see that for $v > 100\ \mu$eV/ns, the loss of coherence is limited by Q_{LZ}. For $v \approx 100\,\mu$eV/ns the loss of coherence in Si (red triangles and squares) is well approximated by the charge transfer error caused by single transition from ground to excited state, i.e. Q_{SEAL} from Eq. (8.22) drawn using red dashed line. In the same regime of sweeps

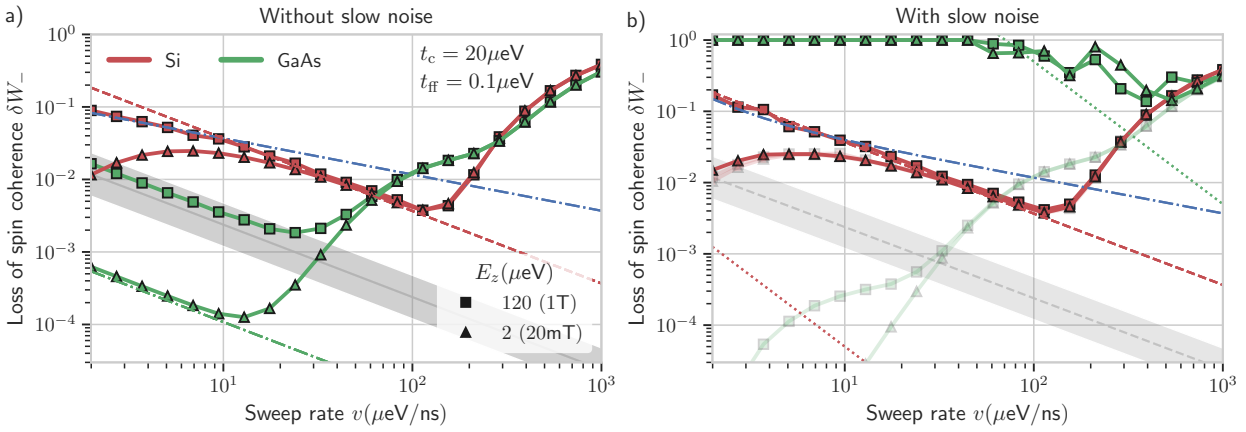

Figure 12.2: Loss of spin coherence during DQD transition δW_- as a function of sweep rate v for $t_c = 20\,\mu$eV, $t_{\mathrm{ff}} = 0.1\,\mu$eV and two Zeeman splittings of $E_z = 120\,\mu$eV (squares) and $E_z = 2\,\mu$eV (triangles). We plot results of adiabatic Master equation method (symbols and solid line for guidance), described in the Appendix A: (a) without averaging over quasistatic fluctuations of $\delta\epsilon, \delta t_c, \delta E_z$ and (b) with averaging over their $N = 100$ realisations. The results are shown for two models of DQD system GaAs (green) and SiGe (red) from Tab. 6.1. We plot analytical predictions corresponding to: spin relaxation at the avoided crossing in GaAs from Eq. (11.35) (green dashed-dotted line), spin-flip interference from Eq. (11.16) (upper bound of gray region for constructive interference limit, and solid line for fully dephased result), single excitation limit in Si from Eq. (8.22) (red dashed line) and the sum of dephasing errors $\langle\delta\phi^2\rangle$ (blue dashed-dotted line): dephasing during excitation from Eq. (12.27) in panels a) and b) and dephasing due to low-frequency detuning noise from Eq. (12.13) (only in b). In b) we separately plot spin dephasing due to nuclear spins using dotted lines for Si (red) and GaAs (green). Finally in b) we show the charge transfer error $\frac{1}{2}(Q_\uparrow + Q_\downarrow)$ using semi-transparent lines. We use the relaxation rates from Fig. 11.7 and parameters given in Tab. 11.1.

the loss of coherence in GaAs is larger due to stronger coupling to environment, i.e. larger transition rates, and only a partial recovery of ground state occupation. In this regime $\delta W \approx \frac{1}{2}(Q_\uparrow + Q_\downarrow)$ is dominated by charge error and the results look analogous to Fig. 8.8, where charge transfer error for spin-down component $Q_\downarrow$ was plotted.

For slower sweeps the results for two magnetic fields starts to differ. In GaAs for $E_z = 120\,\mu\text{eV} > t_c$ (green squares) the loss of coherence is dominated by the spin-flip interference, i.e. $\delta W_- \approx \frac{1}{2}\overline{Q}_\uparrow$, where the dephased result is plotted using gray line from Eq. (11.16). The additional contribution from dephasing due to many inelastic transitions (Eq. (12.35)) can be observed. For weak magnetic field of $E_z = 2\,\mu\text{eV} < t_c$ (green triangles), the spin relaxation dominates the error $\delta W_- \approx \frac{1}{2}Q_{\uparrow\downarrow}$, which in Fig. 12.2a can be seen by green dashed-dotted line corresponding to $\delta W_- = \frac{1}{2}Q_{\uparrow\downarrow}$ from Eq. (11.35). In Si (red) the two magnetic fields differ significantly only at $v \leq 10\,\mu\text{eV/ns}$. For large magnetic field (red squares), the loss of coherence is caused by non-zero value of $\Delta E_z = 0.12\,\mu\text{eV}$ which leads to dephasing during excitation process from Eq. (12.27), that we plot using blue dashed-dotted line. As a result $\delta W_- \propto 1/\sqrt{v}$ is visible for $v < 10\,\mu\text{eV/ns}$, where the red squares fall below the red dashed line of Q_{SEAL}. For low magnetic field (red triangles) as a result of small $\Delta E_z = 0.002\,\mu\text{eV}$ the loss of coherence is effectively the same as the charge transfer error $\delta W_- \approx Q_{\text{HEAL}}$ from Eq. (8.23), which means that recovery of ground state occupation by charge relaxation process is approximately coherent.

We now include the low-frequency fluctuations in the analysis. As it can be seen in Fig. 12.2b, δW_- remains almost the same in Si devices. The only difference is visible at slowest sweeps of $v \approx 5\,\mu\text{eV/ns}$, and for the large magnetic field (red squares). In this region, the loss of coherence is additionally increased by the low-frequency detuning noise (Eq. (12.13)) that produces $\delta W_- \propto 1/v^2$ scaling. In Fig. 12.2b we plot the sum of the two processes activated by $\Delta E_z = 0.1\,\mu\text{eV}$: dephasing due to excitation-relaxation and due to low-frequency charge noise, using dashed-dotted blue line. Note that the contribution from the nuclear spins (red dotted line) is at least two orders of magnitude below these contributions to dephasing. In contrast, the dephasing due to nuclear spins in GaAs completely dominates the loss of coherence. We plot the theoretical value related to T_2^* time by the dotted green line, and prove that the rapidly oscillating numerical result stays above that line for both considered values of E_z.

Finally, to highlight the relation between the spin dephasing and charge transfer, in Fig. 12.2b) we additionally plot the charge transfer error $\frac{1}{2}(Q_\uparrow + Q_\downarrow)$,[8] using semi-transparent lines with symbols. As it can be seen the incoherent charge transfer in GaAs is relatively easy to achieve even at $v \approx 10\,\mu\text{eV/ns}$ at which the charge transfer error reads $\frac{1}{2}(Q_\uparrow + Q_\downarrow) \approx 10^{-4}$.[9] In contrast in Si the charge transfer error in Si follows δW_- for lower values of the Zeeman splitting (red triangles in Fig. 12.2b)), hence in this regime of parameters the coherent transfer is limited only by the charge transfer error.

8: i.e. probability of the electron staying in the initial dot $|L\rangle$

9: Note that in the limit of small magnetic fields the spin relaxation around avoided crossing does not modify charge transfer error $\frac{1}{2}(Q_\uparrow + Q_\downarrow)$, since the electron still ends up in the target dot but with its spin state flipped. As a result the charge transfer error (semi-transparent line in Fig. 12.2b)) can go below the values of δW_- from Fig. 12.2a)

Large tunnel coupling

We now move the larger tunnel coupling of $t_c = 60\,\mu$eV, which as we will show in the discussion in 13.2 could enable the charge transfer across $N = 100$ dot array, i.e. allow for $L = 10\mu$m charge transfer.

Loss of coherence

As before we start by considering the transfer in absence of low-frequency noise and in Fig. 12.3a plot the loss of coherence δW_- as a function of sweep rate v. For both devices, plotted using red (Si) and green (GaAs)

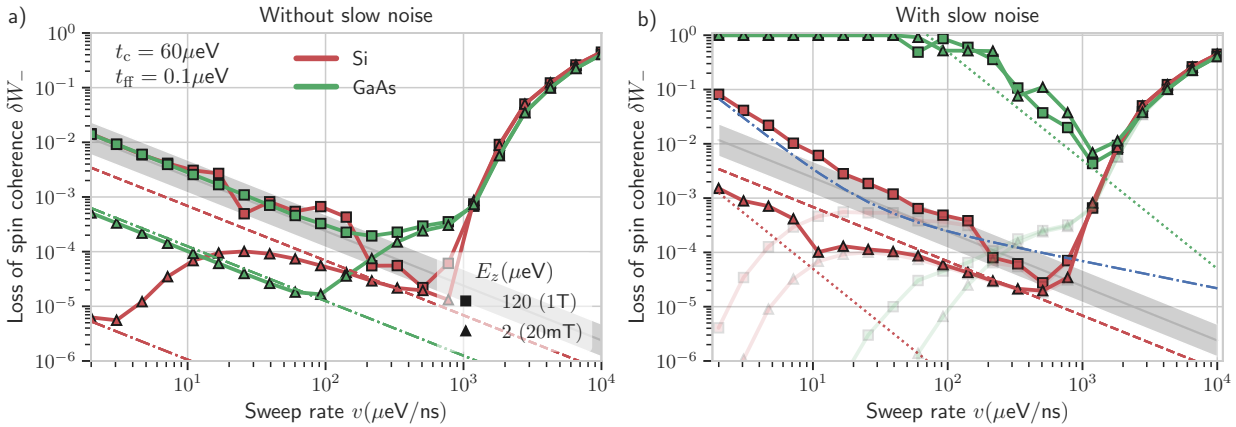

Figure 12.3: Loss of spin coherence during DQD transition δW_- as a function of sweep rate v for $t_c = 60\,\mu$eV, $t_{ff} = 0.1\,\mu$eV and two Zeeman splittings of $E_z = 120\,\mu$eV (squares) and $E_z = 2\,\mu$eV (triangles). We plot the results of adiabatic Master equation method (symbols and solid line for guidance) described in the Appendix A: (a) without averaging over quasistatic fluctuations of $\delta\epsilon, \delta t_c, \delta E_z$ and (b) with averaging over their $N = 100$ realisations. The results are shown for two models of DQD system GaAs (green) and SiGe (red) from Tab. 6.1. We plot analytical predictions corresponding to: spin relaxation at the avoided crossing in GaAs (green dashed-dotted line) and Si (red dashed-dotted line) from Eq. (11.35), spin-flip interference from Eq. (11.16) (upper bound of gray region for constructive interference limit, and solid line for fully dephased result) and Single Excitation Limit in Si from Eq. (8.22) (red dashed line). In b) we additionally plot sum of dephasing errors $\langle\delta\phi^2\rangle$ (blue dashed-dotted line) caused by dephasing during excitation from Eq. (12.27) and dephasing due to low-frequency detuning noise from Eq. (12.13). In b) we also separately plot spin dephasing due to nuclear spins using dotted lines for Si (red) and GaAs (green). Finally in b) we show charge transfer error $\frac{1}{2}(Q_\uparrow + Q_\downarrow)$ using semi-transparent lines. We use relaxation rates from Fig. 11.7 and parameters given in Tab. 11.1.

lines with symbols, the large magnetic field of $E_z = 120\,\mu$eV results in loss of coherence caused by the spin-flip interference. In Si, the contributions from this mechanism, given by $\overline{Q}_\uparrow$ (gray line in Fig. 12.3a from Eq. (11.16)), are larger than the charge excitation line Q_{SEAL} (red dashed line and Eq. (8.22)), which means that the transfer is limited by the error in the transfer of spin-up component, i.e. $\delta W_- \approx \frac{1}{2}Q_\uparrow$ and by the Landau-Zener processes for large v. In GaAs, an additional small region of relaxation aided transfer can bee seen around $v \approx 500\mu$eV/ns, in which $\delta W_- \approx Q_{\text{HEAL}}$ from Eq. (8.23).[10] For slower sweeps, $v < 100\,\mu$eV/ns, the difference in coupling strengths to the environment means the spin-flip oscillations are absent in GaAs and visible in Si. In the latter, the additional contribution to δW_- due to dephasing during inelastic transitions can be observed around $v \approx 100\,\mu$eV/ns.

In smaller magnetic fields of $E_z = 2\,\mu\text{eV} < t_c$ (triangles in Fig. 12.3a)) the spin-flip interference is absent and the δW_- is dominated by the charge transfer error for faster sweep rates, and by the spin relaxation at the avoided crossing for the slowest ones. However the transition between the two regimes is taking place at different v for the two devices, i.e.

10: Note that the factor of 1/2 is missing, since
$$Q_\uparrow \approx Q_\downarrow \approx Q_{\text{HEAL}}$$
.

$v \approx 100\,\mu$eV/ns for GaAs and $v \approx 2\,\mu$eV/ns for SiGe. In Fig. 12.3b) we plot the probability of spin relaxation $\frac{1}{2}Q_{\uparrow,\downarrow}$ by the dashed-dotted lines (green for GaAs, red for SiGe). The two-orders of magnitude difference between such contribution reflects the difference of corresponding relaxation rates at the avoided crossing[11] .

11: See relaxation rates in Fig. (11.7)

Finally we add the low-frequency fluctuations, and plot the sum of all the contribution to δW_- in Fig. 12.3b. As before, the loss of coherence in GaAs is determined by the interplay between charge transfer error due to Landau-Zener physics and dephasing due to nuclear spin noise. Using the Landau-Zener formula, we predict that the minimum of δW_- in GaAs can be made as small as 10^{-4} only for $v \approx 10^4\,\mu$eV/ns and $t_c > 200\,\mu$eV. Note that in Fig. 12.3b a similar value of δW_- for the Si device was achieved at an order of magnitude slower sweep. Below this value the loss of coherence in Si depends on the value of E_z, as $\Delta E_z = 10^{-3}E_z$. In the limit of large $E_z > t_c$ (squares) the presence of slow noise on one hand reduces amplitude of the oscillations of the spin-flip interference (shaded region and gray line for dephased result), and on the other gives $\delta W_- \propto 1/v^2$ behaviour at $v < 10\,\mu$eV/ns due to slow-fluctuations of detuning (Eq. 12.13). Since small dephasing due to inelastic transitions can be observed around $v = 100\,\mu$eV/ns, we plot the sum of those two dephasing contributions, i.e. low-frequency charge noise and inelastic transitions, using the blue dashed-dotted line.

For the case of low-magnetic field in Si (red triangles), the slow fluctuations modify δW_- only at $v < 10\,\mu$eV/ns, where the loss of coherence is caused by remaining nuclear spins (Eq. (12.22) and red dotted line). Note that in principle in Si at low-magnetic fields one might expect two local-minima of δW_-, where additionally to charge-transfer related $v_{\text{opt}} \approx 10^3\,\mu$eV/ns (see discussion below Eq. (13.1)), another minimum $v_\phi \approx 10\,\mu$eV/ns can be observed as an effect of the interplay between the charge relaxation mechanism (in the form of Q_{HEAL}) and the spin dephasing $\delta W_- \propto 1/v^2$. Note that the error at this v_ϕ can be decreased by further isotopic purification[12] , however at some point $\delta W_-(v_\phi)$ will become dominated by the spin relaxation dephasing from Fig. 12.3a).

12: such that the contribution of nuclear spins effectively vanishes

Finally in Fig. 12.3b we add the semi-transparent lines to illustrate the corresponding charge transfer error $\frac{1}{2}(Q_\uparrow + Q_\downarrow)$. Crucially, for the Si-based device we can observe that the phase error δW_- is dominated by the charge errors for sweep rates $v > 100\,\mu$eV/ns. For slower sweeps $\delta W_- \propto \langle\delta\varphi^2\rangle$, the contribution from dephasing mechanisms analyzed in this chapter in a typical range of parameters, prevents us form achieving significantly lower values of δW_- than the one obtained at the charge transfer minimum $v_{\text{opt}} \approx 10^3\,\mu$eV/ns (See Chapter 8 for discussion). As a consequence, we can claim that the minimal achievable phase error is very close to the minimaal achievable charge transfer error,r $\delta W_-(v_{\text{opt}}) \approx Q(v_{\text{opt}})$. We will use this result in Sec. 13.2 to estimate the range of tunnel couplings needed for coherent transfer across $N = 100$ dots.

IV. Outlook and discussion

13 Summary and discussion

13.1 Summary

Possibility of moving the spin-qubit without loss of the spin-coherence would enable coherent communication of distant quantum registers in the future quantum computer based on semiconductor quantum dots. The main objective of the thesis was to identify possible threads in realising this task. We concentrated on the single electron transition between two realistic semiconductor quantum dots. The main challenge was associated with the presence of the environment of the electron, which combines the sources of low- and high-frequency noise. Apart from nuclear spins, which are expected to directly affect the spin coherence, we have considered the effect of the environmental electric fields in form of lattice vibrations (phonons) and the charge noise. Their effect on the spin degree of freedom was mediated by the finite spin-orbit interaction, that correlates spin states with the charge degree of freedom. We have shown that in its presence the dynamical drive of the charge states can modify the initial spin state and due to non-deterministic evolution leads to spin dephasing. We found that most dephasing is activated by the dot-dependant Zeeman splitting, however in the relevant regime of relatively fast sweeps the error in coherent transfer has been dominated by the charge transfer error.

System of interest

As mentioned above, we have focused on transitions between two tunnel-coupled quantum dots. In a commonly used model, in which only ground orbital states of the dots are used, the double quantum dot system is treated as two-level system. In a typical experimental scenario, charge transfer can be mapped onto the Landau-Zener problem of adiabatic transfer across an avoided crossing, where the size of the crossing is given by the tunnel coupling. From the L-Z solution we know that in the closed system case, the sufficiently slow sweep of dots energy detuning should keep the electron in the ground state, which is being moved between the dots. As we have shown in this thesis, this picture is modified in presence of an environment. If a thermal energy of the environment is non-negligible in comparison to the tunnel coupling, the environment can provide the energy needed for inelastic transition between the levels of the system, and in this way populate the excited state that ends up in the initial dot. In the language of qubit shuttling it introduces a charge transfer error.

Theoretical tools

To model the above phenomenon in a realistic scenario, we have devoted the first part of the thesis to introduction of theoretical tools needed

to describe interactions between an environment and a driven two-level system (TLS), the double quantum dot system. In particular in Chapter 2 we have introduced the basic description of undriven TLS, and have shown the emergence of non-unitary evolution. In the subsequent Chapter 3 we have related the transverse coupling to dissipative evolution, associated with the energy exchange between the TLS and the bath. In the process we have derived GKLS Master equation starting from Bloch-Redfield treatment, and performing the Born-Markov approximation in the limit of weak coupling and relatively short correlation time of environment. Next in Chapter 4 we have then considered the pure dephasing process, which is associated with the longitudinal coupling. We have introduced there a classical noise model, using which we have shown that dephasing is typically dominated by the slow fluctuations of the environment. We have argued that in the limit of small error, the separation of timescales between dissipative and dephasing effects allows for their independent treatment. As a result, in the following parts of the thesis the inelastic transition between the instantaneous states is computed using the Master equation approach, while low-frequency noise is included by additional averaging over classical quasistatic noise. Finally. in Chapter 5 we have generalized the above-described treatments of open system dynamics to the case of a driven TLS. We have modeled the presence of the environment with an adiabatic Master equation and classical noise approach. Most importantly, we have shown there that due to rotation of the basis caused by the adiabatic drive, the character of longitudinal and transverse noise is dynamically changed.

Modeling a realistic semiconductor environment

It is not obvious if strong coupling between the electron and environment will hinder or help successful charge transfer. On one hand, stronger coupling increases probability of excitation from ground to excited state. On the other, at the same time it increases the probability of ground state recovery by subsequent relaxation. The probability of charge transfer results from competing processes of excitation and relaxation, each depending in a distinct way on temperature, sweep rate, tunnel coupling and a specific model of environmental noise. We have attempted to find parameters reflecting realistic environments of semiconductor double quantum dots. In Chapter 7, we have used the previously defined models of DQD systems to compute the corresponding transition rates, which later served as an input for numerical calculations. In particular, we have shown that relaxation and excitation rates in GaAs are dominated by the piezoelectric phonons, while their absence in non-polar Si-based device resulted in order of magnitude smaller rates, caused by the charge noise. We have argued there that detuning noise is expected to be orders of magnitude stronger than noise in tunnel coupling, which means that most inelastic transitions are expected to take place in the vicinity of the avoided crossing.

Charge transfer

For an estimation of charge transfer error we have concentrated on the lowest-lying energy states in the 4-level spin-dot system. Using the

theory from the previous chapters, in Chapter 8 we have compared charge transfer errors in Si-based and GaAs-based devices, which were effectively treated as realistic examples of weakly- and strongly-coupled electron-environment systems, respectively. As expected, for fast sweep rates the transfer was limited by Landau-Zener physics, however at slower sweeps the effects caused by coupling to the environment completely dominated the error probability. In case of strongly coupled GaAs, monotonic behaviour of charge transfer error with sweep rate (qualitatively similar to that known from the L-Z solution) is expected to be preserved, since for slower sweeps the strong coupling to environment drives the system towards equilibrium occupation of the ground state, which increases with the size of orbital gap.

The situation is very different in weakly coupled Si-based devices, for which the similar relaxation aided transfer is observed only for the slowest sweeps. For a relatively wide regime of intermediate sweep velocities, we have found that the charge transfer is limited by at most a single excitation from the ground to the excited state. At these intermediate timescales the relaxation back to the lowest energy state, corresponding to the electron finally getting transferred to the "right" dot, is too slow. As the excitation process is proportional to time spent in the vicinity of the avoided crossing, the resulting charge transfer error as a function of sweep rate has a non-monotonic structure, with a local minimum defined by the intersection of Landau-Zener curve and the excitation-induced error, which scales as $\propto 1/v$.

Spin-orbit coupling

We have followed the analysis by adding the spin degree of freedom, which couples to the driven TLS by the spin-orbit interaction. In Chapter 9 we have shown that dephasing and dissipation are mostly sensitive to transverse noise in the orbital basis. We have devoted the whole Chapter 10 to discussion of the adiabatic drive of the charge states in presence of spin degree of freedom, and non-zero spin-orbit coupling. In particular we have defined there two effects of such coupling, ΔE_z which stems from the difference between dot-dependent Zeeman splittings, and t_{ff}, which couples the two spin states and leads to tunneling with a spin-flip. We have related ΔE_z to the value of dot-dependent g-factor, and as such stated that the effects caused by finite ΔE_z are expected to be smaller, and hence less dangerous, at lower magnetic fields. We have found that a sufficiently large ΔE_z leads to a strong correlation of spin and charge degree of freedom in a form of longitudinal Stern-Gerlach apparatus, i.e. spatial separation of spin-up and spin-down states. Based on the previous discussion of spatial correlations of the noise, we have found that such an effect is expected to induce strong spin dephasing in presence of detuning noise.

On the other hand, we have connected the t_{ff} with intrinsic or synthetic spin-orbit interactions, which are needed for an all-electrical control of spin qubit. We have shown that its effect on the spin-down transfer is negligibly small, however it can significantly limit adiabatic transition of the spin-up component. We have found that in the regime of large magnetic fields, it introduces two additional avoided crossings with the excited spin-down state. The resulting interferometric pattern was

highly sensitive to environmental fluctuations of Zeeman splitting (due to nuclear spins) and phonon-induced relaxation (high-frequency noise). We have used the second process to propose a physical realization of Elizur-Veidman bomb testing experiment.

We have shown that for weaker magnetic fields, the highly sensitive to noise interference pattern can be avoided, and the next limiting factor for spin-up transfer is the spin relaxation caused by the mixing of the ground spin-up state with the excited spin-down state around the avoided crossing. This effect is essentially the same as the one used recently to realise spin-photon coupling. As we have shown, due to different relaxation rates this temporal spin-to-charge conversion is not expected to modify transfer of spin-up component in Si-based devices, but becomes relevant in GaAs.

Spin coherence

We have finally combined all of the above techniques and results to analyze the probability of successful transfer of the electron in a coherent spin superposition. As we have shown, the small error limit of this quantity, defined as the absolute value of single off-diagonal element of spin-dot density matrix δW, has three separable contributions. The first two of them, the probability of spin-up and spin-down transfer, have been analyzed above. Thus in the last Chapter 12 we have focused on the remaining pure dephasing error, present due to averaging over stochastic phase, associated with non-deterministic part of the spin evolution during electron transfer. We have identified three most relevant contributions.

The first of them arises trivially from the presence of nuclear spins, and for typically spatially uncorrelated Overhauser fields puts a lower bound on the sweep rate, which comes from dephasing time T_2^* being an upper bound for transfer time. As a result we have found that the δW during electron transfer in GaAs results from the trade-off between the Landau-Zener physics and nucleari-nduced dephasing. Specifically, we have found that $\delta W \geq 10^{-2}$ at $t_c = 60\mu$eV. The second dephasing mechanism was related to the temporal occupation of another orbital state (i.e. the excited one) with Zeeman splitting differing from that of the lowest-energy orbital state. As a result of random time spent in the energy eigenstates, it introduces a stochastic phase which leads to spin dephasing. Finally, the last contribution comes from the low-frequency detuning noise and, as the previous mechanism, it is active in presence of non-zero ΔE_z. It induces dephasing of spin qubit during time spent around the avoided crossing, and for typical amplitudes of charge noise it is expected to overshadow other purely dephasing errors. Furthermore, it scales as $1/v^2$, so the low-frequency charge noise contribution is expected to dominate δW at lowest v.

Generally, the loss of spin coherence during the adiabatic spin qubit shuttling is expected to have a single minimum, as a function of sweep rate, in GaAs devices. In the Si-based devices, for sufficiently small ΔE_z and t_{ff} (Fig. 12.3) we expect δW to have two local minima. For the smallest v, δW is limited by low-frequency charge noise and the error decreases with increasing v, for slightly faster v it is limited by partially recovered ground state occupation (error increases with v), at some v the relaxation

becomes too slow in comparison and the transfer is limited by single excitation only (decreases with v) and finally for the fastest sweeps the coherence is limited by Landau-Zener physics (the error increases with v).

13.2 Discussion

Let us now put our findings in the context of the initial motivation for the research in this thesis: the coherent electron shuttling across distance of the order of 10μm in a realistic semiconductor device. As discussed above, in the GaAs case the coherent transfer is limited by the interplay between the charge noise transfer error in form of Landau-Zener excitations, and the spin dephasing due to presence of nuclear spins. The situation is different in the Si-based devices device. Although similarly to GaAs we have shown that for sufficiently slow sweeps the charge transfer can be arbitrarily successful, it has been achieved using relatively slow DQD passage, which would make long distance communication in large Si-based quantum computer rather impractical. Apart from that, we have argued that for a typical range of tunnel couplings and dot-dependant g-factor differences, transfer that is slow enough for the relaxation assisted charge transfer is associated with a significant loss of spin coherence. Thus, we now concentrate on the regime of relatively fast sweeps $v > 100\,\mu$eV/ns, in which the pure dephasing processes are no longer limiting the loss of coherence. Instead, as we have shown in Fig. 12.3, in Si-based systems the local minimum of δW_- is formed as a result of interplay between the two processes responsible for charge transfer error, the Landau-Zener non-adiabaticity, that increases with the sweep rate v, and the noise-induced excitations that scales as $1/v$. Alternatively, in the regime of lower tunnel couplings, the second contribution can be subdominant in comparison to the error in the transfer of spin-up component $Q_\uparrow \propto 1/v$ as it could be seen in Fig. 12.2.

The optimal sweep rate

We now concentrate on the scaling of such an optimal sweep rate, v_{opt}, with the magnitude of the tunnel coupling. This analysis is naturally limited to Si-based devices, however we compute the charge transfer error in GaAs at the same v_{opt} for comparison. For sufficiently small tunnel coupling with a spin flip, t_{ff}, the optimal sweep rate can be found from the equation:

$$Q_{\text{LZ}}(v_{\text{opt}}) = Q_{\text{SEAL}}(v_{\text{opt}}). \tag{13.1}$$

Taking into account Eq. (5.18) and Eq. (8.22) for the left and right side, the optimal sweep rate is given by

$$v_{\text{opt}} = \frac{\pi t_c^2}{2W(a)}, \tag{13.2}$$

where $W(a)$ is the Lambert W function, which satisfies equation $W(a)\exp(W[a]) = a$. In our case

$$a = \pi/4\sqrt{\beta t_c^3}/\Gamma_+(t_c), \tag{13.3}$$

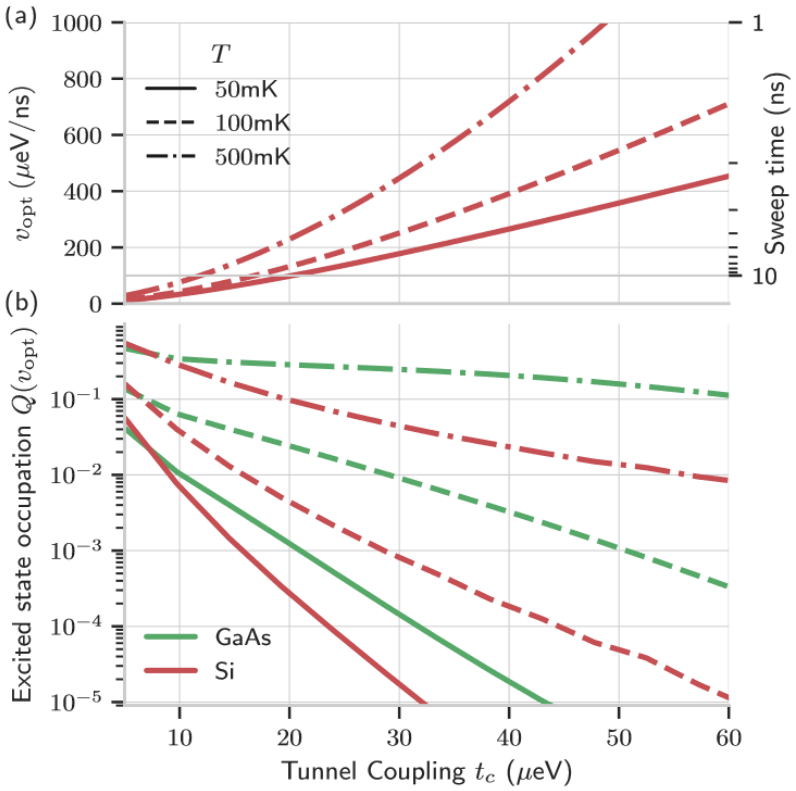

Figure 13.1: a) The optimal sweep rate v_{opt} and b) the charge transfer error computed at the optimal sweep rate $Q(v_{\mathrm{opt}})$ as a function of tunnel coupling. The lines are computed from the Eq. (13.2) in the model of Si device from Tab. 6.1 (red) at various temperatures (solid, dashed and dashed-dotted lines). For comparison we plot the charge transfer error, evaluated at the same sweep rate v_{opt} in the GaAs DQD (green). In (a) we additionally use the right y-axis to show the corresponding transfer time, assuming that the sweep range $\Delta\epsilon = 1$ meV. Adapted from [2].

which in the limit of low-temperature allows to approximate optimal sweep rate as $v_{\mathrm{opt}} \approx \pi k_{\mathrm{B}} T t_c/2$. In Fig. 13.1 we plot the numerically obtained value of v_{opt} and the corresponding charge transfer error as a function of t_c. In the figure we see that the charge transfer at these fast sweeps is about an order of magnitude worse in the GaAs,[1] compared to Si.

Transfer over 10 μm range

For a typical distance between the dots of $d \approx 100$nm, the number of double quantum dot transition needed for coherent transfer is $N \approx 100$. This means that to realize coherent communication at the level compatible with achieving fault-tolerance with quantum error correction, i.e. phase error smaller then $\sim 10^{-3}$,[2] a sufficiently low error rate at each DQD transition has to be achieved. If we assume that error rates in consecutive transitions are uncorrelated, the total phase error, as long as it is < 1, can be approximated as

$$\delta W = \sum_{i=1}^{100} \delta W_i \leq 10^{-3}. \tag{13.4}$$

From the above we see that the average error per single DQD transition cannot by larger then $\delta W \sim 10^{-5}$, which based on results for $T = 100$mK in Fig. 13.1 is expected if every dot pair along the chain has $t_c > 60\mu$eV, and sufficiently low magnetic field is used, so that the additional pure dephasing contributions are negligible compared to charge transfer errors.

1: It is attributed to stronger coupling to environment, which causes more transitions around avoided crossing. As it can be seen from Fig. 8.9 the region of v_{opt} is too fast for the effective recovery of ground state occupation in GaAs

2: Error thresholds for fault-tolerance of quantum computing architecture are between 10^{-4} and 10^{-2}, and we choose here the middle ground of 10^{-3}

Secondly we consider the case in which the error is dominated by a single weak link. This would effectively mean that the overall error is dominated by a single transition, i.e. $\delta W_k = 10^{-3}$, which according to Fig. 13.1 requires that the weakest coupled pair of dots should still have $t_c > 30\mu$eV such that probability of losing the electron is sufficiently small.

Other limitations

We finally comment of the other possible limitations during electron transfer along the chain of $N = 100$ dots. In the thesis we have considered a rather optimistic case of pre-tuned dots, which was reflected in relatively narrow detuning sweep from $\epsilon(t_i) = -500\,\mu$eV to $\epsilon(t_f) = 500\,\mu$eV. However, in presence of large - but realistic - electrostatic disorder one can expect up to $\Delta\epsilon \sim 10$meV to ensure transition through avoided crossing at unknown detuning [3]. Additionally, the uncertainty in the exact location of the avoided crossing will prevent us from using sophisticated time-dependent detuning sweep profiles (with large sweep rate away from the anticrossing, and small rate close to the anticrossing. Taking this into account, in a truly realistic situation involving many dots with $\sim$ meV scale initial detunings due to electrostatic disorder, we should expect an increase of the time of single interdot transition by about an order of magnitude, if we want to keep the charge transfer errors at the previously discussed level. This would imply about two-orders of magnitude larger phase error due to to nuclear spins, which even in isotopically purified Si would become a significant source of dephasing, i.e. $\delta W \approx 10^{-3}$ at $v < 100\,\mu$eV/ns. Another possible limitation is the presence of the valley degree of freedom in the Si devices, which can be treated as an additional internal degree of freedom of transferred electron. In the case of relatively small valley splitting, or different composition of the valley states in two dots, the interdot transfer can lead to non-zero occupation of the excited valley state which is expected to introduce additional spin-dephasing (see discussion below).

13.3 Outlook

In this thesis we have concentrated on the interdot transfer of an electron carrying quantum information encoded in its spin state, and the influence of interactions with the environment on both the fidelity of charge transfer, and the spin coherence of transferred electron. Below we discuss selected connections between the results presented above and other works, and mention a few possible extensions of the theoretical investigations contained in this thesis.

In the first two examples an important role is played by the valley degree of freedom, which we have only briefly mentioned in Sec. 6.1. The short introduction to valley physics can be found in our paper [3], but also in the topical reviews [20, 30]. Below we only highlight close relation between the effect that including another two-level degree of freedom of the electron in Si (valley states) will have on spin coherence, and the results presented in this thesis.

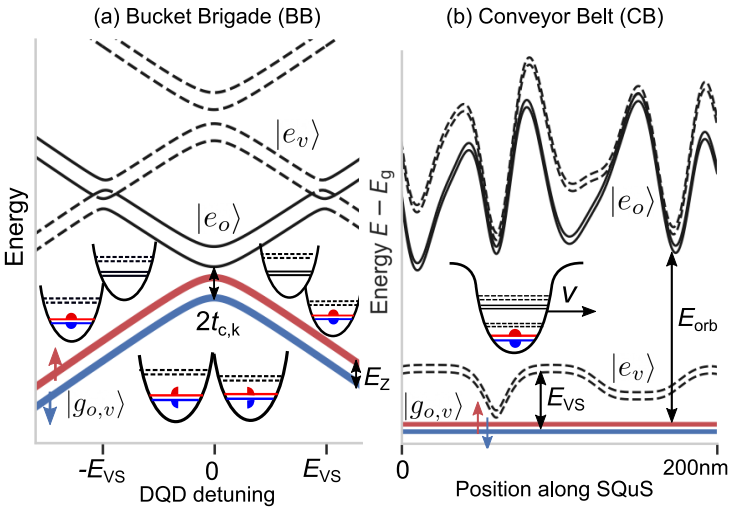

Figure 13.2: Comparison between two modes of the spin qubit shuttling in Si device: (a) the Bucket Bridgade and (b) the Conveyor Belt. In this thesis we have concentrated on the single interdot transition, which is a building block of the BB mode. In the CB method (right) the electron occupies the potential that is being moved along a 1D channel. In the figure we see the instantaneous energy spectrum of the two lowest lying orbital states and the valley states relative to the energy of the ground orbital state. By blue and red colors we denote ground orbital state corresponding to spin-up (red) and spin-down (blue). Dashed lines correspond to the excited valley states. The orbital splitting was denoted by E_{orb}, the valley splitting by E_{VS} and the tunnel coupling is given by $t_c = 2t_{c,k}$. The figure has been adapted from [3]

Conveyor Belt transfer

A method of coherent spin qubit shuttling that is alternative to multiple transitions between pre-defined quantum dots (the Bucket Brigade mode of shuttling), uses a single quantum dot that is being moved along a one-dimensional channel. As we discussed in [3], where a blueprint for such a Conveyor Belt transfer in Si/SiGe is provided, this method is expected to require much less fine-tuning of experimental equipment, and thus allow for easier scalability. The comparison between the Bucket Brigade and Conveyor Belt transfer modes is given in Fig. 13.2. As we will show below, with effectively adiabatic evolution of the charge degree of freedom, the potential loss of spin coherence and spin relaxation in the Conveyer Belt is related to the presence of the valley degree of freedom in Si.

Charge transfer

Firstly in [3], using numerical simulations of the disorder potential for the experimentally relevant parameters, we certified that shape of the moving quantum dot is weakly modified by its motion. The resulting orbital splitting of $E_{\text{orb}} \approx 1\text{meV}$ is large in comparison to thermal energy, which significantly limits the possibility of noise-induced orbital excitation, that are analogous to the ones considered in Chapter 8 in the context of charge transfer. As it can be seen from Fig. 7.1, large energy gap between ground and excited orbital states leads to for fast phonon-induced relaxation to the ground orbital level, i.e. $\Gamma_- \approx 10\,\text{ps}^{-1}$. This means that the electron effectively remains in the ground orbital state during the shuttling.

Next we showed that the motion of the electron turns stationary disorder into a time-dependent classical noise, which in principle can excite the electron into a higher orbital or spin state, if the amplitude of the fluctuations at the frequency corresponding to a gap are in resonance with the corresponding splitting. However for relevant velocity of $v \approx 10$ m/s, the finite size of electron wavefunction acts as a low-pass filter, which suppresses the excitation rate[3] . As a result the evolution of the orbital degrees of freedom can be treated as effectively adiabatic.

3: See [90] for alternative discussion of the spin inelastic transitions in the moving quantum dot in Si and GaAs devices

Valley degree of freedom

However, the role of orbital degrees of freedom from the thesis is played here by the valley degree of freedom, i.e. the non-adiabatic evolution in the valley degree of freedom leads to spin dephasing. The relevant spin-valley system can be described in terms of another four-level system which is formally analogous to an electron in a double quantum dot. Since both the valley splitting and the valley composition of eigenstates are sensitive to typically uncontrolled microscopic details of the interface, the valley eigenstates at any point in space (time) $|v_{\pm}(t)\rangle$, are expected to have different g-factor [200]. This activates spin dephasing channel analogous to DQD system with g-factors being distinct for the two dots, and in particular this means that spending random time in an excited valley state leads to spin dephasing. Since the electric dipole matrix element between the valley states is typically small, the resulting inefficient valley relaxation suggest that occupation of higher energy state should be generally avoided along the channel.

As the first dephasing channel we identified transitions over many atomistic steps* that can be mapped onto multiple Landau-Zener transitions. Their presence can create interference patterns analogous to the ones for transition of spin-up state $Q_{\uparrow}$ in DQD from Chapter 11. In further analogy with those results, random fluctuations of parameters, including expected fluctuations in electron velocity, are preventing usage of the effects of the interference, and lead to a finite occupation of the excited valley state. The typical occupation of excited valley state after two-step passage is shown in Fig. 13.3.

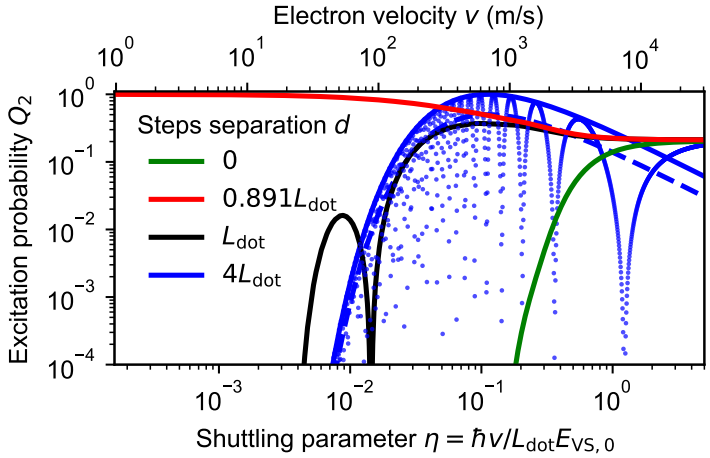

Figure 13.3: The occupation of excited valley state after the electron passage over two atomistic steps as a function of the effective electron velocity η. The interference pattern, visible for sufficiently large distance between the steps $d \gg L_{\mathrm{dot}}$, is the effect of double L-Z transition and is analogous to spin-flip interference during interdot transition from Chapter 11. Due to typical difference in g-factors between the valley states temporal occupation of the excited valley state leads to spin dephasing, which is also analogous to a process of dephasing due to random time spent in the excited state during interdot transition from Sec. 12.3. Adapted from [3].

The second source of spin transfer error was associated with the transition through a spin-valley hot-spot, which takes place if the Zeeman splitting matches the local valley splitting, i.e. at some time $E_z(t) = E_{\mathrm{vs}}(t)$. This effect is in full mathematical analogy to the flip-flop avoided crossing in the DQD case, and also can be avoided if sufficiently small magnetic field $E_z < \min(E_{\mathrm{VS}}(t))$ is used. In this case, the adiabatic transition through typically small avoided-crossing between $|v_{-}(t), \uparrow\rangle$ and $|v_{+}(t), \downarrow\rangle$ adiabatic states, leads to a spin-flip which can then be possibly followed by a relaxation to the lowest lying spin-down state, and in this way

* Such atomistic steps occur naturally at Si/SiGe interface due to the fact that the crystal growth requires the presence of a miscut of the substrate, i.e. the surface of the growing crystal is not exactly at 90 degree angle to the growth direction.

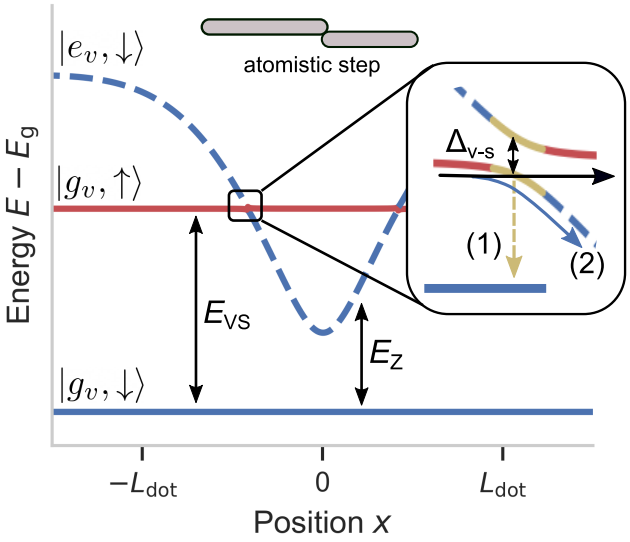

Figure 13.4: The instantaneous energy spectrum of the spin-valley Hamiltonian in the vicinity of the spin-valley hot spot, i.e. $E_z = E_{vs}$ with respect to lowest lying valley state $|g_v,\downarrow\rangle$. In full analogy to a passage through the spin-flip avoided crossing during interdot transition (See Fig. 11.3, the finite coupling between the $|v_+,\downarrow\rangle$ and $|v_-,\uparrow\rangle$ states can lead to unwanted adiabatic transition trough their avoided crossing. As a result both spin-relaxation to the lowest lying energy and uncontrolled interference can occur (see Chapter 11). Adapted from [3]

destroy quantum information encoded in the spin superposition. This phenomenon is schematically showed in Fig. 13.4

Predicted error

We finally share the main result of [3], and in Fig. 13.5 we plot the predicted loss of spin coherence after transfer over 10μm distance. The ddephasing

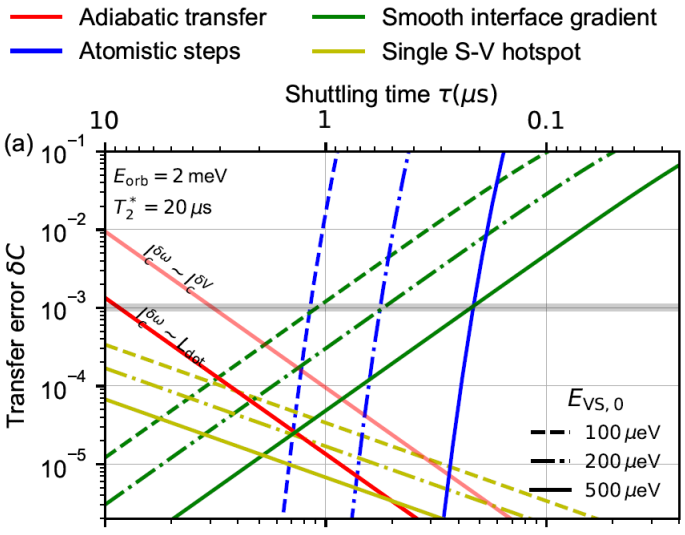

Figure 13.5: The main result of [3], which predicts the loss of spin coherence during 10 μm conveyor belt transfer as a function of electron velocity. As it can be seen we predict a relatively wide range of velocity around $v = 10$m/s which would allow to keep the coherence error $\delta C < 10^{-3}$. We highlight that in the alternative the similar distance could be covered by $N \approx 100$ interdot transitions using modelled in this thesis BB mode. Hence obtained error should be compared against $\delta C \approx 100\overline{\delta W_-}$, where $\overline{\delta W_-}$ is the average error of coherent transition per DQD transfer. Adapted from [3].

channels escribed above were denoted using blue and yellow lines in order of description. The red line corresponds to dephasing during completely adiabatic evolution, analogous to the processes described in Sec. (12.2). The contribution from the nuclear spins is reduced due to motional narrowing process, which for the DQD case could be observed in the reduced fluctuations of average Zeeman splitting $\delta\overline{E}_z$ from Eq. (9.16). The second contribution to adiabatic dephasing is from low-frequency charge noise and similarly to Eq. (12.13) is mediated by spatially dependent g-factor, which is a continuous version of the dot-dependent Zeeman splitting, or equivalently non-zero ΔE_z.

Interdot transfer in presence of valley degree of freedom

Let us now discuss how the presence of valley degree of freedom can be incorporated in the theory developed in this thesis. Together with spin and charge degrees of freedom the addition of the valley states would give rise to eight instantaneous states of the composite system. However, for the coherent interdot transition of the spin superposition, only two of them are initially populated. The typical situation is depicted in Fig. 13.6 where the two spin superposition states are marked using blue (spin-down) and red (spin-up) color. For the regime from Fig. 13.6a) of relatively large valley splitting (or small magnetic field), $E_{\mathrm{VS}} > E_z$, the low-energy transfer is effectively the same as the one in the thesis, with possible modification of the value of the tunnel coupling (see discussion below).

In the opposite case depicted in Fig. 13.6b), i.e. $E_{\mathrm{VS}} > E_z$, the modification of the adiabatic evolution of the spin-down state (blue) can be still effectively analyzed using the two-level model from Chapter 8. However, for the excited spin state, the additional crossings between the states with different valley composition occur, which together with the spin-flip crossings lead to a rich interference structure analogous to the spin-flip interference from Chapter 11. The size of each orbit-valley avoided crossing is determined by the "valley-orbit interaction", which analogously to synthetic spin-orbit interaction from Chapter 9 is caused by a different orientation and the magnitude of the valley field in two quantum dots. We highlight, however, that the orientation of the valley fields in two dots can be almost orthogonal, which might be associated with the presence of an atomistic step in-between the dots, and lead to a creation of relatively large avoided crossing between excited and ground valley states, and effectively suppress the intravalley tunnel coupling compared to the the bare coupling t_c. In such a case the interdot transfer would lead to a significant valley excitation, and hence spin dephasing (see the discussion above). Additionally, different composition of the valley states in the two dots would activate inelastic transitions between valley states, and as a result lead to even more valley mixing. From

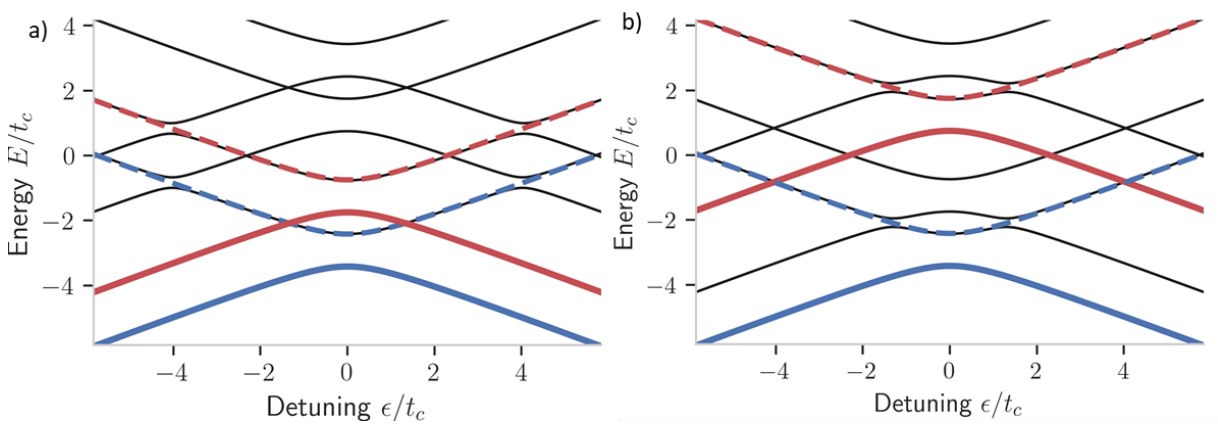

Figure 13.6: Instantanous spectrum of the Hamiltonian, corresponding to the transition of the spin qubit in presence of the valley degree of freedom. By the blue (red) solid lines we denote the ground orbital states corresponding to spin-down (spin-up). By dashed line the corresponding excited states. a) The case of large valley splitting $E_{\mathrm{VS}} < E_z$ in which the transition can be effectively described using methods from the thesis. b) The case of small valley splitting splitting $E_{\mathrm{VS}} > E_z$, in which the spin-up state experiences additional avoided crossings, which can additionally affect coherence of transferred spin qubit.

the above, we highlight that no improvement of spin coherence of the transferred electron should be expected if the valley states are added to the analysis. Hence, the results of the thesis can be treated as a good estimation of the lower bound of the spin coherence error.

Characterisation of environmental noise

We finally comment on the possibility of using the transfer-induced dephasing to characterize the spatio-temporal correlations of the charge noise. In principle this idea can be used in both BB and CB modes of the electron transfer, but here for simplicity we show its principle using the discrete case of repeating transitions between two dots. We also concentrate on the noise in dots' detuning $\delta\epsilon(t)$ only. We use here an approach form Sec. (5.4) and write the longitudinal dephasing noise in the spin basis as:

$$\xi_\phi(t) = d_\phi(t)\delta\epsilon(t), \tag{13.5}$$

where we have used the longitudinal dipole moments given by

$$d_\phi(t) = \langle\tilde{\uparrow}(t)|\hat{\sigma}_z|\tilde{\downarrow}(t)\rangle, \tag{13.6}$$

expressed in terms of $\hat{\sigma}_z = |L\rangle\langle L| - |R\rangle\langle R|$ and $|\tilde{\downarrow}(t)\rangle$ $|\tilde{\uparrow}(t)\rangle$ as the instantaneous eigenstates of spin qubit. As we have shown in the case of adiabatic evolution, they can correspond to dressed states from Eq. (9.20). We now follow Eq. (4.20)) and compute the contribution to dephasing in the second order in the fluctuations, i.e. $W'(t) = 1 - \frac{1}{2}\langle\delta\phi^2\rangle$, where $\delta\phi = \int_0^T \xi_\phi(t)$ and $\langle\ldots\rangle$ denotes classical averaging, such that

$$\langle\delta\phi^2\rangle = \int_0^T \mathrm{d}t_1 \int_0^T \mathrm{d}t_2 \Big(\big\langle\delta\epsilon(t_1)\delta\epsilon(t_2)\big\rangle d_\phi(t_1)d_\phi(t_2)\Big). \tag{13.7}$$

The above expression shows that the rotation of the basis during driven evolution acts as an effective filter of detuning noise. In the language of our previous works on characterising environmental noise using qubits undergoing pure dephasing [4–7], the longitudinal dipole moment $d_\phi(t)$ acts as a filter function, which for more sophisticated detuning sweeps could be used for the spectroscopy of environmental fluctuations encoded in the spectral density $S_\epsilon(\omega) = \int_{-\infty}^{\infty} \mathrm{d}\omega\langle\delta\epsilon(t)\delta\epsilon(0)\rangle e^{-i\omega t}$. This can be conveniently seen in the Fourier picture

$$\langle\delta\phi^2\rangle = \int_{-\infty}^{\infty} \frac{\mathrm{d}t}{2\pi} S_\epsilon(\omega)|D_t(\omega)|^2, \tag{13.8}$$

where we have defined the windowed Fourier transform of the longitudinal dipole moment as:

$$D_t(\omega) = \int_0^T d_\phi(t)e^{-i\omega t}\mathrm{d}t. \tag{13.9}$$

Crucially, if $d_\phi^{\mathrm{spin}}(t)$ can be engineered to be frequency selective, it can be use to characterize $S_\epsilon(\omega)$.

As we showed around Eq. (12.13), a single interdot passage effectively induces a non-zero $d_\phi^{\mathrm{spin}}(t)$ around the avoided crossing. Thus, perform-

ing multiple passage, for instance in the form of LZSM interference experiment [97], will result in a periodic $d_\phi^{\text{spin}}(t)$. The low-frequency part, which otherwise dominates the dephasing, can be filtered out by applying a single spin-flip operation (a spin echo) in the middle of the evolution, such that $d_\phi^{\text{spin}}(T/2 - t) = -d_\phi^{\text{spin}}(T/2 + t)$. This means that the effective filter $d_\phi^{\text{spin}}(t)$ has zero average, and based on Eq. (13.7) the quasistatic contribution to $\delta\epsilon$ vanishes. As a result, the dephasing error will be related to a spectral density of detuning noise at frequencies commensurate with the frequency of the drive.

The above method can be extended to characterise also spatial correlations of the noise in the arrays of many quantum dots. In such a case the movement of the electron between the dots in an array would result in more sophisticated filter functions, and additionally relate the dephasing to a correlations between the detunings of distinct pairs of dots.

Appendix

A Averaged Master equation method

In this section we discuss the approach used in the thesis to simultaneously treat low- and high- frequency noise for the driven and undriven systems.

A.1 Method description

The numerical method of *averaged Master equation*, that is being used in the thesis is now summarized in a diagram plotted in Fig. A.1. As it can

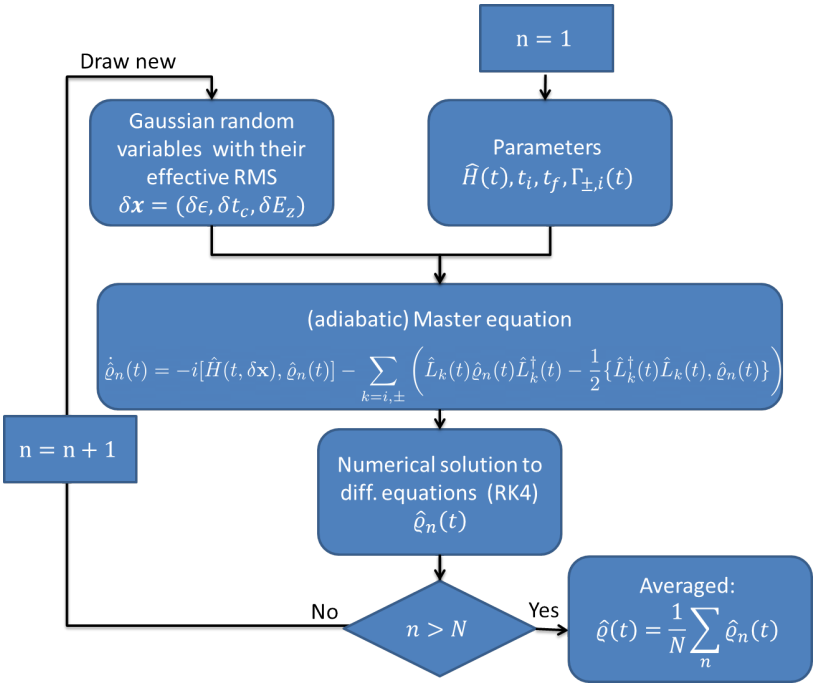

Figure A.1: The scheme of averaged Adiabatic master equation, used in this thesis for computing the reduced density matrix of the density matrix corresponding to spin and charge degrees of freedom. For each realization of the quasistatic fluctuations of detuning $\delta\epsilon$, tunnel coupling δt_c and the Zeeman splitting δE_z we numerically solve the system of coupled differential equations obtained using Adiabatic master equation methods. The final density matrix is obtained by averaging over N realisations of the quasistatic noise.

be seen in each loop we first draw new realisation of quasitatic random variables, which together with deterministic but possibly time-dependant parameters enters the Master equation or adiabatic Master equation for driven systems. The resulting equations of motion for each element of the density matrix of a four-level system are solved using numerical methods, which for our case was done using Runge-Kutta 4th order method. This procedure is repeated for N realisations of quasistatic random variables, and the final result, i.e. the elements of the density matrix for spin-charge system are averaged over them. Due to complicated structure related to the adiabatic basis, we now describe the procedure in details for the adiabatic drive of four-level system of interest, i.e. the spin in a double dot. Its application to the undriven case, and driven case of the two-level system can be deduced from below.

Driven system

Low-frequency noise

We first deal with the low-frequency noise and compute the effective rms of the detuning, tunnel coupling and Zeeman spliting fluctuations, using method of effective quasistatic noise from Eq. (4.49). For each of the above, we draw the first realisation from the independent Gaussian distributions with respective RMS $\tilde{\sigma}_\epsilon$, $\tilde{\sigma}_{t_c}$, $\tilde{\sigma}_{E_z}$ and zero average. Together they form a random "vector"

$$\delta\mathbf{x} = (\delta\epsilon, \delta t_c, \delta E_z) \tag{A.1}$$

As described in Chapter 10, we next consider diagonal spin-orbit coupling and go to the adiabatic frame, with respect to the Hamiltonian

$$\hat{H}_{\text{diag}}(t, \delta\epsilon, \delta t_c, \delta E_z) = \frac{\epsilon(t) + \delta\epsilon + \frac{1}{2}\Delta E_z \hat{s}_z}{2}\hat{\sigma}_z + \frac{t_c + \delta t_c}{2}\hat{\sigma}_x + \frac{E_z + \delta E_z}{2}\hat{s}_z, \tag{A.2}$$

which means we find the operator $\hat{S}(t, \delta\mathbf{x})$, which diagonalize the above. This can be done analytically for any $\delta\mathbf{x}$ as it was done in Sec. 5.2. With the help of the operator $\hat{S}(t, \delta\mathbf{x})$ we move to the adiabatic picture, i.e.

$$\hat{\mathscr{H}}_0(t, \delta\mathbf{x}) = \hat{S}^\dagger(t, \delta\mathbf{x})\hat{H}_{\text{diag}}(t, \delta\mathbf{x})\hat{S}(t, \delta\mathbf{x}) = \frac{\Omega(t,\delta\mathbf{x})}{2}\hat{\varsigma}_z - \frac{\Delta\Omega(t,\delta\mathbf{x})}{4}\hat{\varsigma}_z\hat{s}_z, \tag{A.3}$$

where the Hamiltonian in the adiabatic picture is now defined in terms of spin-averaged orbital splitting :

$$\Omega(t, \delta\mathbf{x}) \approx \sqrt{(\epsilon + \delta\epsilon)^2 + (t_c + \delta t_c)^2}, \tag{A.4}$$

and the difference in orbital splittings for each spin components

$$\begin{aligned}\Delta\Omega(t, \delta\mathbf{x}) = &\sqrt{(\epsilon(t) + \delta\epsilon + \tfrac{\Delta E_z}{2})^2 + (t_c + \delta t_c)^2} \\ &- \sqrt{(\epsilon(t) + \delta\epsilon - \tfrac{\Delta E_z}{2})^2 + (t_c + \delta t_c)^2},\end{aligned} \tag{A.5}$$

both evaluated for a particular realization of $\delta\mathbf{x}$. Now we add non-diagonal coupling between the spin and the charge degree of freedom $[\hat{V}_{so}]_{\text{non-diag}}$ from Eq. (10.4) and move to the adiabatic picture (See Eq. (10.22)), such that the unitary part of the AME reads:

$$\dot{\hat{\varrho}}_n(t) = -i\left[\hat{\mathscr{H}}(t, \delta\mathbf{x}), \hat{\varrho}_n(t)\right], \tag{A.6}$$

where $\hat{\varrho}_n$ can be understood as the density matrix for the nth realization of $\delta\mathbf{x}$. Its unitary evolution is generated by the Hamiltonian

$$\hat{\mathscr{H}}(t, \delta\mathbf{x}) = \hat{\mathscr{H}}_0(t, \delta\mathbf{x}) + \hat{\mathscr{V}}_{\text{so}}(t, \delta\mathbf{x}) + \frac{1}{2}\dot{\hat{\vartheta}}(t, \delta\mathbf{x})\hat{\varsigma}_y, \tag{A.7}$$

where $\dot{\hat{\vartheta}}(t, \delta\mathbf{x}) = \sum_{s=\uparrow,\downarrow} \dot{\vartheta}_s(t, \delta\mathbf{x})\,|s\rangle\langle s|$,[1] and the spin-coupling operator was given by $\hat{\mathscr{V}}_{\text{so}}(t, \delta\mathbf{x}) = \hat{S}^\dagger(t, \delta\mathbf{x})[\hat{V}_{\text{so}}]_{\text{non-diag}}\hat{S}(t, \delta\mathbf{x})$, which is given by Eq. (10.22) but with realisation-dependent $\vartheta_s(t, \delta\mathbf{x})$.

1: where

$$\vartheta_s(t, \delta\mathbf{x}) = \operatorname{acot}\left(\frac{\epsilon(t) + \delta\epsilon}{t_c + \delta t_c}\right)$$

High-frequency noise

We now deal with high-frequency noise related to transverse coupling between the charge degree of freedom and the environment, i.e.:

$$\hat{V}_{\mathrm{oe}} = \frac{1}{2}\left(\hat{\sigma}_z\hat{V}_z + \hat{\sigma}_x\hat{V}_x\right). \tag{A.8}$$

We assume that the $\delta\mathbf{x}$ is too small to modify the spectral density of the environment, but will possibly modify the orbital angle $\vartheta_s(t,\delta\mathbf{x})$. We start by computing relaxation rates as a function of the energy gap for each relaxation mechanism $\Gamma_{-,i}(\Omega[t])$ for $i = x, z$. From Eq. (3.7) we associate the relaxation rate for the s spin component with the spectral density of the transverse coupling, i.e.

$$\Gamma_{-,i}(\Omega_s[t],\delta\mathbf{x}) = \frac{1}{4}|d_{\perp,i,s}(t,\mathbf{x})|^2 S_i(\Omega_s[t]), \tag{A.9}$$

where $S_i(\Omega_s[t]) = \int \mathrm{d}t\,\mathrm{Tr}\{\hat{V}_i'(t)\hat{V}_i'(0)\hat{\rho}_e\}e^{-i\Omega_s t}$ with $\hat{\rho}_e$ as a density matrix of the environment, and $\hat{V}_i'(t)$ is the environmental operator in the interaction picture with respect to environmental Hamiltonian $\hat{H}_e$. To compute the transverse dipole moment for each spin component, we use the instantaneous states of the Hamiltonian $\hat{\mathscr{H}}_0(t,\delta\mathbf{x})\,|\pm(t),s\rangle$ from Eq. (A.3) i.e.

$$|d_{\perp,i,s}(t,\delta\mathbf{x})|^2 = \langle +(t),s|\,\hat{\sigma}_i\,|-(t),s\rangle + \mathrm{h.c.}, \tag{A.10}$$

which for considered Landau-Zener drive of the orbital states give $|d_{\perp,x,s}|^2 = \cos^2\vartheta_s = (\epsilon + \sigma_s\frac{\Delta E_z}{2})^2/\Omega_s^2$ and $|d_{\perp,z,s}|^2 = t_c^2/\Omega_s^2 = \sin^2\vartheta_s$ for each spin component $s = \uparrow,\downarrow$. Finally we relate the relaxation rates with the excitation rates using the Boltzman Factor $\Gamma_{+,i}(\Omega_s[t]) = \Gamma_{-,i}(\Omega_s[t])e^{-\beta\Omega_s(t)}$ and with their help construct the Linblad operators for each spin component $s = \uparrow,\downarrow$:

$$\hat{L}_{s,\pm}(t,\delta\mathbf{x}) = \sqrt{\Gamma_{\pm,i}(\Omega_s[t],\delta\mathbf{x})}\hat{\varsigma}_{\pm}, \tag{A.11}$$

where $\Omega_s(t) = \Omega(t) + \frac{1}{2}\sigma_s\Delta\Omega(t)$ with $\sigma_\uparrow = 1$ and $\sigma_\downarrow = -1$. The resulting parameters are substituted to the adiabatic Master equation in the Linblad form:

$$\dot{\hat{\varrho}}_n(t) = -i[\hat{\mathscr{H}}(t),\hat{\varrho}_n(t)] - \sum_{k=s,\pm}\left(\hat{L}_k(t)\hat{\varrho}_n(t)\hat{L}_k^\dagger(t) - \frac{1}{2}\{\hat{L}_k^\dagger(t)\hat{L}_k(t),\hat{\varrho}_n(t)\}\right), \tag{A.12}$$

where for brevity we neglected dependance on $\delta\mathbf{x}$, i.e. in the above $\hat{\mathscr{H}}(t) \equiv \hat{\mathscr{H}}(t,\delta\mathbf{x})$ and $\hat{L}_k(t) \equiv \hat{L}_k(t,\delta\mathbf{x})$. The above differential equation for the operators can generate at least 10 coupled differential equations for the possibly complex elements of four-by-four density matrix $\langle d,s|\,\varrho_n(t)\,|d',s'\rangle$, the time evolution of which can be solved numerically. We use here Runge-Kutta method of the 4th order with sufficiently small step size, which in the units of time correspond to $\delta t = 10^{-4}$ns.

We finally average each element of density matrix over N realizations of $\delta\mathbf{x}$ such that for instance the spin coherence in the ground state is given by:

$$W_-(t) = \frac{1}{N}\sum_n \langle -,\uparrow|\,\hat{\varrho}_n(t)\,|-,\downarrow\rangle\,. \tag{A.13}$$

A.2 Physical justification and limitations of the model

The presented above numerical approach to some extend treats low- and high-frequency noise as independent, using classical quasistatic model for the former and quantum Master equation approach for the latter. Additionally in the analytical analysis we related the dephasing to longitudinal coupling and dissipation with the transverse coupling and dealt with their effects on two-level systems separately. We now discuss physics of such separate treatment and discuss its limitations.

Statistical independence

In many physical situations the longitudinal and transverse noise, are caused by a different weakly coupled physical system, which makes the above assumption natural. Even if this is not the case, we showed that both contributions depends on distinct frequencies of environmental noise. The effect of transverse noise depends on the fluctuations with frequency close to the gap Ω, while longitudinal noise depends on the environmental frequencies below the inverse of experimental time π/t. As a result as long as relation $\Omega t \geq \pi$ holds, both effects are well separated in frequency space and hence can be regarded as independent. For instance for the qubit Larmor frequency of 10GHz (Energy gap of $\sim 40\mu$eV) this condition is fulfilled for any experiment that lasts for at least $t > 10$ns.

In principle both transverse and longitudinal contributions are expected to come from the sum of macroscopic number of the fluctuators, with various correlation times (see 1/f noise modeling in Sec. 12). In such case the slowly varying fluctuators would contribute only to dephasing, while only the ones with characteristic frequency in resonance with the gap, can exchange the energy with the qubit. In such a model statistical independence between fast and slow fluctuators depends on the mutual coupling between them. For small enough coupling it can be neglected on the timescales of the experiment. Additionally in the typical experiments the possibility to initialize in the qubit ground state requires to keep the thermal energy of environment below the gap $\beta\Omega \geqslant 1$. This means high-frequency (transverse) part of environment has non-trivial Boltzman factor $e^{-\beta\Omega} \leq 1$, while the low-frequency (longitudinal) part is typically classical, i.e. $e^{-i\beta\omega_{\mathrm{qs}}} \approx 1$ as it related to the frequencies (energies) below the $\omega_{\mathrm{qs}} = \pi/t$.

Small error regime

Motivated by recent progress in quantum information process we concentrated on relatively small error regime in which the expression for the transverse and longitudinal coupling can be treated in the leading order in the coupling (See Chapter 3 and Chapter 4). For the transverse noise of the short correlation time weak coupling is enough to justify Master equation approach. Secondly as shown in Sec. Chapter 4, the dephasing

errors due to dissipative and non-dissipative terms are additive in the leading order, i.e.

$$\delta W = \delta W_\phi + \delta W_\perp, \tag{A.14}$$

where contribution from pure dephasing term $\hat{V}_\phi$ is denoted as δW_ϕ and given by Eq. (4.13), while contribution from the dissipative evolution denoted as $\delta W_\perp$ was derived in Eq. (3.22). The weak coupling limit additionally justifies Gaussian approximation of the classical noise.

Based on the arguments above we conclude that separate treatment of low- and high-frequency noise should be suitable for near-term devices operating close to the estimated threshold, needed for operating error correction codes $\Delta \leq 10^{-2}$.

We expect the approximation to be invalid, when the transition rates becomes significantly modified by the shift of energy gap due to longitudinal noise. This can happen either due to strong coupling between qubit and environment $\Delta\Omega \sim \Omega$ or in presence of not flat enough spectral density of the environment, where in both cases $\Gamma' \propto S(\Omega + \xi) \neq S(\Omega)$. Also strong environment-qubit coupling would put in question validity of secular approximation leading to a Linblad form of master equation from Eq. (5.70), which eventually would introduce additional Ω-dependant phases in the equations of motion and correlate effects of low- and high-frequency environment.

A.3 Numerical tests

We now use the method of *averaged adiabatic Master equation* described in Sec. A.1 and verify it against direct averaging over the classical Ornstein-Uhlenbeck process from Sec. 4.4 for various correlation times, and for the cases of undriven and driven TLS and also compute the resulting loss of spin coherence during interdot transition.

Undriven case

For the undriven case of TLS we use a single O-U process, which has been introduced in Sec. 4.4. We use the relative angle between the quantization axis of the qubit and the direction along which the noise fluctuates α_{ou}, which can be used to switch between transverse $\alpha_{\mathrm{ou}} = \pi/2$ and longitudinal coupling $\alpha_{\mathrm{ou}} = 0$. The Hamiltonian thus reads:

$$\hat{H} = \frac{\Omega}{2}\hat{\sigma}_z + \frac{\xi_{\mathrm{ou}}(t)}{2}\left(\cos\alpha_{\mathrm{ou}}\hat{\sigma}_z + \sin\alpha_{\mathrm{ou}}\hat{\sigma}_x\right). \tag{A.15}$$

where the correlation function of $\langle\xi_{\mathrm{ou}}(t)\xi_{\mathrm{ou}}(0)\rangle = \sigma^2 e^{-|t|/\tau_c}$ is parameterized by the noise power σ^2 and the correlation time τ_c.

We now compute transition rates $\Gamma_\pm$ and amplitude of effective dephasing noise $\tilde{\sigma}$. Due to classical nature of the noise the relaxation and excitation rates are equal and given by:

$$\Gamma_- = \Gamma_+ = \frac{1}{2}\frac{\sigma^2 \sin^2\alpha_{\mathrm{ou}}\tau_c}{1 + (\Omega\tau_c)^2}. \tag{A.16}$$

Next, the amplitude of dephasing noise can be computed as:

$$\tilde{\sigma}^2(t) = \cos^2\alpha_{\rm ou}\int_{-\pi/t}^{\pi/t}\frac{S_{\rm ou}(\omega)}{2\pi} = \cos^2\alpha_{\rm ou}\frac{2}{\pi}\sigma_\phi^2\arctan(\pi\tau_c/t). \quad \text{(A.17)}$$

Due to lack of divergence at low-frequencies we neglect here effect of finite data acquisition time T_a (see Sec. 4.4 for the case of 1/f where it is relevant).

Numerical results

To test the evolution generated by the noise we initialize the qubit in the weighted superposition state for azimuth angle $\theta = \pi/3$:

$$|\psi(0)\rangle = \frac{\sqrt{3}}{2}|\uparrow\rangle + \frac{1}{2}|\downarrow\rangle\,, \quad \text{(A.18)}$$

for which initial polarization $Z(0) = 1/2$ and coherence $W(0) = \sqrt{3}/2$. Due to infinite temperature $Z_\beta = 0$ and hence according to fast-slow approximation the time-dependence of the observables reads:

$$\begin{aligned} Z(t) &= \frac{1}{2}\exp\left(-\frac{\sigma^2\sin^2\alpha_{\rm ou}\tau_c t}{1+(\Omega\tau_c)^2}\right),\\ W(t) &= \sqrt{\frac{3}{2}Z(t)}\exp\left\{-\frac{(\sigma\cos\alpha_{\rm ou}t)^2}{\pi}\arctan(\pi\tau_c/t)\right\} = W_0 e^{-\chi(t)}, \end{aligned} \quad \text{(A.19)}$$

where decoherence factor reads:

$$\chi(t) = \frac{1}{2}\sigma^2 t\left(t\cos^2\alpha_{\rm ou}\frac{2\arctan(\pi\tau_c/t)}{\pi} + \sin^2\alpha_{\rm ou}\frac{\tau_c}{1+(\Omega\tau_c)^2}\right) \quad \text{(A.20)}$$

Below in Fig. A.2 we compare analytical predictions (lines) against numerical simulations of qubit evolution averaged over $N = 10000$ realizations of O-U process (points). We fix evolution time as $\Omega t_f = 10$ and use two methods to obtain noise amplitude. In Fig. A.2a) we fix the noise power, i.e. $\sigma^2 = (0.1\Omega)^2$ and in the Fig. A.2b) we fix the spectrum at $\omega = 0$, i.e. $S_{\rm ou}(0) = 2$, or equivalently $\sigma^2\tau_c = 1$. In general the analytical predictions based on the independent treatment of transverse and longitudinal noise component (symbols) agree with the numerical simulations. As expected in the limit of slow noise, i.e. $\Omega\tau_c \gg 1$ the influence of the noise, independent of the tilt angle and noise power the $Z(t_f) \approx Z(0)$ (dashed lines and crosses). For fixed noise power $\sigma = \text{const}$ in Fig. A.2a) decreasing correlation time (i.e making the noise faster) decreases spectral density at the gap and hence the modification to $Z(t)$ is visible only around $\Omega\tau_c \approx 1$. In the same figure in the regime of slow noise $\Omega\tau_c \gg 1$ the dephasing becomes stronger as the noise is more longitudinal and effectively vanishes for purely transverse noise (blue solid line and dots). In fact slow decay of coherence can be observed for the numerical data (blue points), which is associated with the renormalization of the energy gap due to slow transverse noise. This effect cannot be encapsulated by the current model, but it is relatively small for relevant here weak coupling (small σ)

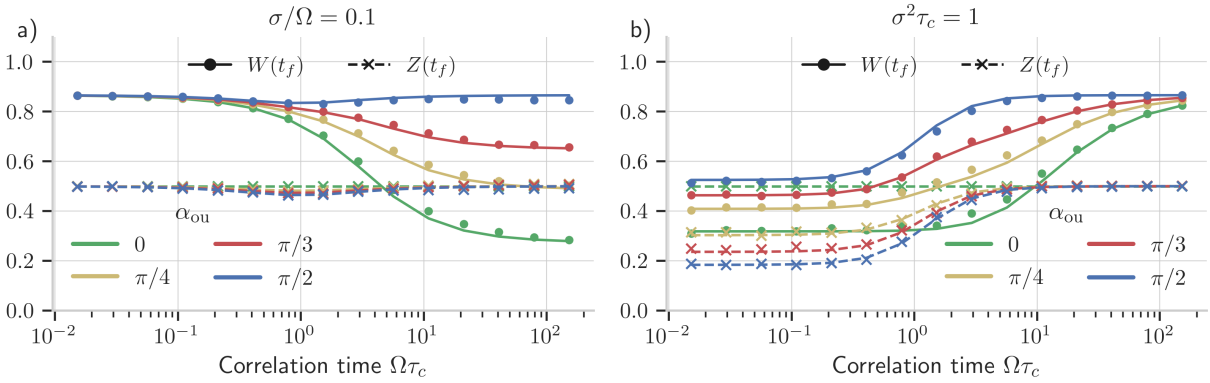

Figure A.2: Dephasing and dissipation of the stationary two-level system. We compare the analytical result based on the independent treatment of low- and high-frequency noise from Eq. (A.19) (solid lines) and numerical simulation of the evolution averaged over realization of the O-U process (symbols) with a) $\sigma = 0.1\Omega$ and b) $\sigma = \sqrt{1/\tau_c}$. With each color we denote different orientation of the noise field (See Eq. (A.15), i.e. $\alpha = 0$ (green) means longitudinal and $\alpha = \pi/2$ (blue) full transverse noise. We plot simultaneously coherence $W(t)$ (solid lines and dots) and polarization $Z(t)$ (dashed line and crosses) of the two-level system. We average over $N = 10000$ realizations of the noise.

In the opposite case of fixed relaxation rate Fig. A.2a) the dephasing in the fast noise limit $\Omega\tau_c \ll 1$ is mostly caused by the disssipative evolution, which can be seen by the simultaneous change in $Z(t)$ and $W(t)$. With fixed relaxation rate, the limit of slow noise $\Omega\tau_c \gg 1$ means the power of decreases as τ_c is larger and hence in the right hand side of the plot both dephasing and dissipation are weak.

Driven two-level system

For a test of driven two-level system we refer to Fig. 8.4 and discussion around it, where we concentrated on the charge transfer without considering spin degree of freedom. In the figure we clearly see the correspondence between the results of the adiabatic master equation for driven two-level system (solid lines) and the results obtained by directly averaging classical realizations of the noise process, which here was associated with 1/f noise constructed from multiple O-U processes.

Driven four-level system

We finally compare the prediction of the averaged Adiabatic master approach against direct averaging over two independent O-U noise process, representing classical noise in tunnel coupling δt_c and detuning $\delta\epsilon$, such that for each realization:

$$\hat{H}_{\mathrm{ou}}(t) = \frac{\epsilon(t) + \delta\epsilon(t)}{2}\hat{\sigma}_z + \frac{t_c + \delta t_c(t)}{2}\hat{\sigma}_x + \frac{E_z}{2}\hat{\sigma}_z + \hat{V}_{so}(t). \qquad \text{(A.21)}$$

We compute the evolution using the RK4 method using $N = 100$ realisations of the O-U processes with $\sigma_\epsilon = 5\mu\mathrm{eV}^2$ and $\sigma_{t_c} = 0.5\mu\mathrm{eV}$ and compare against method of averaged Master equation with the relaxation rates computed using spectral density of the O-U noise. The results are plotted in Fig. A.3, where the spin coherence in the ground orbital state is plotted as a function of sweep rate, which is analogous figure to the one presented in Chapter 12. In the figure we can observe the general agreement between the averaged Master equation method (lines) and the averaging over noise processes (symbols). Note however that in order

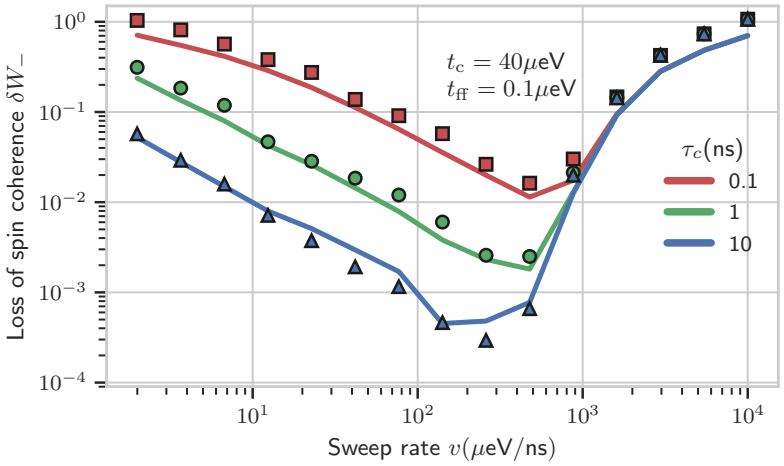

Figure A.3: Loss of spin coherence during adiabatic transition computed by averaging the evolution over realizations of Ornstein-Uhlembeck process (symbols) and the averaged adiabatic Master equation method in infinite temperature (lines). We use $N = 100$ realisations of the tunnel coupling and detuning noise of the respective powers $\sigma_\epsilon^2 = 5^2\ \mu\text{eV}^2$ and $\sigma_{t_c}^2 = 0.5^2\ \mu\text{eV}^2$. $t_c = 40\,\mu$eV, $t_{\text{ff}} = 0.1\mu\,$eV

to compare the two we had to assume effectively infinite temperature, such that the excitation rate was equal to relaxation rate. For this reason the physical analysis of the result is difficult. We highlight however that for assumed here fixed noise amplitude $\sigma_\epsilon^2 = 5^2\mu$eV the relaxation (and excitation) rate at the avoided crossing decreases as the correlation time increase. This is visible, as the smallest phase error is provided by the blue line corresponding to longest correlation time. Apart from small region around $v \approx 100\mu$eV/ns the $\delta W_- \propto v$ points towards phase error caused by high frequency noise and possibly charge transfer error. Note that due to classical nature of the noise, the relaxation aided transfer is impossible in this case.

Bibliography

Here are the references in citation order.

[1] J. A. Krzywda and Ł. Cywiński, 'Adiabatic electron charge transfer between two quantum dots in presence of 1/f noise', Physical Review B **101**, 035303 (2020) (cited on pages v, 7, 8, 15, 38, 85, 88, 89, 133).

[2] J. A. Krzywda and Ł. Cywińnski, 'Interplay of charge noise and coupling to phonons in adiabatic electron transfer between quantum dots', Physical Review B **104**, 075439 (2021) (cited on pages v, 8, 15, 48, 49, 67, 70, 85, 91, 92, 95, 97, 98, 113, 156).

[3] V. Langrock, J. A. Krzywda, N. Focke, I. Seidler, L. R. Schreiber, and Ł. Cywiński, 'Blueprint of a scalable spin qubit shuttle device for coherent mid-range qubit transfer in disordered Si/SiGe/SiO$_2$', 10.48550/arXiv.2202.11793 (2022) (cited on pages v, 6, 8, 63, 157–160).

[4] J. Krzywda, P. Szańkowski, and Ł. Cywiński, 'The dynamical-decoupling-based spatiotemporal noise spectroscopy', New Journal of Physics **21**, 043034 (2019) (cited on pages v, 34, 162).

[5] J. Krzywda, P. Szańkowski, J. Chwedeńczuk, and Ł. Cywiński, 'Decoherence-assisted detection of entanglement of two qubit states', Physical Review A **98**, 022329 (2018) (cited on pages v, 34, 162).

[6] P. Szańkowski, G. Ramon, J. Krzywda, D. Kwiatkowski, and Ł. Cywiński, 'Environmental noise spectroscopy with qubits subjected to dynamical decoupling', Journal of Physics: Condensed Matter **29**, 333001 (2017) (cited on pages v, 3, 34, 36, 74, 162).

[7] J. Krzywda, Ł. Cywiński, and P. Szańkowski, 'Localization of a magnetic moment using a two-qubit probe', Physical Review A **96**, 042108 (2017) (cited on pages v, 34, 162).

[8] J. Krzywda and K. Roszak, 'Phonon-mediated generation of quantum correlations between quantum dot qubits', Scientific Reports **6**, 23753 (2016) (cited on page v).

[9] L. K. Grover, 'A fast quantum mechanical algorithm for database search', in Proceedings of the twenty-eighth annual ACM symposium on Theory of computing - STOC '96 (1996), pp. 212–219 (cited on page 1).

[10] P. W. Shor, 'Polynomial-time algorithms for prime factorization and discrete logarithms on a quantum computer', SIAM Journal on Computing **26**, 1484–1509 (1997) (cited on page 1).

[11] S. Lloyd, 'Universal Quantum Simulators', Science **273**, 1073–1078 (1996) (cited on page 1).

[12] F. Arute et al., 'Quantum supremacy using a programmable superconducting processor', Nature **574**, 505–510 (2019) (cited on page 1).

[13] Y. Wu et al., 'Strong quantum computational advantage using a superconducting quantum processor', Physical Review Letters **127**, 180501 (2021) (cited on page 1).

[14] I. Pogorelov et al., 'Compact Ion-Trap Quantum Computing Demonstrator', PRX Quantum **2**, 020343 (2021) (cited on page 1).

[15] A. Bouland, B. Fefferman, C. Nirkhe, and U. Vazirani, 'On the complexity and verification of quantum random circuit sampling', Nature Physics **15**, 159–163 (2019) (cited on page 1).

[16] K. Bharti et al., 'Noisy intermediate-scale quantum algorithms', Reviews of Modern Physics **94**, 015004 (2022) (cited on page 1).

[17] J. Preskill, 'Quantum Computing in the NISQ era and beyond', Quantum **2**, 79 (2018) (cited on page 1).

[18] E. Bäumer, N. Gisin, and A. Tavakoli, 'Demonstrating the power of quantum computers, certification of highly entangled measurements and scalable quantum nonlocality', npj Quantum Information **7**, 117 (2021) (cited on page 1).

[19] C. Wang et al., 'Towards practical quantum computers: transmon qubit with a lifetime approaching 0.5 milliseconds', npj Quantum Information **8**, 3 (2022) (cited on page 1).

[20]F. A. Zwanenburg et al., 'Silicon quantum electronics', Reviews of Modern Physics **85**, 961–1019 (2013) (cited on pages 1, 2, 63, 68, 157).

[21]D. Loss and D. P. DiVincenzo, 'Quantum computation with quantum dots', Physical Review A **57**, 120–126 (1998) (cited on pages 1, 3).

[22]L. M. K. Vandersypen et al., 'Interfacing spin qubits in quantum dots and donors—hot, dense, and coherent', npj Quantum Information **3**, 34 (2017) (cited on pages 1, 4).

[23]J. M. Boter et al., 'The spider-web array–a sparse spin qubit array', `10.48550/arXiv.2110.00189` (2021) (cited on pages 1, 4).

[24]G. Scappucci et al., 'The germanium quantum information route', Nature Reviews Materials **6**, 926–943 (2021) (cited on pages 1, 68).

[25]D. P. DiVincenzo, 'The Physical Implementation of Quantum Computation', Fortschritte der Physik **48**, 771–783 (2000) (cited on page 1).

[26]A. V. Kuhlmann et al., 'Charge noise and spin noise in a semiconductor quantum device', Nature Physics **9**, 570–575 (2013) (cited on page 1).

[27]E. J. Connors, J. Nelson, L. F. Edge, and J. M. Nichol, 'Charge-noise spectroscopy of Si/SiGe quantum dots via dynamically-decoupled exchange oscillations', Nature Communications **13**, 940 (2022) (cited on pages 1, 37, 74, 80).

[28]H. Bluhm, S. Foletti, I. Neder, M. Rudner, D. Mahalu, V. Umansky, and A. Yacoby, 'Dephasing time of GaAs electron-spin qubits coupled to a nuclear bath exceeding 200 μs', Nature Physics **7**, 109–113 (2011) (cited on pages 2, 3, 68).

[29]F. K. Malinowski et al., 'Spectrum of the Nuclear Environment for GaAs Spin Qubits', Physical Review Letters **118**, 177702 (2017) (cited on pages 2, 21).

[30]G. Burkard, T. D. Ladd, J. M. Nichol, A. Pan, and J. R. Petta, 'Semiconductor Spin Qubits', (2021) (cited on pages 2, 64, 68, 103, 104, 157).

[31]K. M. Itoh and H. Watanabe, 'Isotope engineering of silicon and diamond for quantum computing and sensing applications', MRS Communications **4**, 143–157 (2014) (cited on pages 2, 68).

[32]E. Kawakami et al., 'Electrical control of a long-lived spin qubit in a Si/SiGe quantum dot', Nature Nanotechnology **9**, 666–670 (2014) (cited on pages 2, 3, 68).

[33]R. Hanson, L. P. Kouwenhoven, J. R. Petta, S. Tarucha, and L. M. Vandersypen, 'Spins in few-electron quantum dots', Reviews of Modern Physics **79**, 1217–1265 (2007) (cited on pages 2, 64, 108).

[34]Z. Shi et al., 'Coherent quantum oscillations and echo measurements of a Si charge qubit', Physical Review B **88**, 075416 (2013) (cited on page 2).

[35]K. Wang, C. Payette, Y. Dovzhenko, P. W. Deelman, and J. R. Petta, 'Charge Relaxation in a Single-Electron Si / SiGe Double Quantum Dot', Physical Review Letters **111**, 046801 (2013) (cited on page 2).

[36]A. Hollmann et al., 'Large, Tunable Valley Splitting and Single-Spin Relaxation Mechanisms in a Si / Si x Ge 1 - x Quantum Dot', Physical Review Applied **13**, 034068 (2020) (cited on pages 2, 69).

[37]I. A. Merkulov, A. L. Efros, and M. Rosen, 'Electron spin relaxation by nuclei in semiconductor quantum dots', Physical Review B **65**, 205309 (2002) (cited on page 2).

[38]A. Ekert, 'Quantum Interferometers as Quantum Computers', Physica Scripta **T76**, 218 (1998) (cited on page 2).

[39]K. Takeda et al., 'A fault-tolerant addressable spin qubit in a natural silicon quantum dot', Science Advances **2**, e1600694 (2016) (cited on pages 2, 4).

[40]Ł. Cywiński, 'Dephasing of Electron Spin Qubits due to their Interaction with Nuclei in Quantum Dots', Acta Physica Polonica A **119**, 576–587 (2011) (cited on page 2).

[41]E. A. Chekhovich, M. N. Makhonin, A. I. Tartakovskii, A. Yacoby, H. Bluhm, K. C. Nowack, and L. M. K. Vandersypen, 'Nuclear spin effects in semiconductor quantum dots', Nature Materials **12**, 494–504 (2013) (cited on page 2).

[42]R. Zhao et al., 'Single-spin qubits in isotopically enriched silicon at low magnetic field', Nature Communications **10**, 5500 (2019) (cited on page 2).

[43]J. Yoneda et al., 'A quantum-dot spin qubit with coherence limited by charge noise and fidelity higher than 99.9%', Nature Nanotechnology **13**, 102–106 (2018) (cited on pages 2, 3, 37, 68).

[44]T. Struck et al., 'Low-frequency spin qubit energy splitting noise in highly purified 28Si/SiGe', npj Quantum Information **6**, 40 (2020) (cited on pages 2, 37).

[45]L. Viola, E. Knill, and S. Lloyd, 'Dynamical Decoupling of Open Quantum Systems', Physical Review Letters **82**, 2417–2421 (1999) (cited on page 3).

[46]A. M. Steane, 'Error Correcting Codes in Quantum Theory', Physical Review Letters **77**, 793–797 (1996) (cited on pages 3, 12).

[47]E. Knill and R. Laflamme, 'Theory of quantum error-correcting codes', Physical Review A **55**, 900–911 (1997) (cited on pages 3, 12).

[48]R. Laflamme, C. Miquel, J. P. Paz, and W. H. Zurek, 'Perfect Quantum Error Correcting Code', Physical Review Letters **77**, 198–201 (1996) (cited on pages 3, 12).

[49]S. J. Devitt, W. J. Munro, and K. Nemoto, 'Quantum error correction for beginners', Reports on Progress in Physics **76**, 076001 (2013) (cited on pages 3, 12).

[50]L. Childress and R. Hanson, 'Diamond NV centers for quantum computing and quantum networks', MRS Bulletin **38**, 134–138 (2013) (cited on pages 3, 61).

[51]B. E. Kane, 'A silicon-based nuclear spin quantum computer', Nature **393**, 133–137 (1998) (cited on pages 3, 61).

[52]A. Bracker et al., 'Optical Pumping of the Electronic and Nuclear Spin of Single Charge-Tunable Quantum Dots', Physical Review Letters **94**, 047402 (2005) (cited on pages 3, 61).

[53]J. Levy, 'Universal Quantum Computation with Spin- 1 / 2 Pairs and Heisenberg Exchange', Physical Review Letters **89**, 147902 (2002) (cited on page 3).

[54]F. Fedele, A. Chatterjee, S. Fallahi, G. C. Gardner, M. J. Manfra, and F. Kuemmeth, 'Simultaneous Operations in a Two-Dimensional Array of Singlet-Triplet Qubits', PRX Quantum **2**, 040306 (2021) (cited on page 3).

[55]J. R. Petta et al., 'Coherent Manipulation of Coupled Electron Spins in Semiconductor Quantum Dots', Science **309**, 2180–2184 (2005) (cited on pages 3, 4, 68).

[56]M. Russ and G. Burkard, 'Three-electron spin qubits', Journal of Physics: Condensed Matter **29**, 393001 (2017) (cited on page 3).

[57]J. Medford, J. Beil, J. M. Taylor, E. I. Rashba, H. Lu, A. C. Gossard, and C. M. Marcus, 'Quantum-Dot-Based Resonant Exchange Qubit', Physical Review Letters **111**, 050501 (2013) (cited on pages 3, 66, 133).

[58]M. Friesen, C. Tahan, R. Joynt, and M. A. Eriksson, 'Spin Readout and Initialization in a Semiconductor Quantum Dot', Physical Review Letters **92**, 037901 (2004) (cited on page 3).

[59]D. Press, T. D. Ladd, B. Zhang, and Y. Yamamoto, 'Complete quantum control of a single quantum dot spin using ultrafast optical pulses', Nature **456**, 218–221 (2008) (cited on page 3).

[60]M. Xiao, I. Martin, E. Yablonovitch, and H. W. Jiang, 'Electrical detection of the spin resonance of a single electron in a silicon field-effect transistor', Nature **430**, 435–439 (2004) (cited on page 3).

[61]J. M. Elzerman, R. Hanson, L. H. Willems van Beveren, B. Witkamp, L. M. K. Vandersypen, and L. P. Kouwenhoven, 'Single-shot read-out of an individual electron spin in a quantum dot', Nature **430**, 431–435 (2004) (cited on pages 3, 4).

[62]M. A. Nielsen and Isaac L. Chuang, Quantum computation and quantum information (Cambridge University Press, Cambridge, England, 2000) (cited on pages 3, 4).

[63]K. W. Chan et al., 'Assessment of a Silicon Quantum Dot Spin Qubit Environment via Noise Spectroscopy', Physical Review Applied **10**, 044017 (2018) (cited on pages 3, 68).

[64]F. H. L. Koppens, K. C. Nowack, and L. M. K. Vandersypen, 'Spin Echo of a Single Electron Spin in a Quantum Dot', Physical Review Letters **100**, 236802 (2008) (cited on pages 3, 68).

[65]F. K. Malinowski et al., 'Notch filtering the nuclear environment of a spin qubit', Nature Nanotechnology **12**, 16–20 (2017) (cited on pages 3, 68).

[66]N. I. Dumoulin Stuyck, F. A. Mohiyaddin, R. Li, M. Heyns, B. Govoreanu, and I. P. Radu, 'Low dephasing and robust micromagnet designs for silicon spin qubits', Applied Physics Letters **119**, 094001 (2021) (cited on page 4).

[67]C. H. Yang et al., 'Spin-valley lifetimes in a silicon quantum dot with tunable valley splitting', Nature Communications **4**, 2069 (2013) (cited on pages 4, 69).

[68]I. I. Rabi, S. Millman, P. Kusch, and J. R. Zacharias, 'The Molecular Beam Resonance Method for Measuring Nuclear Magnetic Moments. The Magnetic Moments of Li 6 3 , Li 7 3 and F 19 9', Physical Review **55**, 526–535 (1939) (cited on page 4).

[69]C. H. Yang et al., 'Operation of a silicon quantum processor unit cell above one kelvin', Nature **580**, 350–354 (2020) (cited on page 4).

[70]M. Pioro-Ladrière et al., 'Electrically driven single-electron spin resonance in a slanting Zeeman field', Nature Physics **4**, 776–779 (2008) (cited on page 4).

[71]K. C. Nowack, F. H. L. Koppens, Y. V. Nazarov, and L. M. K. Vandersypen, 'Coherent control of a single electron spin with electric fields', Science **318**, 1430–1433 (2007) (cited on page 4).

[72]M. Veldhorst et al., 'A two-qubit logic gate in silicon', Nature **526**, 410–414 (2015) (cited on page 4).

[73]T. F. Watson et al., 'A programmable two-qubit quantum processor in silicon', Nature **555**, 633–637 (2018) (cited on page 4).

[74]D. M. Zajac, A. J. Sigillito, M. Russ, F. Borjans, J. M. Taylor, G. Burkard, and J. R. Petta, 'Resonantly driven CNOT gate for electron spins', Science **359**, 439–442 (2018) (cited on page 4).

[75]K. Takeda, A. Noiri, T. Nakajima, T. Kobayashi, and S. Tarucha, 'Quantum error correction with silicon spin qubits', 10.48550/arXiv.2201.08581 (2022) (cited on page 4).

[76]D. P. DiVincenzo, D. Bacon, J. Kempe, G. Burkard, and K. B. Whaley, 'Universal quantum computation with the exchange interaction', Nature **408**, 339–342 (2000) (cited on page 4).

[77]K. W. Chan et al., 'Exchange Coupling in a Linear Chain of Three Quantum-Dot Spin Qubits in Silicon', Nano Letters **21**, 1517–1522 (2021) (cited on page 4).

[78]H. Qiao, Y. P. Kandel, S. Fallahi, G. C. Gardner, M. J. Manfra, X. Hu, and J. M. Nichol, 'Long-Distance Superexchange between Semiconductor Quantum-Dot Electron Spins', Physical Review Letters **126**, 017701 (2021) (cited on page 4).

[79]F. Vigneau et al., 'Probing quantum devices with radio-frequency reflectometry', 10.48550/arXiv.2202.10516 (2022) (cited on page 4).

[80]B. Buonacorsi et al., 'Network architecture for a topological quantum computer in silicon', Quantum Science and Technology **4**, 025003 (2019) (cited on page 4).

[81]M. Friesen, A. Biswas, X. Hu, and D. Lidar, 'Efficient Multiqubit Entanglement via a Spin Bus', Physical Review Letters **98**, 230503 (2007) (cited on page 5).

[82]A. J. Sigillito, M. J. Gullans, L. F. Edge, M. Borselli, and J. R. Petta, 'Coherent transfer of quantum information in a silicon double quantum dot using resonant SWAP gates', npj Quantum Information **5**, 110 (2019) (cited on page 5).

[83]A. D. Greentree, J. H. Cole, A. R. Hamilton, and L. C. L. Hollenberg, 'Coherent electronic transfer in quantum dot systems using adiabatic passage', Physical Review B **70**, 235317 (2004) (cited on page 5).

[84]Y. P. Kandel, H. Qiao, and J. M. Nichol, 'Perspective on exchange-coupled quantum-dot spin chains', Applied Physics Letters **119**, 030501 (2021) (cited on page 5).

[85]M. Benito, X. Mi, J. M. Taylor, J. R. Petta, and G. Burkard, 'Input-output theory for spin-photon coupling in Si double quantum dots', Physical Review B **96**, 235434 (2017) (cited on pages 5, 7, 72).

[86]P. Harvey-Collard, J. Dijkema, G. Zheng, A. Sammak, G. Scappucci, and L. M. K. Vandersypen, 'Circuit quantum electrodynamics with two remote electron spins', 10.48550/arXiv.2108.01206 (2021) (cited on page 5).

[87]N. Samkharadze et al., 'Strong spin-photon coupling in silicon', Science **359**, 1123–1127 (2018) (cited on pages 5, 7).

[88]X. Mi, M. Benito, S. Putz, D. M. Zajac, J. M. Taylor, G. Burkard, and J. R. Petta, 'A coherent spin–photon interface in silicon', Nature **555**, 599–603 (2018) (cited on pages 5, 7, 66).

[89]A. J. Skinner, M. E. Davenport, and B. E. Kane, 'Hydrogenic Spin Quantum Computing in Silicon: A Digital Approach', Physical Review Letters **90**, 087901 (2003) (cited on page 5).

[90]P. Huang and X. Hu, 'Spin qubit relaxation in a moving quantum dot', Physical Review B **88**, 075301 (2013) (cited on pages 5, 75, 158).

[91]C. H. W. Barnes, J. M. Shilton, and A. M. Robinson, 'Quantum computation using electrons trapped by surface acoustic waves', Physical Review B **62**, 8410–8419 (2000) (cited on page 5).

[92]S. Takada et al., 'Sound-driven single-electron transfer in a circuit of coupled quantum rails', Nature Communications **10**, 4557 (2019) (cited on pages 6, 73).

[93]B. Jadot et al., 'Distant spin entanglement via fast and coherent electron shuttling', Nature Nanotechnology **16**, 570–575 (2021) (cited on pages 6, 68, 73).

[94]H. Flentje, P.-A. Mortemousque, R. Thalineau, A. Ludwig, A. D. Wieck, C. Bäuerle, and T. Meunier, 'Coherent long-distance displacement of individual electron spins', Nature Communications **8**, 501 (2017) (cited on pages 6, 46, 73).

[95]B. Bertrand et al., 'Fast spin information transfer between distant quantum dots using individual electrons', Nature Nanotechnology **11**, 672–676 (2016) (cited on pages 6, 73).

[96]I. Seidler, T. Struck, R. Xue, N. Focke, S. Trellenkamp, H. Bluhm, and L. R. Schreiber, 'Conveyor-mode single-electron shuttling in Si/SiGe for a scalable quantum computing architecture', 10.48550/arXiv.2108.00879 (2021) (cited on page 6).

[97]S. N. Shevchenko, S. Ashhab, and F. Nori, 'Landau-Zener-Stückelberg Interferometry', Physics Reports **492**, 1–30 (2010) (cited on pages 6, 7, 9, 45, 124, 163).

[98]A. R. Mills, D. M. Zajac, M. J. Gullans, F. J. Schupp, T. M. Hazard, and J. R. Petta, 'Shuttling a single charge across a one-dimensional array of silicon quantum dots', Nature Communications **10**, 1063 (2019) (cited on pages 6, 67, 98).

[99]T. A. Baart, M. Shafiei, T. Fujita, C. Reichl, W. Wegscheider, and L. M. K. Vandersypen, 'Single-spin CCD', Nature Nanotechnology **11**, 330–334 (2016) (cited on page 6).

[100]J. Yoneda et al., 'Coherent spin qubit transport in silicon', Nature Communications **12**, 4114 (2021) (cited on pages 6, 92).

[101]A. Noiri, K. Takeda, T. Nakajima, T. Kobayashi, A. Sammak, G. Scappucci, and S. Tarucha, 'A shuttling-based two-qubit logic gate for linking distant silicon quantum processors', 10.48550/ARXIV.2202.01357 (2022) (cited on pages 6, 67, 92).

[102]V. L. Pokrovsky and D. Sun, 'Fast quantum noise in the Landau-Zener transition', Physical Review B **76**, 024310 (2007) (cited on pages 6, 7).

[103]M. Yamaguchi, T. Yuge, and T. Ogawa, 'Markovian quantum master equation beyond adiabatic regime', Physical Review E **95**, 012136 (2017) (cited on pages 6, 7).

[104]A. J. Leggett, S. Chakravarty, A. T. Dorsey, M. P. A. Fisher, A. Garg, and W. Zwerger, 'Dynamics of the dissipative two-state system', Reviews of Modern Physics **59**, 1–85 (1987) (cited on page 6).

[105]S. Javanbakht, P. Nalbach, and M. Thorwart, 'Dissipative Landau-Zener quantum dynamics with transversal and longitudinal noise', Physical Review A: Atomic, Molecular, and Optical Physics **91**, 052103 (2015) (cited on page 6).

[106]D. Zueco, P. Hänggi, and S. Kohler, 'Landau–Zener tunnelling in dissipative circuit QED', New Journal of Physics **10**, 115012 (2008) (cited on page 6).

[107]K. Saito and Y. Kayanuma, 'Nonadiabatic Electron Manipulation in Quantum Dot Arrays', Physical Review B **70**, 1–4 (2004) (cited on page 6).

[108]M. B. Kenmoe and L. C. Fai, 'Adiabatic Landau-Zener transitions at avoided level crossings with fast noise', Annals of Physics **362**, 814–837 (2015) (cited on page 6).

[109]P. Nalbach, 'Adiabatic-Markovian bath dynamics at avoided crossings', Physical Review A **90**, 042112 (2014) (cited on pages 7, 51).

[110]T. Albash, S. Boixo, Daniel A Lidar, and Paolo Zanardi, 'Quantum adiabatic Markovian master equations', New Journal of Physics **14**, 123016 (2012) (cited on pages 7, 51).

[111]L. Arceci, S. Barbarino, R. Fazio, and G. E. Santoro, 'Dissipative Landau-Zener problem and thermally assisted Quantum Annealing', Physical Review B **96**, 054301 (2017) (cited on pages 7, 51, 96).

[112]P. Ao and J. Rammer, 'Influence of dissipation on the Landau-Zener transition', Physical Review Letters **62**, 3004–3007 (1989) (cited on page 7).

[113]Y. Kayanuma and H. Nakayama, 'Nonadiabatic transition at a level crossing with dissipation', Physical Review B **57**, 13099–13112 (1998) (cited on page 7).

[114]V. L. Pokrovsky and N. A. Sinitsyn, 'Fast noise in the Landau-Zener theory', Physical Review B **67**, 1–11 (2003) (cited on page 7).

[115]Z.-X. Luo and M. E. Raikh, 'Landau-Zener transition driven by slow noise', Physical Review B **95**, 064305 (2017) (cited on pages 7, 48).

[116]R. K. Malla, E. G. Mishchenko, and M. E. Raikh, 'Suppression of the Landau-Zener transition probability by weak classical noise', Physical Review B **96**, 075419 (2017) (cited on pages 7, 43, 48).

[117]J. I. Vestgarden, J. Bergli, and Y. M. Galperin, 'Nonlinearly driven Landau-Zener transition with telegraph noise', Physical Review B **77**, 014514 (2008) (cited on page 7).

[118]T. Nakajima et al., 'Coherent transfer of electron spin correlations assisted by dephasing noise', Nature Communications **9**, 2133 (2018) (cited on pages 7, 67).

[119]N. A. Sinitsyn and N. Prokof'ev, 'Nuclear spin bath effects on Landau-Zener transitions in nanomagnets', Physical Review B **67**, 1–5 (2003) (cited on page 7).

[120]J.-D. Chen, X.-D. Wen, G.-Z. Sun, and Y. Yu, 'Landau—Zener—Stückelberg interference in a multi-anticrossing system', Chinese Physics B **20**, 088501 (2011) (cited on page 7).

[121]S. Ashhab, 'Landau-Zener transitions in an open multilevel quantum system', Physical Review A **94**, 042109 (2016) (cited on page 7).

[122]J. Stehlik, M. Z. Maialle, M. H. Degani, and J. R. Petta, 'Role of multilevel Landau-Zener interference in extreme harmonic generation', Physical Review B **94**, 075307 (2016) (cited on page 7).

[123]M. B. Kenmoe, H. N. Phien, M. N. Kiselev, and L. C. Fai, 'Effects of colored noise on Landau-Zener transitions: Two- and three-level systems', Physical Review B **87**, 10.1103/PhysRevB.87.224301 (2013) (cited on page 7).

[124]I. Nyisomeh, M. Ateuafack, and L. Fai, 'Noise-induced multilevel Landau–Zener transitions: Density matrix investigation', Physics Letters A **383**, 1350–1356 (2019) (cited on page 7).

[125]F. Ginzel, A. R. Mills, J. R. Petta, and G. Burkard, 'Spin shuttling in a silicon double quantum dot', Physical Review B **102**, 195418 (2020) (cited on page 7).

[126]X. Zhao and X. Hu, 'Coherent electron transport in silicon quantum dots', 10.48550/arXiv.1803.00749 (2019) (cited on page 7).

[127]B. Buonacorsi, B. Shaw, and J. Baugh, 'Simulated coherent electron shuttling in silicon quantum dots', Physical Review B **102**, 125406 (2020) (cited on page 7).

[128]S. N. Shevchenko, A. I. Ryzhov, and F. Nori, 'Low-frequency spectroscopy for quantum multilevel systems', Physical Review B **98**, 1–8 (2018) (cited on page 7).

[129]T. Bonsen, P. Harvey-Collard, M. Russ, J. Dijkema, A. Sammak, G. Scappucci, and L. M. K. Vandersypen, 'Probing the Jaynes-Cummings ladder with spin circuit quantum electrodynamics', 10.48550/arXiv.2203.05668 (2022) (cited on page 7).

[130]M. Gawełczyk, M. Krzykowski, K. Gawarecki, and P. Machnikowski, 'Controllable electron spin dephasing due to phonon state distinguishability in a coupled quantum dot system', Physical Review B **98**, 075403 (2018) (cited on page 7).

[131]R. J. Schoelkopf, A. A. Clerk, S. M. Girvin, K. W. Lehnert, and M. H. Devoret, 'Qubits as Spectrometers of Quantum Noise', in Quantum Noise in Mesoscopic Physics, edited by Y. V. Nazarov (Springer Netherlands, Dordrecht, 2003), pp. 175–203 (cited on page 10).

[132]A. A. Clerk, M. H. Devoret, S. M. Girvin, F. Marquardt, and R. J. Schoelkopf, 'Introduction to quantum noise, measurement, and amplification', Reviews of Modern Physics **82**, 1155 (2010) (cited on page 10).

[133]Ł. Cywiński, 'Dynamical-decoupling noise spectroscopy at an optimal working point of a qubit', Physical Review A **90**, 042307 (2014) (cited on page 21).

[134]H. Bruus and K. Flensberg, Many-body quantum field theory in condensed matter physics (Oxford University Press, Oxford, 2004) (cited on page 23).

[135]H. B. Callen and T. A. Welton, 'Irreversibility and Generalized Noise', Physical Review **83**, 34–40 (1951) (cited on page 25).

[136]X. You, A. A. Clerk, and J. Koch, 'Positive- and negative-frequency noise from an ensemble of two-level fluctuators', Physical Review Research **3**, 013045 (2021) (cited on pages 25, 74, 80).

[137]K. Blum, Density matrix theory and applications (Plenum Press, New York, 1981) (cited on page 26).

[138]M. Winczewski, A. Mandarino, M. Horodecki, and R. Alicki, 'Bypassing the Intermediate Times Dilemma for Open Quantum System', 10.48550/arXiv.2106.05776 (2021) (cited on pages 28, 119).

[139]G. Lindblad, 'On the generators of quantum dynamical semigroups', Communications in Mathematical Physics **48**, 119–130 (1976) (cited on page 29).

[140]V. Gorini, 'Completely positive dynamical semigroups of N-level systems', Journal of Mathematical Physics **17**, 821 (1976) (cited on page 29).

[141]N. Vogt, J. Jeske, and J. H. Cole, 'Stochastic Bloch-Redfield theory: Quantum jumps in a solid-state environment', Physical Review B **88**, 174514 (2013) (cited on page 29).

[142]P. R. Eastham, A. O. Spracklen, and J. Keeling, 'Lindblad theory of dynamical decoherence of quantum-dot excitons', Physical Review B **87**, 195306 (2013) (cited on page 29).

[143]M. Vogelsberger, D. A. Garanin, and R. Schilling, 'Butterfly hysteresis curve is a signature of adiabatic Landau-Zener transition', 10.1103/PhysRevB.73.092412 (2005) (cited on page 30).

[144]D. Kwiatkowski, P. Szańkowski, and Ł. Cywiński, 'Influence of nuclear spin polarization on the spin-echo signal of an NV-center qubit', Physical Review B **101**, 155412 (2020) (cited on page 32).

[145]G. A. Paz-Silva, L. M. Norris, and L. Viola, 'Multiqubit spectroscopy of Gaussian quantum noise', Physical Review A **95**, 022121 (2017) (cited on page 32).

[146]P. Szańkowski and Ł. Cywiński, 'Noise representations of open system dynamics', Scientific Reports **10**, 22189 (2020) (cited on page 34).

[147]P. Szańńkowski, 'Measuring trajectories of environmental noise', Physical Review A: Atomic, Molecular, and Optical Physics **104**, 022202 (2021) (cited on page 34).

[148]J. R. Klauder and P. W. Anderson, 'Spectral diffusion decay in spin resonance experiments', Physical Review **125**, 912–932 (1962) (cited on page 34).

[149]Ł. Cywiński, R. M. Lutchyn, C. P. Nave, and S. Das Sarma, 'How to enhance dephasing time in superconducting qubits', Physical Review B **77**, 1–11 (2008) (cited on page 34).

[150]C. L. Degen, F. Reinhard, and P. Cappellaro, 'Quantum sensing', Reviews of Modern Physics **89**, 035002 (2017) (cited on page 34).

[151]P. Szańkowski, M. Trippenbach, and Ł. Cywiński, 'Spectroscopy of cross correlations of environmental noises with two qubits', Physical Review A **94**, 012109 (2016) (cited on pages 34, 50).

[152]M. J. Biercuk, A. C. Doherty, and H. Uys, 'Dynamical decoupling sequence construction as a filter-design problem', Journal of Physics B: Atomic, Molecular and Optical Physics **44**, 154002 (2011) (cited on page 34).

[153]L. M. Norris, D. Lucarelli, V. M. Frey, S. Mavadia, M. J. Biercuk, and L. Viola, 'Optimally band-limited spectroscopy of control noise using a qubit sensor', Physical Review A: Atomic, Molecular, and Optical Physics **98**, 032315 (2018) (cited on page 34).

[154]J. Marcinkiewicz, 'Sur une peropri'et'e de la loi de Gauss', Mathematische Zeitschrift **44**, 612 (1939) (cited on page 35).

[155]N. G. V. Kampen, Stochastic processes in physics and chemistry (Elsevier, New York, 1992) (cited on pages 36, 37).

[156]E. Paladino, Y. M. Galperin, G. Falci, and B. L. Altshuler, '1 / f noise: Implications for solid-state quantum information', Reviews of Modern Physics **86**, 361–418 (2014) (cited on pages 37, 38, 74).

[157]B. M. Freeman, J. S. Schoenfield, and H. Jiang, 'Comparison of low frequency charge noise in identically patterned Si/SiO $_2$ and Si/SiGe quantum dots', Applied Physics Letters **108**, 253108 (2016) (cited on pages 37, 80).

[158]O. E. Dial, M. D. Shulman, S. P. Harvey, H. Bluhm, V. Umansky, and A. Yacoby, 'Charge noise spectroscopy using coherent exchange oscillations in a singlet-triplet qubit', Physical Review Letters **110**, 146804 (2013) (cited on pages 37, 80).

[159]W. I. L. Lawrie et al., 'Quantum dot arrays in silicon and germanium', Applied Physics Letters **116**, 080501 (2020) (cited on page 37).

[160]L. Petit et al., 'Spin lifetime and charge noise in hot silicon quantum dot qubits', Physical Review Letters **121**, 076801 (2018) (cited on pages 37, 80).

[161]G. E. Uhlenbeck and L. S. Ornstein, 'On the theory of the brownian motion', Physical Review **36**, 823–841 (1930) (cited on page 37).

[162]J. Schriefl, Y. Makhlin, A. Shnirman, and G. Schön, 'Decoherence from ensembles of two-level fluctuators', New Journal of Physics **8**, 1 (2006) (cited on page 38).

[163]G. Ramon, 'Non-Gaussian signatures and collective effects in charge noise affecting a dynamically decoupled qubit', Physical Review B **92**, 155422 (2015) (cited on page 39).

[164]N. V. Vitanov and B. M. Garraway, 'Landau-Zener Model: Effects of Finite Coupling Duration', Physical Review A **53**, 4288–4304 (1996) (cited on page 43).

[165]B. Damski and W. H. Zurek, 'Adiabatic-impulse approximation for avoided level crossings: From phase-transition dynamics to Landau-Zener evolutions and back again', Physical Review A: Atomic, Molecular, and Optical Physics **73**, 063405 (2006) (cited on page 45).

[166]T. N. Ikeda, S. Tanaka, and Y. Kayanuma, 'Floquet-Landau-Zener interferometry: Usefulness of the Floquet theory in pulse-laser-driven systems', 10.48550/arXiv.2202.04973 (2022) (cited on page 45).

[167]D. Porras and J. I. Cirac, 'Effective quantum spin systems with trapped ions', Physical Review Letters **92**, 207901 (2004) (cited on page 61).

[168]T. Chakraborty, Quantum dots : a survey of the properties of artificial atoms (North-Holland, Amsterdam, 1999) (cited on page 61).

[169]P. Y. Yu and M. Cardona, Fundamentals of Semiconductors, Graduate Texts in Physics (Springer Berlin Heidelberg, Berlin, Heidelberg, 2010) (cited on pages 61, 73, 104).

[170]R. Winkler, Spin-orbit coupling effects in two-dimensional electron and hole systems (Springer-Verlag, Berlin, 2003) (cited on page 61).

[171]M. Friesen, S. Chutia, C. Tahan, and S. N. Coppersmith, 'Valley Splitting Theory of SiGe/Si/SiGe Quantum Wells', Physical Review B **75**, 1–12 (2007) (cited on page 63).

[172]A. L. Saraiva, M. J. Calderón, X. Hu, S. Das Sarma, and B. Koiller, 'Physical mechanisms of interface-mediated intervalley coupling in Si', Physical Review B **80**, 081305 (2009) (cited on pages 63, 69).

[173]G. Bastard, Wave mechanics applied to semiconductor heterostructures (New York, NY (USA); John Wiley and Sons Inc., 1990) (cited on page 64).

[174]Platt, Edward, 'WKB Analysis of Tunnel Coupling in a Simple Model of a Double Quantum Dot', MA thesis (UWSpace, 2008) (cited on page 66).

[175]L. Gaudreau et al., 'Coherent control of three-spin states in a triple quantum dot', Nature Physics **8**, 54–58 (2012) (cited on page 66).

[176]G. Burkard, D. Loss, and D. P. DiVincenzo, 'Coupled quantum dots as quantum gates', Physical Review B **59**, 2070 (1999) (cited on page 67).

[177]Q. Li, Ł. Cywiński, D. Culcer, X. Hu, and S. Das Sarma, 'Exchange coupling in silicon quantum dots: Theoretical considerations for quantum computation', **81**, 085313 (2010) (cited on page 67).

[178]J. M. Nichol et al., 'Quenching of dynamic nuclear polarization by spin–orbit coupling in GaAs quantum dots', Nature Communications **6**, 7682 (2015) (cited on pages 68, 114).

[179]L. Kranz, S. K. Gorman, B. Thorgrimsson, Y. He, D. Keith, J. G. Keizer, and M. Y. Simmons, 'Exploiting a Single-Crystal Environment to Minimize the Charge Noise on Qubits in Silicon', Advanced Materials **32**, 2003361 (2020) (cited on pages 69, 74, 80).

[180]J. Klos, F. Hassler, P. Cerfontaine, H. Bluhm, and L. R. Schreiber, 'Calculation of tunnel couplings in open gate-defined disordered quantum dot systems', Physical Review B **98**, 1–9 (2018) (cited on page 74).

[181]J. Klos, B. Sun, J. Beyer, S. Kindel, L. Hellmich, J. Knoch, and L. R. Schreiber, 'Spin Qubits Confined to a Silicon Nano-Ridge', Applied Sciences **9**, 3823 (2019) (cited on page 74).

[182]R. Maurand et al., 'A CMOS silicon spin qubit', Nature Communications **7**, 13575 (2016) (cited on page 74).

[183]R. M. Jock, N. T. Jacobson, M. Rudolph, D. R. Ward, M. S. Carroll, and D. R. Luhman, 'A silicon singlet-triplet qubit driven by spin-valley coupling', Nature Communications **13**, 641 (2022) (cited on page 74).

[184]F. Marquardt and V. A. Abalmassov, 'Spin relaxation in a quantum dot due to Nyquist noise', Physical Review B **71**, 165325 (2005) (cited on page 75).

[185]U. Weiss, Quantum dissipative systems (World Scientific, Singapore, 1999) (cited on page 75).

[186]P. Dutta and P. M. Horn, 'Low-frequency fluctuations in solids: 1 f noise', Reviews of Modern Physics **53**, 497–516 (1981) (cited on page 80).

[187]J. M. Boter et al., 'Spatial noise correlations in a Si/SiGe two-qubit device from Bell state coherences', Physical Review B **101**, 235133 (2020) (cited on pages 83, 107).

[188]S. Yang et al., 'High-fidelity transfer and storage of photon states in a single nuclear spin', Nature Photonics **10**, 507–511 (2016) (cited on page 90).

[189]J. M. Hornibrook et al., 'Cryogenic Control Architecture for Large-Scale Quantum Computing', Physical Review Applied **3**, 024010 (2015) (cited on page 90).

[190]E. I. Rashba, 'Theory of electric dipole spin resonance in quantum dots: Mean field theory with Gaussian fluctuations and beyond', Physical Review B **78**, 195302 (2008) (cited on page 104).

[191]M. Raith, P. Stano, and J. Fabian, 'Theory of single electron spin relaxation in Si/SiGe lateral coupled quantum dots', Physical Review B **83**, 195318 (2011) (cited on page 105).

[192]T. Tanttu et al., 'Controlling Spin-Orbit Interactions in Silicon Quantum Dots Using Magnetic Field Direction', Physical Review X **9**, 021028 (2019) (cited on page 105).

[193]A. Hofmann, V. F. Maisi, T. Krähenmann, C. Reichl, W. Wegscheider, K. Ensslin, and T. Ihn, 'Anisotropy and Suppression of Spin-Orbit Interaction in a GaAs Double Quantum Dot', Physical Review Letters **119**, 176807 (2017) (cited on pages 105, 113, 114).

[194]L. V. C. Assali, H. M. Petrilli, R. B. Capaz, B. Koiller, X. Hu, and S. D. Sarma, 'Hyperfine interactions in silicon quantum dots', Physical Review B **83**, 165301 (2011) (cited on pages 106, 108, 132).

[195]A. Abragam, The principles of nuclear magnetism (Oxford University Press, New York, 1983) (cited on page 106).

[196]D. Paget, G. Lampel, B. Sapoval, and V. I. Safarov, 'Low field electron-nuclear spin coupling in gallium arsenide under optical pumping conditions', Physical Review B **15**, 5780–5796 (1977) (cited on page 108).

[197]P. Harvey-Collard et al., 'Spin-orbit Interactions for Singlet-Triplet Qubits in Silicon', Physical Review Letters **122**, 217702 (2019) (cited on pages 114, 132).

[198] H. Munoz-Bauza, H. Chen, and D. Lidar, 'A double-slit proposal for quantum annealing', npj Quantum Information **5**, 51 (2019) (cited on page 124).

[199] A. C. Elitzur and L. Vaidman, 'Quantum mechanical interaction-free measurements', Foundations of Physics **23**, 987–997 (1993) (cited on pages 130, 131).

[200] R. Ruskov, M. Veldhorst, A. S. Dzurak, and C. Tahan, 'Electron g -Factor of valley states in realistic silicon quantum dots', Physical Review B **98**, 1–19 (2018) (cited on page 159).